

**Biochemical and structural characterization
of novel drug targets regulating polyamine
biosynthesis in the human malaria parasite,
*Plasmodium falciparum***

By

Marni Williams

Submitted in partial fulfilment of the requirements for the degree

Philosophiae Doctor Biochemistry

in the Faculty of Natural & Agricultural Science

Department of Biochemistry

University of Pretoria

Pretoria

July 2011



Submission declaration

I, Marni Williams declare that this dissertation, which is herewith submitted for the degree *Philosophiae Doctor* at the University of Pretoria, is my own work and has not previously been submitted by me for a degree at this or any other tertiary institution.

Signature: Date:



Plagiarism declaration

**UNIVERSITY OF PRETORIA
FACULTY OF NATURAL AND AGRICULTURAL SCIENCES
DEPARTMENT OF BIOCHEMISTRY**

Full name: Student number:
Title of work:

Declaration

1. I understand what plagiarism entails and am aware of the University's policy in this regard.
2. I declare that this thesis is my own, original work. Where someone else's work was used (whether from a printed source, the internet or any other source) due acknowledgement was given and reference was made according to departmental requirements.
3. I did not make use of another student's previous work and submit it as my own.
4. I did not allow and will not allow anyone to copy my work with the intention of presenting it as his or her own work.

Signature: Date:

Acknowledgements

Prof Lyn-Marié Birkholtz (supervisor) and Prof Abraham I. Louw (co-supervisor) from the University of Pretoria. Thank you for teaching me not only about science but also about life, for believing in me as a scientist and for investing the time and money that allowed me to travel the world to attend conferences and courses.

My co-supervisor Prof Lo Persson (Lund University) for collaborating with us on this project and for hosting me in your laboratory as well as in your beautiful country.

Prof Salam Al-Karadaghi (Lund University) for collaborating with us on this project and for hosting me in your laboratory and teaching me about protein crystal structures.

Janina Sprenger (Lund University) for your contributions to the AdoMetDC project and for all the interesting discussions, advice and friendship.

Dr Gordon A. Wells (University of Pretoria) for all the bioinformatics-related questions.

Dr Pieter B. Burger (University of Pretoria) for the design and identification of the SpdS inhibitory compounds. Shaun B. Reeksting and Dina le Roux (University of Pretoria) for the enzyme kinetics and whole cell-based testing of the identified compounds.

Maria Håkansson (Crystallisation facility at Max Lab, Lund) for protein crystallisation screens and Prof Marjolein Thunnissen for help with the X-ray data collection.

Esmaré Human (University of Pretoria) for your help in the cloning experiments and general assistance in the laboratory. Jandeli Niemand (University of Pretoria) for your assistance in the testing of the O1 insert peptide probes.

Prof Marina Rautenbach (University of Stellenbosch) for your advice on the design of the peptide probes.

Dr Janet Mans for your scientific contributions to the protein crystallisation chapter.

The PhD students at Lund University including Dr Raymond Yengo for your assistance with SEC, Dr Christopher Söderberg and Dr Sreekanth Rajan for advice on crystallisation drop set up and manual screens.

My parents, husband and sisters for your devoted love and motivation during my PhD studies.

Finally, I would like to thank the funding organisations, which enabled me to complete my PhD studies, including the National Research Foundation, the Swedish International Cooperation Development Agency (NRF-SIDA, Swedish Research Links Programme), the South African Malaria Initiative and the Ernst and Ethel Eriksen Trust.

Summary

Malaria is prevalent in over 100 countries which is populated by half of the world's population and culminates in approximately one million deaths per annum, 85% of which occurs in sub-Saharan Africa. The combined resistance of the mosquitoes and parasites to the currently available pesticides and antimalarial chemotherapeutic agents requires the concerted effort of scientists in the malaria field to identify and develop novel mechanisms to curb this deadly disease.

In this study, a thorough understanding of the role players in the polyamine pathway of the parasite was obtained, which could aid future studies in the development of novel inhibitory compounds against these validated drug targets. The uniquely bifunctional *S*-adenosylmethionine decarboxylase/ornithine decarboxylase (AdoMetDC/ODC) of *Plasmodium falciparum* forms an important controlling node between the polyamine and methionine metabolic pathways. It has been speculated that the unique bifunctional association of the rate-limiting enzymes allows for the concerted regulation of the respective enzyme activities resulting in polyamine synthesis as per requirement for the rapidly proliferating parasite while the methionine levels are strictly controlled for their role in the methylation status. The results of this study showed that the enzyme activities of the bifunctional complex are indeed coordinated and subtle conformational changes induced by complex formation is suggested to result in these altered kinetics of the individual AdoMetDC and ODC domains. Studies also showed that the identification of the interaction sites between the domains, which allows for communication across the complex, may be targeted for specific interference with the enzyme activities. Furthermore, these studies showed that the current knowledge on the different subclasses of the AdoMetDC family should be re-evaluated since *P. falciparum* AdoMetDC shows diverse properties from orthologues and therefore points towards a novel grouping of the plasmodial protein. The extensive biochemical and biophysical studies on AdoMetDC has also provided important avenues for the crystallisation and solving of this protein's 3D structure for subsequent structure-based identification of drug-like lead compounds against AdoMetDC activity.

The application of structure-based drug design on malarial proteins was additionally investigated and consequently proved that the rational design of lead inhibitory compounds can provide important scaffold structures for the identification of the key aspects that are required for the successful inhibition of a specific drug target. Spermidine synthase, with its intricate catalytic mechanism involving two substrate binding sites for the products of the reactions catalysed by

AdoMetDC/ODC, was used to computationally identify compounds that could bind within its active site. Subsequent testing of the compounds identified with a dynamic receptor-based pharmacophore model showed promising inhibitory results on both recombinant protein and *in vitro* parasite levels. The confirmation of the predicted interaction sites and identification of aspects to improve inhibitor interaction was subsequently investigated at atomic resolution with X-ray protein crystallography.

The outcome of this doctoral study shows the benefit in applying a multidisciplinary and multinational approach for studying drug targets within the malaria parasite, which has led to a thorough understanding of the targets on both biochemical and structural levels for future drug design studies.

Table of Contents

List of Figures	IV
List of Tables	VI
List of Abbreviations	VII
1. Chapter 1	1
Introduction	1
1.1. Malaria	1
1.1.1. The <i>P. falciparum</i> life cycle	3
1.2. Treating malaria	5
1.2.1. Vector control	5
1.2.2. Vaccine development	7
1.2.3. Current antimalarials	8
1.3. Novel antimalarial targets	13
1.3.1. Polyamine biosynthesis as a drug target	14
1.3.2. Polyamines.....	14
1.3.3. Polyamine metabolism in <i>P. falciparum</i>	17
1.3.4. Polyamine transport in <i>P. falciparum</i>	18
1.3.5. The <i>P. falciparum</i> polyamine biosynthetic enzymes as drug targets	20
1.4. Research objectives	27
1.5. Outputs	28
2. Chapter 2	30
A conserved parasite-specific insert is a key regulator of the activities and interdomain interactions of <i>Plasmodium falciparum</i> AdoMetDC/ODC	30
2.1. Introduction	30
2.1.1. Parasite-specific inserts within the polyamine biosynthetic enzymes of <i>P. falciparum</i>	31
2.2. Methods.....	34
2.2.1. Secondary structure predictions of the O1 parasite-specific insert	34
2.2.2. Expression constructs and site-directed mutagenesis.....	34
2.2.3. Protein expression and isolation	35
2.2.4. Activity analysis of the recombinantly expressed proteins	36
2.2.5. Analysis of the oligomeric status of the mutant monofunctional and bifunctional proteins.....	37
2.2.6. Western immunodetection of monofunctional <i>Pf</i> ODC and bifunctional <i>Pf</i> AdoMetDC/ODC proteins following SEC	37
2.2.7. Computational studies on the homology models of the monofunctional <i>Pf</i> AdoMetDC and <i>Pf</i> ODC proteins.....	38
2.2.8. Incubation of <i>Pf</i> AdoMetDC/ODC with synthetic peptide probes.....	38
2.3. Results	39
2.3.1. The O1 parasite-specific insert contains specific structural features	39
2.3.2. Mutagenesis of the flanking Gly residues and disruption of the α -helix within	

O1 insert affects enzyme activity	40
2.3.3. The O1 insert α -helix mediates inter- and intradomain protein-protein interactions	41
2.3.4. Peptide probe-mediated modulation of <i>PfAdoMetDC</i> and <i>PfODC</i> activities via interference of the O1 insert interactions	44
2.4. Discussion	48
2.5. Conclusion.....	52
3. Chapter 3:.....	54
Biochemical and structural characterisation of monofunctional <i>Plasmodium falciparum</i> AdoMetDC	54
3.1. Introduction	54
3.2. Methods.....	57
3.2.1. Cloning of the harmonised <i>PfAdometdc</i> gene sequence.....	57
3.2.2. Protein expression and purification	60
3.2.3. Refolding of the <i>PfAdoMetDC</i> from insoluble inclusion bodies.....	61
3.2.4. Determination of enzyme activity and protein stability	61
3.2.5. Investigations into the oligomeric status of monofunctional <i>PfAdoMetDC</i>	62
3.2.6. Secondary structure analysis of <i>PfAdoMetDC</i> using far-UV CD spectroscopy.....	65
3.2.7. Analyses of residues involved in the autocatalytic processing reaction.....	66
3.2.8. <i>PfAdoMetDC</i> enzyme and inhibition kinetics.....	66
3.3. Results	68
3.3.1. Codon harmonisation improves the purity and stability of monofunctional <i>PfAdoMetDC</i>	68
3.3.2. Refolding of <i>PfAdoMetDC</i> from inclusion bodies yields a significant amount of unprocessed protein	70
3.3.3. <i>PfAdoMetDC</i> enzyme activity and protein stability	72
3.3.4. Determination of the oligomeric status of monofunctional <i>PfAdoMetDC</i>	74
3.3.5. Far-UV analyses of <i>PfAdoMetDC</i> indicates a similar fold as the human protein.....	82
3.3.6. Studies of the mechanism of processing in <i>PfAdoMetDC</i>	83
3.3.7. Enzyme kinetics of monofunctional <i>PfAdoMetDC</i>	86
3.4. Discussion	90
3.5. Conclusion.....	101
4. Chapter 4:.....	103
Validation of pharmacophore-identified inhibitors against <i>Plasmodium falciparum</i> SpdS with X-ray crystallography	103
4.1. Introduction	103
4.1.1. Identification of novel compounds against <i>PfSpdS</i> with the use of a dynamic pharmacophore model	106
4.2. Methods.....	111
4.2.1. Enzyme kinetics of <i>PfSpdS</i> treated with lead inhibitor compounds	111
4.2.2. <i>In vitro</i> growth inhibition of <i>P. falciparum</i>	111

4.2.3.	Near-UV CD of <i>Pf</i> SpdS in the presence of active site ligands	112
4.2.4.	Protein crystallisation of <i>Pf</i> SpdS in complex with lead inhibitor compounds ..	113
4.3.	Results	115
4.3.1.	Enzyme kinetics and <i>in vitro</i> parasite treatment of novel inhibitory compounds against <i>Pf</i> SpdS	115
4.3.2.	Preparation of high yields of pure <i>Pf</i> SpdS for protein crystallography	117
4.3.3.	Near-UV CD analyses of <i>Pf</i> SpdS in the presence of NAC or NACD	120
4.3.4.	Growth of diffraction quality <i>Pf</i> SpdS protein crystals in complex with NAC or NACD	121
4.3.5.	X-ray crystallography verifies binding of NAC and NACD in the active site of <i>Pf</i> SpdS.....	122
4.4.	Discussion	135
4.5.	Conclusion.....	141
5.	Chapter 5:.....	142
	Concluding discussion.....	142
6.	References.....	149
	Appendix I: PROCHECK results for the <i>Pf</i> SpdS-NACD-MTA crystal structure.....	164
	Appendix II: PROCHECK results for the <i>Pf</i> SpdS-NACD crystal structure	171
	Appendix III: PROCHECK results for the <i>Pf</i> SpdS-NAC-MTA crystal structure.....	178

List of Figures

Figure 1.1: The worldwide distribution of malaria and its association with economic growth.....	3
Figure 1.2: A <i>P. falciparum</i> merozoite showing the apical complex and other major cellular organelles and structures.	4
Figure 1.3: The asexual and sexual life cycles of the malaria parasite.	5
Figure 1.4: Selected malaria vaccines targeting different antigens in specific stages of the parasite life cycle.....	8
Figure 1.5: A schematic diagram of the <i>P. falciparum</i> life cycle within the human host showing the targets of different antimalarials during the developmental stages.	9
Figure 1.6: Polyamine biosynthetic pathways of various parasites compared with that of the human host.	16
Figure 1.7: Polyamine levels during the intra-erythrocytic developmental cycle of <i>P. falciparum</i>	17
Figure 1.8: Summary of the polyamine metabolic pathways in the human host and <i>P. falciparum</i> parasite.	18
Figure 1.9: Schematic diagram of the bifunctional <i>P. falciparum</i> AdoMetDC/ODC protein.	22
Figure 1.10: The $\alpha\beta\alpha$ -sandwich fold of monofunctional, monomeric <i>P. falciparum</i> AdoMetDC superimposed with the dimeric human protein.	23
Figure 1.11: The head-to-tail organisation of <i>P. falciparum</i> ODC superimposed with the human protein.....	25
Figure 1.12: The structure of homodimeric SpdS from <i>P. falciparum</i> superimposed with the human protein.....	26
Figure 2.1: Multiple sequence alignment and secondary structure prediction of the O1 insert...39	39
Figure 2.2: The effect of O1 insert mutations on the <i>PfAdoMetDC</i> and <i>PfODC</i> enzyme activities within the bifunctional complex.	40
Figure 2.3: Western blots of the sequential fractions obtained from SEC of the (A) bifunctional <i>PfAdoMetDC/ODC</i> and (B) monofunctional <i>PfODC</i> proteins.	42
Figure 2.4: The wild-type homodimeric <i>PfODC</i> and immobile insert ODC G2A mutant protein after minimisation and MD.	43
Figure 2.5: <i>PfAdoMetDC</i> (A) and <i>PfODC</i> (B) activities after co-incubation with different peptide probes.	46
Figure 2.6: Folding of the α -helix O1 insert peptides as predicted by PEP-FOLD.	47
Figure 2.7: Protein-protein docking results to determine the proximity of the O1 insert to the <i>PfAdoMetDC</i> protein.	48
Figure 3.1: Schematic diagrams of the gene fragments used in the comparative <i>PfAdoMetDC</i> protein expression study.....	59
Figure 3.2: SDS-PAGE analyses of <i>PfAdoMetDC</i> , <i>PfAdoMetDC</i> -hinge and wt <i>PfAdoMetDC</i> -hinge proteins followed by Western immunodetection of these recombinantly expressed monofunctional proteins.....	69
Figure 3.3: Non-reducing SDS-PAGE analyses of the insoluble protein extracts of expressed (A) <i>PfAdoMetDC</i> and (B) <i>PfAdoMetDC</i> -hinge proteins.	71
Figure 3.4: Purification of <i>PfAdoMetDC</i> and <i>PfAdoMetDC</i> -hinge from inclusion bodies and visualisation on 7.5% (A) and 12.5% (B) SDS-PAGE gels.....	72
Figure 3.5: Fluorescence intensity curves obtained upon incubation of <i>PfAdoMetDC</i> with different molar excesses of MDL73811 and CGP48664.	74
Figure 3.6: Analyses of the oligomeric status of monofunctional <i>PfAdoMetDC</i> with SEC.	75
Figure 3.7: Protein gel bands of the <i>PfAdoMetDC</i> and <i>PfAdoMetDC</i> -hinge proteins that were analysed with MALDI-MS.....	77
Figure 3.8: Analyses of the oligomeric status of the C505S mutant of <i>PfAdoMetDC</i> with SEC.....	78

Figure 3.9: Predicted structural description of <i>PfAdoMetDC/ODC</i> showing the proposed domain-domain interaction sites.	81
Figure 3.10: SEC of <i>PfAdoMetDC</i> -C505S in the presence of DTT and n-butanol.....	82
Figure 3.11: Far-UV CD analyses of the <i>PfAdoMetDC</i> and C505S mutant proteins.	83
Figure 3.12: The charged-buried site of <i>PfAdoMetDC</i>	84
Figure 3.13: SDS-PAGE analysis of the S421A <i>PfAdoMetDC</i> mutant protein to determine the role of this residue in autocatalytic processing.	85
Figure 3.14: SDS-PAGE analysis of the R11L <i>PfAdoMetDC</i> mutant protein to determine the role of this residue in autocatalytic processing.	86
Figure 3.15: Activity analyses of the S421A and R11L <i>PfAdoMetDC</i> mutant enzymes.....	86
Figure 3.16: Michaelis-Menten curve (A) and linear Hanes-Woolf plot (B) of <i>PfAdoMetDC</i> reaction velocity measured at different substrate concentrations.....	87
Figure 3.17: Inhibition kinetics of <i>PfAdoMetDC</i> treated with MDL73811 and CGP48664.....	89
Figure 3.18: Model of monofunctional <i>PfAdoMetDC</i> oligomerisation <i>in vitro</i>	95
Figure 3.19: Schematic diagram describing the coordinated activities of the domains within the bifunctional AdoMetDC/ODC complex from <i>P. falciparum</i>	99
Figure 4.1: Chemical structures of various SpdS inhibitors.	104
Figure 4.2: Clustering of the MD trajectory of <i>PfSpdS</i> in the absence of ligands.....	107
Figure 4.3: 2D representation of the active site of <i>PfSpdS</i> illustrating different regions used to explore and construct DPMs.	108
Figure 4.4: PhFs selected to describe the most important binding characteristics of the DPM2 binding cavity as well as the proposed docking poses of NAC and NACD within <i>PfSpdS</i>	110
Figure 4.5: Inhibition kinetics of <i>PfSpdS</i> treated with NAC.	116
Figure 4.6: Dose response curves of <i>P. falciparum</i> cultures treated with NAC (A) and NACD (B) for determination of IC ₅₀ values.	117
Figure 4.7: The aLEX chromatogram (A) and subsequent SDS-PAGE analysis (B) of the <i>PfSpdS</i> fractions.....	118
Figure 4.8: SEC of affinity-purified <i>PfSpdS</i> (A) followed by SDS-PAGE analysis (B).....	119
Figure 4.9: Western immunodetection of the ProTEV cleavage products collected after affinity chromatography using HisProbe [®] -HRP (A) and a polyclonal <i>PfSpdS</i> antibody (B).....	119
Figure 4.10: Near-UV CD analyses of <i>PfSpdS</i> in the presence of various ligands.	120
Figure 4.11: Images of <i>PfSpdS</i> crystals in complex with NAC or NACD.	122
Figure 4.12: Ramachandran plot of the <i>PfSpdS</i> -NACD structure.	125
Figure 4.13: Ramachandran plot of the <i>PfSpdS</i> -NACD-MTA crystal structure.	126
Figure 4.14: Ramachandran plot of the <i>PfSpdS</i> -NAC-MTA crystal structure.	126
Figure 4.15: Diagram to illustrate the crystal packing of <i>PfSpdS</i> -NACD crystallised in spacegroup C121.	127
Figure 4.16: Overall fold of <i>PfSpdS</i> (A) and superimposition of the solved crystal structures (B).....	128
Figure 4.17: Stereo view of the <i>PfSpdS</i> -NACD-MTA active site.	129
Figure 4.18: The active site of <i>PfSpdS</i> -NACD-MTA superimposed with the 2PSS (A) and 2PT9 (B) crystal structures.....	130
Figure 4.19: Electrostatic surface potential of the <i>PfSpdS</i> active site.	131
Figure 4.20: Stereo view of the <i>PfSpdS</i> -NACD active site.	132
Figure 4.21: Stereo view of the <i>PfSpdS</i> -NAC-MTA active site.	133
Figure 4.22: Stereo view of the <i>PfSpdS</i> -NAC-MTA active site superimposed with the apo structure.	134
Figure 4.23: Derivatives of NAC and NACD as alternative chemical compounds to test for inhibition of <i>PfSpdS</i> activity.	140
Figure 4.24: The <i>PfSpdS</i> -NACD-MTA active site superimposed with the human structure....	141

List of Tables

Table 1.1: Antimalarial drug classes	10
Table 1.2: Selected inhibitors of <i>P. falciparum</i> ODC, AdoMetDC and SpdS	21
Table 2.2: Mutagenesis primers used for the introduction of point mutations in the O1 parasite-specific insert.....	35
Table 2.3: The synthetic peptides used as probes to determine the role of the O1 insert in protein-protein interactions across <i>PfAdoMetDC</i> /ODC	44
Table 3.1: Primers used for the amplification of the <i>PfAdometdc</i> and <i>PfAdometdc-hinge</i> fragments from the pASK-IBA3 containing partially harmonised <i>PfAdometdc/Odc</i>	60
Table 3.2: Primers used for the mutagenesis of residues predicted to be involved in the autocatalytic processing reaction of <i>PfAdoMetDC</i>	66
Table 3.3: Yields obtained for the <i>PfAdoMetDC</i> and <i>PfAdoMetDC-hinge</i> proteins isolated from soluble and insoluble protein extracts	71
Table 3.4: Comparison of the <i>PfAdoMetDC</i> and wt <i>PfAdoMetDC-hinge</i> enzyme activities after storage for two weeks at different temperatures	73
Table 3.5: Hydrodynamic radii of <i>PfAdoMetDC</i> in the presence and absence of DTT as determined by DLS	76
Table 3.6: Hydrodynamic radii of <i>PfAdoMetDC-C505S</i> at two different protein concentrations.....	79
Table 3.7: Dissociation constants for <i>PfAdoMetDC</i> and the C505S mutant from analytical SEC.....	80
Table 3.8: Alignment of residues involved in the active site, processing reaction and the putrescine-binding site or charged-buried site for AdoMetDC from three organisms	84
Table 3.9: Comparison of enzyme kinetics for AdoMetDC from different organisms	88
Table 3.10: Subclasses of AdoMetDCs from different organisms.....	101
Table 4.1: Crystallography data collection and refinements statistics	124
Table 4.2: Inhibitors tested <i>in vitro</i> on <i>PfSpdS</i> or in whole-cell assays against <i>P. falciparum</i>	135

List of Abbreviations

AbeAdo:	5'-([(Z)-4-amino-2-butenyl]methylamino)-5'-deoxyadenosine
AdoDATO:	<i>S</i> -adenosyl-1,8-diamino-3-thio-octane
ACT:	artemisinin-based combination therapy
AdoMet:	<i>S</i> -adenosyl-L-methionine
AHT:	anhydrotetracycline
aIEX:	anion exchange chromatography
AMA-1:	apical membrane antigen 1
APA:	3-aminooxy-1-aminopropane
APE:	5-amino-1-pentene
ASU:	asymmetric unit
CD:	circular dichroism
CGP48664:	4-amidinoindan-1-one-2'-amidinohydrazone
CHA:	cyclohexylamine
CSP:	circumsporozoite protein
2D:	two-dimensional
3D:	three-dimensional
Da:	Dalton
dcAdoMet:	decarboxylated <i>S</i> -adenosyl-L-methionine
DDT:	bis(4-chlorophenyl)-1,1,1-trichloroethane
DEAE:	diethylaminoethyl-cellulose
DFMO:	D,L- α -difluoromethylornithine
DHFR:	dihydrofolate reductase
DHPS:	dihydropteroate synthase
DLS:	differential light scattering
DMSO:	dimethyl sulfoxide
DPM:	dynamic pharmacophore model
DSF:	differential scanning fluorimetry
DTT:	dithiothreitol
EDTA:	ethylenediaminetetraacetic acid
eIF-5A:	eukaryotic translation initiation factor 5A
GLURP:	glutamine-rich protein
G6PD:	glucose 6-phosphate dehydrogenase
HBA:	hydrogen bond acceptor
HBD:	hydrogen bond donor
HEPES:	4-(2-hydroxyethyl)-1-piperazineethanesulfonic acid
HRP:	horseradish peroxidase
Hsp70:	heat shock protein 70 kDa
HYD:	hydrophobic
IC ₅₀ :	inhibitory concentration at 50%
IRS:	indoor residual spraying
ITN:	insecticide-treated mosquito net
JCSG:	Joint Structural Genomics Consortium

kDa:	kilodalton
LB:	Luria-Bertani
LC-MS:	liquid chromatography-mass spectrometry
LSA-1:	liver stage antigen 1
MALDI-MS:	matrix-assisted laser desorption/ionisation-mass spectrometry
4MCHA:	<i>trans</i> -4-methylcyclohexyl amine
MD:	molecular dynamics
MDL73811:	5'-([(Z)-4-amino-2-butenyl]methylamino)-5'-deoxyadenosine
MES:	2-(<i>N</i> -morpholino)ethanesulfonic acid
MGBG:	methylglyoxal bis(guanylhydrazone)
MIF:	molecular interaction field
MSP-1:	merozoite stage protein 1
MTA:	5'-methylthioadenosine
MWCO:	molecular weight cut-off
NAC:	<i>N</i> -(3-aminopropyl)-cyclohexylamine
NACD:	<i>N</i> -(3-aminopropyl)- <i>trans</i> -cyclohexane-1,4-diamine
Ni-NTA:	nickel-nitrilo triacetic acid
OD:	optical density
pABA:	<i>p</i> -aminobenzoic acid
PBS:	phosphate buffered saline
PdI:	polydispersity index
<i>Pf</i> AdoMetDC:	<i>Plasmodium falciparum</i> <i>S</i> -adenosylmethionine decarboxylase
<i>Pf</i> AdoMetDC/ODC:	<i>Plasmodium falciparum</i> <i>S</i> -adenosylmethionine decarboxylase/ornithine decarboxylase
<i>Pf</i> CRT	<i>Plasmodium falciparum</i> chloroquine transporter
<i>Pf</i> DHFR/TS:	<i>Plasmodium falciparum</i> dihydrofolate reductase/thymidylate synthase
<i>Pf</i> EMP1:	<i>Plasmodium falciparum</i> erythrocyte membrane protein 1
<i>Pf</i> ODC:	<i>Plasmodium falciparum</i> ornithine decarboxylase
<i>Pfs</i> :	<i>Plasmodium falciparum</i> surface antigen
<i>Pf</i> SpdS:	<i>Plasmodium falciparum</i> spermidine synthase
<i>Pf</i> TIM:	<i>Plasmodium falciparum</i> triosephosphate isomerase
Pgh1:	P-glycoprotein homologue 1
PhFs:	pharmacophore features
PLP:	pyridoxal-5'-phosphate
PMSF:	phenylmethylsulphonyl fluoride
PPPK:	hydroxymethyl-dihydropterin pyrophosphokinase
PVDF:	polyvinylidene fluoride
qPCR:	quantitative PCR
RMSD:	root mean square deviation
RT:	room temperature
SDS-PAGE:	sodium dodecyl sulphate polyacrylamide gel electrophoresis
SEC:	size-exclusion chromatography
S.E.M:	standard error of the mean

SGC:	Structural Genomics Consortium
TEV:	tobacco etch virus
TFA:	trifluoroacetic acid
T _m :	melting temperature
TOF:	time-of-flight
TRAP:	thrombospondin-related adhesive protein
TS:	thymidylate synthase
UTR:	untranslated region
UV:	ultra violet
WHO:	World Health Organisation
wt:	wild-type

Chapter 1

Introduction

1.1. Malaria

The first decade of the 21st century has been met with many successes as well as disappointments in the area of malaria control. From a scientific research perspective the achievements have been extraordinary and include developments such as 1) the sequencing of the *Plasmodium falciparum* (causative parasite) [1] and *Anopheles gambiae* (insect vector) [2] genomes; which has resulted in 2) the development of vast, freely available databases such as PlasmoDB [3]; 3) the release of the transcriptomic [4-7], proteomic [8,9] and metabolomic [10] profiles of the intra-erythrocytic infectious stages of the parasite within the human host; and 4) the promising results of the RTS,S/AS vaccine against falciparum malaria, which is currently in phase III clinical trials [11]. In terms of vector control, the WHO has revised the use of DDT (bis(4-chlorophenyl)-1,1,1-trichloroethane) in 2006 as a means to control the transmission of malaria by mosquitoes (<http://www.who.int/whopes/>), despite the resistance met from environmental protection agencies [12]. The creation of transgenic mosquitoes has also received attention in the scientific community to reduce the capacity of parasites to infect humans [13].

The 2010 World Malaria Report (WHO 2010) stated that nearly 289 million insecticide-treated mosquito nets (ITNs) were delivered to sub-Saharan Africa between 2008 and 2010, which conferred malaria transmission protection to 578 million people, including children and pregnant women (http://www.who.int/malaria/world_malaria_report_2010/). In 2009, 75 million Africans were also protected by indoor residual spraying (IRS) and these preventative efforts have resulted in measurable effects on public health as follows: 1) the number of malaria cases decreased from 244 million in 2005 to 225 million in 2009 (~7%); 2) the number of deaths decreased from 985 000 in 2000 to 781 000 in 2009 (~20%); 3) the number of countries that have reduced their malaria burden by 50% over the past decade continues to rise resulting in fewer countries that are endemic for malaria; and 4) in 2009 not a single case of cerebral malaria was reported in the WHO European Region. The decrease in malaria deaths can be attributed to improved access to treatment, vector control measures and diagnostic testing, which is reflected in the fact that most cases of fever in Africa are no longer due to malaria infection and the availability of inexpensive, easy-to-use, quality-assured rapid diagnostic tests for this disease (WHO 2010). Despite these successes, malaria resurgence is still observed in some African countries and even though funding for malaria control has increased dramatically in recent years

(from \$592 million in 2006 to over \$1 billion in 2008, and \$1.7 billion in 2009). The Roll Back Malaria Partnership estimates that \$5.2-6 billion is required per annum in order to achieve the targets by 2015 that have been set by the Global Malaria Action Plan. Furthermore, the current global economic recession is likely to decrease aid as reflected by the 5-10% cut in the USA science and technology budget for 2011 and 2012, which makes malaria funding uncertain.

The chief disappointment with regards to malaria control remains the ongoing development of parasite resistance, which has rendered several antimalarial medicines ineffective especially in the parts of the world where malaria remains cataclysmic. The most dreadful being the resistance threats of the most promising and highly effective artemisinin derivatives, which was confirmed at the Cambodia-Thailand border in 2009 [14]. However, despite the observed changes in parasite sensitivity to artemisinins, ACT (artemisinin-based combination therapy) remains in effect and has been combined with efforts to limit the spread of resistant parasites. Another alarming event observed in the last decade was the inclusion of *P. knowlesi*, common in macaque monkeys, as the fifth species than can cause malaria in humans [15].

More than 40% of the world's population reside in areas where they are at risk of malaria transmission (Figure 1.1, upper panel). Most deaths due to malaria occur in Africa, which is also one of the poorest regions of the world (Figure 1.1, lower panel). The disease contributes to poor economic growth, which has a further negative impact on malaria treatment and prevention. Malaria is a complicated disease and its spread may be attributable to a variety of factors such as ecological and socio-economic conditions, displacement of large population groups, agricultural malpractices causing an increase in vector breeding, global warming, parasite resistance to antimalarial drugs and vector resistance to insecticides.

A number of promising antimalarial drug and vaccine discovery projects have been launched. This includes the Medicines for Malaria Venture (MMV, <http://www.mmv.org/>) funded by a number of organisations including the Bill and Melinda Gates Foundation (<http://www.gatesfoundation.org/>) for the development of novel antimalarials. The identification of new drug targets for malaria chemotherapeutic development is an ongoing process and is dependent on the study of disease pathology, parasite invasion and immune defence strategies, parasite transmission as well as parasite growth and development.

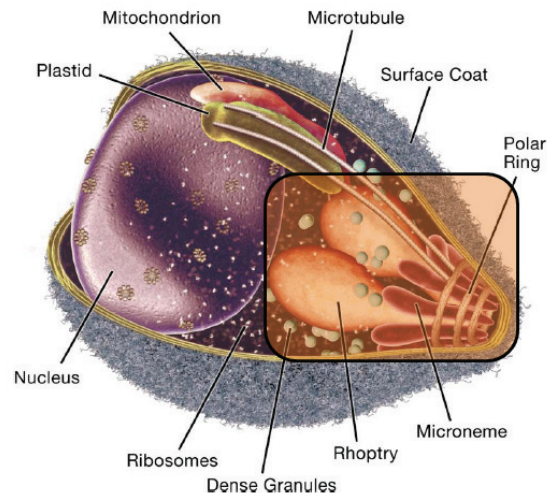


Figure 1.2: A *P. falciparum* merozoite showing the apical complex and other major cellular organelles and structures.

The apical complex is shaded. Adapted from [17].

P. falciparum invades host cells to acquire a rich source of nutrients and at the same time, these cells protect the parasites from host immune responses. The parasites are transmitted by the female *A. gambiae* and *A. funestus* (southern Africa) mosquitoes, which serve as vectors for the sexual reproduction of the parasites while the mammalian host provides the parasites with a niche for asexual development. During a blood meal the mosquitoes inject a sporozoite form of the parasites into the subcutaneous layer of the host skin. The sporozoites rapidly move to the liver where they infect the hepatocytes and differentiate into thousands of merozoites. *P. vivax* and *P. ovale* have a dormant stage which persists in the liver and cause relapses by invading the bloodstream sometime thereafter (Figure 1.3A). Merozoites are subsequently released into the bloodstream where they invade erythrocytes. This invasion characterises the onset of the intra-erythrocytic asexual blood stage of the parasitic life cycle. The parasite cycles through ring, trophozoite and schizont stages and in so doing produce between 16 and 32 daughter merozoites per erythrocyte egression, which is accompanied by the characteristic bursts of fever and anaemia associated with the disease, occurring every 24 hours. The daughter merozoites repeat the asexual cycle by invading free erythrocytes (Figure 1.3B) [18].

Some ring stage parasites develop into male or female gametocytes that are ingested by the mosquito during its next blood meal. These develop into male and female gametes inside the mosquito's gut where they fuse to form diploid zygotes. The zygotes differentiate into ookinetes that subsequently cross the midgut and develop into oocysts from which sporozoites are released. These sporozoites are stored in the salivary glands and are injected into the human host by the mosquito to repeat the parasitic life cycle resulting in its successful transmission (Figure 1.3C) [18].

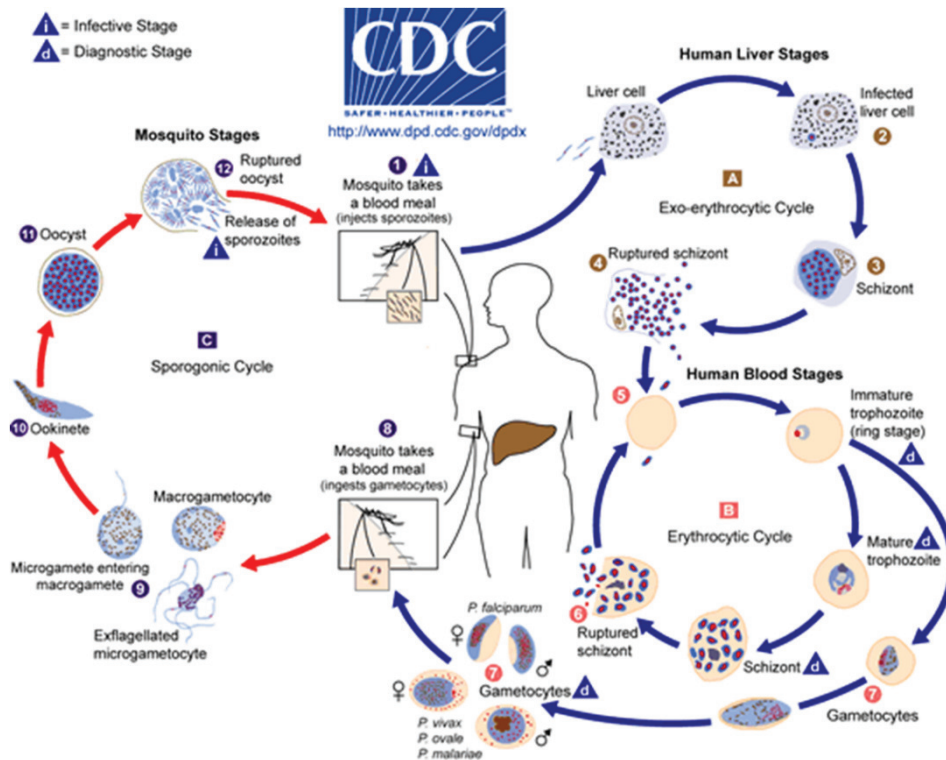


Figure 1.3: The asexual and sexual life cycles of the malaria parasite.

(1A) During a blood meal the malaria-infected female *Anopheles* mosquito injects sporozoites into the human host where they are transported to the liver cells (2A) and mature into schizonts (3A). The schizonts rupture and release merozoites (4A), which infect red blood cells (intra-erythrocytic asexual blood stage) (5B). The trophozoites mature into schizonts, which once again rupture to release merozoites (6B). Some parasites differentiate into sexual erythrocytic stages (7B) or gametocytes, which are ingested by another mosquito during a blood meal (8C). The male and female gametocytes fuse to form zygotes (9C), which differentiate into motile and elongated ookinets (10C) that invade the midgut wall where they develop into oocysts (11C). These then grow and rupture to release sporozoites (12C), which move to the mosquito's salivary glands in order to be injected into a new human host during the next blood meal (1A). Obtained from <http://www.cdc.gov/malaria/about/biology/>.

1.2. Treating malaria

The areas where malaria prevalence is at epidemic proportions are mostly devoid of trained physicians and health workers who possess the skills necessary for the early diagnosis of the disease as well as its efficient treatment. Novel antimalarials must therefore adhere to several pre-requisites such as oral bio-availability, since diseased individuals mostly do not have access to healthcare facilities, a short treatment period to reduce the risks associated with parasite resistance development and the drugs must be inexpensive with extended shelf lives [19].

1.2.1. Vector control

Strategies to reduce the prevalence of malaria include the use of ITNs and reduction of the vector population with IRS. DDT remains the most powerful and successful pesticide to date and is responsible for the eradication of malaria from both the North American and European continents. In South Africa, the discontinued use of DDT in the 1990s resulted in the worst

malaria epidemic this country has experienced since the introduction of IRS in the 1950s. The subsequent re-introduction of DDT spraying in 2000 once again resulted in an overall decrease in the number of malaria cases by approximately 50% [20]. DDT is not only effective against malaria vectors but is equally potent at alleviating various other arthropod-borne diseases such as yellow fever, African sleeping sickness, dengue fever and typhus. However, DDT was also used extensively in agriculture during which enormous quantities were aerially sprayed onto crops to curb pests. This widespread and uncontrolled use of DDT raised concerns amongst environmentalists in the 1960s who described possible catastrophic consequences for both the environment and humans, ultimately leading to the ban of DDT in the 1980s [21]. However, the controlled use of DDT at the low concentrations required for malaria vector control [22] as well as the combined efforts of several public health officials and malaria experts, have resulted in the approval of restricted use of DDT for malaria control by the WHO Pesticide Evaluation Scheme (WHOPES) (<http://www.who.int/whopes/>).

Malaria parasite transmission can also be prevented by blockage of the sexual development of the parasites within the mosquito host. Coleman *et al.* tested the effect of 8-aminoquinolines on the sexual development of *P. berghei* and *P. falciparum* parasites in *A. stephensi* mosquitoes and showed that the drug-fed mosquitoes produced fewer oocysts than the control-fed group, and the sporozoites that did manage to develop from the oocysts could not enter the salivary glands [23]. The antifolate drugs proguanil and pyrimethamine have also been shown to be sporontocidal by causing a reduction in oocysts in drug sensitive strains while pyrimethamine directly damages ookinetes [24]. DL- α -difluoromethylornithine (DFMO), a polyamine pathway inhibitor, also interferes with *P. berghei* sporozoite development in *A. stephensi* mosquitoes [25].

A more recent development to control malaria transmission is the radical concept of rendering mosquitoes refractory to *Plasmodium* infection by creating transgenic mosquitoes. This can be obtained by either altering the lifespan of the female mosquitoes so that they cannot transmit the parasite or to introduce an agent into the mosquito that kills the parasite and thereafter becomes hereditary. Malaria transmitting mosquitoes are harmless for the first two weeks and only a small proportion of the female population actually live long enough to transmit parasites. Additionally, a problem that contributed to the rapid development of insecticide resistance was the instantaneous killing of the mosquitoes, which placed large resistance pressure on the mosquitoes to combat the insecticide. If the lifespan of the females could therefore be shortened by a few days, the transmission capacity would be reduced tremendously while the development of insecticide resistance would also be delayed [26]. Transgenic mosquitoes can be created by

using an antimalarial fungus, such as *Metarhizium anisopliae* that naturally infects mosquitoes, and inserting a gene for e.g. a human antibody into it, which is then transferred to the mosquito during the fungal infection. The mosquitoes are then sprayed with the transgenic fungus soon after being infected by the malaria parasite [27]. In addition, it has also been shown that fungus infection actually increases the susceptibility of resistant mosquitoes to the insecticide for which they have developed resistance [28].

1.2.2. Vaccine development

Some malaria experts are of the opinion that vaccination represents the most valuable strategy to reduce the mortality associated with malaria [29]. This is due to the fact that people residing in malaria endemic areas do eventually develop low levels of protective immunity against *P. falciparum* infection but this immunity is never complete and seems to be specific for the parasite strain residing in a specific area. Protective immunity is therefore lost once the host moves into an area where a different strain resides and also once the host is no longer chronically infected [30].

The complex life cycle of the malaria parasite, which allows it to co-exist with the host immune response, is largely responsible for the lack of a successful vaccine [31]. Current vaccine development strategies focus on different protein antigens that are expressed during particular stages of the life cycle, namely the pre-erythrocytic (sporozoite and schizont-infected hepatic cells), the asexual intra-erythrocytic (merozoite-infected erythrocytes) and sexual exo-erythrocytic (gametocyte) stages (Figure 1.4) [31]. An ideal vaccine against plasmodial infection should therefore induce a multistage, multivalent and multi-immune response for it to be successful in the treatment of malaria [32].

Antibodies directed against antigens on the surface of extracellular sporozoites e.g. circumsporozoite protein (CSP) would result in the neutralisation of sporozoite infectivity in the bloodstream. Preliminary studies of the RTS,S/AS malaria vaccine (GlaxoSmithKline Biologicals) in African infants showed that the vaccine is safe, well-tolerated and reduces parasite infection and clinical illness related to malaria. The vaccine consists of two polypeptides; RTS corresponds to CSP residues 207-395 of *P. falciparum* 3D7 fused to the N-terminus of the hepatitis B surface antigen (HBsAg) and S consists of 226 residues of HBsAg [33]. Testing of the vaccine in Phase II, or mid-stage, clinical trials showed a 53% reduction of clinical malarial episodes in young children administered over a period of eight months. A

success rate of 80% is expected and combined with vector control strategies and antimalarials the vaccine is predicted to be extremely effective in reducing malaria infections. Currently, the vaccine has entered pivotal Phase III trials and, if approved, is expected to be available by 2015 [11].

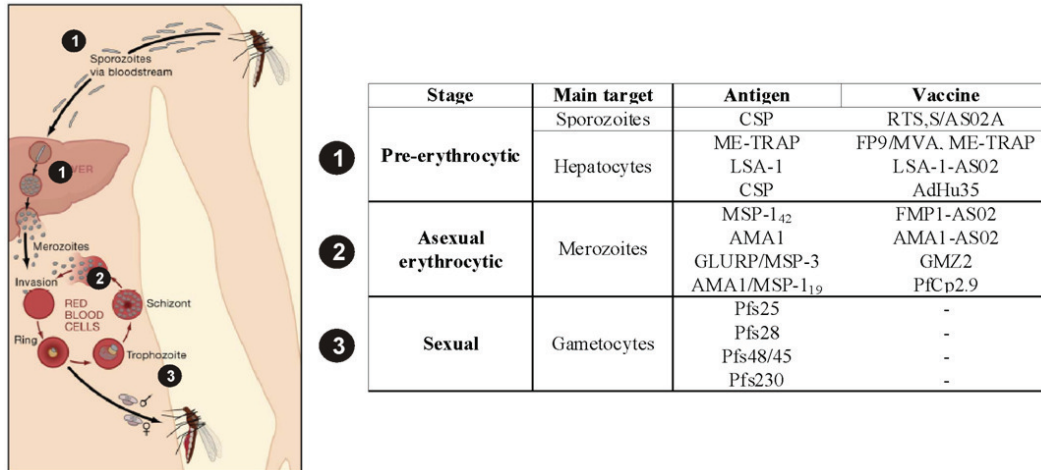


Figure 1.4: Selected malaria vaccines targeting different antigens in specific stages of the parasite life cycle.

(1) Pre-erythrocytic stage vaccines prevent host parasitic infection and disease development; (2) asexual erythrocytic stage vaccines block the multiplication of daughter merozoites; and (3) sexual stage vaccines prevent parasite transmission [12,31]. Abbreviations: AdHu35, human adenovirus serotype 35; AMA-1, apical membrane antigen 1; CSP, circumsporozoite protein; FMP-1, *falciparum* merozoite protein-1; FP, fowl pox; GLURP, glutamine-rich protein; LSA-1, liver stage antigen 1; ME-TRAP, multi-epitope thrombospondin-related adhesive protein; MSP, merozoite surface protein; MVA, modified vaccinia virus Ankara; PfCp2.9, *P. falciparum* chimeric protein 2.9; Pfs, *P. falciparum* surface antigens. Figure adapted from [17].

Extensive research is also being conducted on antibodies raised to antigens on the erythrocyte plasma membrane (e.g. *P. falciparum* erythrocyte membrane protein 1, *PfEMP1*) as this would result in the destruction of the infected erythrocyte or prevent the cytoadherence of these infected cells [32,33]. Blood-stage vaccines are, however, limited by the polymorphic character of the antigens, which creates diversity and restricts the efficacy of the vaccine representative of a particular genotype [34].

1.2.3. Current antimalarials

Various drugs have been developed and used in the fight against malaria. As with malaria vaccines, antimalarials target different stages of the parasite life cycle within the human host and specifically interfere with processes that are essential to parasite survival. Figure 1.5 shows the different stages of the parasite life cycle and current drugs that specifically target these stages of parasite development. Eradication of malaria with the use of antimalarials is continuously compromised by the increased prevalence of parasite resistance to the small number of available commercial drugs.

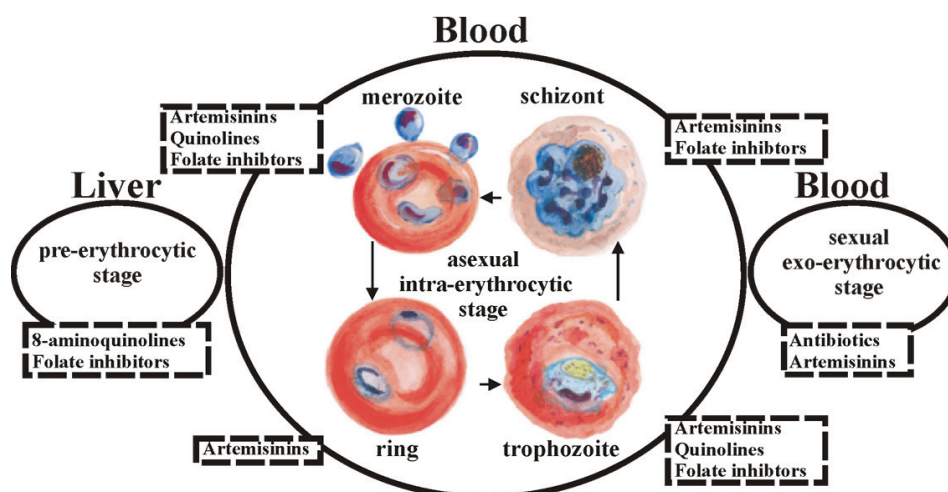


Figure 1.5: A schematic diagram of the *P. falciparum* life cycle within the human host showing the targets of different antimalarials during the developmental stages.

The pre-erythrocytic, asexual intra-erythrocytic and sexual exo-erythrocytic stages as well as the different intra-erythrocytic phases of malaria parasite development are shown. Examples of drugs that have been used at each stage are listed in the dashed boxes [35-37].

1.2.3.1. Quinolines

The bark of the Cinchona tree has been used for centuries to treat fever associated with malaria from which the active ingredient is quinine [38]. It remained the antimalarial of choice until the 1940s, where after it was replaced by the chloroquine derivative. Quinine is, however, still used today to treat clinical malaria. Chloroquine is a 4-aminoquinoline derivative of quinine and for many years it was the main antimalarial drug used in malaria treatment caused by *P. falciparum* until parasite resistance developed in the 1950s (Table 1.1). However, it remains the most popular antimalarial developed to date due to its safety, low cost and efficacy [39,40]. Currently, the widespread resistance to the drug has rendered its use as a therapeutic agent useless, but it is still used to treat falciparum malaria in certain critical situations and shows some efficacy against the other *Plasmodium* spp (WHO 2010) [41].

Despite more than three decades of research, the exact molecular mechanism of chloroquine action remains controversial. It is believed that the weak-base drug accumulates in the acidic food vacuole of the parasite where it prevents haem detoxification [43]. Chloroquine resistance in malaria parasites has been attributed to reduced concentrations of the drug in the food vacuole possibly due to drug efflux, pH modification in the vacuole, the role of a Na^+/H^+ exchanger and transporters [43-45]. Two genes have been implicated in this resistance, namely *Pfmdr1* and *Pfcrt*, which encode P-glycoprotein homologue 1 (Pgh1) and *P. falciparum* chloroquine transporter (*PfCRT*), respectively [45,46]. Both these proteins are localised to the food vacuole membrane. Mutations in these genes could lead to small increases in the food vacuole pH thus reducing chloroquine accumulation [47]. Alternatively, *PfCRT* may increase the efflux of

chloroquine by directly interacting with the drug [48]. Resistance is associated with several mutations in the *PfCRT* protein, while the loss of Lys76 has been shown as the critical mutation that renders the *P. falciparum* parasites resistant to the drug [49].

Table 1.1: Antimalarial drug classes

Stage	Drug class	Drug compounds	Mechanism of action
Pre-erythrocytic	Aminoquinolines	Primaquine (and gametocytocidal)	Unknown
	Hydroxynaphthoquinone	Atovaquone (and sporontocidal)	Interferes with cytochrome electron transport
Asexual intra-erythrocytic	Aminoquinolines	Chloroquine (and gametocytocidal) Quinine (and gametocytocidal)	Inhibits haem detoxification
	Sulphonamides	Sulphadoxine	Inhibits DHPS
	Sulphones	Dapsone	Inhibits DHPS
	Amidines	Proguanil (active as cycloguanil, also active against pre-erythrocytic forms and sporontocidal)	Inhibits DHFR
	Pyrimidines	Pyrimethamine (also sporontocidal and interferes with sexual reproduction)	Inhibits DHFR (used in combination with sulphadoxine or dapsone)
	4-Methanolquinoline	Mefloquine	Inhibits haem detoxification
	Sesquiterpene lactone	Artemisinin and derivatives (and gametocytocidal)	Unknown
Exo-erythrocytic	Antibiotics	Tetracycline (and active against intra-erythrocytic forms) Doxycycline (and active against intra-erythrocytic forms)	Inhibitors of aminoacyl-tRNA binding during protein synthesis

Abbreviations: DHFR, dihydrofolate reductase; DHPS, dihydropteroate synthase. Compiled from WHO 2005 and [35,37].

A number of related aminoquinolines have been developed (Table 1.1) and are clinically applied including: Amodiaquine, Atovaquone (used in combination with proguanil, Malarone[®]), Lumefantrine (highly effective against multi-drug resistant *P. falciparum* when co-formulated with artemether, Co-Artem[™]), Halofantrine (Halfan), Mefloquine (Lariam[®]), and Primaquine (WHO 2005 and [42]). Mutations in the *Pfmdr1* gene have also been associated with resistance to these derivatives including quinine, Mefloquine and Halofantrine [43].

1.2.3.2. Antifolates

The antifolates are some of the most widely used antimalarials but their role in malaria prevention is increasingly hampered by the rapid emergence of resistance once the parasites are placed under drug pressure. The direct effect of folate biosynthesis inhibition is a reduction in

the synthesis of serine, methionine and pyrimidines, which leads to decreased DNA synthesis (Table 1.1) [37].

The antifolates can generally be divided into two classes; the type-1 antifolates mimic the *p*-aminobenzoic acid (pABA) substrate of dihydropteroate synthase (DHPS) and include the sulphonamides (sulphadoxine) and sulphones (dapson), while the type-2 antifolates (pyrimethamine and cycloguanil, the active metabolite of the prodrug proguanil) inhibit dihydrofolate reductase (DHFR) (Table 1.1) [37]. Interestingly both of these classes of target proteins are arranged on separate bifunctional enzymes; hydroxymethyldihydropterin pyrophosphokinase/DHPS (PPPK/DHPS) and DHFR/thymidylate synthase (DHFR/TS) [44]. In addition, malaria parasites are capable of *in vivo* folate salvage from the extracellular environment as well as *de novo* synthesis of folate derivatives from simple precursors. The mechanism of exogenous folate uptake by a carrier-mediated process has important implications in the sensitivity of the antifolate inhibitors and is being investigated as a novel drug target [45].

Pyrimethamine is a diaminopyrimidine and is mostly used in combination with sulphadoxine (FansidarTM) or dapson leading to the simultaneous inhibition of DHFR and DHPS (Table 1.1). Pyrimethamine crosses the blood-brain barrier and the placenta. Resistance to sulphadoxine-pyrimethamine combination therapy emerged rapidly due to the appearance of point mutations in the active sites of the target enzymes resulting in reduced drug binding capacity [46,47]. The Ser108 (AGC) to Asn (AAC) mutation is present in all pyrimethamine-resistant parasites and mutations of Asn51 to Ile, Cys59 to Arg and Ile164 to Leu confer additional resistance [48-50]. In addition, the DHFR and TS activities were found to be up-regulated upon challenge with antifolate drugs, independent of the mutational status of the gene [51]. Quantitative trait locus analysis on the rodent parasite *P. chabaudi*, of a genetic cross between clones with different resistance patterns to pyrimethamine, sulphadoxine and a combination thereof also showed the influence of one or more genes other than *dhfr* and *dhps* on the observed levels of resistance in the cross progeny [52]. A new combination of antifolates, chlorproguanil and dapson (LapDapTM), with shorter half-lives than pyrimethamine and sulphadoxine, were subsequently investigated as a means to delay drug resistance and was shown to clear FansidarTM-resistant parasites [53], but was later discontinued (see below) [54].

1.2.3.3. Artemisinin

Artemisinin is a sesquiterpene lactone extracted from the leaves of *Artemisia annua* and is a

potent, fast acting blood schizontocide that shows efficacy against all *Plasmodium* spp. Its efficacy is especially broad and shows activity against all the asexual stages of the parasites including the gametocytes, which results in reduced transmission potential (Figure 1.5) [55]. The exact mechanism of action of artemisinin remains vague and different studies have produced contradicting results (reviewed in [56,57]). Evidence to suggest that the primary activator of artemisinin is an iron source and protein alkylation due to artemisinin treatment is well established but a single molecular target that has a direct role in cell death due to artemisinin has not been identified. The multi-faceted nature of the plasmodial cellular response to artemisinin may explain the use of this drug against multi-drug resistant strains of *P. falciparum* and its effect on practically all stages of the parasite life cycle (Figure 1.5) [56].

The low aqueous solubility of artemisinin resulting in poor absorption upon oral administration has led to the development of several artemisinin derivatives including dihydroartemisinin, artesunate and artemether [58]. Despite the appearance of artemisinin resistance [14], the WHO still recommends ACTs as the first-line treatment against malaria infections where resistance to other antimalarials is prevalent (WHO 2010). One of the obvious disadvantages of using ACT for malaria case management in Africa is the increased costs involved in combining therapies, but several reasons exist for combining antimalarials with an artemisinin derivative, namely: 1) the increase in the efficacy of the antimalarials involved; 2) the decrease in the duration of treatment; and 3) the reduced risk of resistant parasites arising through mutation [59].

Originally, the appearance of parasite resistance to artemisinin was thought to be unlikely or at least delayed for several reasons, including 1) the short exposure of the parasites to the drug due to its short half-life; 2) the gametocytocidal effect of artemisinin, which reduces the transmission potential and therefore spread of the parasite; and 3) the frequent use of ACTs was specifically introduced to delay the onset of resistance [60]. The appearance of artemether resistance in field isolates from French Guiana in 2005 resulted in increased inhibitory concentrations and was attributed to inappropriate drug use that exerted selection pressures, favouring the emergence of parasites with an artemether-resistant *in vitro* profile [61]. Even though reduced *in vitro* drug susceptibility is not tantamount to diminished therapeutic effectiveness, it could lead to complete resistance and thus called for the rapid deployment of drug combinations [61]. Lapdap™, a combination of chlorproguanil (targeting DHFR), dapsone (targeting DHPS) and the artemisinin derivative artesunate (Table 1.1), was introduced in 2003 as malaria therapeutic to replace sulphadoxine-pyrimethamine treatment in Africa [62]. However, resistance to artesunate monotherapy appeared on the Thai-Cambodian border in 2009 and it was also discontinued due

to significant haemoglobin reductions in patients with glucose 6-phosphate dehydrogenase (G6PD) deficiency [63].

Currently the WHO recommends the following ACTs for malaria treatment, which should be combined with a single dose of primaquine as gametocytocidal (provided the risks of haemolysis in patients with G6PD deficiency have been established) and should be combined with knowledge on the efficacy of the specific combination therapy in the area of use: 1) artemether + lumefantrine (Co-Artem™); 2) artesunate + amodiaquine (ASAQ); 3) artesunate + mefloquine; 4) artesunate + sulphadoxine-pyrimethamine; and 5) dihydroartemisinin + the quinoline-based drug piperazine (Artekin™) (WHO 2010 and [64]).

1.2.3.4. Antibiotics

Several antibiotics such as tetracycline, doxycycline and minocycline are active against the exo-erythrocytic as well as the asexual blood stages of the *P. falciparum* parasite. Tetracycline was originally derived from *Streptomyces* species, but is now synthetically prepared. They interfere with aminoacyl-tRNA binding and therefore inhibit protein synthesis in the parasite's apicoplast and additionally have been shown to block apicoplast genome replication [65]. This is due to the presence of a genome in the apicoplast that encodes prokaryote-like ribosomal RNAs, tRNAs and various proteins [66]. Doxycycline is a synthetic tetracycline derivative with a longer half-life than tetracycline, but shows a disadvantageous property in that it causes photosensitivity, which is an obvious drawback for tourists entering malaria areas (WHO 2005).

1.3. Novel antimalarial targets

Despite the availability of various antimalarials and attempts aimed at preventing parasite infection with the use of suitable vaccines, high malaria mortality continues to persist in endemic areas. The identification of novel drug targets that can reduce the prevalence of malaria without inducing rapid resistance thus remains imperative and a major challenge for researchers in the field of infectious diseases. A good starting point for the identification of drug targets is to pinpoint differences between essential metabolic pathways of the host and parasite, which are more easily identified once the parasite physiology and host-parasite relationships are better understood. The presence or absence of specific essential pathway enzymes and special features thereof can subsequently be identified and investigated in possible chemotherapeutic intervention strategies.

1.3.1. Polyamine biosynthesis as a drug target

Several studies have investigated the importance of polyamines and their involvement in various processes within the cell. In most organisms, the polyamine pathway has been fully elucidated and extensive research has resulted in major advances in our understanding of polyamine biosynthesis in the malaria-causing parasite. Previous studies have shown that interruption of polyamine biosynthesis hampers the development of disease-causing *Trypanosoma brucei gambiense* and *P. falciparum* parasites [67,68]. Further studies have identified unique parasite-specific properties in the *P. falciparum* polyamine pathway, which present possible targets for chemotherapeutic intervention [69-71]. A sensible approach is thus the structural and functional characterisation of the pathway's constituent enzymes for rational drug development strategies. The polyamine biosynthesis pathway as drug target in *P. falciparum* will thus be the main focus of this study.

1.3.2. Polyamines

The physiologically important polyamines putrescine, spermidine and spermine are found in all living organisms except the Methano- and Halobacteriales [72]. The widespread prevalence of these polyamines signifies its considerable contribution to the survival of living cells and as such they have been implicated in many growth processes such as cell differentiation and proliferation [73-76]. This is reflected by the general abundance of polyamines and increased activities of its biosynthetic enzymes during stages of rapid growth [67,77]. Polyamine levels are thus controlled by tight regulation of its synthesis, degradation, uptake and secretion as their depletion may lead to growth arrest and aberrant embryonic development while their accumulation may cause apoptosis [78-80].

Electrostatic associations between polyamines and DNA result in the stabilisation of these nucleic acids, which often promotes DNA bending and facilitates binding of gene regulatory elements thereby indirectly influencing DNA transcription [81-84]. Polyamines additionally influence transcription by modifying chromatin structure via the stimulation of histone acetyltransferase [85]. One of the most unique post-translational protein modifications is the spermidine-dependent hypusination of eukaryotic translation initiation factor (eIF-5A) of which the function is not entirely understood but it appears to be essential for cell proliferation since its depletion arrests yeast cells in the G1 stage of the cell cycle [86,87]. Cells therefore maintain optimal levels of polyamines as they play paradoxical roles in the prevention as well as in the stimulation of cell death; increased levels protect cells by steering them into the proliferative

pathway and away from cell death [88]. However, the accumulation of excess intracellular putrescine has been shown to trigger apoptosis possibly as a result of an imbalance in intracellular positive and negative charges as well as decreased formation of modified eIF-5A [80,89].

The importance of the naturally occurring polyamines as well as their regulation by various biosynthetic and catabolic enzymes has led to the identification of various enzymes in the polyamine pathway as drug targets for the treatment of cancer and parasitic diseases [90-92]. The limited success, however, in finding an anti-tumour drug specifically targeting the polyamine pathway in humans has opened new possibilities in finding a drug against rapidly proliferating parasites [93] such as *P. falciparum* (malaria), *T. brucei* (African trypanosomiasis), *T. cruzi* (Chagas' disease) and *Leishmania donovani* (leishmaniasis) [91,92]. An overview of the polyamine biosynthetic pathways within these organisms as compared to the human host is shown in Figure 1.6 (Birkholtz *et al.*, Biochemical Journal, in press).

Polyamines are synthesised via the decarboxylation of L-ornithine to putrescine by the enzyme ornithine decarboxylase (ODC). This enzyme catalyses the first and rate-limiting step of the polyamine biosynthetic pathway and an increased growth rate of rapidly proliferating cells is observed when this enzyme is over-expressed [84,101]. The diamine putrescine then acts as the precursor of spermidine and spermine synthesis. Another decarboxylation enzyme, *S*-adenosylmethionine decarboxylase (AdoMetDC), synthesises decarboxylated *S*-adenosyl-L-methionine (dcAdoMet), which serves as a donor of aminopropyl moieties to putrescine for the synthesis of spermidine and spermine (Figure 1.6). The latter reactions are catalysed by spermidine synthase (SpdS) and spermine synthase (SpmS), respectively [77].

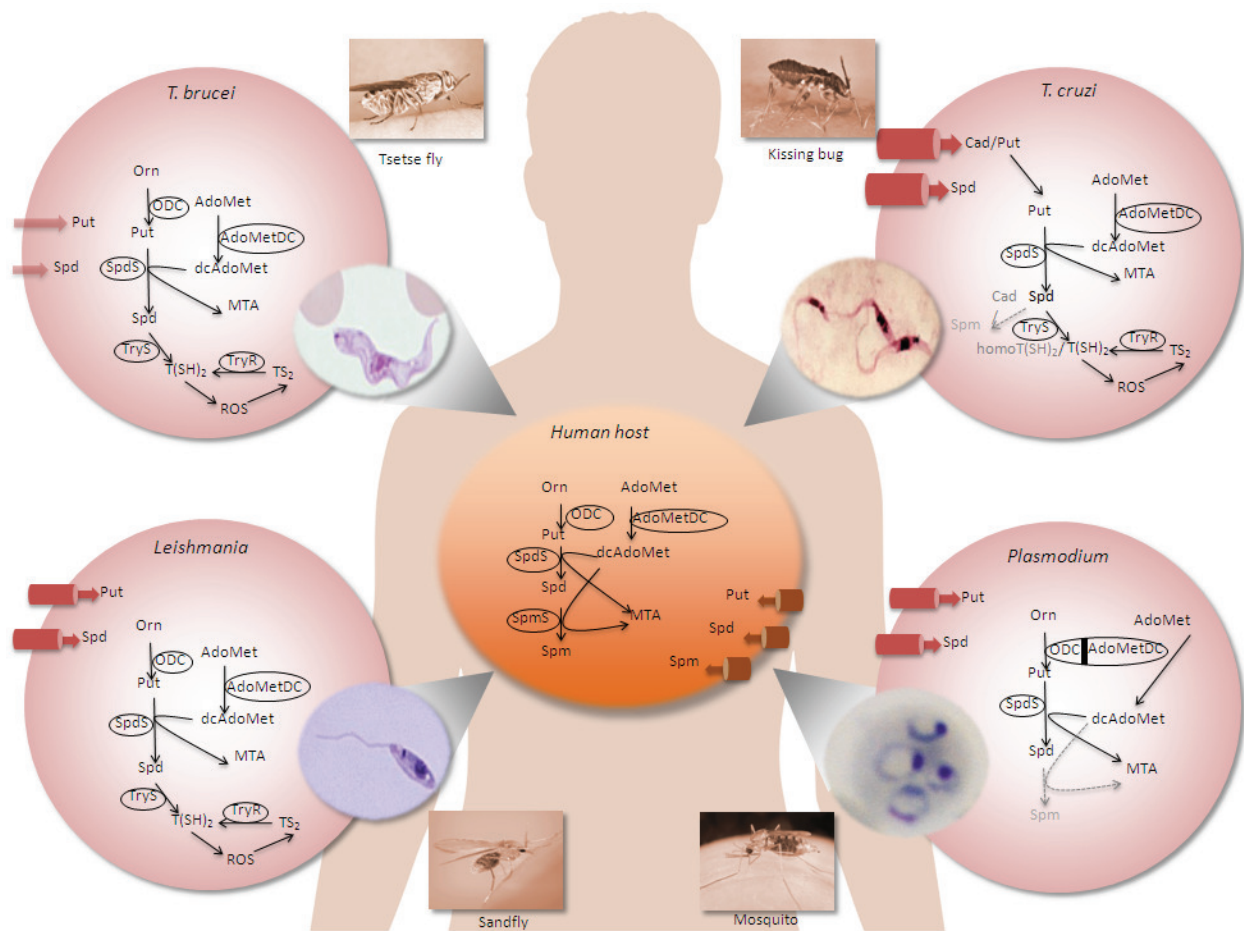


Figure 1.6: Polyamine biosynthetic pathways of various parasites compared with that of the human host.

The parasites and their vectors are shown. *T. brucei* is transmitted by tsetse flies while *T. cruzi* is transmitted by kissing bugs resulting in sleeping sickness and Chagas' disease within the human host, respectively. *Leishmania* spp are transmitted by sand flies and malaria-causing *Plasmodium* parasites are transmitted by *Anopheles* mosquitoes. Abbreviations: AdoMet, *S*-adenosyl-L-methionine; AdoMetDC, AdoMet decarboxylase; cad, cadaverine; dcAdoMet, decarboxylated AdoMet; homoT(SH)₂, homotrypanothione; MTA, 5'-methylthioadenosine; ODC, L-ornithine decarboxylase; put, putrescine; ROS, reactive oxygen species; spd, spermidine; SpdS, spermidine synthase; spm, spermine; TryS, trypanothione synthetase; TryR, trypanothione reductase; TS₂, oxidised trypanothione; T(SH)₂, reduced trypanothione. Taken from Birkholtz *et al.* (Biochemical Journal, in press).

Mammalian cells can also interconvert polyamines for the production of spermidine from spermine and putrescine from spermidine, which is successively catabolised by spermidine/spermine-*N*¹-acetyltransferase and polyamine oxidase [94]. *T. brucei* and other trypanosomatids are uniquely capable of synthesising a conjugate between glutathione and spermidine called trypanothione [*N*¹,*N*⁸-bis(glutathionyl)spermidine] by trypanothione synthetase, which is involved in the parasite's redox metabolism (Figure 1.6) [95]. *T. cruzi* lacks ODC and is therefore auxotrophic for putrescine, which is taken up from the host and converted into spermidine by AdoMetDC and SpdS [96]. Furthermore, similar to *Thermotoga maritima* SpdS, it appears that *T. cruzi* SpdS activity may be promiscuous since the active site can accommodate both putrescine and spermidine to synthesise spermidine and spermine, respectively [97]. *Leishmania* parasites possess a complete intact polyamine biosynthetic

pathway and are capable of synthesising putrescine and spermidine as well as trypanothione for redox control. As in prokaryotes, SpmS is absent in *Trypanosoma* spp, *L. donovani* and *P. falciparum* (Figure 1.6) [98,99].

1.3.3. Polyamine metabolism in *P. falciparum*

Human erythrocytes contain trace amounts of polyamines and lack the necessary enzymes for active polyamine biosynthesis. However, in *P. falciparum*-infected erythrocytes there is a significant increase in polyamine levels during the trophozoite and schizonts stages of parasitic infection, with large variation in the spermidine and to a lesser extent putrescine levels. In contrast, it was found that spermine levels are only slightly elevated in the parasitised cells (Figure 1.7). In general, polyamine synthesis increases from the ring to the schizont stages during intra-erythrocytic parasite infection with spermidine being the major polyamine present at all stages. These increases in polyamine levels were found to be proportional to the parasitaemia, the activities of the polyamine biosynthetic enzymes as well as the biosynthetic activities of the parasite such as macromolecular synthesis and replication (Figure 1.7) [67,100].

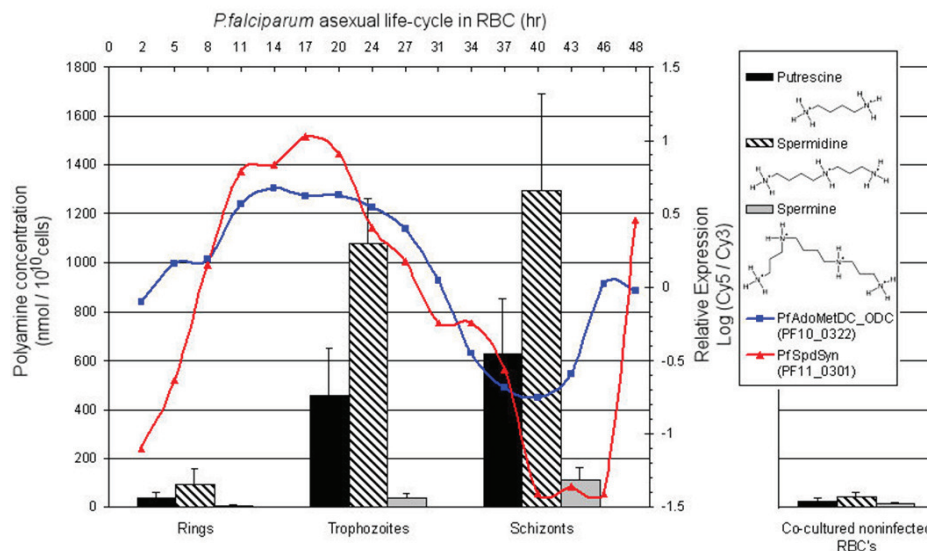


Figure 1.7: Polyamine levels during the intra-erythrocytic developmental cycle of *P. falciparum*.

The levels of the three polyamines (structures on the right) are shown together with the transcript abundance of the polyamine biosynthetic genes (*PfAdometdc/Odc* and *PfSpds*) [4] during the asexual intra-erythrocytic stages of *P. falciparum*. The polyamine levels within uninfected erythrocytes are also shown. Taken from [101].

The *P. falciparum* parasite polyamine pathway is distinctly different from that of the human host, which means that interference with the parasite's polyamine biosynthetic pathway could have more severe consequences on the parasite than its host [92]. Obvious differences between the pathways and the main polyamine biosynthetic enzymes between the two organisms are highlighted in Figure 1.8.

In *P. falciparum*, a single open reading frame encoding a bifunctional protein with both *Pf*AdoMetDC and *Pf*ODC activities uniquely facilitates polyamine synthesis [70]. In contrast to the short half-lives (~15 min) of the monofunctional mammalian AdoMetDC and ODC enzymes, *Pf*AdoMetDC/ODC has a half-life of more than two hours [92]. The short half-life of human ODC is due to the polyamine-dependant effect of antizyme and recruitment of the 26S proteasome [77,102]. While mammalian ODC is barely inhibited by putrescine, *Pf*ODC activity is susceptible to feedback inhibition by putrescine [103] and *Pf*AdoMetDC activity is not stimulated by putrescine [71]. In contrast to the mammalian pathway, the SpmS enzyme [98] and a retro-conversion pathway [92] have not been identified in *P. falciparum*. In the absence of SpmS, *Pf*SpdS has been shown to be capable of synthesising low levels of spermine [98]. Mammalian cells are not only capable of synthesising and interconverting polyamines, but can also take up polyamines from their environment via a poorly understood transport system [104]. These differences may provide possible drug target development opportunities for the treatment of parasitic infectious diseases.

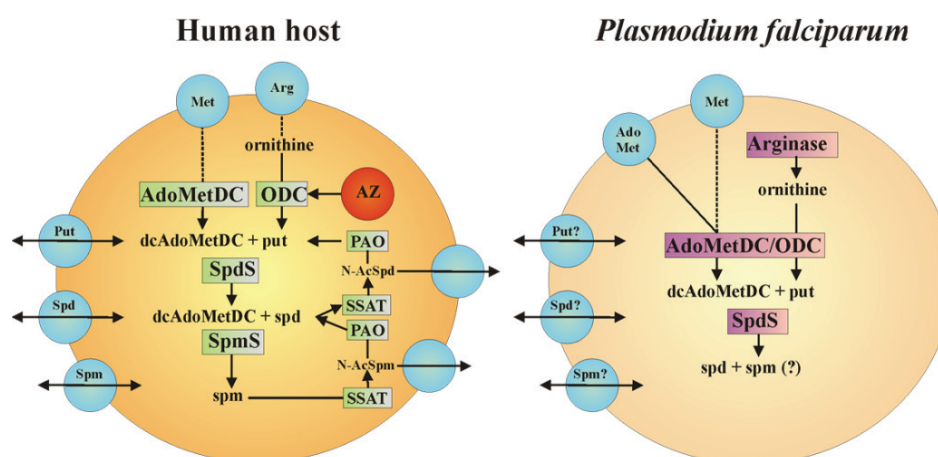


Figure 1.8: Summary of the polyamine metabolic pathways in the human host and *P. falciparum* parasite. Transporters or channels are shown as blue circles. Intermediates and reaction products are written in plain text while the enzymes producing these are given in green (human host) and purple (parasite) boxes. Abbreviations: AdoMet, *S*-adenosyl-L-methionine; AdoMetDC, AdoMet decarboxylase; Arg, arginine; AZ, antizyme; dcAdoMet, decarboxylated AdoMet; Met, methionine; *N*-AcSpd and *N*-AcSpm, *N*¹-acetylated spermidine and spermine; ODC, ornithine decarboxylase; PAO, polyamine oxidase; put, putrescine; spd, spermidine; SpdS, spermidine synthase; spm, spermine; SpmS, spermine synthase; SSAT, spermidine/spermine-*N*¹-acetyltransferase. Adapted from [92].

1.3.4. Polyamine transport in *P. falciparum*

The presence of a specific polyamine transport system in malaria parasite-infected erythrocytes remains a controversial subject but evidence has suggested their presence based on three specific observations: 1) parasites induce numerous biochemical, structural and functional changes in infected erythrocytes resulting in the membrane becoming more permeable to various solutes via new permeability pathways [105,106]; 2) evidence suggests that the replenishment of

intracellular polyamine pools in parasites treated with polyamine biosynthesis enzyme inhibitors is due to an influx of polyamines across the membrane [107,108]; and 3) the exogenous addition of putrescine rescues DFMO-treated *P. falciparum* cultures, suggesting that the parasites are able to internalise and metabolise putrescine for growth and macromolecular synthesis [67,109].

To date, the only polyamine transporter that has been characterised in plasmodia is the *P. knowlesi*-induced putrescine-specific transporter [108], which was shown to be temperature-dependent and competed for by both spermidine and spermine. Haider *et al.* showed that parasites treated with the *PfSpdS* inhibitor, *trans*-4-methylcyclohexylamine (4MCHA), could not be rescued with the exogenous addition of spermidine, which indicated inefficient uptake of this polyamine by the infected erythrocytes and an apparent absence of a spermidine-specific transporter in *P. falciparum*-infected erythrocytes [98]. However, since the exact targets of this inhibitor are unknown it is possible that additional sites may be affected in *P. falciparum* and thereby prevented parasite rescue [98]. *PfAdoMetDC* inhibition could also not be rescued with the addition of putrescine or spermidine while the effects of *PfODC* inhibition with DFMO could be reversed by putrescine supplementation, suggesting the presence of a putrescine transporter system [100].

In a recent study it was shown that both putrescine and spermidine are indeed taken up across the membrane of viable isolated parasites with a saturable, temperature-dependent process that competed for different polyamines, L-ornithine and other basic amino acids [110]. Further inhibition of polyamine biosynthesis in the isolated parasites resulted in an increased uptake of these polyamines while the rate of uptake was shown to be independent of extracellular Na^+ and K^+ . However, uptake was shown to be dependent on the extracellular pH, which was increased with an increase in pH; putrescine and spermidine uptake therefore decreased with membrane depolarisation and increased with membrane hyperpolarisation [110]. In contrast to *L. major* and *T. cruzi*, a molecular candidate of polyamine transport in *P. falciparum* remains to be identified.

In the process of drug discovery it is empirical to take into account the strategies that parasites employ to counteract the depletion of an essential metabolic compound. The most effective drug would be one that interferes with the biosynthesis of the compound, such as putrescine, and at the same time obstructs its uptake into the *P. falciparum*-infected erythrocyte. Alternatively, the putrescine and spermidine uptake systems may provide a mechanism for the selective delivery of antimalarials via their conjugation to polyamines, which might result in improved inhibitory activities of currently available antimalarials [111,112].

1.3.5. The *P. falciparum* polyamine biosynthetic enzymes as drug targets

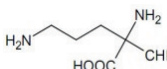
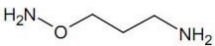
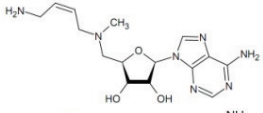
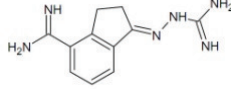
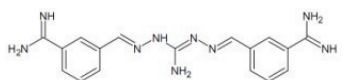
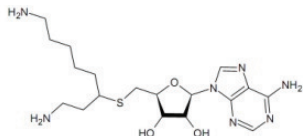
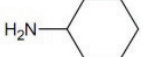

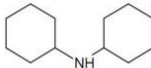
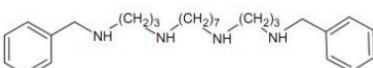
The importance of polyamines in parasitic growth suggests that the inhibition of the polyamine pathway would interfere with the proliferation of the parasites [67], which can be approached by three general routes: 1) by the application of active site-based inhibitors targeting the pathway's essential biosynthetic enzymes; 2) by interfering with polyamine transport; and 3) by using non-functional polyamine structural analogues to replace functional polyamines resulting in altered intracellular polyamine homeostasis [92].

The ability of substrate analogues to interfere with polyamine enzyme activity as well as their effects on parasite growth has been investigated. DFMO is a well-known enzyme-activated, irreversible inhibitor of ODC and causes the alkylation of the enzyme's active site. Even though its effect on *P. falciparum* growth is only cytostatic, it has been successfully applied in the treatment of West African sleeping sickness caused by *T. b. gambiense* [67,68]. The success of DFMO treatment of the latter infection may be attributed to several factors including 1) the rapid division of parasitic cells resulting in a higher polyamine requirement than the host cells; 2) trypanosomes also use spermidine to produce trypanothione, which maintains the intracellular redox state (Figure 1.6) [113]; 3) the trypanosomal ODC is more stable and has a longer half-life than the host [114]; and 4) DFMO may be effectively transported into the trypanosomal parasites since the drug does not have to cross several membranes as is the case for the intracellular malaria parasites [71].

The ODC inhibitor 3-aminooxy-1-aminopropane (APA) and its derivatives CGP52622A and CGP54169A as well as the AdoMetDC inhibitors CGP40215A and CGP48664A (both analogues of methylglyoxal bis(guanylhydrazone), MGBG), severely affect *PfAdoMetDC* and *PfODC* activities and result in reduced intracellular polyamine concentrations (Table 1.2) [100]. Additionally, 5'-([(Z)-4-amino-2-butenyl]methylamino)-5'-deoxyadenosine (MDL73811 or AbeAdo) irreversibly inhibits *PfAdoMetDC* and is roughly a 1000-fold more effective than DFMO treatment [115]. Furthermore, Bitonti *et al.* showed that the bis(benzyl)-polyamine analogue, MDL27695, rapidly inhibits the *in vitro* growth of both chloroquine-sensitive and resistant *P. falciparum* strains, and if administered in combination with DFMO, cures malaria in *P. berghei*-infected mice [116]. Treatment of *P. falciparum* with the *PfSpdS* inhibitor, dicyclohexylamine, completely arrests parasite growth of both chloroquine-sensitive and resistant strains [117] and its derivative, 4MCHA, results in up to 85% growth arrest within 48 h when used in micromolar quantities (Table 1.2) [98].

Table 1.2: Selected inhibitors of *P. falciparum* ODC, AdoMetDC and SpdS

The *in vitro* inhibitory concentrations (IC_{50} in μM) of these drugs against *P. falciparum* parasites and recombinant enzyme (K_i in μM) are indicated.

		IC_{50}	K_i	Reference
ODC inhibitors				
DFMO		1250	87.6	[100,103,118]
APA		1	2.7	[100]
AdoMetDC inhibitors				
MDL73811		3	1.6	[100]
CGP48664A		8.8	3	[100]
CGP40215A		1.8	0.8	[100]
SpdS inhibitors				
AdoDATO		-	8.5	[98,119]
CHA		19.7	198	[98]
4MCHA		1.4	0.18	[98]
Dicyclohexylamine		>1 000	342	[98]
Polyamine analogue				
MDL27695		3	-	[116]

Adapted from Birkholtz *et al.* (Biochemical Journal, in press). Abbreviations: AdoDATO, *S*-adenosyl-1,8-diamino-3-thiooctane; APA, 3-aminooxy-1-aminopropane; CHA, cyclohexylamine; DFMO, DL- α -difluoromethylornithine; 4MCHA, *trans*-4-menthylcyclohexylamine.

The combined use of inhibitor treatment and protein X-ray crystallography of the polyamine metabolic enzymes allows the visualisation of the interactions between the inhibitor and the active site residues, providing a physical glimpse into a formerly unknown chemical space. These structures are particularly helpful in the identification and *in silico* testing of a specific set of lead chemical compounds, which would have been painstaking to test experimentally [128]. Homology models provide an alternative to protein crystal structures due to the challenges involved in expressing pure and sufficient amounts of *P. falciparum* proteins required for crystallisation studies [129,130]. Models of the three *P. falciparum* polyamine biosynthetic

enzymes have been solved, i.e. monofunctional *Pf*AdoMetDC [131], monofunctional *Pf*ODC [132] and *Pf*SpdS [133] (also crystallised [127]).

1.3.5.1. The bifunctional *P. falciparum* AdoMetDC/ODC complex

In *P. falciparum*, the *Pf*AdoMetDC and *Pf*ODC domains are uniquely assembled into a bifunctional complex of approximately 330 kDa (Figure 1.9) [70]. The N-terminal *Pf*AdoMetDC domain (residues 1-529) exists as a protomer that is post-translationally cleaved into a large ~55 kDa α -subunit, and a smaller β -subunit of approximately 9 kDa. This domain is covalently linked to *Pf*ODC at the C-terminus (residues 805-1419) via a hinge region that spans residues 530-804 [70,71]. The quaternary structure of the functional ~165 kDa heterodimeric polypeptide thus consists of two subunits, the ~155 kDa α -*Pf*AdoMetDC/ODC and the ~9 kDa post-translationally cleaved β -*Pf*AdoMetDC subunit. Two of these polypeptides have an obligatory association through the *Pf*ODC domain, to form the active ~330 kDa bifunctional complex (Figure 1.9) [70,71,120].

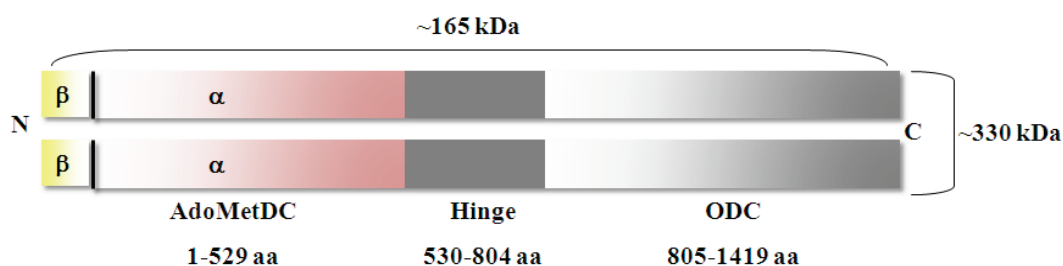


Figure 1.9: Schematic diagram of the bifunctional *P. falciparum* AdoMetDC/ODC protein.

The N-terminal *Pf*AdoMetDC domain consists of α - and β -subunits. This domain is connected to the C-terminal *Pf*ODC via a hinge region. The sizes of the heterodimeric and heterotetrameric complexes are shown [70].

The 275-residue hinge region connects the *Pf*AdoMetDC and *Pf*ODC domains (Figure 1.9) [70] and is involved in the conformational stability and quaternary structure formation of the *Pf*ODC domain [103]. Previous studies have shown that the hinge stabilises the heterotetrameric *Pf*AdoMetDC/ODC complex by mediating interdomain interactions [69]. Several secondary structures are present within this region, notably two α -helices and a β -sheet that have been shown to have indirect effects on the catalytic activities of both domains due to contributions to interdomain interactions [121]. The importance of the hinge region in the activity of monofunctional *Pf*ODC (see below) has led to investigations of possible protein-protein interactions between the domains of the bifunctional protein [71,103]. Interdomain interactions have been reported to play a role in other bifunctional proteins of *P. falciparum* such as DHFR/TS where the catalytic activity of the TS domain is dependent on its interaction with the DHFR domain [122]. In *Pf*AdoMetDC/ODC it was shown that although the specific activities of

the respective enzymes (referred to here as monofunctional protein domains) are not affected upon inhibition or substrate removal of the neighbouring enzyme [71], interdomain interactions occur within the bifunctional complex that are essential for domain activities [69]. A possible explanation for the bifunctional arrangement could therefore be that the control of the abundance and activity of a single protein regulates polyamine biosynthesis within *P. falciparum* [92].

1.3.5.2. Monofunctional S-adenosylmethionine decarboxylase from *P. falciparum*

PfAdoMetDC utilises pyruvoyl as a co-factor, which is formed from an internal autocatalytic processing event at Ser73 resulting in the formation of the α - and β -subunits (Figure 1.9). The native bifunctional protein isolated from the *P. falciparum* parasites showed a K_m of 33.5 μ M for its substrate AdoMet and a specific activity of 14.8 pmol/min/mg [70]. In contrast to the human enzyme, *PfAdoMetDC* activity is not stimulated by putrescine, indicating that *PfAdoMetDC* lacks the regulatory mechanism proposed for mammalian cells to relate putrescine abundance with spermidine synthesis [71,120]. Similarly to the human protein, monofunctional *PfAdoMetDC* exists as an $(\alpha\beta)_2$ dimer within the bifunctional complex [71,120,123] where each active site is located between the β -sheets of the monomeric $\alpha\beta\alpha$ -sandwich fold (Figure 1.10) [120].



Figure 1.10: The $\alpha\beta\alpha$ -sandwich fold of monofunctional, monomeric *P. falciparum* AdoMetDC superimposed with the dimeric human protein.

The crystal structure of dimeric human AdoMetDC (1JEN, α - and β -subunits in yellow and orange, respectively) [123] superimposed with the homology model of the monofunctional, monomeric *PfAdoMetDC* (pink and grey for α - and β -subunits, respectively) [120]. Putrescine within the charged-buried site is shown in green.

The monofunctional *PfAdoMetDC* homology model showed that the residues within the active site are in a similar orientation to those of the human protein with only four substitutions in the active site and surrounding surface of *PfAdoMetDC*. Interactions with the substrate analogue MeAdoMet (methyl ester of AdoMet) are conserved where the adenine ring is hydrophobically stacked between residues Phe5 and Phe415 [120], which are contributed from both β -sheets. Mutagenesis studies confirmed the involvement of these aromatic residues in substrate and inhibitor binding of the human protein [124]. Glu438 forms two hydrogen bonds with the hydroxyl groups on the ribose moiety while a third hydrogen bond is also present between N^1 on the adenine ring and the amide nitrogen of Glu72. Lastly, the model showed that the pyruvoyl group in *PfAdoMetDC* is more out-of-plane while the carbonyl group remains in plane for its purpose as an electron sink during the decarboxylation reaction [120]. The model could also explain the lack of *PfAdoMetDC* activity stimulation by putrescine. The putrescine-binding site of the human protein is lined with acidic residues that can interact with the positive amines of putrescine [125]. In *PfAdoMetDC*, these residues are substituted by the basic residues Arg11, Lys15 and Lys215. Subsequent mutagenesis of these residues to non-polar ones showed that especially Arg11 is essential for activity and therefore suggests that these residues assume the function of putrescine binding [120].

1.3.5.3. Monofunctional ornithine decarboxylase from *P. falciparum*

PfODC decarboxylates L-ornithine to form putrescine in a reaction that is dependent on the vitamin B₆-derived co-factor, pyridoxal-5'-phosphate (PLP) [126]. ODC exists as an obligate homodimer as a consequence of the two active sites that are formed at the dimer interface and consist of residues contributed from both monomers of ~70 kDa each. This interface is distinguished by an aromatic amino acid zipper, formed by the head-to-tail association of the two *PfODC* monomers, placing the C-terminus of one monomer vertical to the N-terminus of the other and *vice versa*. The *PfODC* monomer consists of two distinct structural domains, an N-terminal α/β triosephosphate isomerase (TIM)-barrel (typical of the alanine racemase-like family) and a C-terminal modified Greek-key β -barrel (Figure 1.11) [127].

Several differences exist between the human and *PfODC* enzymes including the feedback inhibition of *PfODC* activity by putrescine and the extended *PfODC* half-life of more than two h compared to the ~15 min half-life of the human protein [77]. The instability of the latter protein is due to the action of antizyme and the presence of a C-terminal PEST region involved in the recruitment of the 26S proteasome (Figure 1.8) [84,110]. This difference has also provided a rationale for the differential host-parasite responses to DFMO treatment [99].

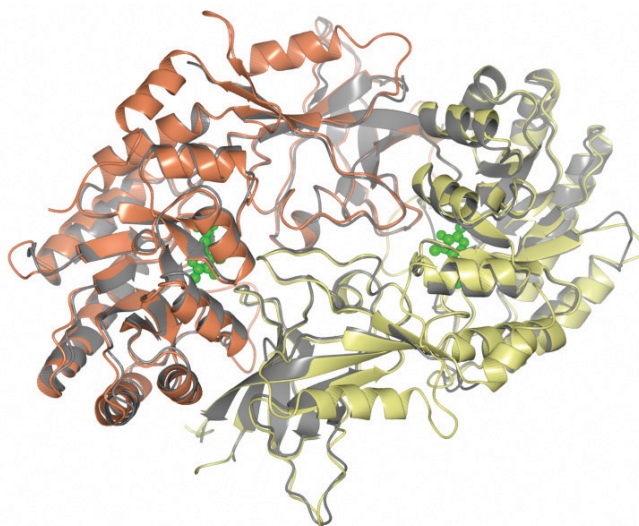


Figure 1.11: The head-to-tail organisation of *P. falciparum* ODC superimposed with the human protein. Crystal structure of homodimeric human ODC (1D7K, grey) [128] superimposed with the homology model of *Pf*ODC (monomers shown in yellow and orange) [127]. PLP within the active sites are shown in green.

The specific activity of the native bifunctional protein isolated from the *P. falciparum* parasites is 93.2 pmol/min/mg while it binds substrate with an affinity of 42.4 μM [70]. Investigations into the expression and catalytic properties of two recombinant constructs of monofunctional *Pf*ODC showed that the hinge region is involved in *Pf*ODC substrate binding while its presence also increases the specific activity of the enzyme [103]. Several residues that are essential for catalytic activity (co-factor and DFMO binding) and dimerisation are conserved in the *Pf*ODC sequence, with only three unique residue substitutions in the *Pf*ODC PLP-binding site [127]. The aromatic Phe1392, Tyr1305 and Phe1319 residues (numbering according to bifunctional protein) make hydrophobic contacts across the dimer interface resulting in an antiparallel-stacked interaction. Lys970 has in particular been predicted to interact with various residues surrounding the active site including Asp1356, Gly1352, Gly1357 and Asp1359. These residues also form part of the DFMO-binding region in the Gly1352-Gln-Ser-Cys-Asp-Gly-Leu-Asp1359 motif of *Pf*ODC [23,127,129].

1.3.5.4. Spermidine synthase from *P. falciparum*

*Pf*SpdS catalyses an aminopropyl transferase reaction to produce spermidine and MTA from dcAdoMet and putrescine. In addition, this enzyme is also responsible for the low levels of spermine within *P. falciparum* [98]. *Pf*SpdS consists of 321 residues with a monomeric molecular mass of ~ 37 kDa and associates to form a homodimer (Figure 1.12). The removal of 29 residues from an N-terminal extension allowed the recombinant expression in *Escherichia coli*. This extension is believed to have a signal peptide-like character and was also identified in plant SpdS [98]. Recombinant *Pf*SpdS catalyses spermidine synthesis with a k_{cat} of 0.48 s^{-1} and

substrate affinities of 52 μM and 35.3 μM for putrescine and dcAdoMet, respectively. MTA is produced as a stoichiometric by-product in this reaction and acts as a feedback inhibitor of the enzyme [98]. *PfSpdS* is part of the aminopropyl transferase family of proteins that characteristically consists of a small N-terminal and a large C-terminal catalytic domain. The crystal structure showed that the N-terminal domain consists of a six-stranded β -sheet while the Rossmann-like C-terminal domain contains a seven-stranded β -sheet followed by nine α -helices (Figure 1.12).

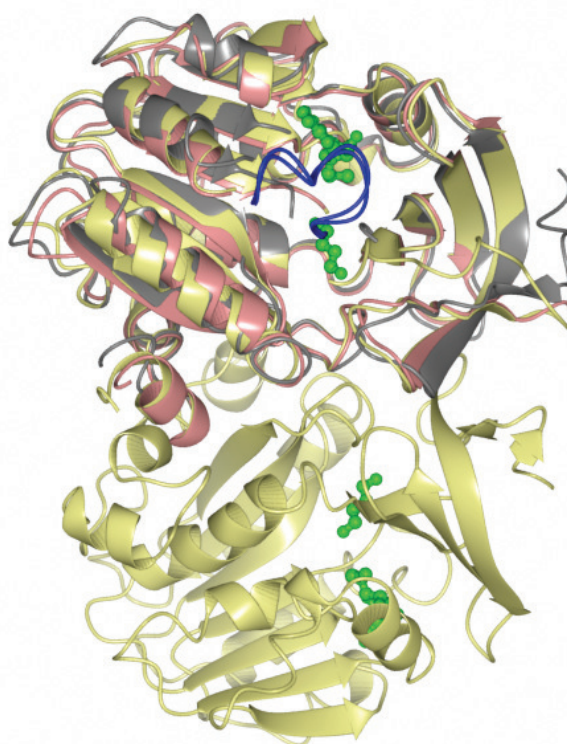


Figure 1.12: The structure of homodimeric SpdS from *P. falciparum* superimposed with the human protein.

The crystal structure of homodimeric human SpdS (2O06, yellow) [97] superimposed with the crystal structures of *T. cruzi* (3BWC, grey) (Bosch *et al.* unpublished results) and *P. falciparum* (2I7C, pink) [119]. MTA and putrescine within the active site are shown in green. The gate-keeping loops of human and *P. falciparum* SpdS are shown in blue.

A homology model of *PfSpdS*, created with the *Arabidopsis thaliana* and *T. maritima* crystal structures as templates, identified essential features which were supported by mutagenesis studies [130]. The putrescine-binding cavity contains a hydrophobic region that is flanked by two negatively-charged regions that allow binding of the hydrophobic and positive termini of putrescine, respectively. Water molecules were predicted to form hydrogen bonds between the active site residues and the substrates to position and anchor them within the cavity. Several hydrogen bonds also form between dcAdoMet and the active site residues that are responsible for positioning of the aminopropyl chain for nucleophilic attack by putrescine [130]. In 2007, the model was superseded by the crystal structures of *PfSpdS* in complex with dcAdoMet, 4MCHA

and the transition state analogue, *S*-adenosyl-1,8-diamino-3-thio-octane (AdoDATO). dcAdoMet binding was shown to be stabilised by an active site gate-keeping loop that controls access of the substrates into the active site pocket [131,132]. The flexible loop covers the entrance to the active site and opens to allow the exit of MTA followed by spermidine (Figure 1.12). The established interactions with the inhibitors also revealed important binding sites that may be modified for the synthesis of improved inhibitory compounds in the near future [119].

1.4. Research objectives

This study was aimed at the identification of novel aspects of the *P. falciparum* polyamine biosynthetic enzymes (both individual domains of the bifunctional *Pf*AdoMetDC/ODC as well as *Pf*SpdS) and ultimately forms part of a larger study to investigate possible antimalarial strategies via inhibition of polyamine synthesis within the malaria-causing parasite. The study involved the structural and functional characterisation of *Pf*AdoMetDC and *Pf*ODC in order to gain a better insight into their activities, protein-protein interactions as well as their arrangement within the bifunctional complex as a means to regulate catalytic activities. Lastly, and for the first time attempted by the Malaria Research group at the University of Pretoria, protein X-ray crystallisation was investigated as a means to validate the predicted binding sites of novel inhibitory compounds against *Pf*SpdS, which were identified by a pharmacophore-based approach.

The work involving the biophysical characterisation of *Pf*AdoMetDC as well as the crystallisation, diffraction data collection and components of the 3D structure solving of *Pf*SpdS were performed at Lund University (Sweden) as part of a South African-Swedish collaboration funded by the National Research Foundation-Swedish International Cooperation Development Agency (NRF-SIDA, Swedish Research Links Programme). The methodology and results of this study therefore forms part of a combination of work that was performed in South Africa and during research visits to Sweden.

Three distinct studies were thus undertaken:

- **Chapter 2: A conserved parasite-specific insert is a key regulator of the activities and interdomain interactions of *Plasmodium falciparum* AdoMetDC/ODC.**

In this chapter the roles of a conserved parasite-specific insert within the *Pf*ODC domain in both activities of the bifunctional *Pf*AdoMetDC/ODC complex were investigated. The

native interaction sites of this insert were subsequently studied with the use of interface peptide probes. Novel insights were obtained that allowed us to better understand the unique arrangement of the decarboxylase domains within a bifunctional complex in the *Plasmodium* spp.

- **Chapter 3: Biochemical and structural characterisation of monofunctional *Plasmodium falciparum* AdoMetDC.**

In this chapter the recombinant expression of the monofunctional *PfAdoMetDC* domain is described that was subsequently used in a structure-function relationship study of this protein. The biochemical and biophysical characteristics of monofunctional *PfAdoMetDC* are discussed, which provided insights into unique parasite-specific properties. The results of this study were also used to establish if the co-existence of the two domains in the bifunctional complex impacts on each other's properties and these were compared to that of the human protein to gain an understanding of the *in vitro* functional arrangement of the monofunctional protein.

- **Chapter 4: Validation of pharmacophore-identified inhibitors against *Plasmodium falciparum* SpdS with the use of X-ray crystallography.**

This study focussed on novel drug development strategies of *PfSpdS*, which resulted in the identification of promising inhibitory compounds by using a dynamic, receptor-based pharmacophore model. These compounds were tested *in vitro* and their interactions within the *PfSpdS* active site were subsequently investigated with co-crystallisation studies of the enzyme-inhibitor complexes. These results validated the use of an *in silico* drug discovery approach to streamline the identification of compounds that could result in the parasite-specific inhibition of a drug target.

- **Chapter 5: Concluding discussion**

1.5. Outputs

The results within this dissertation have been published and/or presented as follows:

Chapter 2:

1. Williams, M., Wells, G.A., Roux, S., Niemand, J., Rautenbach, M., Louw, A.I. and Birkholtz, L. "Insert-mediated regulation of the activities and interactions of the rate-limiting polyamine biosynthetic enzyme of *Plasmodium falciparum*. A

conserved parasite-specific insert is a key regulator of the activities and interdomain interactions of *Plasmodium falciparum* S-adenosylmethionine decarboxylase/ornithine decarboxylase.” (Manuscript to be submitted to Experimental Parasitology)

2. Conference proceeding: “A conserved parasite-specific insert influences the activities and interdomain interactions of the malarial S-adenosylmethionine decarboxylase/ornithine decarboxylase.” Invited oral presentation, 5th Symposium on Polyamines in Parasites, Detroit, USA in July 2008

Chapter 3:

1. Williams, M., Sprenger, J., Human, E., Al-Karadaghi, S., Persson, L., Louw, A.I. and Birkholtz, L. “Biochemical and structural characterisation of S-adenosylmethionine decarboxylase from *Plasmodium falciparum*.” (Biochemical Journal, accepted with minor revision)
2. Conference proceeding: “Towards finding the structure of *Plasmodium falciparum* S-adenosylmethionine decarboxylase.” Invited oral presentation, 6th Symposium on Polyamines in Parasites, Phalaborwa, South Africa in August 2010
3. Conference proceeding: “Malaria polyamine biosynthesis: The road from drug target validation to drug development.” Oral presentation, Biology of Parasitism course at The Marine Biology Laboratories, Woods Hole, USA in June 2009
4. Conference proceeding: “Structural and functional characterisation of malarial S-adenosylmethionine decarboxylase.” Poster presentation, 7th Protein Expression, Purification and Crystallisation course, Hamburg, Germany in August 2010

Chapter 4:

1. *Burger, P.B., *Williams, M., Reeksting, S.B., Al-Karadaghi, S., Briggs, J.M., Joubert, F., Birkholtz, L., Louw, A.I. “Design of novel inhibitors against *Plasmodium falciparum* Spermidine Synthase using structurally-derived binding descriptors.” (Manuscript to be submitted to Journal of Medicinal Chemistry)
*Authors contributed equally to this work.
2. Conference proceeding: “The development of a dynamic receptor-based pharmacophore model for *Plasmodium falciparum* spermidine synthase.” Poster presentation, 6th Symposium on Polyamines in Parasites, Phalaborwa, South Africa in August 2010
3. Conference proceeding: “Crystal structure of *Plasmodium falciparum* spermidine synthase containing a novel inhibitor identified with a dynamic receptor-based pharmacophore model.” Poster presentation, Gordon Research Conference: Polyamines, Waterville Valley Resort, USA in June 2011

Reviews:

1. Clark, K., Niemand, J., Reeksting, S., Smit, S., van Brummelen, A., Williams, M., Louw, A.I. and Birkholtz, L. (2010) “Functional consequences of perturbing polyamine metabolism in the malaria parasite, *Plasmodium falciparum*.” Amino Acids. **38**, 633-644
2. Birkholtz, L., Williams, M., Niemand, J., Louw, A.I., Persson, L. and Heby, O. “Polyamine homeostasis as a drug target in pathogenic protozoa: peculiarities and possibilities.” (Biochemical Journal, in press)

Chapter 2

A conserved parasite-specific insert is a key regulator of the activities and interdomain interactions of *Plasmodium falciparum* AdoMetDC/ODC

2.1. Introduction

ODC and AdoMetDC are rate-limiting enzymes in the polyamine biosynthetic pathway and in *P. falciparum* are uniquely located on one polypeptide encoded by a single open reading frame to form a ~330 kDa heterotetrameric, bifunctional *Pf*AdoMetDC/ODC complex [70]. The heterotetrameric nature is due to an autocatalytic processing event within the *Pf*AdoMetDC domain of one *Pf*AdoMetDC/ODC polypeptide, resulting in the formation of two non-identical α - and β -subunits with the essential pyruvoyl moiety covalently bound to the N-terminus of the α -subunit for catalysis [70]. Although the two decarboxylase activities of the bifunctional complex can function independently [71], inter- and intradomain interactions have been shown to stabilise the active bifunctional *Pf*AdoMetDC/ODC complex while unique parasite-specific inserts within the two domains mediate these physical interactions and thereby regulate the activities of both domains [69]. The interdomain interactions therefore support a proposed regulatory mechanism of both decarboxylase activities within the bifunctional complex, which has not been experimentally investigated. Recently, it was shown that an N-terminal non-homologous insert of *P. falciparum* hydroxymethylpterin pyrophosphokinase/dihydropteroate synthase, which is not located within the active site, affects the activities of both enzymes and it was suggested that this insert could be involved in the interaction of the two catalytic domains of the bifunctional complex [133].

The *Pf*ODC domain occurs at the C-terminus of the bifunctional protein and includes residues 805-1419. The protein contains regions of homology to mammalian ODC, especially concerning the residues involved with co-factor binding and catalytic activity as well as several quaternary structural features. These regions of homology are interspersed with parasite-specific inserts [69,70]. Similar to other eukaryotes, the activity of *Pf*ODC is dependent on the formation of a homodimer, where the two active sites are formed by residues contributed from both monomers at the dimer interface. The aromatic Phe1392, Tyr1305 and Phe1319 residues form hydrophobic contacts across the dimer interface, which result in an antiparallel-stacked interaction. A number of studies have investigated features of ODC such as the contribution of long-range interactions

mediated by residues distant from the active site in the promotion of catalytic efficiency (Lys294 of *T. brucei*) [134] and the rapid exchange of mammalian ODC subunits [23]. In the latter study it was shown the active sites consisted of Lys69, Lys169 and His197 (from one subunit) and Cys360 (from the second subunit). Subsequent mutagenesis of these residues and mixing of the mutated monomer with a wild-type one resulted in a rapid exchange of subunits between the enzyme dimers at physiological conditions. The authors suggested that the rapid association and dissociation of ODC facilitates antizyme binding and thus the short half-life of ODC *in vivo* [23].

Comparison of the residues involved in PLP binding of *Pf*ODC to those of *T. brucei* and human ODC (Cys1355, Asp887, Arg955, His998, Ser1001, Gly1037, Gly1114, Gly1116, and Tyr1384, numbered according to the bifunctional protein) showed only three unique residues for *Pf*ODC PLP binding, while two residues were also specific in *Pf*ODC substrate binding (Tyr966 and Arg1117) [127]. Subsequent mutagenesis studies of these residues confirmed their importance in both PLP and substrate binding. These unique properties provide important starting points for the identification of compounds that could be used to selectively target the plasmodial enzyme in an otherwise highly conserved protein.

2.1.1. Parasite-specific inserts within the polyamine biosynthetic enzymes of *P. falciparum*

Compared to the size of the independent monofunctional AdoMetDC and ODC orthologues in humans, the size of the *Pf*AdoMetDC/ODC bifunctional protein is much larger than just the combination of these proteins. This is due to the presence of several parasite-specific inserts within both of the domains that interrupt sequence homology [69,120,127] and, excluding the contribution of the hinge region, increases the size of *Pf*AdoMetDC/ODC by 366 residues (~40 kDa).

Parasite-specific inserts are an interesting feature of plasmodial proteins that form long insertions separating well-conserved blocks that are adjacent in the homologous proteins [135]. These inserts can be present as tandem repeats or sparsely distributed insertions between globular domains and show species-specific characteristics such as rapid divergence, non-globularity and low-complexity. The inserts are mostly flexible and hydrophilic due to the high abundance of Asn and Lys residues, which form loops on the surface of the protein. The frequency of low-complexity regions (subsequences of biased composition) in parasite-specific inserts in *P. falciparum* proteins is particularly high and can be found in enzymes such as RNA polymerases [136], glutamylcysteine synthetase [137], DHFR/TS [138] and DNA topoisomerase [139]. It has

been hypothesised that these low-complexity regions in proteins may promote protein-protein interactions [140] and their high prevalence within *P. falciparum* proteins raises questions about their origin and maintenance within the parasite genome as well as influence on the evolution of the parasite's unusual genome [135,141,142]. Furthermore, these inherently flexible protein elements that do not spontaneously fold into stable globular structures and are often characterised as intrinsically unstructured [143,144], may allow the proteins to recognise several biological targets by becoming structured upon interaction with specific targets [145]. A recent study to identify intrinsically unstructured proteins in the *P. falciparum* proteome showed a high correlation between the presence of these large segments of disordered structures in proteins that play a role in host-parasite interactions (specifically in the sporozoite life cycle stage) [143] as well as in proteins that self-assemble into large multiprotein complexes [140].

Both the *Pf*AdoMetDC and *Pf*ODC domains contain parasite-specific inserts that disrupt regions of homology and range in size from 6 to 180 residues [120,127]. The *Pf*AdoMetDC domain contains three inserts (A1: residues 57-63; A2: residues 110-137; and A3: residues 259-408) [120]. The hinge occupies residues 530-804 and is for all purposes also considered as an insert, while two inserts are present in the *Pf*ODC domain (O1: residues 1047-1085 and O2: residues 1156-1302) [127]. Although the roles of these inserts in enzyme activity have been investigated [69], the specific details of the interaction between the *Pf*AdoMetDC and *Pf*ODC domains and the contributions of the inserts to interdomain protein-protein interactions remain unclear.

The 39-residue O1 insert of *Pf*ODC differs from the other inserts since it is: 1) devoid of low-complexity regions; 2) better conserved between plasmodia in terms of sequence composition and length; and 3) contains an area of well-defined predicted secondary structure [69,121]. These features suggest a distinct function for the O1 insert compared to the other less-conserved and larger inserts in terms of protein folding, stability, organisation and activity [146]. This was confirmed by the observed 94% and 77% reduction in *Pf*ODC and *Pf*AdoMetDC activities, respectively, within the bifunctional complex after deletion of this insert. Moreover, O1 insert deletion prevented *Pf*ODC homodimerisation as well as association with the *Pf*AdoMetDC domain [69], possibly by altering the conformation of *Pf*ODC at the dimer interface. The homology model of monofunctional *Pf*ODC showed that the O1 insert appears to lie parallel to the protein core and loops from the protein surface out towards the C-terminus at the same side as the entrance to the active site [127]. The insert is also flanked by mobile Gly residues (Gly1036-1038 and Gly1083, numbered according to the bifunctional protein) [121] suggesting

that the insert may be acting as a flexible gate-keeping loop for substrate entry into the active site pocket. The O1 insert is thus implicated in both inter- and intradomain protein-protein interactions, mediated by long-range effects across the bifunctional complex and might function as a modulator of interactions between the decarboxylase domains in *Pf*AdoMetDC/ODC. In contrast, the larger O2 insert does not form significant secondary structures and was shown to be more important for *Pf*ODC activity, possibly due to it being spatially removed from the N-terminal *Pf*AdoMetDC domain [69]. However, this insert contains a low-complexity region of (NND)-repeats that are thought to play an important role in the formation of the *Pf*ODC homodimer through the formation of a polar zipper.

The interaction sites between the domains of *Pf*AdoMetDC/ODC therefore remains to be identified while the noteworthy effect that the deletion of the O1 parasite-specific insert has on the entire protein indicates that this insert may be involved in protein-protein interactions across the bifunctional complex. This is based on previous studies that showed the presence of these inserts between structured domains of multiprotein complexes as well as in proteins that have diverse protein binding partners [140]. Analysis of the specific functions of this insert could therefore provide an indication of the arrangement of the domains within the bifunctional *Pf*AdoMetDC/ODC complex. Furthermore, it was postulated that the predicted flexibility of the O1 insert may allow the modulation of the catalytic activity of the *Pf*ODC domain by stabilising the substrate and/or co-factor interactions within the active site pocket, followed by product release. This postulate is substantiated by the homology model of *Pf*ODC in which the O1 insert was shown to be positioned on the same side of substrate entry into the *Pf*ODC active site pocket [135]. Alternatively, the conserved α -helix within the O1 insert may mediate specific protein-protein interactions for *Pf*ODC homodimerisation (intradomain interactions) and/or subsequent complex formation with *Pf*AdoMetDC (interdomain interactions). In this study, mutagenesis, biochemical, computational and peptide probe studies were therefore employed to investigate the possibility that the O1 insert acts as a flexible, catalytically essential loop and to delineate the function(s) of the conserved secondary structure within this insert. The results provide specific evidence for the functional role of the O1 insert in the activities and interdomain associations of *Pf*AdoMetDC/ODC. Furthermore, the role of this insert in protein-protein interactions could in future be used as a platform for the design and application of compounds that could interfere with these interfaces [130].

2.2. Methods

2.2.1. Secondary structure predictions of the O1 parasite-specific insert

The *Odc* gene sequences of *Homo sapiens* (GenBank ID: P11926) and *T. b. gambiense* (Q9TZZ6) as well as the full-length bifunctional plasmodial *Adometdc/Odc* sequences of *P. falciparum* (Q8IJ77), *P. berghei* (Q4YHB2) and *P. yoelii* (Q7RFF2) were subjected to the CLUSTALW2 multiple sequence alignment tool [147] followed by secondary structure predictions with the Jnet v2.0 algorithm within Jpred 3 [148].

2.2.2. Expression constructs and site-directed mutagenesis

The pASK-IBA3 vector (C-terminal Strep-tag, Institut für Bioanalytik, IBA) containing the bifunctional wild-type *PfAdometdc/Odc* coding sequence [70] was used as template for site-directed mutagenesis. The codons encoding the three conserved N-terminal Gly residues (Gly1036-1038, numbering according to bifunctional protein) flanking the O1 insert were mutated to Ala to produce the *A/O G1A* triple mutant. This mutated gene was subsequently used as template to introduce the C-terminal Gly1083Ala mutation resulting in the *A/O G2A* quadruple mutant. The predicted α -helix within O1 was disrupted by the introduction of a Pro codon at residue position 1068 giving rise to the *A/O I1068P* mutant. The primers used for PCR-mediated mutagenesis are listed in Table 2.1.

To create mutations within the monofunctional *Pf*ODC domain, *PfOdc* together with 432 nucleotides of the hinge region, previously cloned into pASK-IBA7 (N-terminal Strep-tag) [103], was used as template with the same primers listed in Table 2.1. Mutagenesis resulted in the monofunctional quadruple *ODC G2A* and helix breaker *ODC I1086P* mutations.

Pfu DNA Polymerases (2.5 U, Fermentas) was used in the presence of 10 fmol template and 10 pmol of each of the primers. Temperature cycling was performed as follows: 94°C for 3 min followed by 30 cycles of 94°C for 30 s, 60°C for 1 min, 68°C for 2 min/kb with a final extension step at 68°C for 10 min. Post-PCR manipulation was performed as described previously [150]. Briefly, the PCR products were visualised with DNA gel electrophoresis and the correctly-sized bands were excised and purified with the NucleoSpin® Extract II PCR cleanup kit (Macherey-Nagel). Purified products were then treated with *DpnI* (Fermentas) to remove the parental templates for 3 h at 37°C and cleaned as before.

Table 2.1: Mutagenesis primers used for the introduction of point mutations in the O1 parasite-specific insert

Primer	T _m (°C) ^a	Primer Sequence (5' to 3') ^b	Alteration
G1A_F	69	GGATTTAATTTTTATATAATAAATTTAGCAGCAG CATATCCAGGAGGATTAG	Triple N-terminal Gly1036-1038 to Ala inflexibility mutation
G1A_R	69	CTAATCCTCCTGGATATGCTGCTGCTAAATTTATT ATATAAAAATTAAATCC	
G2A_F	68	CATTTCTCAAGACGAAATATGCATACTATAGTTTT GAAAAAATAACATTGG	Single C-terminal Gly1083 to Ala inflexibility mutation
G2A_R	68	CCAATGTTATTTTTTTTCAAACACTATAGTATGCATA TTTCGTCCTTGAGAAATG	
I1068P_F	67	GTCTTCAAGAAATTAATAAAGATCCACAAAAATT TCTTAATGAAGAAACATTTCTC	Ile1068 to Pro helix breaker
I1068P_R	67	GAGAAATGTTTCTTCATTAAGAAATTTTTGTGGAT CTTTTTTAATTTCTTGAAGAC	

^a The T_m's were calculated according to: $69.3+0.41(\%GC)-(650/N)$, where N is the number of nucleotides [149].

^b Mutations are underlined.

The linear PCR fragments were ligated overnight to form circular plasmids with 3 U of T4 DNA Ligase (Promega) at 22°C. The plasmids as well as a wild-type control (*A/Owt* and *ODCwt*) were electroporated into DH5α cells. The plasmids (monofunctional *ODCwt*, *ODC I1068P*, *ODC G2A* and bifunctional *A/Owt*, *A/O I1068P*, *A/O G2A*) were isolated with the peqGOLD Plasmid Miniprep kit I (Biotechnologie) and all mutations were confirmed with automated nucleotide sequencing using a BigDye[®] Terminator v3.1 Cycle Sequencing kit (Applied Biosystems) with the ODCseq1 sequencing primer (5'-TATGGAGCTAATGAATATGAATG-3').

2.2.3. Protein expression and isolation

The pASK-IBA3 and -IBA7 plasmids containing the wild-type *PfAdometdc/Odc* and *PfOdc* sequences, respectively, or the various confirmed mutations (above) were transformed into AdoMetDC and ODC deficient *E. coli* EWH331 expression cells kindly provided by Dr. H. Tabor (National Institutes of Health, MD, USA). Proteins were recombinantly expressed and isolated as Strep-tag fusion proteins as described previously [70]. Colonies were inoculated in Luria-Bertani (LB)-ampicillin (50 µg/ml) and incubated at 37°C for 16 h. These cultures were subsequently diluted 1:100 in 1 litre LB-ampicillin medium and incubated at 37°C with agitation until an OD₆₀₀ of 0.5 was reached and protein expression was induced with 200 µg anhydrotetracycline (AHT, IBA). The cultures were incubated for 16 h at 22°C before the cells were harvested. The pelleted cells were diluted in 10 ml wash buffer (100 mM Tris/HCl, pH 8.0, 150 mM NaCl, 1 mM EDTA) per litre of culture. Lysozyme and 0.1 mM phenylmethylsulphonyl fluoride (PMSF, Roche Diagnostics) was added to the suspension and incubated on ice for 30

min. The cells were disrupted with sonication and the soluble proteins were collected in the supernatants after ultracentrifugation was performed at 4°C for 1 h at 100 000g. The pellets were discarded while the supernatants were kept for subsequent affinity chromatography.

The Strep-tagged fusion proteins were purified from the total soluble protein extracts using Strep-*Tactin* affinity chromatography (IBA). Each protein extract was loaded at 4°C onto a Chromabond® 15 ml PP column (Macherey-Nagel) containing a 1 cm³ bed volume of Strep-*Tactin* beads. The beads were subsequently washed three times with 10 ml wash buffer and the bound protein was eluted with 5 ml elution buffer (wash buffer containing 2.5 mM desthiobiotin, IBA) and collected in fractions on ice. Desthiobiotin reversibly competes with binding to the streptavidin and thus releases the Strep-tagged proteins. The beads were regenerated for future use with regeneration buffer (wash buffer containing 1 mM 4-hydroxy azobenzene-2-carboxylic acid, Sigma-Aldrich), which in turn displaces the desthiobiotin from the affinity beads. Protein concentration was determined by the Bradford assay [150] and visualised with denaturing SDS-PAGE and silver staining [151]. The protein samples were kept at 4°C until further use.

2.2.4. Activity analysis of the recombinantly expressed proteins

AdoMetDC and ODC activities were measured by trapping released ¹⁴CO₂ from *S*-[carboxy-¹⁴C]adenosyl-L-methionine (60.7 mCi/mmol, Amersham Biosciences) and L-[1-¹⁴C]ornithine (55 mCi/mmol, Amersham Biosciences) as previously described [70]. Briefly, 5 µg of the bifunctional or monofunctional proteins were incubated in AdoMetDC (50 mM KH₂PO₄, pH 7.5, 1 mM EDTA, 1 mM DTT) or ODC (50 mM Tris/HCl, pH 7.5, 40 µM PLP, 1 mM EDTA, 1 mM DTT) assay buffers in a total reaction volume of 250 µl containing 100 µM total substrate. The reactions were incubated at 37°C for 30 min followed by reaction termination via protein precipitation with the addition of 0.5 ml of 30% (v/v) trichloroacetic acid. ¹⁴CO₂ was captured with hydroxide of hyamine-treated filter papers (PE Applied Biosystems, USA) for an additional 30 min at 37°C. The filter papers were transferred to 4 ml Pony-Vial H/I tubes (PE Applied Biosystems) to which 4 ml of Ultima Gold XR scintillation fluid (PE Applied Biosystems) was added. The radioactivity was counted with a Tri-Carb series 2800 TR liquid scintillation counter (PE Applied Biosystems). Specific enzyme activity was expressed as the amount of CO₂ produced in nmol/min/mg and performed in duplicate for three individual experiments. The specific activities of the mutant proteins were normalised against the specific activity of the wild-type protein performed in parallel. Statistical analysis was performed using paired Students t-test.

2.2.5. Analysis of the oligomeric status of the mutant monofunctional and bifunctional proteins

The ability of the wild-type and O1 insert mutated proteins to form either monofunctional *Pf*ODC homodimeric (~170 kDa) or bifunctional *Pf*AdoMetDC/ODC heterotetrameric (~330 kDa) proteins [69,70] via protein-protein interactions were determined by size-exclusion chromatography (SEC) using an Äkta Prime System (Amersham Pharmacia Biotech). A Superdex[®]-S200 10/300 GL SE column (Tricorn, GE Healthcare) was calibrated with the Gel Filtration Standard kit (BioRad), which separated into five peaks corresponding to thyroglobulin (670 kDa), γ -globulin (158 kDa), ovalbumin (44 kDa), myoglobin (17 kDa) and Vitamin B₁₂ (1.35 kDa). A standard curve obtained from the elution of the standard proteins was used to identify the fractions in which the monofunctional *Pf*ODC homodimeric (~170 kDa) or monomeric (~85 kDa) and bifunctional *Pf*AdoMetDC/ODC heterotetrameric (~330 kDa) or heterodimeric (~165 kDa) proteins were expected to elute. The column was equilibrated with wash buffer and equal amounts of separately expressed and isolated monofunctional *Pf*ODC (ODCwt, ODC I1068P and ODC G2A) and bifunctional *Pf*AdoMetDC/ODC (A/Owt, A/O I1068P and A/O G2A) proteins (~120 μ g) were each applied to the SEC column and 1.5 ml fractions were collected at a flow rate of 0.5 ml/min in wash buffer.

2.2.6. Western immunodetection of monofunctional *Pf*ODC and bifunctional *Pf*AdoMetDC/ODC proteins following SEC

The *Pf*AdoMetDC/ODC and *Pf*ODC proteins were detected in each fraction with dot-blot Western immunodetection. Briefly, 0.5 ml of the sequential fractions collected from SEC were dot-blotted onto Immobilon-P PVDF transfer membranes (Millipore) using a BioDot apparatus (Bio-Rad). The membranes were subsequently blocked for 16 h at 4°C with blocking buffer (1xPBS containing 3% (w/v) BSA, 0.5% (v/v) Tween-20). For immunodetection of the Strep-tag fusion protein the membranes were incubated for 1 h at 37°C in membrane wash buffer (1xPBS containing 1% BSA, 0.5% Tween-20) and 1:4000 monoclonal Strep-tag II horseradish peroxidase (HRP)-conjugated mouse antiserum (Acris antibodies). The antibody is coupled to keyhole limpet haemocyanin and is supplied as a liquid Protein G purified immunoglobulin fraction, conjugated to HRP and therefore does not require the incubation with a secondary antibody. The membranes were washed six times in the membrane wash buffer followed by incubation for 5 min in equal volumes of the Luminol/Enhancer and Stable Peroxidase solutions (SuperSignal[®] West Pico Chemiluminescent Substrate, Pierce). Hyperfilm High Performance chemiluminescence films (Amersham Biosciences) were exposed for various times to the membranes and subsequently developed (3 min) and fixed (1 min) with ILFORD Universal

Paper Developer and Rapid Fixer, respectively (ILFORD Imaging Ltd., UK). Images of the developed film were captured with a VersaDoc™ Imaging System (BioRad).

2.2.7. Computational studies on the homology models of the monofunctional PfAdoMetDC and PfODC proteins

The following *in silico* simulations were performed by G. A. Wells [152] to visualise the flexibility of the O1 insert and the subsequent role of the flanking Gly residues on this flexibility upon their mutagenesis to Ala. Briefly, homology models for both AdoMetDC and ODC domains were constructed for all full-length *Plasmodium* spp listed in PlasmoDB (*P. falciparum*, *P. vivax*, *P. knowlesi*, *P. yoelii* and *P. berghei*) [3]. The monomeric AdoMetDC domain was modelled with the human (1I7B) and *S. tuberosum* (1MHM) as templates, while the homology model of dimeric ODC was optimised from earlier models [127] using MODELLER 9v2. Model qualities were determined using PROCHECK [153] and WHATIF [154].

For molecular dynamics (MD) simulations of *P. falciparum* ODC, 30 models were constructed with the O1 insert included. Based on the secondary structure predictions, the backbone conformation of residues 1054-1060, 1061-1072 and 1074-1076 of the O1 insert were restricted to a β -strand, α -helix and α -helix, respectively. A model of the A/O G2A mutant was constructed in VMD [155] using the wild-type structure as template. MD was performed on the wild-type and A/O G2A models using NAMD 2.6 [156].

For protein-protein docking, multiple (~100) models were constructed for the AdoMetDC and ODC domains, including an average or cluster model. All parasite-specific inserts were excluded from modelling to avoid additional uncertainty. Wild-type AdoMetDC models were docked against wild-type dimeric ODC models using FTDOCK2 [157] with AdoMetDC being treated as the mobile species while ODC was kept static.

2.2.8. Incubation of PfAdoMetDC/ODC with synthetic peptide probes

Synthetic peptides were designed to specifically target and compete with the inter- and intradomain interacting sites of the O1 insert: 1) NY-39 is identical to the entire O1 insert and is expected to bind to the insert's interaction site; 2) LK-21 is identical to the α -helix within the O1 insert and would thus also bind to the α -helix interaction site; while 3) LE-21, was designed as the charge complement of the helix within the O1 insert by replacing the positively-charged Lys with negatively-charged Glu residues in the peptide and *vice versa* to enable binding to the helix

2.3.2. Mutagenesis of the flanking Gly residues and disruption of the α -helix within O1 insert affects enzyme activity

To test the hypothesis that the Gly residues flanking the O1 insert provide loop flexibility and are involved in the decarboxylase activities of *Pf*AdoMetDC/ODC, the N- and C-terminal O1 insert Gly residues were replaced with Ala. This resulted in a triple mutant A/O G1A (Gly1036-1038 to Ala) protein where only the flanking N-terminal Gly residues were mutated, and a quadruple A/O G2A mutant (Gly1036-1038 and Gly1083 to Ala) where both the N- and C-terminal Gly residues were mutated. Secondly, to investigate the possible role of the conserved O1 insert α -helix in the decarboxylase activities of the bifunctional *Pf*AdoMetDC/ODC enzyme by mediating inter- and intradomain protein-protein interactions, a helix-breaker Pro residue was inserted within this helix resulting in the A/O I1068P mutant protein. The secondary structure prediction of this mutant using the Jnet algorithm did not predict the presence of an α -helix (results not shown).

Compared to the wild-type enzyme, the specific activity of the *Pf*AdoMetDC domain in the bifunctional protein was significantly ($P < 0.01$) reduced by 83% and 67% in the triple (A/O G1A) and quadruple (A/O G2A) mutant enzymes, respectively. In addition, the *Pf*ODC domain in both Gly mutant enzymes were essentially inactivated ($P < 0.01$) (Figure 2.2).

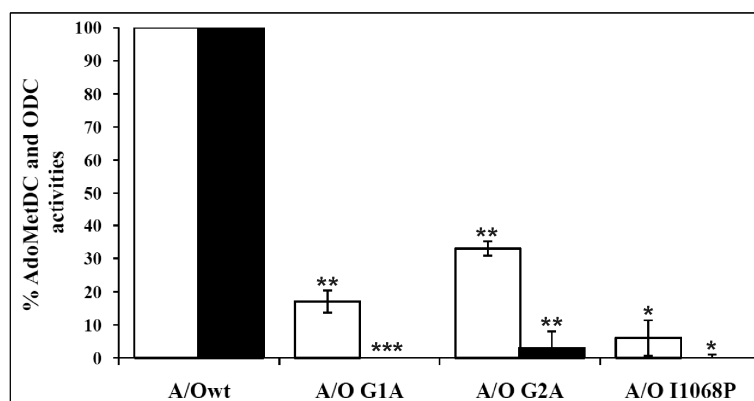


Figure 2.2: The effect of O1 insert mutations on the *Pf*AdoMetDC and *Pf*ODC enzyme activities within the bifunctional complex.

The AdoMetDC (white bars) and ODC (black bars) specific activities of the mutant enzymes (A/O I1068P, A/O G1A and A/O G2A) were normalised to the wild-type activity (A/Owt) and are given as a percentage. The results are shown as mean \pm S.E.M with error bars on each graph from three independent experiments carried out in duplicate ($n=3$). Significant differences at a confidence level of 95% are represented as follows: * for $P < 0.05$; ** for $P < 0.01$; *** for $P < 0.001$.

Disruption of the O1 insert α -helix (A/O I1068P) also resulted in complete loss in *Pf*ODC specific activity and significantly decreased *Pf*AdoMetDC activity ($P < 0.05$) (Figure 2.2). It is therefore possible that the helix within the O1 insert is involved in protein-protein interactions

with both domains of the bifunctional complex and that the flexibility of the insert may allow these interactions to take place. Disruption of the helix may therefore be communicated to the respective sites via long-range interactions [134] resulting in the reduced activities of both domains. Alternatively, mutagenesis may hinder substrate binding to the *Pf*ODC active site due to its proximate location to the active site entrance [127]. However, increased substrate concentrations of up to 400 μ M (8-fold K_m) did not restore AdoMetDC or ODC activity for any of the mutant enzymes, which indicates that altered K_m 's were not responsible for the loss of enzyme activities (results not shown). The results therefore show that the flexibility of the O1 insert (imparted by the flanking Gly residues), as well as the α -helix within this insert are functionally important for both the *Pf*AdoMetDC and *Pf*ODC domains.

2.3.3. The O1 insert α -helix mediates inter- and intradomain protein-protein interactions

SEC on affinity-purified wild-type and mutated monofunctional and bifunctional proteins was performed to qualitatively determine if loss of catalytic activity could be ascribed to the inability of the mutant proteins to form obligate *Pf*ODC homodimers and to associate into bifunctional *Pf*AdoMetDC/ODC complexes. Interestingly, even though equal amounts of total protein were applied to SEC, the quantities of proteins in specific fractions of the mutated protein samples were decreased for both the mutant bifunctional *Pf*AdoMetDC/ODC and monofunctional *Pf*ODC protein preparations. These differences in protein levels between the wild-type and the mutant samples were also detected with SDS-PAGE analysis (results not shown) and are probably due to the formation of larger, soluble protein aggregates upon mutagenesis.

The expected sizes of the wild-type heterotetrameric *Pf*AdoMetDC/ODC protein (A/Owt) and its heterodimeric form are shown in Figure 2.3A. *Pf*ODC was also expressed in its monofunctional form resulting in a homodimeric protein (with half of the hinge region) with a size of ~170 kDa, due to the association of two ~85 kDa monomeric proteins (Figure 2.3B) [103]. Prevention of heterotetrameric complex formation or dimerisation of the *Pf*ODC domains as a result of the introduced mutations would therefore be reflected in the SEC profiles. As expected, the wild-type bifunctional A/Owt protein eluted as both heterotetrameric (~330 kDa, fractions 44-46 of the SEC) and heterodimeric (~165 kDa, fractions 53-55) proteins (Figure 2.3A) due to the equilibration between bound and unbound states of the *Pf*ODC domains in the bifunctional protein [23]. Moreover, disruption of the α -helix in the O1 insert prevented not only heterotetramer complex formation but also dimerisation of the *Pf*ODC domain, which is obligatory for activity [127]. This is evident for both the bifunctional A/O I1068P protein that

eluted as a heterodimer of ~165 kDa (Figure 2.3A) as well as the monofunctional ODC I1068P protein that eluted as a monomer of ~85 kDa (Figure 2.3B). These results support previous findings, which have shown that dimeric *Pf*ODC is a prerequisite for heterotetrameric complex formation [69].

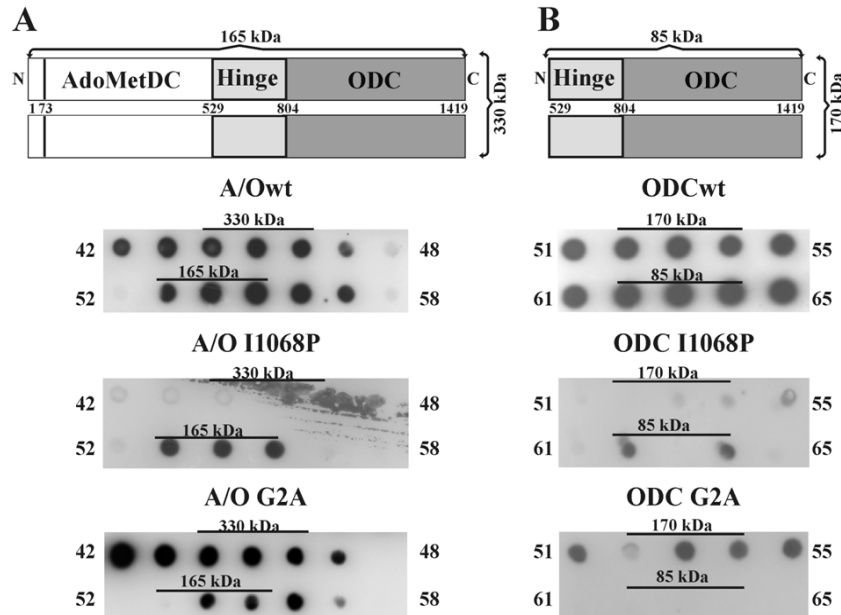


Figure 2.3: Western blots of the sequential fractions obtained from SEC of the (A) bifunctional *Pf*AdoMetDC/ODC and (B) monofunctional *Pf*ODC proteins.

From the top to the bottom panel the blots are shown for the wild-type (wt), the α -helix disrupted (I1068P) and the immobile (G2A: Gly1036-1038, 1083 to Ala) proteins. The sizes of the proteins in the SEC fractions as determined from a standard curve are indicated with black bars. Schematic diagrams to show the predicted sizes of the bifunctional *Pf*AdoMetDC/ODC (~330 or ~165 kDa) and monofunctional *Pf*ODC (~170 or ~85 kDa) proteins are shown above the blots.

These results also show that the protein-protein interactions that are required for complex formation are independent of the proposed flexibility of the O1 insert since SEC showed that the inflexible and inactive A/O G2A mutant could still form the ~330 kDa heterotetrameric complex (Figure 2.3A, fractions 44-46). Furthermore, while the equilibration of the bound and unbound states of wild-type *Pf*ODC was maintained (Figure 2.3B), the Gly mutations shifted the equilibrium towards the formation of the inactive ~170 kDa *Pf*ODC homodimer (Figure 2.3B, fractions 52-54). It therefore seems that the Gly residues are more important for the O1 insert's involvement in the decarboxylase activities of *Pf*AdoMetDC/ODC (Figure 2.2) than in complex formation.

Since the Gly to Ala mutations in the A/O G2A did not influence dimerisation, the loss of activity for this mutant may therefore be ascribed to a loss of insert flexibility. Therefore, to localise the O1 insert and to show the inflexibility of the quadruple Gly mutant, MD simulations were preformed (Figure 2.4). MD can be used to simulate the movement of the insert and

thereby provide information on the effect of the flanking Gly residues on the insert movement, which would not be possible in laboratory experiments.

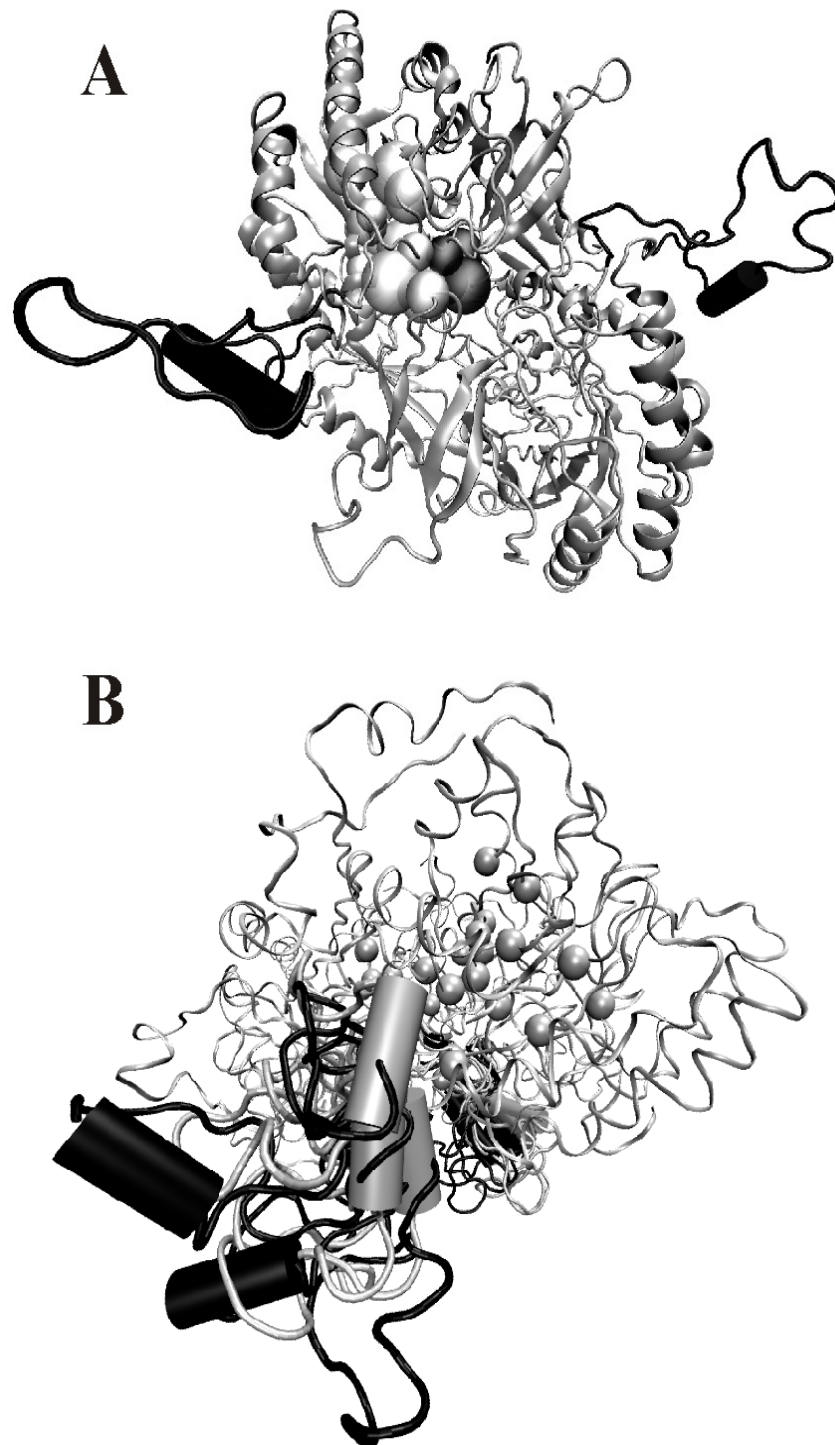


Figure 2.4: The wild-type homodimeric *Pf*ODC and immobile insert ODC G2A mutant protein after minimisation and MD.

(A) To give an indication of the protein and insert arrangement prior to MD, the two monomers of the wild-type *Pf*ODC minus its O1 inserts, prior to 5 million dynamic steps are shown in grey while only the O1 inserts of the ODC G2A mutant are shown in black relative to the active site (grey spheres). (B) A side view of the protein with the inserts (wild-type and mutant inserts shown in grey and black, respectively) at the front and back of the page after MD. The *Pf*ODC active sites and interface residues of the wild-type protein are shown as spheres while the α -helices within the inserts are shown as cylinders.

The results showed that, compared to the mutant insert at the start of the simulation (Figure 2.4A), the O1 insert of the wild-type *Pf*ODC protein appeared more tightly folded against the monomeric *Pf*ODC subunit at the site of substrate entry into the active site pocket (Figure 2.4B) [135]. The insert of the mutant protein projects away from the protein where it is unlikely to interact with the protein core. Interestingly, the α -helix within the O1 insert of the wild-type protein also moves closer to the protein to allow for possible interactions or to stabilise co-factor or substrate binding whereas the α -helix in the ODC G2A mutant protein remains more distant from the protein.

Experimental evidence therefore suggests the involvement of the O1 parasite-specific insert and specifically its predicted α -helix, in the functioning and dimerisation of the bifunctional *Pf*AdoMetDC/ODC protein. However, deletion or disruption of the O1 insert as well as mutations of *Pf*AdoMetDC/ODC and *Pf*ODC can have unpredictable effects on protein conformation, which may be communicated through long-range interactions to active site centres and protein-protein interaction sites. In addition, the appearance of soluble aggregates upon mutagenesis could also have an effect on the activities of the protein samples. Peptides were therefore used as novel probes to further aid the interpretation of the mutagenesis results.

2.3.4. Peptide probe-mediated modulation of *Pf*AdoMetDC and *Pf*ODC activities via interference of the O1 insert interactions

Various peptides were designed to be used either as competitors to simulate the functions of the O1 insert i.e. NY-39, which is identical to the entire O1 insert and LK-21, which is identical to the predicted α -helix within insert O1. In addition, a peptide was also designed as a blocking probe to prevent insert-mediated inter- and intradomain interactions (LE-21, a charge complement peptide of the predicted α -helix within insert O1) (Table 2.2).

Table 2.2: The synthetic peptides used as probes to determine the role of the O1 insert in protein-protein interactions across *Pf*AdoMetDC/ODC

Peptide	Peptide sequence ^a
NY-39	NAKKHDKIHYCTLSLQEIKKDIQKFLNEETFLKTKYGY
LK-21	<u>LSLQEIKKDIQKFLNEETFLK</u>
LE-21	<u>LSLQKIEEIQEFLQKKTFL</u>

^a The common sequences that are predicted to form the α -helix within insert O1 are underlined. The charge complement residues in peptide LE-21 are shown in bold italics.

Treatment of *Pf*AdoMetDC/ODC with the peptides significantly increased ($P < 0.05$) *Pf*AdoMetDC activity by ~60% at the highest concentrations tested (Figure 2.5A) by presumably

interacting with the respective target sites of these peptides within the *Pf*AdoMetDC and/or *Pf*ODC domains. Peptide NY-39 (corresponding to the complete O1 insert) also significantly increased ($P < 0.05$) both *Pf*AdoMetDC and *Pf*ODC activities (Figure 2.5). It can be speculated that the increase in activity could be due to stabilisation of the *Pf*ODC protein-protein interactions that are mediated by the O1 insert. However, the effect of this insert on *Pf*ODC dimerisation was not investigated due to the large quantities of the peptide that are required to determine the oligomeric status of the protein:peptide complex with SEC. In contrast, the α -helix insert peptide (LK-21) increased both domain activities within the bifunctional *Pf*AdoMetDC/ODC in an almost dose-dependent manner but only the highest peptide concentration significantly ($P < 0.05$) affected *Pf*AdoMetDC and *Pf*ODC activities (Figure 2.5A and B). The results show that the NY-39 peptide has additional effects beyond the proposed O1 insert α -helix effects on both domains due to the significant increases in both domain activities at all concentrations tested.

The O1 insert charge complement peptide LE-21, significantly decreased *Pf*ODC activity by 43% ($P < 0.05$) at a 1000-fold molar excess of the peptide (Figure 2.5B). This peptide possibly interferes with beneficial inter- and/or intradomain protein-protein interactions that are normally mediated by the O1 insert. One consequence could be prevention of *Pf*ODC homodimer formation, which is translated to inhibition of the interaction of this domain with the *Pf*AdoMetDC domain, but this was not determined due to the limited quantities of the peptide that was available.

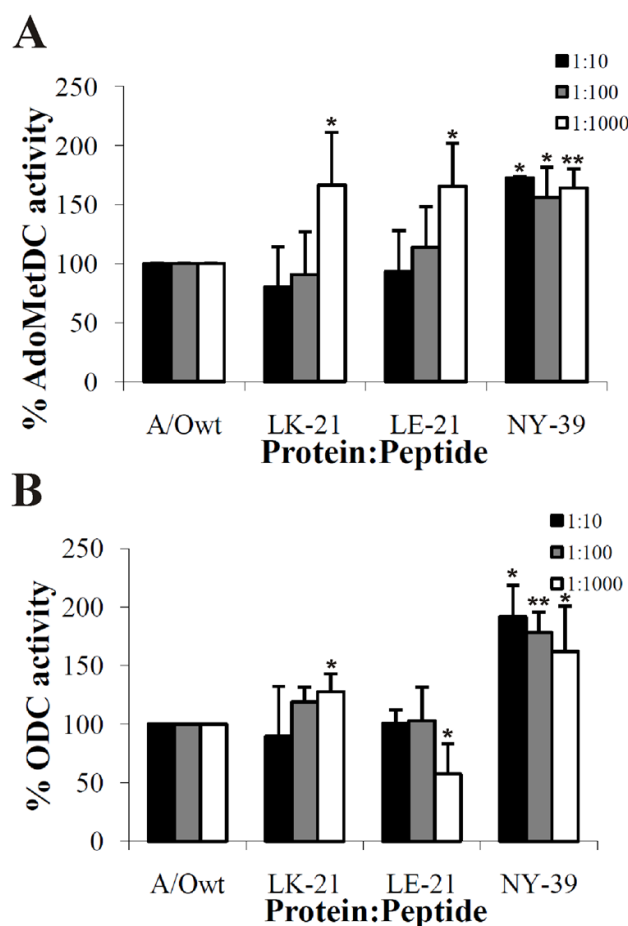
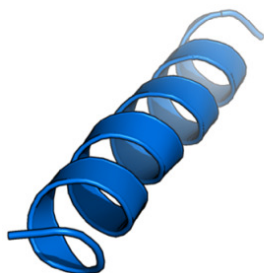


Figure 2.5: *Pf*AdoMetDC (A) and *Pf*ODC (B) activities after co-incubation with different peptide probes. The specific activities (nmol/min/mg) of the peptide-treated enzymes were normalised to the untreated, positive control's activity (A/Owt) and are given as a percentage. The values were determined from three independent experiments carried out in duplicate (n=3) after a 2 h incubation at 22°C of the wild-type bifunctional protein with three different peptides at three different molar quantities (protein to peptide ratio in molar quantities of 1:10, 1:100, 1:1000). The standard deviations of the mean are indicated as error bars on each graph. Significant differences at a confidence level of 95% are represented as follows: * for $P < 0.05$ and ** for $P < 0.01$.

From these results it is plausible that the O1 insert forms direct interactions with both domains in the bifunctional protein to modulate the decarboxylase activities. The peptides (LK-21 and NY-39) behave as O1 insert mimics and simulate inter- and intradomain protein-protein interactions of the O1 insert as reflected by the increases in *Pf*AdoMetDC and *Pf*ODC activities. The LE-21 charge complement peptide increases *Pf*AdoMetDC activity to the same extent as LK-21 but inhibited the activity of the *Pf*ODC domain by blocking the interactions normally mediated by the α -helix within the O1 insert (Figure 2.5A and B). Non-specific stabilisation and inhibitory effects of peptide binding seem unlikely since specific up- and down-regulation of the enzymatic activities were observed and the increase in peptide concentrations affected the enzyme activities in a dose-dependent manner. Furthermore, in the absence of CD analysis, the peptides in solution are predicted to fold into α -helices as determined by PEP-FOLD (Figure 2.6) [159]. The folding of the peptides into their 3D shapes is expected to allow the peptides to form interactions with their predicted target sites.

LK-21



LE-21



Figure 2.6: Folding of the α -helix O1 insert peptides as predicted by PEP-FOLD.

To determine whether the α -helix within the O1 insert of the *Pf*ODC domain is positioned in such a way that it is capable of forming direct interactions with the *Pf*AdoMetDC protein, protein-protein docking was employed to monitor the interaction between *Pf*AdoMetDC and *Pf*ODC. Even though the parasite-specific inserts were removed from these models prior to docking, their approximate positions on the *Pf*ODC protein could still be established (Figure 2.7).

In general, the docking results predicted that *Pf*AdoMetDC only makes contact with one face of the *Pf*ODC homodimeric protein, which is the same region where the *Pf*ODC active site and the O1 insert are located [152]. Fewer contacts are predicted for the non-active site face (Figure 2.7). Conversely, only one face of *Pf*AdoMetDC is favoured for contact with *Pf*ODC (results not shown) [152]. By taking into consideration the volume that would be occupied by the *Pf*AdoMetDC protein (identified as spheres in Figure 2.7) it is conceivable that the O1 insert (identified by the positions of the red spheres) is positioned in such a way that an interaction between the insert and the *Pf*AdoMetDC domain would be allowed. The same result was observed for AdoMetDC and ODC proteins from the five plasmodial species that were modelled, which indicates that the mechanism of protein-protein interactions between the domains is preserved and emphasises the importance of the conserved O1 parasite-specific insert in possibly mediating these essential inter- and intradomain interactions that are required for optimal enzyme activities within the bifunctional *Pf*AdoMetDC/ODC.

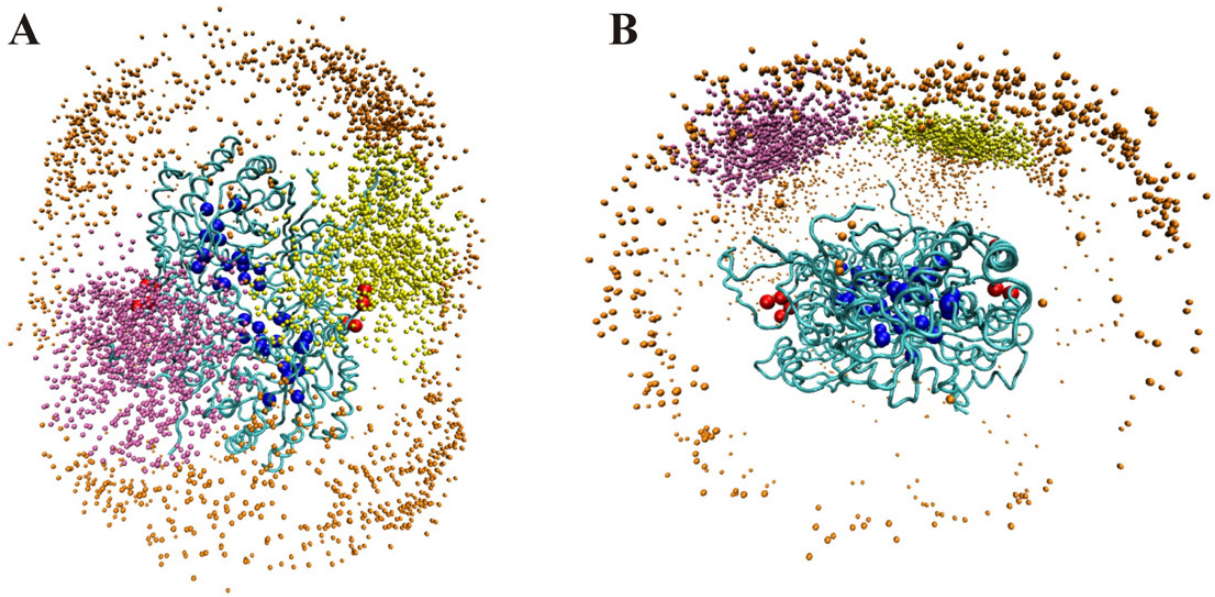


Figure 2.7: Protein-protein docking results to determine the proximity of the O1 insert to the *Pf*AdoMetDC protein.

(A) The view from the bottom of the ODC dimer at the site of substrate entry into the active site pockets and (B) a side view of the protein with the ODC active sites at the top. The orange, yellow and magenta spheres represent the centre of mass of different AdoMetDCs around the homodimeric ODC protein (blue ribbon). These spheres are the favoured positions of the AdoMetDCs, which are approximately symmetrical. The entire inserts were not included in the model but the positions of the O1 inserts can be identified by the red spheres. The ODC active site residues at the homodimer interface are shown as blue spheres (numbered according to the bifunctional protein): Chain A: Lys868, Asp887, Glu893, Arg955, His998, Ser1001, Asn1034, Gly1037, Glu1114, Gly1116, Arg1117, Asp1320, Tyr1384; Chain B: Tyr1311, Asp1356, Phe1392, Asn1393, Phe1395.

2.4. Discussion

Investigations into the roles of the hinge region connecting the *Pf*AdoMetDC and *Pf*ODC domains as well as parasite-specific inserts within both domains showed that the *Pf*ODC domain is more refractory to interference and possibly acts as the nucleation site for the formation of the active bifunctional complex in *P. falciparum* [69,103]. Such interdomain associations have also been observed for *P. falciparum* DHFR/TS, in which the catalytic activities of DHFR and TS are increased when the adjacent domain is in its activated, ligand-bound conformation [160]. *P. falciparum* TS is also dependent on its physical interaction with the DHFR domain for catalytic activity and possible allosteric regulation [122]. Furthermore, a crossover helix within a non-active site region of *Cryptosporidium hominis* DHFR has been shown to physically interact with the active site of the other DHFR monomer, thereby modulating its activity [161].

In the absence of known regulatory mechanisms of both *Pf*AdoMetDC and *Pf*ODC, the arrangement of the proteins within the bifunctional complex has been proposed to allow for the regulation of the enzyme activities via protein-protein interactions as has been observed in other

organisms. Mammalian ODC is rapidly degraded by its association with an inhibitory, polyamine-dependent antizyme protein [162] and the efficiency of the catalytic activity of trypanosomal AdoMetDC is dependent on its association with a catalytically dead, but allosterically active, AdoMetDC homologue or prozyme [163,164]. However, in *P. falciparum*, while antizyme is absent and the presence of a prozyme seems improbable, *Pf*AdoMetDC/ODC may behave in an analogous fashion to the DHFR/TS association where the enzyme properties are co-regulated to control polyamine biosynthesis.

Previous studies showed depletion of *Pf*ODC activity upon the deletion of the O1 parasite-specific insert from the bifunctional *Pf*AdoMetDC/ODC protein as a result of the inability to form active *Pf*ODC homodimers [69]. Two possible roles for the O1 insert were therefore investigated in this study. The first hypothesis, which is supported by a *Pf*ODC homology model [127], implies that the position and the proposed flexibility imparted by the flanking Gly residues of the O1 insert allows it to function as a catalytically essential loop. Secondly, it was postulated that the position of the O1 insert on the surface of the protein could allow the insert to mediate essential inter- and intradomain protein-protein interactions.

Flexible active site loops have been described for the Lys169 trypsin-sensitive loops of *L. donovani* [165] and *T. brucei* ODC [134] as well as for *Pf*ODC [127], where they retain the substrate within the active site pocket for catalysis and then open to allow the release of product. In addition to this trypsin-sensitive flexible loop, the O1 insert of *Pf*ODC is also sensitive to trypsin digestion, which suggests that it is located on the surface of the protein and exposed to the solvent [166]. This insert may additionally enable the stabilisation of the PLP co-factor within the *Pf*ODC active site as predicted by the *Pf*ODC homology model [127]. Similarly, the PLP-dependent *E. coli* D-serine dehydratase contains a flexible Gly-rich region that interacts with the co-factor [167]. For the *T. brucei* ODC enzyme, the presence of a highly flexible and conserved Gly-rich region (Gly235-237, corresponding to Gly1036-1038 in *Pf*ODC) and a salt bridge to Arg277 (corresponding to Arg1117 in *Pf*ODC) was shown to stabilise binding of PLP within the active site [168]. In this study, it was shown that the proposed restriction of O1 insert flexibility through mutation of the flanking Gly residues to Ala resulted in a loss of the specific activities of both domains of the bifunctional *Pf*AdoMetDC/ODC complex (Figure 2.2). The N-terminal Gly residues (Gly1036-1038) are also conserved within plasmodial ODCs and could thus serve as a binding site for PLP, which would explain the depletion of the specific activities of both the triple and quadruple mutants (A/O G1A and G2A). The observed decrease in

*Pf*AdoMetDC activity could be due to long-range effects communicated to this domain's active site upon inactivation of the *Pf*ODC domain. Enzyme kinetics to determine whether PLP binding to *Pf*ODC was affected was not performed due to the inactivation of the enzymes upon mutagenesis. On the other hand, the C-terminal Gly residue of the O1 insert (Gly1083) is not conserved among plasmodial ODCs (Figure 2.1) and is not predicted to play a role in the activity of *Pf*ODC activity. It therefore seems that the mutagenesis of the Gly residues resulting in inactive enzymes were due to prevention of co-factor binding and not as a result of insert inflexibility.

SEC of the G2A mutant protein showed that the protein was still capable of forming the homodimeric *Pf*ODC domain. However, disruption of the α -helix within the O1 insert through the introduction of a Pro residue showed that this I1068P mutant could no longer form the obligate *Pf*ODC homodimer (Figure 2.3). Additionally, this mutation prevented the formation of the bifunctional heterotetrameric *Pf*AdoMetDC/ODC complex, which resulted in significant losses in both enzyme activities (Figure 2.2). This result emphasises the importance of *Pf*ODC homodimer formation as nucleation sites for heterotetrameric bifunctional complex association [69].

Previous studies have shown that monofunctional *Pf*AdoMetDC has an increased substrate affinity when associated with *Pf*ODC in the bifunctional *Pf*AdoMetDC/ODC complex [71]. The identification of the interaction sites that mediate the interdomain interactions would therefore provide interesting opportunities to simultaneously influence both decarboxylase domains of the bifunctional complex. In this study, the disruption of the conserved α -helix within the O1 insert significantly decreased both *Pf*AdoMetDC and *Pf*ODC activities within the bifunctional complex but also prevented complex formation. This helix thus represents a site that can be targeted for the simultaneous interference of the activities of the bifunctional *Pf*AdoMetDC/ODC. Additionally, protein-protein docking results confirmed that the O1 insert (and possibly the α -helix within this insert) is in close enough proximity to the active site faces of *Pf*AdoMetDC to enable physical interactions with the protein (Figure 2.7).

The possibility that the O1 insert acts as a key enzymatic regulator of decarboxylase activity within the bifunctional complex was further investigated with novel peptides as probes in an attempt to distinguish between the effects of global conformational changes introduced as a result of the mutations as opposed to the effects of more localised interventions. Synthetic

peptides have been successfully applied as inhibitors of *P. falciparum* TIM [169], HIV-1 protease [170,171], *Lactobacillus casei* TS [172] and *T. brucei* farnesyltransferase [173]. For *Pf*TIM, one peptide resulted in a 55% decrease in enzyme activity at a 1000-fold molar excess of the peptide, which indicated that this region is possibly involved in the stabilisation of the dimeric protein [169]. However, the use of peptides to probe interaction sites of a specific protein region in order to obtain information on the structural arrangement of a protein represents a novel application of synthetic probes in biochemistry.

Analysis of the residues within the O1 insert within *Pf*ODC revealed the presence of two dominant motifs: a cationic N-terminal motif (high abundance of Lys residues) and an aromatic C-terminal motif (high abundance of aromatic residues) (Table 2.2). These may be involved in different interactions with the core protein such as electrostatic interactions/hydrogen bonds and aromatic stacking/hydrophobic interactions, respectively. Therefore, synthetic peptides were specifically designed based on these areas to probe the functional roles of the O1 insert.

The NY-39 peptide, which mimics the entire O1 insert and thus contains both the N-terminal cationic and C-terminal aromatic motifs, is expected to compete for binding to the native sites of the insert on *Pf*ODC (intradomain interactions) and/or *Pf*AdoMetDC (interdomain interactions). The significant increase by the peptide in the specific activities of both enzymes after treatment with this peptide suggests relief of restraints imposed on the domains through interactions that are natively mediated by the O1 insert. The role of the peptide in mediating complex formation could not be determined but would provide additional information on the role of the insert in mediating complex formation as was observed with the SEC results of the α -helix mutant. These effects were less pronounced when the shorter peptide LK-21 was used.

The LK-21 peptide is identical to the α -helix within O1 and was also expected to compete with the native interaction sites of specifically the α -helix within the O1 insert as the NK-39 peptide would. Treatment of the bifunctional protein with this peptide resulted in a dose-dependent increase of the specific activities of both *Pf*AdoMetDC and *Pf*ODC, which was less pronounced in *Pf*ODC activity. Subsequently, and to gain a better understanding of the function of the α -helix, the effects of a charge complementary peptide of the helix on *Pf*AdoMetDC/ODC activity were investigated. This mostly anionic peptide is expected to bind to the cationic motif of the O1 insert helix and not to the helices' interaction sites. Whereas the increase in *Pf*AdoMetDC activities by this peptide was indistinguishable from those of the other peptides, the activity of

the *Pf*ODC domain significantly decreased in a dose-dependent manner. The results therefore suggest that this peptide could form stable ionic interactions with the α -helix in the O1 insert. Peptide binding to the insert then resulted in either the prevention of obligate *Pf*ODC homodimer formation, which decreased its activity and/or prevented the native functioning of the loop in intradomain interactions.

It is feasible that an increase in the proportions of *Pf*AdoMetDC-peptide complexes (peptides LK-21 and NY-39) relieved inhibitory constraints imposed by *Pf*ODC on the *Pf*AdoMetDC domain and this resulted in higher activity. Alternatively, in the absence of kinetic data it can be speculated that peptide binding could have resulted in an altered K_m and/or better substrate accessibility to the catalytic site, which increased the catalytic efficiency of the *Pf*AdoMetDC enzyme. However, with the charge complement LE-21 peptide, the significant increase in *Pf*AdoMetDC activity could be due to prevention of the interaction of the α -helix within the O1 insert to this protein resulting in increased activities.

2.5. Conclusion

The results indicate that *Pf*ODC constrain the activity of *Pf*AdoMetDC in the bifunctional complex whereas *Pf*AdoMetDC is required for the optimal activity of *Pf*ODC [103]. These effects are mediated by protein-protein interactions, which could be similar in mechanism to that observed for antizyme and mammalian ODC [162] as well as prozyme and trypanosomal AdoMetDC [163,164]. The peptide probe studies showed that interference with the interaction sites of the O1 insert within the *Pf*ODC domain decreased its activity while *Pf*AdoMetDC activity was increased, indicative of a relieve of constraint placed on the *Pf*AdoMetDC domain by *Pf*ODC. The *Pf*ODC domain of *Pf*AdoMetDC/ODC may therefore coordinate the activities of both the domains within the bifunctional complex through long-range interdomain protein-protein interactions to simultaneously supply dcAdoMet and putrescine. In turn, investigations into the *Pf*AdoMetDC domain to identify specific features that mediate possible regulatory effects within the bifunctional protein should be performed. Together these results could provide an explanation for the evolutionary advantage of maintaining such a large open reading frame in the plasmodial genome. The bifunctional arrangement of *Pf*AdoMetDC/ODC is also reminiscent of the essential protein-protein interactions involved in the *Pf*DHFR/TS bifunctional protein in which the C-terminally located TS is dependent on the presence of the N-terminal DHFR domain [122]. Additionally, such a fusion of genes that encode two proteins linked with a hinge region enhances the effective concentration of protein domains that are involved in a common

metabolic pathway with respect to each other [174].

These studies are revealing the regulatory mechanisms employed by plasmodia to maintain optimum levels of the essential polyamines. Advances are therefore being made towards the identification of areas amenable to polyamine biosynthesis inhibition or uncoupling of the methionine and polyamine biosynthesis, essentially joined by the bifunctional *Pf*AdoMetDC/ODC complex, which could hopefully interfere with parasite survival.

Chapter 3:

Biochemical and structural characterisation of monofunctional *Plasmodium falciparum* AdoMetDC

3.1. Introduction

Targeting of AdoMetDC activity has previously been shown to be effective in antiparasitic strategies such as *T. b. brucei*-infected rats. Treatment of the infected rats with MDL73811 resulted in a 20-fold increase in AdoMet levels [175]. In addition, DFMO treatment of trypanosomes isolated from these infected rats also resulted in a 50-fold increase in AdoMet levels. In the latter study a massive >4 000-fold increase in dcAdoMet levels was also observed since putrescine as acceptor of the aminopropyl moiety from dcAdoMet was depleted upon inhibition of ODC activity with DFMO [176]. These results showed that inhibition of *T. brucei* AdoMetDC with MDL73811 leads to a trypanosome-specific increase in AdoMet, which could be responsible for the trypanosomal-specific hypermethylation of nucleic acids and/or proteins via the inhibition of the polyamine biosynthesis pathway [175-177]. Histone and DNA methylation has transcriptional regulatory effects [178,179] and hypermethylation may result in the down-regulation of transcription [180].

In *P. falciparum*, MDL73811 has also been shown to irreversibly inhibit *Pf*AdoMetDC activity resulting in the prevention of parasite growth *in vitro* [115] and resulted in the prevention of hypusine formation for eIF-5A synthesis [181]. In contrast to the observed effect in trypanosomes, metabolomic studies have shown that, while co-inhibition of *Pf*AdoMetDC and *Pf*ODC with MDL73811 and DFMO causes cytoostasis, inhibition does not alter AdoMet levels, possibly due to the observed down-regulation of AdoMet synthetase [116]. However, another study has shown that plasmodial AdoMet synthase is not allosterically regulated by AdoMet [93], which indicates that a different mechanism exists for the homeostatic control of AdoMet levels within *P. falciparum* to prevent hypermethylation. The polyamine pathway in the plasmodial parasite therefore seems to be highly regulated in order to link methionine metabolism with that of polyamine levels. Further investigations are needed to identify possible allosteric effector/s of the bifunctional *Pf*AdoMetDC/ODC activities, while the bifunctional arrangement in itself could allow for the simultaneous regulation of both activities exerted by the effector/s.



Extensive studies on the bifunctional *Pf*AdoMetDC/ODC protein provided important insights into several biochemical properties of the bifunctional protein such as its oligomeric arrangement as a heterotetramer, obligate homodimer formation of *Pf*ODC, effects of putrescine on *Pf*ODC and *Pf*AdoMetDC activities, the role of the hinge region and *Pf*AdoMetDC domain in *Pf*ODC activity, the presence and functional roles of parasite-specific inserts and the effects of various inhibitors on enzyme activities [69-71,100,103]. Homology models have also been solved for both monofunctional domains, which provided important insights into the active sites as well as inhibitor binding to *Pf*ODC [120,127]. Apart from the predictions obtained from the *Pf*AdoMetDC homology model, comparatively few studies have been performed on this monofunctional *Pf*AdoMetDC domain and aspects such as its functional oligomeric status, the details of its mechanism of autocatalytic processing, role as a partner protein to *Pf*ODC and regulator of enzyme activities within the bifunctional complex remains to be identified. In context of the well-studied *Pf*ODC domain [103] and the proposed role of the bifunctional *Pf*AdoMetDC/ODC arrangement in mediating the decarboxylase domain activities as identified in Chapter 2, the *Pf*AdoMetDC domain should be investigated to determine its biochemical properties as well as its role within the bifunctional complex. These results could provide novel insights into the observed differences in parasite responses upon treatment with polyamine biosynthesis inhibitors as well as possibilities to improve the mainly cytostatic effect observed with DFMO and MDL73811 treatment [118,182].

Previous studies of *Pf*AdoMetDC in either its monofunctional or bifunctional form showed that the *Pf*AdoMetDC active site can function independently while the optimal activity of *Pf*ODC is dependent on the presence of the hinge region as well as the *Pf*AdoMetDC domain [71,103]. A follow-up study showed that interdomain interactions within the bifunctional complex are mediated by parasite-specific inserts [69]. Recently, it was shown that trypanosomal AdoMetDC is activated by a catalytically inactive AdoMetDC homologue, or prozyme [163,164] while human ODC is inhibited by the presence of antizyme [128]. In contrast to the human and trypanosomal proteins, *Pf*AdoMetDC activity and autocatalytic processing is not stimulated by putrescine [71], making this enzyme a comparatively less catalytic efficient enzyme and indicates that an as of yet unidentified effector could mediate the kinetic properties of this enzyme. As mentioned previously it has been speculated that the bifunctional arrangement in *P. falciparum* could allow for the simultaneous regulation of both the domains within the *Pf*AdoMetDC/ODC complex [71], which is similar to the domains within the *Pf*DHFR/TS bifunctional protein [122].



The crystal structures of various AdoMetDC and ODC proteins have been solved, which provided insights into several aspects concerning protein function, regulation and druggability. For AdoMetDC, the structures of human, plant (*S. tuberosum*) and prokaryotic (*T. maritima*) AdoMetDCs have been determined [123,183,184]. The quaternary structure of the active, human AdoMetDC revealed a four-layer $\alpha\beta\beta\alpha$ -sandwich fold, which at the time of publishing, had not been observed in any other protein structure in the Protein Data Bank [123]. It has previously been suggested that AdoMetDC might be a product of an ancient gene duplication event that resulted in its structural similarity [184]. The protein exists as an $(\alpha\beta)_2$ dimer where the α - and β -subunits are formed by an autocatalytic processing event (non-hydrolytic serinolysis) that takes place at hSer68 (human residue Ser68), which simultaneously results in the formation of the active site pyruvoyl co-factor. The mechanism of processing has been studied in human and *T. cruzi* AdoMetDC and the specific residues involved in the autocatalytic reaction have been characterised [125,185-189]. Several human AdoMetDC crystal structures of unprocessed mutants or a protein locked as an ester intermediate have been solved, which provided novel insights into the autocatalytic reaction mechanism. Each $(\alpha\beta)$ monomer contains two central eight-stranded β -sheets that are flanked by several α - and 3_{10} -helices on either side. The two monomers are then joined by an edge-on association of the β -sheets at the dimer interface to form the dimeric protein. The active sites of the monomers are located between the α - and β -subunits of each monomer where the pyruvoyl group is formed and is thus located distant from the dimer interface. An unusual collection of charged residues between the β -sheets of each monomer, well-removed from the active site, has been shown as the site where the positively-charged putrescine binds. The crystal structure of plant AdoMetDC showed that the protein adopts the same $\alpha\beta\beta\alpha$ -fold as the dimeric human protein but revealed two major differences, namely: 1) plant AdoMetDC is constitutively active since putrescine does not stimulate autocatalytic processing nor catalytic activity; and 2) plant AdoMetDC exists as a monomeric protein. Even though plant AdoMetDC also contains most of the charged-buried residues present in the human putrescine-binding site, three positively-charged residues and several water molecules were shown to mimic putrescine binding [184,189].

The homology model of *PfAdoMetDC* with the plant and human structures as templates showed that the protein also adopts the same $\alpha\beta$ -fold as seen for the template AdoMetDCs [120]. The model has an equal number of strands as in the human template but differences exist in the number of α - and 3_{10} -helices flanking the β -sheets of the $\alpha\beta\beta\alpha$ -fold. Like plant AdoMetDC, *PfAdoMetDC* activity is not affected by putrescine nor does it require putrescine for the



autocatalytic processing reaction [71]. In the absence of putrescine these proteins may be constitutively active to allow for continuous supply of product, which is nonsensical in the case of the plant *AdoMetDC* due to the various essential functions that the polyamines mediate while *PfAdoMetDC* activity may be regulated by a different mechanism. As mentioned earlier, the inhibition of *PfAdoMetDC* does not lead to accumulation of *AdoMet*, nor would *dcAdoMet* be synthesised if it is not required by the parasite since *dcAdoMet* is exclusively used as a substrate in the polyamine pathway [178], thus once produced it is committed to this pathway. Furthermore, previous studies have shown that within the bifunctional complex, the *PfODC* domain affects the kinetic properties of *PfAdoMetDC* [71]. Therefore, instead of the product of the ODC reaction stimulating *PfAdoMetDC* activity, the entire protein may conformationally contribute to mediate catalytic activity. Activity analyses of the monofunctional and bifunctional forms of *PfAdoMetDC* showed an increase in substrate affinity from 58 μM to 43 μM , respectively, while the specific activities remained similar (as recalculated in nmol/min per mol protein) [71].

In this chapter, the expression and purification of soluble, monofunctional *PfAdoMetDC* within *E. coli* was improved, which allowed investigations of various biochemical and structural aspects of this protein such as enzyme kinetics and oligomeric status. Comparisons could subsequently be drawn with trypanosomal and human *AdoMetDCs* in terms of the oligomeric status, secondary structure and the mechanism of autocatalytic processing of the *PfAdoMetDC* protein. The results obtained in this study support previous studies that were performed on the *PfODC* domain, which suggested that the unique arrangement of *PfAdoMetDC* and *PfODC* in the bifunctional complex allows for the concurrent regulation of the enzyme activities and could provide a possible explanation for the absence of *PfAdoMetDC* stimulation by putrescine.

3.2. Methods

3.2.1. Cloning of the harmonised *PfAdometdc* gene sequence

Codon harmonisation was carried out in an attempt to improve the heterologous expression of the *PfAdoMetDC* domain within *E. coli* with the use of a web interface algorithm (<http://www.sami.org.za/equalize/>). Nucleotides 1 to 1461 were replaced by synonymous codons that ensured the positional codon frequency of low/intermediate and high usage codons to remain similar to the frequency used by that of the *E. coli* host [190]. This region corresponds to approximately the first third of the entire bifunctional *PfAdometdc/Odc* gene and encodes for the



487-residue catalytic domain of *PfAdoMetDC* (Figure 3.1A and B).

Custom gene synthesis was performed by GeneArt, (Regensburg, Germany) and the shipping plasmid containing the harmonised insert was received in dried form. The plasmid was dissolved and then transformed into electrocompetent *E. coli* SURE cells (Stratagene). Transformed cells were selected for ampicillin resistance on LB-agar plates and grown overnight at 37°C. A single colony was picked and inoculated for 16 h at 30°C in LB-ampicillin (50 µg/ml) for subsequent plasmid purification. The shipped and the pASK-IBA3 plasmids containing the wild-type, unharmonised *PfAdometdc/Odc* insert (Figure 3.1A, pASK-IBA3 *A/Owt*) [70] were both digested with *Xba*I and *Kpn*I (Promega) at 37°C for 1 h in order to replace the corresponding wild-type, unharmonised *PfAdometdc* sequence with the harmonised *PfAdometdc* insert from the shipping plasmid with restriction enzyme-mediated cloning (Figure 3.1C). The bands corresponding to the 1461 bp harmonised insert and the 5911 bp pASK-IBA3 *A/Owt* fragment (with wild-type unharmonised *PfAdometdc* removed) were excised and purified from an agarose gel and ligated at 4°C for 48 h using T4 DNA Ligase (Promega). The ligated, circular product was then transformed into electrocompetent *E. coli* SURE cells. Colonies were picked for plasmid extraction and verified with restriction mapping.

However, since the exact C-terminal end of the *PfAdoMetDC* domain within *PfAdoMetDC/ODC* is unclear, a harmonised fragment was created that included 255 wild-type, unharmonised nucleotides at the C-terminus of the gene encoding the catalytic domain of *PfAdometdc* (Figure 3.1E). This fragment was amplified from the construct containing the partially harmonised *PfAdometdc/Odc* sequence described above (Figure 3.1C). The length of this 572-residue protein was based on the portion used for the *PfAdoMetDC* homology model, which consisted of 526 residues [128] with a buffer of 45 residues since the extent of the *PfAdoMetDC* domain is unknown. A second construct was also created that included 519 wild-type, unharmonised nucleotides (Figure 3.1F, total of 1980 nucleotides) in order to mimic the size of the published monofunctional *PfAdoMetDC* domain (Figure 3.1D, wt*PfAdoMetDC*-hinge) and includes half of the hinge region [78].

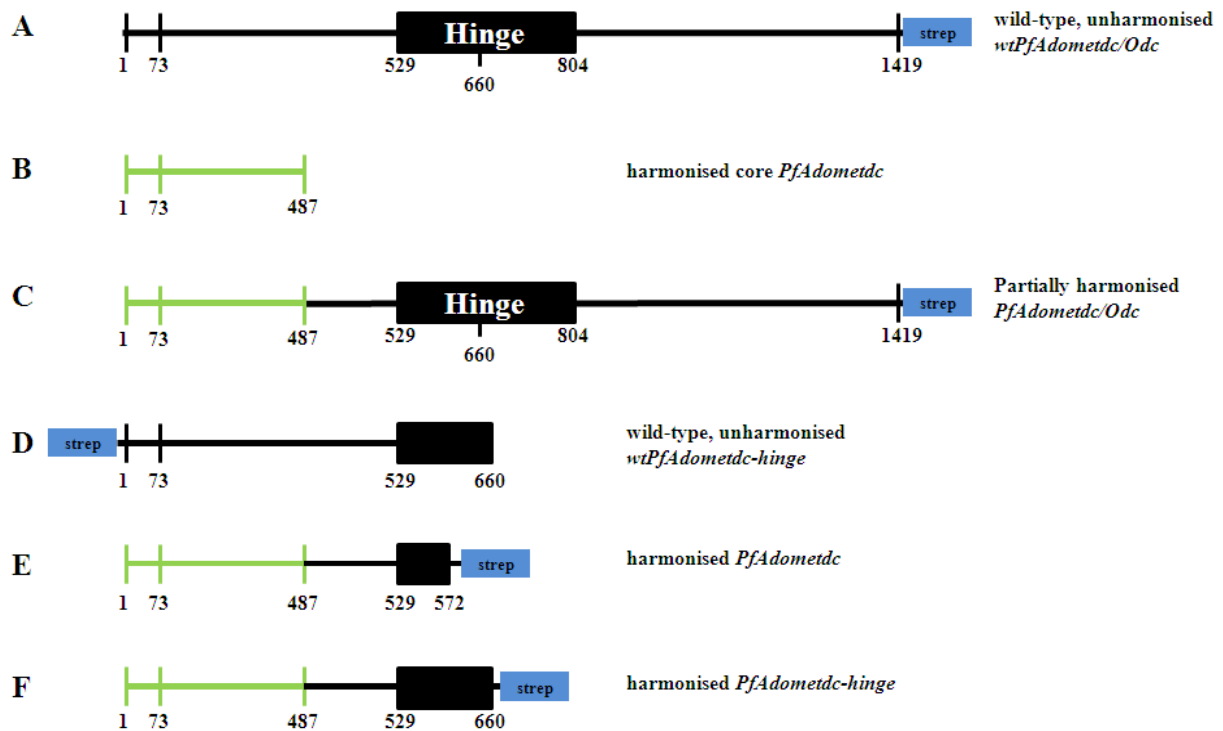


Figure 3.1: Schematic diagrams of the gene fragments used in the comparative *PfAdoMetDC* protein expression study.

(A) The plasmid containing the wild-type, unharmonised full-length gene sequence (black line) of *PfAdoMetdc/Odc* [77] cloned into the pASK-IBA3 vector (C-terminal Strep-tag) was used to replace the core sequence of *PfAdoMetdc* with the codon-harmonised one (green line) in (B) to create a partially harmonised full-length gene (C). Two gene fragments were subsequently amplified from this partially harmonised full-length gene, namely (E) *PfAdoMetdc* (nucleotides 1-1716) encoding a C-terminally strep-tagged protein (572 residues) and (F) *PfAdoMetdc-hinge* (nucleotides 1-1980) encoding a C-terminally Strep-tagged protein (660 residues). The latter protein was compared to the expression of the (D) wt*PfAdoMetDC-hinge* protein (660 residues) encoded from the wild-type, unharmonised gene (N-terminal Strep-tag) that was previously used in a study of the monofunctional *PfAdoMetDC* protein [78].

The primers that were used for the amplification of these two fragments are listed in Table 3.1. PCR SuperMix (Invitrogen) was used with 5 fmol of template and 10 pmol of each of the forward and reverse primers. Temperature cycling was performed as follows: 94°C for 3 min, 85°C for 30 s followed by 25 cycles of 94°C for 30 s, 50°C for 1 min and 65°C for 4 min. The sizes of the PCR products were verified with DNA gel electrophoresis and the parental template DNA was removed by digestion with *DpnI* (New England Biolabs) at 37°C for 1 h followed by digestion with *BsaI* (New England Biolabs) at 50°C for 3 h. The pASK-IBA3 vector was also digested with *BsaI* and used for the ligation with the *BsaI*-digested PCR amplified fragments (pASK-IBA3 *PfAdoMetdc* and *PfAdoMetdc-hinge*). Ligation was carried out with T4 DNA Ligase at 4°C for 16 h. The ligated products were subsequently transformed into heat shock competent DH5 α *E. coli* cells and positive colonies were selected using ampicillin resistance. Plasmids containing the harmonised *PfAdoMetdc* and *PfAdoMetdc-hinge* inserts were verified with automated nucleotide sequencing using a BigDye[®] Terminator v3.1 Cycle Sequencing kit (Applied Biosystems).

**Table 3.1: Primers used for the amplification of the *PfAdometdc* and *PfAdometdc-hinge* fragments from the pASK-IBA3 containing partially harmonised *PfAdometdc/Odc***

Primer	Sequence (5' to 3')
domain_F	ATGGTAGGTCTCAAATGAATGGCATTTCGAAGGCATTGAAA
domain_R	ATGGTAGGTCTCAGCGCTCAAAGTTTCTTTTCTACACATTTAAC
hinge_R	ATGGTAGGTCTCAGCGCTATCTTTCTCATTGTGTTGTACCTTTTC

The expression constructs used for subsequent comparative protein expression therefore included the pASK-IBA7 vector containing wild-type, unharmonised *PfAdometdc* with half of the hinge region (Figure 3.1D, residues 1-660, N-terminal Strep-tag, wt*PfAdoMetDC*-hinge) generously provided by Dr. C. Wrenger [71], the pASK-IBA3 vector containing harmonised *PfAdometdc* (Figure 3.1E, residues 1-572, C-terminal Strep-tag, *PfAdoMetDC*) and the pASK-IBA3 vector containing harmonised *PfAdometdc* with half of the hinge region (Figure 3.1F, residues 1-660, C-terminal Strep-tag, *PfAdoMetDC*-hinge).

3.2.2. Protein expression and purification

The plasmids containing unharmonised wt*PfAdometdc-hinge* [71], harmonised *PfAdometdc* and harmonised *PfAdometdc-hinge* were transformed into heat shock competent BL21 Star™ *E. coli* cells (Invitrogen). Colonies were inoculated in LB-ampicillin and incubated at 37°C for 16 h. These cultures were subsequently diluted 1:100 in 1 litre LB-ampicillin and incubated at 37°C with agitation. Protein expression was induced at an OD₆₀₀ of 0.7-0.8 with 200 µg AHT (IBA). The cultures were incubated at 37°C for another 4 h before the cells were harvested. The pelleted cells were diluted in 10 ml wash buffer (100 mM Tris/HCl, pH 8.0, 150 mM NaCl, 1 mM EDTA) per litre of culture. Lysozyme and 0.1 mM PMSF was added to the suspension and incubated on ice for 30 min. The cells were subsequently disrupted with sonication and the soluble proteins were collected in the supernatants after ultracentrifugation was performed at 4°C for 1 h at 100 000g. The Strep-tagged fusion proteins (660-residue wt*PfAdoMetDC*-hinge, 572-residue *PfAdoMetDC* and 660-residue *PfAdoMetDC*-hinge) were purified using Strep-*Tactin* affinity matrix (IBA) as described previously [69]. Samples of the insoluble proteins collected after ultracentrifugation were also kept for further analysis with SDS-PAGE and subsequent refolding from inclusion bodies (section 3.2.3).

The affinity-purified *PfAdoMetDC* protein was separated with SEC using an Äkta Explorer System (Amersham Pharmacia Biotech). The Superdex®-S200 10/300 GL SE column (Tricorn, GE Healthcare) was calibrated with the Gel Filtration Standard kit (BioRad) that separated into five peaks corresponding to thyroglobulin (670 kDa), γ -globulin (158 kDa), ovalbumin (44 kDa),



myoglobin (17 kDa), and Vitamin B₁₂ (1.35 kDa). The calibration curve was used to estimate protein sizes based on observed elution volumes (V_e). The column was subsequently equilibrated with filtered, degassed wash buffer after which protein samples (500 μ l) were loaded and fractions corresponding to dimeric (~140 kDa) and monomeric (~70 kDa) *PfAdoMetDC* were collected, pooled and subsequently concentrated with Amicon Ultra centrifugal filter devices (MWC0 3000, Millipore).

Protein concentrations were determined using protein absorbance at 280 nm and molar extinction coefficients of 69110 and 73580 M⁻¹ cm⁻¹ for *PfAdoMetDC* and *PfAdoMetDC*-hinge, respectively, followed by protein visualisation with SDS-PAGE using NuPAGE[®] 4-12% BisTris pre-cast gels (Invitrogen) and Colloidal Coomassie staining. Protein bands were identified with LC-MS/MS as previously described [8] as well as with Western immunodetection using monoclonal Strep-tag II mouse antiserum conjugated to HRP (Acris antibodies) (section 2.2.6).

3.2.3. Refolding of the *PfAdoMetDC* from insoluble inclusion bodies

The cell pellets of the lysed cells from the expression of *PfAdoMetDC* and *PfAdoMetDC*-hinge were collected and analysed for the presence of the proteins in insoluble inclusion bodies [191]. The method of Sirawaraporn *et al.* was followed to isolate and refold the proteins from the insoluble fractions [192]. Briefly, the pellets were washed three times with wash buffer and the supernatants were discarded. The pellets were redissolved in wash buffer containing 20% (v/v) glycerol, 10 mM DTT, 0.2 M KCl and 6 M guanidinium hydrochloride. The tubes were rotated at 4°C for 1 h to unfold the proteins and subsequently refolded by adding drop-wise a 20-fold dilution of wash buffer containing 20% glycerol, 10 mM DTT and 0.2 M KCl. Refolding was performed overnight at 4°C with gentle stirring. The samples were then centrifuged and the supernatants were used in subsequent protein purification with Strep-*Tactin* affinity chromatography as previously described [69]. The protein eluates were visualised with SDS-PAGE and Colloidal Coomassie Staining.

3.2.4. Determination of enzyme activity and protein stability

The SEC-purified *PfAdoMetDC* and wt*PfAdoMetDC*-hinge enzymes were assayed for decarboxylase activity directly after purification and after two weeks of storage at 4 and -20°C. The assays were performed as previously described ([70] and section 2.2.4). Briefly, 5 μ g (290 nM) protein was incubated in assay buffer (50 mM KH₂PO₄, pH 7.5, 1 mM EDTA, 1 mM DTT) and 100 μ M substrate consisting of [*S*-(5'-adenosyl)-L-methionine chloride] (Sigma-Aldrich)



and 50 nCi AdoMet [*S*-(5'-adenosyl-[carboxy-¹⁴C])-L-methionine] (55 mCi/mmol, Amersham Biosciences) in a total reaction volume of 250 μ l. The reactions were incubated at 37°C for 30 min followed by reaction termination via protein precipitation with the addition of 30% (w/v) trichloroacetic acid. Specific enzyme activity was expressed as the amount of CO₂ produced in nmol/min/mg (or nmol/min per mol protein) and performed in duplicate for three individual experiments.

Differential scanning fluorimetry (DSF) was used to test a range of buffers (http://cassiopeia.maxlab.lu.se/index/dsf_screens/) that could contribute to the stability of the *PfAdoMetDC* protein. Prior to protein stability screening of the SEC-purified *PfAdoMetDC* protein, the wash buffer was exchanged with dialysis buffer (50 mM Tris/HCl, pH 8.0, 150 mM NaCl) to decrease the buffer strength and to remove the EDTA. A volume of 8.3 μ l of each of the 24 buffers was pipetted into the ABgene[®] PCR plate (Thermo Scientific). The protein was diluted to a concentration of 0.15 mg/ml while the 100% DMSO-containing SYPRO orange dye (Sigma-Aldrich) was diluted 1:100 with H₂O. A volume of 25 μ l protein containing 1:10 of the dye (final dilution of 1:1000) was added to each buffer-containing well, mixed briefly, and sealed with clear film. The plate was placed within the Mx3005P qPCR system (Stratagene) and the temperature was increased from 25°C to 95°C. Fluorescence readings with excitation and emission wavelengths of 492 nm and 610 nm, respectively, were measured at 1 min intervals [193]. The results were analysed with the MxPro software.

The stability of *PfAdoMetDC* in the presence of the substrate analogues MDL73811 and CGP48664 was also tested. Protein (1.3 μ M) was incubated with 1x, 5x, and 10x molar excesses of the two analogues for 30 min at RT. Volumes of 25 μ l of the protein:ligand complexes as well as the protein without ligand were added in duplicate to the 96-well plate and analysed as before.

3.2.5. Investigations into the oligomeric status of monofunctional *PfAdoMetDC*

3.2.5.1. Reducing and non-reducing SEC and SDS-PAGE

The oligomeric status of affinity-purified *PfAdoMetDC* at concentrations of 1 mg/ml and 4 mg/ml were analysed with SEC as described in section 3.2.2. Monomeric and dimeric protein fractions collected from SEC were analysed in terms of their elution volumes (V_e) relative to the void volume (V_o) of the column (V_e/V_o). Reducing SEC was also performed by equilibrating the SE column with wash buffer containing 10 mM DTT. Monomeric (~70 kDa) and dimeric (~140 kDa) protein fractions collected from SEC were visualised with reducing (10 mM DTT added to



the sample buffer immediately prior to gel loading and electrophoresis) and non-reducing (reducing agent omitted from the sample buffer) SDS-PAGE.

3.2.5.2. MALDI-MS of affinity-purified proteins

Preliminary peptide mass fingerprinting with MALDI-MS was performed on the bands corresponding to the monomeric and dimeric proteins [191]. Protein sample extraction, dehydration and preparation for MALDI-MS as well as sample derivatisation with iodoacetamide to identify Cystines possibly involved in disulphide-bond formation, was performed as previously described [194]. Briefly, the gel bands were destained followed by dehydration with absolute ethanol and all samples except the dimeric ones were treated with 10 mM DTT in 50 mM NH_4HCO_3 for 30 min at 37°C. All samples were subsequently alkylated for 30 min with 55 mM iodoacetamide, washed with NH_4HCO_3 in 50% (v/v) ethanol and dehydrated as before. Trypsin digestion was performed overnight at 4°C by using 96 ng trypsin in 50 mM NH_4HCO_3 . The supernatants after the overnight digestion were collected and any remaining peptides were extracted with 50% ethanol and 50% (v/v) trifluoroacetic acid (TFA). The latter supernatants were pooled with the previously collected supernatants and dried *in vacuo*. The dried peptides were dissolved in 0.1% TFA and briefly centrifuged. A volume of 0.5 μl of each protein sample was directly spotted into the MALDI target plate, followed by the same volume of matrix solution (5 mg/ml α -cyano-4-hydroxycinnamic acid in 60% (v/v) acetonitrile and 0.1% TFA). MALDI-MS was performed using the Applied Biosystems 4700 Proteomics Analyzer with TOF/TOF™ optics in positive reflection mode. The peak lists were generated using T2D-extractor with default settings and submitted to the MASCOT Peptide Mass fingerprint tool (<http://www.matrixscience.com/>).

3.2.5.3. Site-directed mutagenesis

Based on the MALDI-MS results the role of Cys505 in dimer stabilisation via covalent disulphide bond formation was studied by mutating the Cys codon to a Ser codon (M. Williams and [191]). The mutagenesis reaction to create the *PfAdometdc-C505S* mutant was performed by using the pASK-IBA3 plasmid containing harmonised *PfAdometdc* as template (Figure 3.1E) with the forward 5'-GGTAAAAGTTCCGTTTTATTATCAAG-3' and reverse 5'-CTTGATAAT AAACGGAACTTTTACC-3' primers (mutations are underlined). Ex Taq™ DNA Polymerase (Takara Bio Inc.) was used to amplify the entire template [195] in the presence of 6 fmol template and 10 pmol of each of the primers. Temperature cycling was performed as follows: 95°C for 3 min followed by 25 cycles of 96°C for 30 s, 56°C for 30 s, 68°C for 5 min with a



final extension step at 68°C for 10 min. Post-PCR manipulation was performed as described previously [195]. Briefly, the PCR product was visualised with DNA gel electrophoresis and the correctly-sized band corresponding to the linear pASK-IBA3 plasmid containing *PfAdometdc* and the C505S mutation was purified with the Wizard[®] SV Gel and PCR Clean-up System (Promega). The agarose-purified product was then treated with *DpnI* (Fermentas) for 3 h at 37°C and cleaned as before. The linear plasmids were directly electroporated into DH5 α cells (Gibco BRL) and plated onto LB-ampicillin agar plates and incubated overnight at 37°C. Colonies were picked and grown for 16 h in LB-ampicillin (50 μ g/ml) from which the plasmids were purified with the Zyppy[™] Plasmid Miniprep kit (Zymoresearch). Positive clones were confirmed with restriction enzyme mapping and automated nucleotide sequencing using a BigDye[®] Terminator v3.1 Cycle Sequencing kit (Applied Biosystems).

3.2.5.4. Estimation of dimer dissociation constants

To estimate the order of magnitude of the dissociation constant (K_d) of the *PfAdoMetDC* dimer (M. Williams and [191]) for comparison to other AdoMetDCs, the relative peak heights (and not areas due to peak overlaps) of the monomeric and dimeric proteins in the non-reducing SEC elution profiles (at concentrations of 1 mg/ml and 4 mg/ml of the wild-type and C505S mutant *PfAdoMetDC* proteins) were assumed to approximately represent the relative proportions of monomer and dimer in the samples (X_M and X_D for monomer and dimer, respectively). Since the total amount of protein loaded was known the concentrations of the monomeric and dimeric proteins could be determined based on their relative proportions as analysed with SEC according to the following equations:

$$[M] = [C] \times X_M, [D] = \frac{M_0 - [M]}{2} = \frac{[C] \times X_D}{2}$$

Where M_0 is the total molar concentration, C is the protein concentration applied to the column in μ M, and [M] and [D] are the molar concentrations in μ M of the monomer and dimer, respectively.

Assuming simple monomer-dimer equilibrium (including Cys505 covalently-linked dimers) the dissociation constant of the dimeric protein could then be calculated by using the following formula:

$$K_a = \frac{[D]}{[M][M]} = \frac{1}{K_d}$$

Where K_d is the dissociation constant in units M and the association constant (K_a) in units M^{-1} is calculated by taking the inverse of K_d .

If the total protein concentration in a protein sample is known, the proportion of the monomeric form of the protein could subsequently be calculated as follows:



$$\frac{[M]}{M_0} = \frac{-1 \pm \sqrt{1 + 8(K_a)(M_0)}}{4(K_a)(M_0)}$$

Where $[M]/M_0$ is the proportion of the monomeric form of the protein and M_0 is the total molar concentration in units M.

3.2.5.5. Analyses of protein hydrodynamic radius with Dynamic Light Scattering

Dynamic light scattering (DLS) was used to determine the hydrodynamic radius of the *PfAdoMetDC* and C505S mutant proteins as an indication of their oligomeric status. Fractions of the *PfAdoMetDC* and C505S mutant proteins collected after SEC were pooled and concentrated to 2.8-6 mg/ml. Reduced *PfAdoMetDC* was also analysed by treatment with 10 mM DTT prior to the DLS measurement. Additionally, DLS provides information on sample homogeneity as given by the polydispersity index (PDI). Immediately prior to measurements, the samples were centrifuged for 10 min at 10 000g to remove any aggregates. DLS was measured with the default settings of the Nanoziser Nano S instrument (Malvern Instruments). A 3 mm precision cell cuvette (Hellma) was used in which the protein samples with volumes of 15 μ l were pre-equilibrated for 5 min at 20°C prior to the measurement. The theoretical R_H assuming globular protein shape were calculated with the Zetasizer Nano software v6.01 using default settings to determine the particle size distribution as given by the volume intensity plot.

3.2.6. Secondary structure analysis of *PfAdoMetDC* using far-UV CD spectroscopy

The *PfAdoMetDC* and C505S mutant proteins in wash buffer collected from SEC were dialyzed against a phosphate buffer (10 mM KH_2PO_4 pH 7.7, 50 mM NaF) for 3 h at 4°C due to the optical activity of Cl^- ions in the far-UV range [196]. Dialysis was performed using Slide-A-Lyzer[®] mini dialysis units (Thermo Scientific) each containing 150 μ l of the protein sample. Following dialysis the concentrations of the samples were determined using protein absorbance at 280 nm and a molar extinction coefficient of 69110 $\text{M}^{-1} \text{cm}^{-1}$.

The far-UV spectra of the *PfAdoMetDC* and C505S mutant proteins (0.5 mg/ml or 7.3 μ M) were determined with the JASCO J815 CD instrument. Measurements were conducted in 1 mm cuvettes at a wavelength range of 190 to 250 nm at 20°C, using a wavelength interval of 0.5 nm, a bandwidth of 1 nm and a scanning speed of 20 nm/min. Two readings were accumulated per sample, buffer spectra were subtracted and the data points were averaged. The molar ellipticity ($[\theta]_M$) of each data point in units $\text{deg cm}^2 \text{dmol}^{-1}$ was calculated as follows according to Bale *et al.* [185]:



$$[\theta]_M = \frac{\Delta\theta \times MW}{10 \times l \times C}$$

Where $\Delta\theta$ is the reading in degree, MW is the molecular weight of the protein in g/mol, l is the path length in cm and C is the concentration of the protein in mg/ml.

The contribution of secondary structures were calculated with CDtool v1.4 [197].

3.2.7. Analyses of residues involved in the autocatalytic processing reaction

The alignment of the *PfAdometdc* gene sequence with the sequences from various organisms was previously performed by Wells *et al.* [120]. The corresponding residues involved in the processing of plant and human AdoMetDCs were identified and subsequently mutated on the gene sequence to determine if these play similar roles in the plasmodial protein. For all mutagenesis reactions partially harmonised *PfAdometdc/Odc* cloned into the pASK-IBA3 plasmid was used as template. The mutagenesis primers are listed in Table 3.2. Phusion DNA Polymerase (Finnzymes) was used in the presence of 6 fmol template and 10 pmol of each of the primers. Temperature cycling was performed as follows: 95°C for 3 min followed by 25 cycles of 96°C for 30 s, 56°C for 30 s, 68°C for 5 min with a final extension step at 68°C for 10 min. Post-PCR manipulation was performed as described previously [195].

Table 3.2: Primers used for the mutagenesis of residues predicted to be involved in the autocatalytic processing reaction of *PfAdoMetDC*

Primer	Mutant name	Sequence (5' to 3') ^a
R11L_F	<i>PfAdoMetDC</i> -R11L	GGCATTGAAAAACT <u>CGTTGTC</u>
R11L_R		GACAACGAGTTTTTCAATGCC
S421A_F	<i>PfAdoMetDC</i> -S421A	CCATGCGGCTAC <u>GCCTGTAACG</u>
S421A_R		CGTTACAG <u>GCGTAGCCGCATGG</u>

^a Mutations are underlined.

3.2.8. *PfAdoMetDC* enzyme and inhibition kinetics

The substrate affinity constant as well as V_{max} of the *PfAdoMetDC* protein was determined using the Michaelis-Menten kinetic model. A substrate dilution series ranging from 12.5 to 800 μ M were used to set up a Michaelis-Menten curve. Three independent experiments were performed in duplicate using the enzyme assay described above and the results were analysed with GraphPad Prism v5.0 (GraphPad Software, Inc.).

The linear Hanes-Woolf plot of substrate concentration ($[S]$)/velocity (v) versus $[S]$ was used to determine the K_m and V_{max} values [198]. The linear equation was obtained by a rearrangement of the Lineweaver-Burk equation:



$$\frac{[S]}{v} = \frac{[S]}{V_{\max}} + \frac{K_m}{V_{\max}}$$

Where the slope of the plot is equal to $1/V_{\max}$, the intercept on the $[S]/v$ axis gives K_m/V_{\max} and the intercept on the $[S]$ axis gives $-K_m$.

The inhibition kinetics of *PfAdoMetDC* for two different substrate analogues, namely MDL73811 and CGP48664 were also repeated and compared with previous results of the monofunctional wt*PfAdoMetDC*-hinge protein [71]. Based on literature studies and the mechanisms of inhibition of these two substrate analogues, irreversible and Michaelis-Menten kinetics were applied for MDL73811 and CGP48664, respectively [71].

The rate of enzyme inactivation by the irreversible MDL73811 inhibitor was followed by measurement of residual activity after fixed time intervals (0, 2, 4 and 6 min) of exposure to the inhibitor. *PfAdoMetDC* enzyme (1 μg , 60 nM) was mixed with 0.1, 0.2 and 0.5 μM MDL73811 in the assay buffer at time point zero (25 μl), incubated at 37°C, stopped by transfer to ice and added to the reaction tubes containing 400 μM total AdoMet in a total volume of 225 μl . The reactions were subsequently incubated at 37°C for 30 min after which the experiment was carried out as before to determine the remaining enzyme activity after inhibition. The Kitz-Wilson method was used to determine the efficiency of the inhibitor [199]. The inhibition with time at the different inhibitor concentrations ($[I]$) were plotted against time as follows:

$$\ln \frac{E(t)}{E(0)} = \frac{-k_{\text{inact}} \times t}{1 + \frac{K_i}{[I]}} = -k_{\text{app}} \times t$$

Where $E(t)$ is the maximal enzyme activity following pre-incubation with the inhibitor for time interval t ; $E(0)$ is the maximal enzyme activity following pre-incubation in the absence of inhibitor; and k_{app} is the slope obtained when the left hand side of the equation is plotted against time.

A secondary plot of the reciprocal of the k_{app} value ($-1/\text{primary slope}$) for each $[I]$ against the reciprocal of $[I]$ resulted in a straight line from which the k_{inact} and K_i values could be determined by the intercept and slope, respectively [198,200].

The inhibition of *PfAdoMetDC* with CGP48664 was tested with the use of different substrate (100 to 800 μM) and inhibitor (2.5 to 10 μM) concentrations. These results were plotted on a typical Michaelis-Menten to obtain several hyperbolic curves for each $[I]$ incubation at increasing $[S]$. The enzyme (1 μg , 60 nM) was incubated with 0, 2.5, 5 and 10 μM CGP48664 at each of the $[S]$ for 30 min at 37°C to determine the remaining enzyme activity.



3.3. Results

3.3.1. Codon harmonisation improves the purity and stability of monofunctional *PfAdoMetDC*

The 660-residue wt*PfAdoMetDC*-hinge protein expressed from the unharmonised gene contains an N-terminal Strep-tag while the 572-residue *PfAdoMetDC* protein expressed from the harmonised *PfAdometdc* gene contains a C-terminal Strep tag (Figure 3.1D and E). In this way the tag remains attached to the larger α -subunit after processing has occurred and is therefore not situated in proximate position of the active site co-factor (as is the case for the N-terminally tagged wild-type protein). Although not tested, the position of the Strep-tag may have an influence on enzyme activity but since the aim of this study was to obtain a high amount of pure, active protein a comparative study of the position of the tags were not considered.

Initially, only the first third of the bifunctional *PfAdometdc/Odc* gene was harmonised, which corresponds to the core of the monofunctional *PfAdoMetDC* domain (Figure 3.1B, residues 1-487). Since the exact start site of the hinge region is unknown due to low sequence homology [120], an additional 255 nucleotides of the wild-type sequence (encoding residues 488-572) were added to obtain the harmonised *PfAdometdc* fragment (Figure 3.1E, *PfAdometdc* pASK-IBA3). In addition, to allow for a comparative analysis of the monofunctional construct created here and a previous study on the monofunctional protein (Figure 3.1D, wt*PfAdoMetDC*-hinge, residues 1-660) [71], a second expression construct was created to encode a 660-residue *PfAdoMetDC*-hinge protein where residues 1-487 are encoded by the harmonised codons (Figure 3.1F, *PfAdometdc-hinge* pASK-IBA3).

The *PfAdoMetDC*, *PfAdoMetDC*-hinge and wt*PfAdoMetDC*-hinge proteins were expressed in BL21 Star™ *E. coli*. Figure 3.2 shows the results obtained when the expression of these three proteins were compared. In each case, two subunits are expected to separate with the denaturing conditions of SDS-PAGE as a result of *PfAdoMetDC* autocatalytic processing. These include the smaller ~9 kDa β -subunit (not resolved with the 7.5% acrylamide gel) and the larger α -subunit. The different lengths of the expressed proteins will be reflected by the sizes of the α -subunits; for the 572-residue *PfAdoMetDC* protein (Figure 3.2, top right) this subunit is predicted to have a size of ~61 kDa while the *PfAdoMetDC*-hinge proteins (expressed from wild-type, top left, and harmonised genes, bottom right) would have α -subunits that are ~10 kDa larger. For the latter two proteins a difference would additionally be the positions of the Strep-tags as shown in the diagrams (Figure 3.2, inset figures).

Expression of the wt*PfAdoMetDC*-hinge protein resulted in the presence of the ~70 kDa processed protein (Figure 3.2A, lane 1, band b) where the β -subunit at the N-terminus (containing the Strep-tag) dissociates from the larger α -subunit and was therefore not resolved with the applied denaturing PAGE conditions. However, wt*PfAdoMetDC*-hinge co-purified with an approximately equal amount of *E. coli* heat shock protein 70 (Hsp70) as identified with LC-MS/MS (Figure 3.2A, lane 1, band a), even after extensive optimisation of various conditions during protein expression and purification. Malarial proteins expressed in *E. coli* are often co-purified with HSPs, which gives an indication of the stress that is placed on the system during folding of these proteins [190].

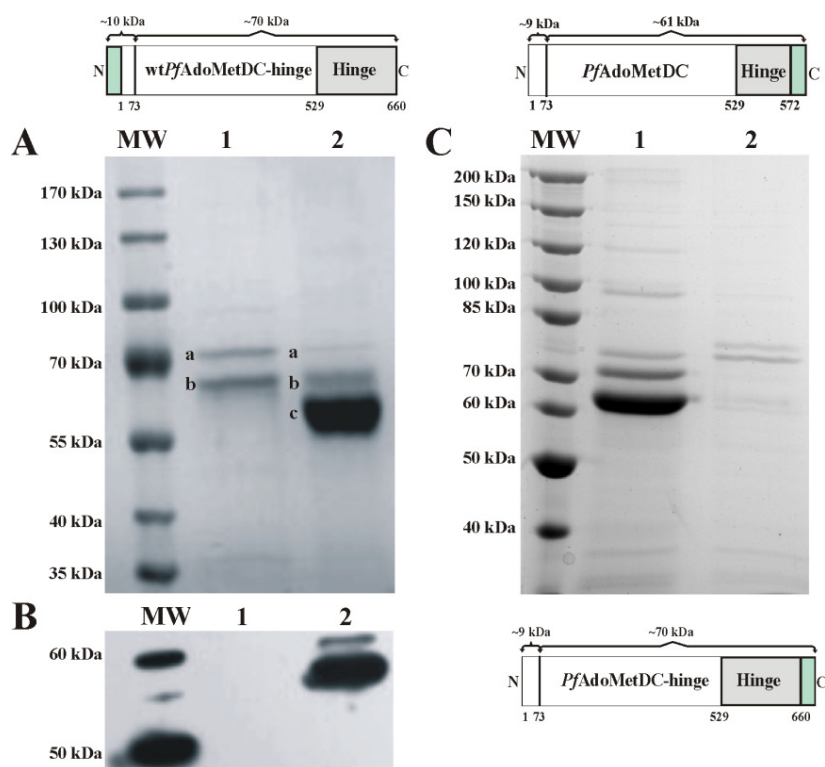


Figure 3.2: SDS-PAGE analyses of *PfAdoMetDC*, *PfAdoMetDC*-hinge and wt*PfAdoMetDC*-hinge proteins followed by Western immunodetection of these recombinantly expressed monofunctional proteins.

(A) SDS-PAGE analysis of wt*PfAdoMetDC*-hinge and *PfAdoMetDC* proteins. MW: PageRuler Prestained Protein Ladder; lane 1: wt*PfAdoMetDC*-hinge protein expressed from the wild-type, unharmonised gene; band a: Hsp70; band b: α -subunit of wt*PfAdoMetDC*-hinge. Lane 2: *PfAdoMetDC* protein expressed from the harmonised gene; band a: Hsp70; band b: unprocessed *PfAdoMetDC* protomer; band c: α -subunit of *PfAdoMetDC*. (B) Western immunodetection of wt*PfAdoMetDC*-hinge (lane 1) and *PfAdoMetDC* (lane 2) proteins with a Strep-tag antibody. (C) SDS-PAGE analyses of the *PfAdoMetDC* (lane 1) and *PfAdoMetDC*-hinge (lane 2) proteins expressed from harmonised genes. The schematic diagrams of the three proteins are also included to show the predicted sizes of the α - and β -subunits of each as well as the positions of the Strep-tags (light green boxes).

PfAdoMetDC separates as a ~61 kDa α -subunit and a ~9 kDa β -subunit and resulted in an almost 10-fold improvement in yield (39.6 $\mu\text{g/ml}$ versus 385.1 $\mu\text{g/ml}$) of the affinity-purified protein compared to total protein yield obtained for the wt*PfAdoMetDC*-hinge protein. Of this,



particularly the ~61 kDa processed form of the protein was present, proven by LC-MS/MS analyses to consist of only *PfAdoMetDC* (Figure 3.2A, lane 2, band c). This protein expressed from the harmonised construct is therefore in a more pure form at a higher yield. However, the results showed that a fraction of the *PfAdoMetDC* protein was present in its unprocessed ~70 kDa protomeric form (Figure 3.2A, lane 2, band b). A decrease in co-purification of contaminating Hsp70 was also observed (Figure 3.2A, lane 2, band a).

Western immunodetection using a Strep-tag antibody confirmed the presence of the *PfAdoMetDC* protein (Figure 3.2B, lane 2), while no protein was identified for wt*PfAdoMetDC*-hinge due to the cleaved ~10 kDa β -subunit with the N-terminal Strep-tag, which was not resolved on this gel (Figure 3.2B, lane 1).

In comparison to *PfAdoMetDC*, expression of the *PfAdoMetDC*-hinge protein yielded much less protein (40.3 μ g/ml), which is similar to the yield obtained for the wt*PfAdoMetDC*-hinge protein. SDS-PAGE analysis showed the presence of two major bands that, in the absence of LC-MS/MS analyses, could represent the processed (~70 kDa) and unprocessed (~79 kDa) forms of the protein and/or Hsp70 (Figure 3.2C, lane 2).

3.3.2. Refolding of *PfAdoMetDC* from inclusion bodies yields a significant amount of unprocessed protein

Protein purification from the soluble extracts of the proteins expressed from codon-harmonised genes (*PfAdometdc* and *PfAdometdc-hinge*) indicated that in the heterologous expression system the processing reaction was not 100% efficient since the unprocessed form of the *PfAdoMetDC* protein was retrieved (Figure 3.2A, lane 2, band b). Subsequent SDS-PAGE analyses of the proteins obtained from the insoluble protein extract showed that an appreciable amount of *PfAdoMetDC* is expressed as insoluble protein (Figure 3.3A) while, in comparison to the protein preparation from the soluble extract (Figure 3.2C), most of *PfAdoMetDC*-hinge was expressed as insoluble protein in inclusion bodies (Figure 3.3B).

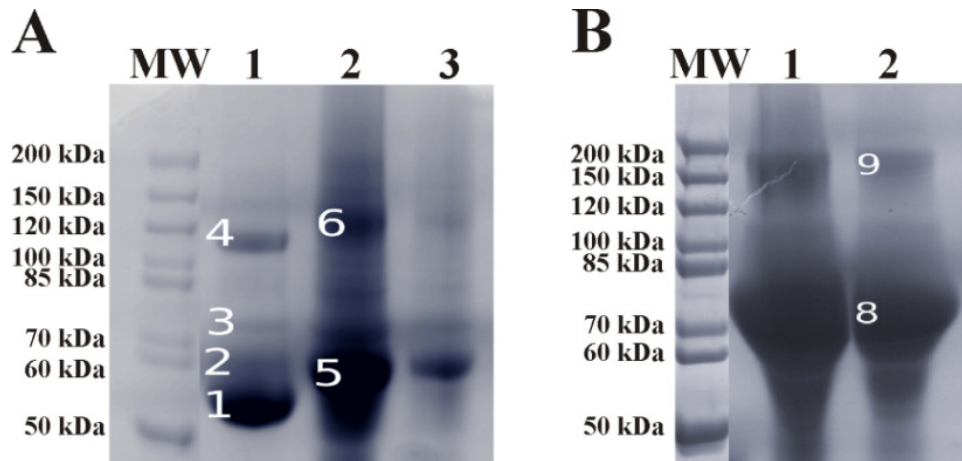


Figure 3.3: Non-reducing SDS-PAGE analyses of the insoluble protein extracts of expressed (A) *PfAdoMetDC* and (B) *PfAdoMetDC*-hinge proteins.

The insoluble protein extracts of (A) *PfAdoMetDC* and (B) *PfAdoMetDC*-hinge were collected after ultracentrifugation of the lysed expression cells. The numbers indicate the proteins that were identified with MALDI-MS (section 3.3.4.1). MW: PageRuler Unstained Protein Ladder. Gel (A) lane 1: *PfAdoMetDC* isolated from the soluble protein extract with Strep-tag affinity chromatography; lane 2: sample from the insoluble protein pellet after expression of *PfAdoMetDC*; lane 3: 10-fold dilution of the insoluble protein pellet in lane 2. Gel (B) lane 1: sample from the insoluble protein pellet after expression of *PfAdoMetDC*-hinge and lane 2: 10-fold dilution of the insoluble protein pellet in lane 1.

The refolding and purification of the monofunctional *PfAdoMetDC* and *PfAdoMetDC*-hinge proteins within the insoluble inclusion bodies were subsequently performed by applying the method of Sirawaraporn *et al.* [192] to determine if correct refolding under favourable *in vitro* conditions could lead to efficient processing of *PfAdoMetDC* into the active form of the protein. Concurrently, proteins were also isolated from the soluble protein extracts for comparison. The yields that were obtained per litre of protein culture for each protein preparation are listed in Table 3.3.

Table 3.3: Yields obtained for the *PfAdoMetDC* and *PfAdoMetDC*-hinge proteins isolated from soluble and insoluble protein extracts

Protein preparation	Concentration (mg/ml)	Yield (mg)
<i>PfAdoMetDC</i> soluble	0.71	4.26
<i>PfAdoMetDC</i> insoluble	0.28	1.68
<i>PfAdoMetDC</i> -hinge soluble	0.22	1.32
<i>PfAdoMetDC</i> -hinge insoluble	0.37	2.22

The highest yield obtained was for the *PfAdoMetDC* protein isolated from the soluble protein extract but another 1.68 mg could be recovered from the insoluble extract (Table 3.3). For *PfAdoMetDC*-hinge more protein could be isolated from the insoluble protein extract, which represented a promising result since a low protein yield was isolated from the soluble fraction presumably due to the presence of the hinge region (Figure 3.2C).

SDS-PAGE analyses showed that the purification of the *PfAdoMetDC* and *PfAdoMetDC*-hinge proteins from the inclusion bodies resulted in the successful retrieval of protein. For *PfAdoMetDC* a single protein band with a size of ~70 kDa was observed (Figure 3.4A, lane 5) while a band at ~79 kDa was observed for the *PfAdoMetDC*-hinge sample (Figure 3.4A, lane 6). The sizes of these bands indicated the presence of only the unprocessed protomers in both samples. In the absence of Hsp70, other contaminating proteins were co-purified, which could probably be removed with secondary purification steps. In order to ascertain that only the unprocessed proteins were purified, SDS-PAGE with a higher acrylamide % gel was also performed. These results showed that, compared to the soluble expression of *PfAdoMetDC* (Figure 3.4B, lane 1), the ~9 kDa subunits were absent in both protein samples obtained from the inclusion bodies (Figure 3.4B, lanes 2 and 4) and indicates that the conformation of the proteins were not correct to allow processing to occur via the Arg11-Lys15-Lys215 triad [120].

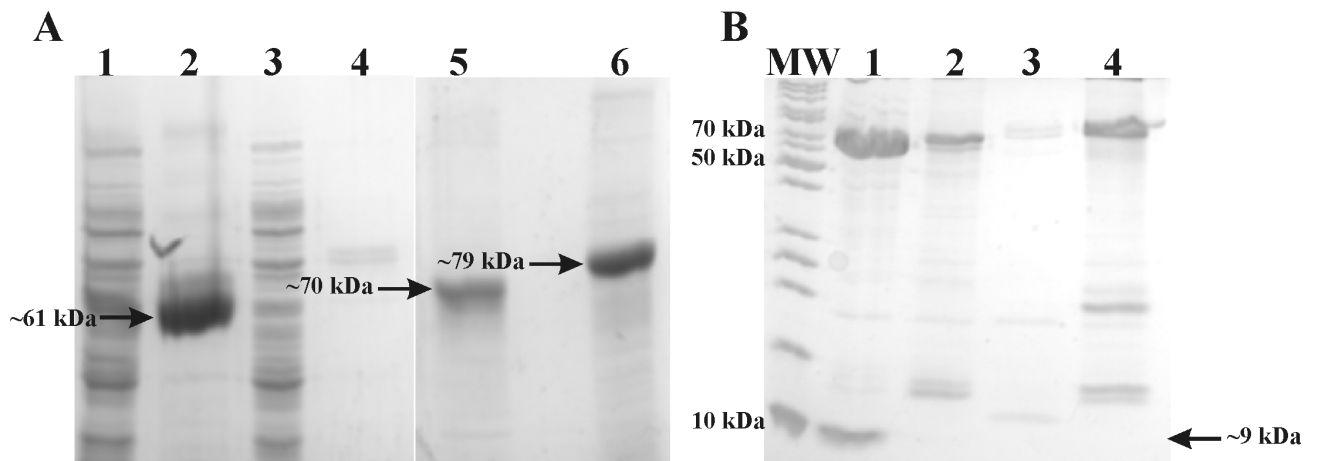


Figure 3.4: Purification of *PfAdoMetDC* and *PfAdoMetDC*-hinge from inclusion bodies and visualisation on 7.5% (A) and 12.5% (B) SDS-PAGE gels.

Gel (A) lane 1: *PfAdoMetDC* total soluble; lane 2: Strep-tag purified *PfAdoMetDC* from soluble extract; lane 3: *PfAdoMetDC*-hinge total soluble; lane 4: Strep-tag purified *PfAdoMetDC*-hinge from soluble extract; lane 5: Strep-tag purified *PfAdoMetDC* refolded from insoluble extract; lane 6: Strep-tag purified *PfAdoMetDC*-hinge refolded from insoluble extract. Gel (B) MW: PageRuler Unstained Protein Ladder; lane 1: Strep-tag purified *PfAdoMetDC* from soluble extract; lane 2: Strep-tag purified *PfAdoMetDC* refolded from insoluble extract; lane 3: Strep-tag purified *PfAdoMetDC*-hinge from soluble extract; lane 4: Strep-tag purified *PfAdoMetDC*-hinge refolded from insoluble extract. The sizes of the protein bands are indicated with arrows.

3.3.3. *PfAdoMetDC* enzyme activity and protein stability

Due to these disappointing results obtained for the *PfAdoMetDC*-hinge protein isolated from the soluble extract, subsequent experiments were performed on *PfAdoMetDC* for its comparison to the expression of the wt*PfAdoMetDC*-hinge protein.

PfAdoMetDC has a specific activity of 140 ± 8 nmol/min per nmol protein compared to wt*PfAdoMetDC*-hinge with an activity of 88 ± 4 nmol/min/nmol (of which approximately half of



the protein sample is Hsp70, Figure 3.2A). Furthermore, *PfAdoMetDC* appeared to be a more stable enzyme than *wtPfAdoMetDC-hinge* since this enzyme remained active when stored for two weeks at 4 and -20°C. In contrast, *wtPfAdoMetDC-hinge* activity was significantly reduced by 16% and 55% (n=2, $P<0.05$) at 4 and -20°C, respectively (Table 3.4).

Table 3.4: Comparison of the *PfAdoMetDC* and *wtPfAdoMetDC-hinge* enzyme activities after storage for two weeks at different temperatures

Mean specific activities in nmol/min/per nmol protein were determined from two independent experiments carried out in duplicate (n=2) and are shown with \pm S.E.M.

Enzyme	Day 1	Day 14 (4°C)	Day 14 (-20°C)
<i>PfAdoMetDC</i>	140 \pm 8	165.8 \pm 2.8	184 \pm 9
<i>wtPfAdoMetDC-hinge</i>	88 \pm 4	74 \pm 10	39.7 \pm 1.5

DSF was subsequently performed to determine if the stability of the *PfAdoMetDC* protein could be improved with a specific buffer system for efficient protein storage. The DSF results showed a general decrease in the T_m of *PfAdoMetDC* with an increase in buffer pH. Buffers containing MES, ammonium acetate or BisTris propane at a pH ~6.0 promoted protein stability to the same extent, and the addition of glycerol did not result in improved protein stabilisation (results not shown). These results were subsequently compared to the dialysis buffer (50 mM Tris/HCl, pH 8.0, 150 mM NaCl) to determine if a difference in protein stability exists with this buffer compared to the most promising buffer identified with DSF (0.4 M MES, pH 6.0, 0.6 M NaCl). The results showed that the T_m of the protein in a buffer where the pH was increased from 6.0 to 8.0 or where Tris/HCl in the dialysis buffer was exchanged with BisTris propane remained similar (62°C versus 61°C) and a different buffer system was therefore not considered for future experiments in which a stable protein is required.

The subsequent co-incubation of *PfAdoMetDC* with two substrate analogues, MDL73811 or CGP48664, showed that molar excesses of either analogue increased the T_m from 62°C to 66°C compared to the apo-protein with a T_m of 62°C (Figure 3.5). These results indicated improved protein stability for the ligand-bound form of the protein.

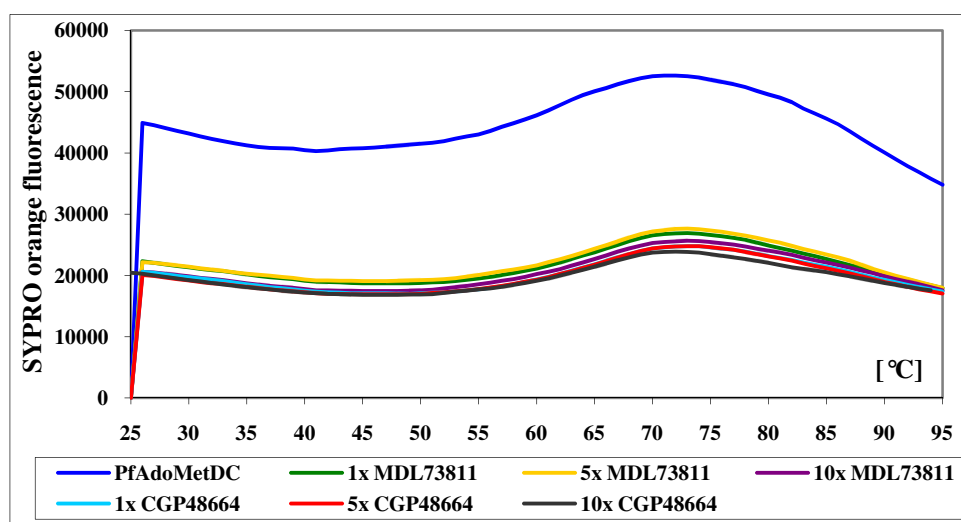


Figure 3.5: Fluorescence intensity curves obtained upon incubation of *PfAdoMetDC* with different molar excesses of MDL73811 and CGP48664.

Incubation of *PfAdoMetDC* (1.3 μ M) in dialysis buffer with MDL73811 and CGP48664 at three different molar excesses (1x, 5x and 10x) of the substrate analogues were tested to determine their effect on the protein's stability as recorded by the T_m . Fluorescence intensities of the SYPRO orange dye bound to the hydrophobic surfaces of the protein were obtained while the temperature was increased from 25°C to 95°C [193].

3.3.4. Determination of the oligomeric status of monofunctional *PfAdoMetDC*

Purification of the *PfAdoMetDC* protein with affinity chromatography allowed further analyses with SEC to determine its oligomeric status. A Superdex S200 column was calibrated from which a calibration curve with a regression coefficient of $R^2=0.98$ could be obtained. Strep-tag purified *PfAdoMetDC* protein separated by SEC is expected to elute at a V_e of the dimeric protein (~140 kDa) in the elution fraction range 12-13 ml (V_e/V_o of ~1.5-1.625) while the monomer (~70 kDa) is expected to elute between 14 and 15 ml (V_e/V_o of ~1.75-1.875).

Concentration-dependent monomer-dimer equilibrium is evident for *PfAdoMetDC* since at 1 mg/ml both monomeric (V_e/V_o of 1.77, calculated MW of ~85 kDa) and dimeric (V_e/V_o of 1.59, calculated MW of ~120 kDa) forms of the protein are present (Figure 3.6A, solid line). At a 4-fold higher concentration of the protein and in the absence of DTT, the proportion of the dimeric fraction (V_e/V_o of 1.60, ~114 kDa) increases relative to that of the monomer (V_e/V_o of 1.73, ~87 kDa). (Figure 3.6A, dotted line). Apart from the peak representing aggregated protein at the void volume (8 ml), a larger oligomer also forms at the shoulder of the dimeric protein peaks (V_e/V_o of 1.44, ~180 kDa) at both protein concentrations tested and could represent a trimeric form of the protein.

Dimerisation as a result of the oxidising conditions was subsequently analysed with the addition of 10 mM DTT to the protein (3-5 mg/ml) prior to SEC, which resulted in a significant shift from

a dimer at an V_e of 12.8 ml (V_e/V_o of 1.61, ~131 kDa) to the monomeric form with an V_e of 13.4 ml (V_e/V_o of 1.68, ~99 kDa) (Figure 3.6B, solid line). A protein sample collected from the dimeric protein peak and visualised with non-reducing SDS-PAGE showed that the intensity of the dimeric protein band was vastly reduced when 10 mM DTT was added to the sample buffer and confirmed the shift of the dimer to the monomeric form under reducing conditions (Figure 3.6C). These results showed that increasing the concentration of the *PfAdoMetDC* protein increased the proportion of the dimeric protein relative to that of the monomer while higher oligomeric forms are also formed. However, both the SDS-PAGE and SEC results show a slight increase in the apparent molecular weight of the reduced protein compared to the non-reduced monomeric protein, which was also confirmed by DLS (see below). The increased proportion of dimeric *PfAdoMetDC* under non-reducing conditions suggests the involvement of Cys residue/s on the protein surface in disulphide bond/s formation between the *PfAdoMetDC* monomers, which is enhanced when the protein is present at concentrations >1 mg/ml.

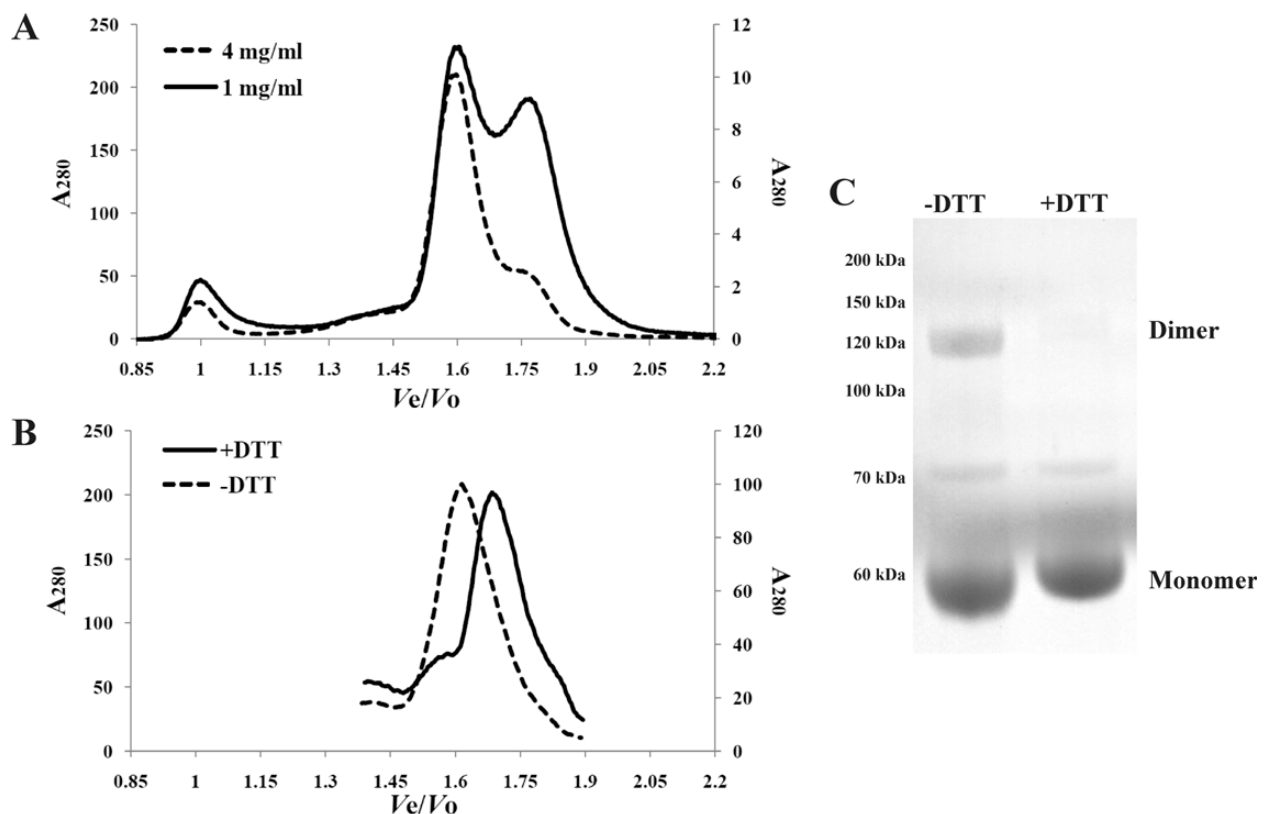


Figure 3.6: Analyses of the oligomeric status of monofunctional *PfAdoMetDC* with SEC.

(A) The *PfAdoMetDC* protein purified with Strep-tag affinity chromatography at concentrations of 1 mg/ml and 4 mg/ml were separated with SEC. The fractions corresponding to the dimeric and monomeric proteins are indicated. The V_e/V_o values are shown on the X-axis while the Y-axes on the left and right of the graph shows the absorbance at 280 nm for the higher or lower concentrated protein samples, respectively. (B) Reducing SEC was performed in the presence or absence of 10 mM DTT, followed by visualisation with non-reducing SDS-PAGE of the 4 mg/ml protein sample in the presence or absence of 10 mM DTT (C). The sizes of the protein ladder as well as the positions of the dimeric and monomeric proteins are shown. Lane 1: no DTT and lane 2: 10 mM DTT included in sample buffer.



Stabilisation of the monomeric form of the protein under reducing conditions was confirmed with DLS analyses. Treatment of *PfAdoMetDC* with DTT reduced the R_H and therefore the size of the protein. The protein sample showed radii of 7.33 nm and 9.07 nm in the presence and absence of DTT, respectively (Table 3.5). This corresponds to a decrease of ~20% in both *PfAdoMetDC* protein diameter and PdI, indicating a fairly monodisperse protein sample since DTT causes a shift in the equilibrium from the dimer to the monomer.

Table 3.5: Hydrodynamic radii of *PfAdoMetDC* in the presence and absence of DTT as determined by DLS

PfAdoMetDC samples at a concentration of 2.8 mg/ml with and without DTT were analysed by DLS and the level of polydispersity was indicated by the PdI value.

Protein sample	Concentration (mg/ml)	R_H (nm)	PdI
<i>PfAdoMetDC</i> -DTT	2.8	9.07	0.23
<i>PfAdoMetDC</i> +DTT	2.8	7.33	0.18

These results suggest that disulphide linkage either induces changes in protein conformation, which is not readily reversed by DTT treatment alone or reflects the average radius of a mixture of the monomeric and dimeric forms of the protein. Alternatively, the increase in protein apparent size could be due to DTT binding to the protein [201,202] although the likelihood that reduction of inner disulphide bonds by DTT that could affect a shape change from e.g. globular to a more expanded and thus a larger size protein [203], cannot be excluded.

3.3.4.1. Cys505 stabilises *PfAdoMetDC* dimerisation

Inspection of the proposed dimer interface of the *PfAdoMetDC* homology model [120] showed the possible involvement of Cys505 from each monomer in disulphide bond formation. This residue is not conserved amongst the AdoMetDCs but structure-based sequence alignment indicated that residue Cys505, which is located on the β 15 strand at the proposed dimer interface of *PfAdoMetDC*, could form a disulphide bond with the same residue from a second monomer. Cys505 in *P. falciparum* AdoMetDC corresponds to Gln311 in the human protein. Gln311 is also located on the β 15 strand at the dimer interface of the human protein with a distance of 6.68 Å between the C_δ atoms and, considering the distance between the residues, could theoretically also form a disulphide bond if replaced by Cys residues as in *PfAdoMetDC*.

To ascertain if Cys505 mediated disulphide bond formation resulting in the appearance of dimeric proteins under oxidising conditions, MALDI-MS peptide mass fingerprinting was performed on the ~120 kDa SDS-resistant dimeric band (Figure 3.7, lane C, band 7), which was

treated with iodoacetamide prior to trypsin digestion both in the presence and in the absence of DTT. Exposed Cys residues would thereby be modified by alkylation while residues involved in disulphide bonds (and not treated with DTT) should be protected resulting in corresponding peptide mass differences. As a control for non-disulphide linked proteins, the monomeric ~61 kDa band was also analysed (Figure 3.7, Lane C, band 4). The MALDI-MS peptide mass fingerprints of the ~120 kDa dimeric band in Figure 3.7 without reduction prior to alkylation was compared to the fingerprints of the dimeric and monomeric bands that were reduced and alkylated after purification from SDS-PAGE.

The results confirmed that the carbamidomethyl-modified Cys505 residue could only be identified in the reduced, alkylated condition and in the mass spectrum of the monomeric band (Figure 3.7). Furthermore, no peptide fragments containing alkylated Cys47, 143, 418, 454 and 481 were identified as these are, like Cys505, surface-localised based on the *PfAdoMetDC* homology model (results not shown) [120].

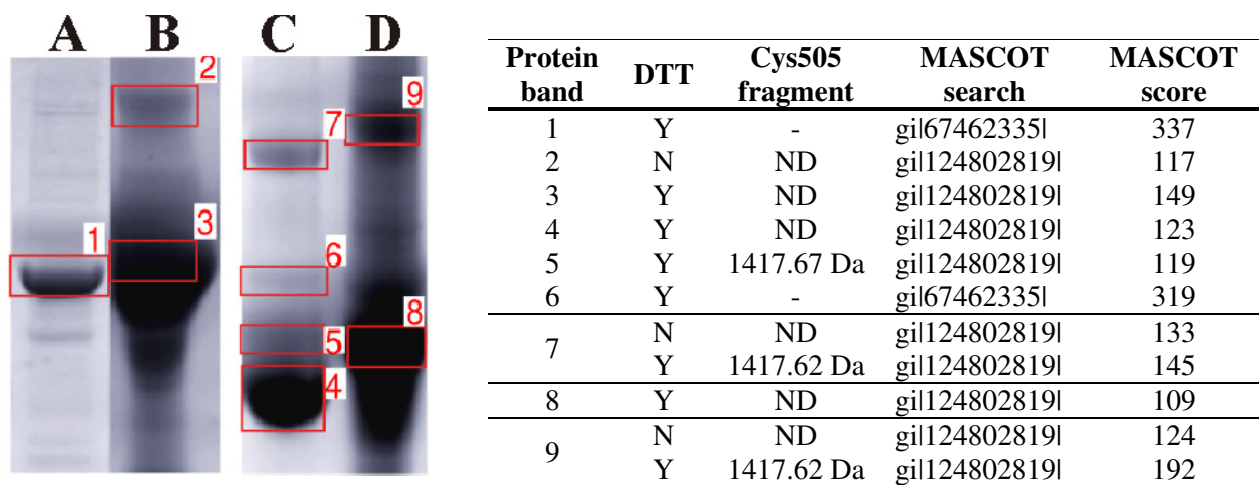


Figure 3.7: Protein gel bands of the *PfAdoMetDC* and *PfAdoMetDC*-hinge proteins that were analysed with MALDI-MS.

Proteins that were eluted for trypsin digestion were extracted from two gels. Lane A: *PfAdoMetDC*-hinge purified with Strep-tag affinity chromatography (band 1); Lane B: the insoluble protein extract after *PfAdoMetDC*-hinge expression (bands 2 and 3); Lane C: *PfAdoMetDC* purified with Strep-tag affinity chromatography (bands 4-7); and Lane D: the insoluble protein extract after *PfAdoMetDC* expression (bands 8 and 9). The protein bands are numbered and the results of the MALDI-MS analyses are shown in the table corresponding to each protein band. The addition of 10 mM DTT during protein preparation for analyses is indicated in the table as yes (Y) or no (N). The detection of a protein fragment containing Cys505 as an indication of a non-disulphide linked protein is indicated in the table as (-) not applicable for the Hsp70 protein, (ND) for not detected i.e. Cys505 could be involved in disulphide bond formation and if Cys505 was detected the size of the fragment in which it was identified is given i.e. as an indication that Cys505 could be in its reduced form in the presence of DTT. The gene accession numbers of the MASCOT search together with the MASCOT scores of the peptides are given as gil67462335l for *Hsp70 E. coli* and gil124802819l for *Adometdc/Odc P. falciparum*.

To further elucidate the possible involvement of Cys505 in disulphide bond formation, a mutant

protein was created in which this residue was changed to a Ser. While the expression level (Figure 3.8A) and specific activity of *PfAdoMetDC*-C505S was identical compared to the wild-type *PfAdoMetDC* (results not shown), the addition of DTT once again resulted in a larger apparent size of the protein (Figure 3.8A) compared to the non-reduced samples (Figure 3.8B) of both the wild-type and mutated monomeric proteins. Subsequent SEC of the mutant protein at a concentration of 1 mg/ml and under non-reducing conditions showed that the *PfAdoMetDC*-C505S protein occurs mainly in its monomeric form (V_e/V_o of 1.74) (Figure 3.8C, solid line). However, the equilibrium was again shifted towards dimer formation at a concentration of 4 mg/ml (V_e/V_o of 1.64) (Figure 3.8C, dotted line). These results indicate that the *PfAdoMetDC* protein is still able to dimerise even in the absence of covalently-linked dimers.

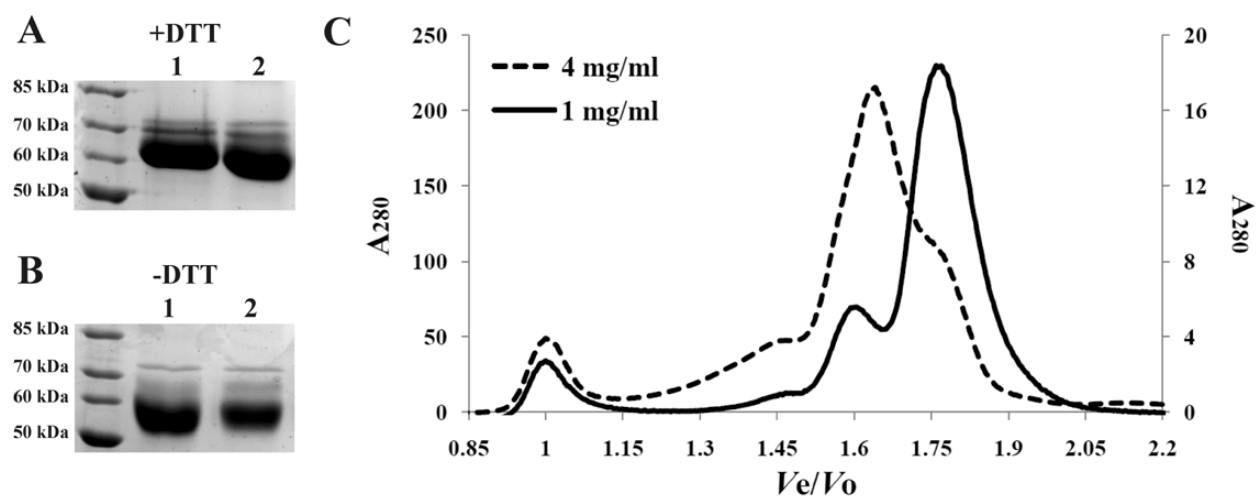


Figure 3.8: Analyses of the oligomeric status of the C505S mutant of *PfAdoMetDC* with SEC.

(A) Reducing and (B) non-reducing SDS-PAGE of the *PfAdoMetDC* (lane 1) and C505S mutant (lane 2) proteins. The sizes of the protein ladder are shown. (C) Analyses of the oligomeric status of the *PfAdoMetDC*-C505S mutant protein purified with *Strep-Tactin* affinity chromatography and at concentrations of 1 and 4 mg/ml with SEC. The V_e/V_o values are shown on the X-axis while the Y-axes on the left and right of the graphs show the absorbance at 280 nm for the higher and lower concentrated protein samples, respectively.

To gain further insight into the affect of the Cys505 mutation on protein dimerisation, DLS was performed to determine the particle size of the mutant protein. DLS showed a radius of 5.79 nm for the C505S mutant in the absence of DTT (3 mg/ml), while treatment of *PfAdoMetDC* at a concentration of 2.8 mg/ml with DTT only decreased the hydrodynamic radius from 9.07 to 7.33 nm (Table 3.5). The mutant protein therefore has a diameter 36% less than that of the wild-type protein, which indicates a smaller particle size of the mutant (Table 3.6). The results show that DTT treatment alone was not as effective as the C505S mutation in stabilising the monomeric form of the protein and therefore reflects an average radius of a mixture of the monomeric and dimeric forms of the wild-type protein resulting in a hydrodynamic radius of 7.33 nm.

**Table 3.6: Hydrodynamic radii of *PfAdoMetDC*-C505S at two different protein concentrations**

Protein sample	Concentration (mg/ml)	R_H (nm)	PdI
<i>PfAdoMetDC</i> -C505S	3	5.79	0.12
<i>PfAdoMetDC</i> -C505S	6.8	6.96	0.13

The more dilute *PfAdoMetDC*-C505S protein showed the smallest diameter as well as the lowest PdI (Tables 3.5 and 3.6) and increasing the protein concentration to 6.8 mg/ml only resulted in a slight increase in the PdI, which was still below that of the wild-type *PfAdoMetDC* protein (Table 3.5) and indicates good sample monodispersity.

3.3.4.2. Estimated dissociation constants of *PfAdoMetDC* and the C505S mutant

SEC results showed the presence of both monomeric and dimeric forms of the *PfAdoMetDC* and C505S mutant proteins. The peaks were not clearly separated but the peak maxima could be clearly identified. In the absence of analytical tools, the SEC results (Figures 3.6 and 3.8) were used to estimate a range of the dissociation constants for the two proteins while keeping in mind that equal amounts of the monomers and dimers were not present. Additionally, simple monomer-dimer equilibrium was assumed where, in the absence of DTT, residues Cys505 could form covalently-linked dimers in a slow, irreversible manner such that the true K_d of *PfAdoMetDC* would be slightly elevated in the presence of DTT.

Table 3.7 lists the relative proportions of the dimer and monomeric proteins for both *PfAdoMetDC* and the C505S mutant protein at concentrations of 1 mg/ml and 4 mg/ml as determined by analytical SEC. The apparent K_d values were found to be in the micromolar range, suggesting relatively weak propensity for dimer formation, with a higher tendency of *PfAdoMetDC* to dimerise than the C505S mutant (K_d value 87% less than that of the mutant) (Table 3.7). The K_d value of dimeric *PfAdoMetDC* in the absence of DTT (9.75 μ M) is a 300-fold higher than the estimated K_d of 33 nM for the human protein [185], showing a comparatively reduced propensity of the plasmodial protein to dimerise. However, this K_d value for *PfAdoMetDC* is similar to that of monomeric plant AdoMetDC (15.38 μ M), its nearest conserved orthologue which has been structurally characterised [184]. Upon concentration of the *PfAdoMetDC*-C505S mutant sample to 4 mg/ml, the K_d value decreased by 75% while the *PfAdoMetDC* protein's constant decreased by 42% (Table 3.7). In general, the K_d values of the *PfAdoMetDC* protein were less than the mutant, indicating that a single mutation at the dimer interface decreased the dimerisation propensity of *PfAdoMetDC*.

Table 3.7: Dissociation constants for *PfAdoMetDC* and the C505S mutant from analytical SEC

The relative proportions of the dimers and monomers for both the wild-type and C505S mutant *PfAdoMetDC* proteins at two different protein concentrations were obtained from SE chromatograms and used to estimate their dissociation constants. These were then compared to the dissociation constants of the confirmed dimeric human and monomeric plant *AdoMetDCs*.

Sample	Concentration		X_D	X_M	[D] (μM)	[M] (μM)	K_d (μM)	K_a (μM^{-1})	Reference
	mg/ml	μM							
<i>PfAdoMetDC</i>	1	14.65	0.53	0.42	3.88	6.15	9.75	0.1	-
	4	58.59	0.74	0.19	21.68	11.13	5.71	0.18	
<i>PfAdoMetDC</i> - C505S	1	14.65	0.22	0.74	1.61	10.84	72.98	0.014	-
	4	58.59	0.58	0.30	16.99	17.58	18.19	0.055	
Human			-				0.033	30.3	[185]
Plant			-				15.38	0.065	[184]

The concentrations of monomer [M] and dimer [D] were calculated as follows: $[M] = [C] \times X_M$, $[D] = \frac{M_0 - [M]}{2} = \frac{[C] \times X_D}{2}$. Where M_0 is the total molar concentration, X_M and X_D are the relative proportions of monomer and dimer, and C (μM) is the protein concentration applied to the SEC column. Assuming simple monomer-dimer equilibrium in the absence of a reducing agent, the apparent dissociation constant of the dimer could then be calculated as follows: $K_a = \frac{[D]}{[M][M]} = \frac{1}{K_d}$.

3.3.4.3. Disulphide-independent dimerisation of *PfAdoMetDC*

Despite the addition of a reducing agent and the mutagenesis of Cys505 at the proposed dimer interface of *PfAdoMetDC*, dimerisation of the protein was still observed, which indicates the presence of an additional dimerisation-mediated process. In the absence of *PfODC*, dimerisation of monofunctional *PfAdoMetDC* may be mediated by a hydrophobic patch on the *PfAdoMetDC* protein surface, which is natively involved in an interaction with the *PfODC* domain within the *PfAdoMetDC/ODC* complex. Based on extensive protein-protein docking results [152], such an interaction between two *PfAdoMetDC* monomers would therefore occur in a side-to-side fashion involving the α -helices that flank the $\alpha\beta\beta\alpha$ -sandwich fold and not the proposed dimer interface that occurs as an edge-on association of the β -strands. The results of docking the *PfAdoMetDC* domain to the *PfODC* domain and *vice versa*, identified the site on *PfAdoMetDC* where *PfODC* is most likely to bind [152]. The *PfAdoMetDC* residues that were predicted to interact with *PfODC* include Phe94, Phe98, Asp101, Phe159, Glu160, Gln161, Glu162, Tyr163, Phe174, Phe177 and Lys180 (Figure 3.9A). These residues are located on the α -helices flanking the core β -strands. In turn, the *PfODC* residues that are likely to interact with *PfAdoMetDC* have also been identified (Figure 3.9B). Interestingly, the latter predicted docking site is in proximate position to the highly conserved *PfODC* domain O1 parasite-specific insert, which was previously shown to mediate protein-protein interactions within the bifunctional complex (Chapter 2).

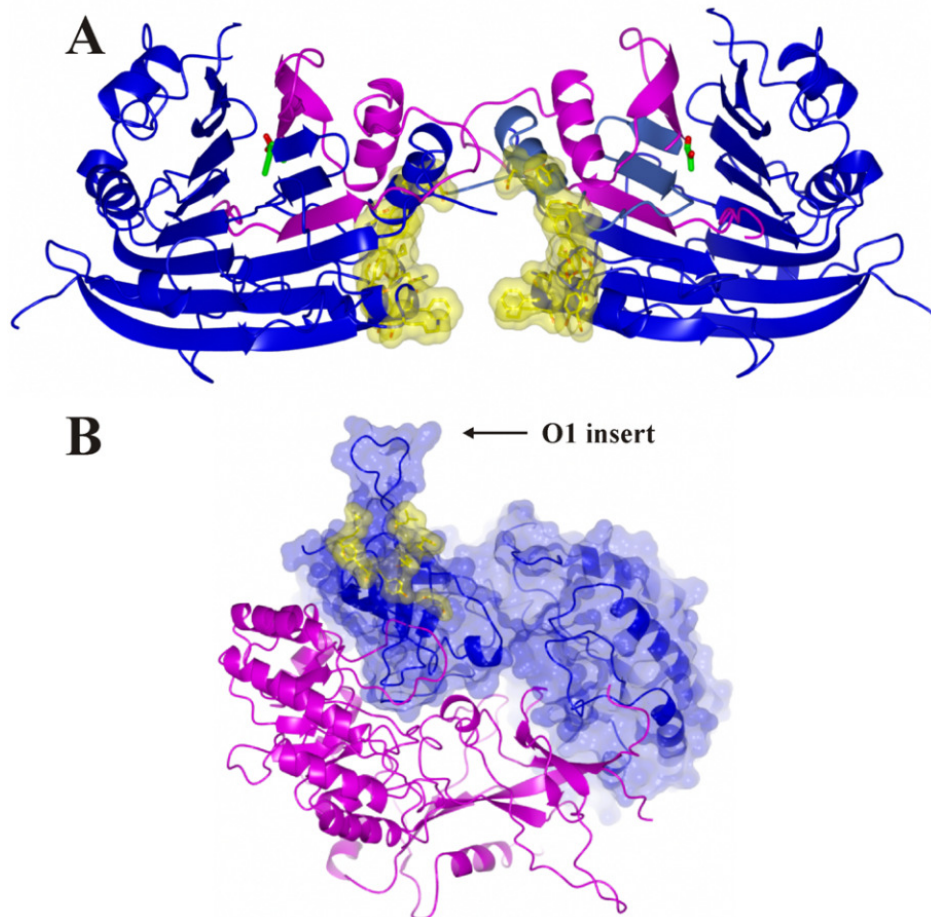


Figure 3.9: Predicted structural description of *Pf*AdoMetDC/ODC showing the proposed domain-domain interaction sites.

(A) The homology model of monomeric *Pf*AdoMetDC (β - and α -subunits shown in magenta and blue, respectively) [120] and (B) homodimeric *Pf*ODC (two monomers shown in magenta and blue) [127] are shown. The residues that are predicted to interact with the *Pf*ODC domain on the surface of *Pf*AdoMetDC and *vice versa* are shown in yellow. Two monomers of monofunctional *Pf*AdoMetDC can interact with each other in a side-to-side fashion at the site where *Pf*ODC natively interacts within the bifunctional complex. The position of the O1 parasite-specific insert is indicated. The pyruvoyl co-factors in the *Pf*AdoMetDC active sites are shown in green.

To confirm the hydrophobic-mediated interaction of the *Pf*AdoMetDC monomers, the mutant C505S protein (~6 mg/ml) was separated with SEC in wash buffer containing 10 mM DTT and 5% (v/v) n-butanol. This organic solvent was identified following the initial testing of a variety of agents at various concentrations that are known to disrupt hydrophobic interactions (results not shown). If a hydrophobic patch is exposed on the surface of *Pf*AdoMetDC the organic solvent is expected to shield this patch and thereby prevent the side-to-side interaction of the protein while DTT and the C505S mutation is expected to prevent the edge-on dimerisation via the proposed dimer interface. Figure 3.10 shows the SEC analysis of *Pf*AdoMetDC-C505S in the presence of DTT and butanol, which resulted in a single protein elution peak at 15.1 ml (V_e/V_o of 1.79) corresponding to a calculated MW of the monomeric protein 77 kDa in size. The addition of butanol therefore protected the hydrophobic patch on *Pf*AdoMetDC and constrained the protein to its monomeric form.

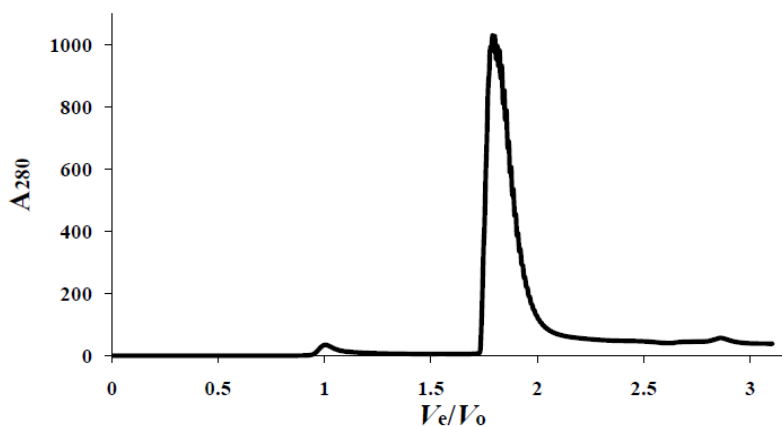


Figure 3.10: SEC of *PfAdoMetDC*-C505S in the presence of DTT and n-butanol.

The *PfAdoMetDC*-C505S mutant protein at a concentration of 6 mg/ml was separated with SEC on a column equilibrated with 50 mM Tris/HCl, pH 8.0, 150 mM NaCl, 10 mM DTT and 5% n-butanol.

Subsequent activity analysis of the protein collected from SEC showed that the enzyme is inactive while extensive dialysis with wash buffer recovered 65% of the activity of the butanol-treated enzyme in comparison to the untreated *PfAdoMetDC* activity (results not shown).

3.3.5. Far-UV analyses of *PfAdoMetDC* indicates a similar fold as the human protein

Far-UV CD was performed to determine the secondary structure of the *PfAdoMetDC* protein (in the absence of DTT) for comparison to dimeric human AdoMetDC [185] as well as to observe any secondary structural changes that might take place in the predominantly monomeric C505S mutant protein. Prior to CD analyses, the R_H of the proteins were analysed with DLS to ensure that the Cl⁻-free phosphate buffer did not cause protein aggregation or affect the oligomeric state of the proteins (results not shown).

At the concentration of 0.5 mg/ml (7.2 μ M) used in these analyses, mainly monomeric protein is expected based on the SEC result, however, by using the estimated K_d values that were determined for the wild-type *PfAdoMetDC* and C505S mutant proteins (Table 3.7), the dimeric proportions within these samples were estimated to be present at 45% and 15%, respectively. The results showed that *PfAdoMetDC* conforms to proteins with significant β -sheet content (40%), with a minimum at 209.5 nm and a maximum at 191 nm (Figure 3.11). This correlates well with what has been predicted in the homology model of *PfAdoMetDC* [120] and dimeric human AdoMetDC, which showed a minimum at 218 nm and a maximum at 195 nm [185]. It is conceivable that parasite-specific inserts of unknown structure (constituting 32% of the 572-residue *PfAdoMetDC* protein [120]), contribute to the differences in the spectra with 34% of the *PfAdoMetDC* secondary structure indicated to be disordered with Far-UV CD.

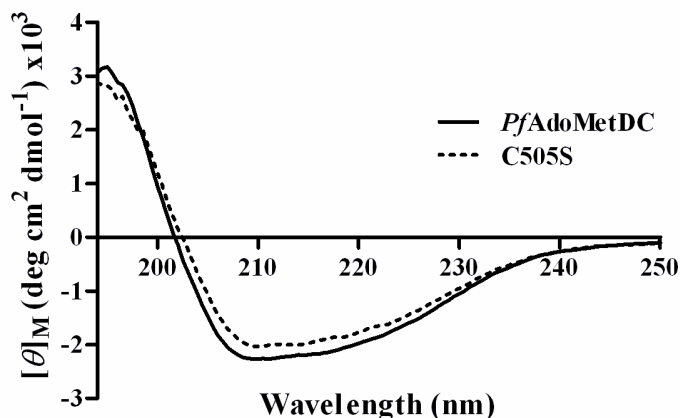


Figure 3.11: Far-UV CD analyses of the *PfAdoMetDC* and C505S mutant proteins.

Far-UV CD analysis was performed on the *PfAdoMetDC* and C505S mutant proteins in a phosphate buffer between wavelengths of 190 nm and 150 nm to detect possible differences in secondary structures of the mainly dimeric and mainly monomeric proteins, respectively.

The spectra of *PfAdoMetDC* and the C505S mutant proteins are similar with minimum peaks at ~210 nm (Figure 3.11). These results provided confidence in the fact that, while the C505S mutation in *PfAdoMetDC* stabilised the monomeric form and showed a reduced propensity of the protein to covalently dimerise, neither the mutation nor the monomeric status affected the secondary structure of the proteins.

Thus far the results have shown that monofunctional *PfAdoMetDC* has a lower propensity than the human protein to dimerise. Furthermore, at the concentration used in the activity assays and by applying the K_d value of *PfAdoMetDC* (Table 3.7) it can be calculated that >95% of the protein will be in its monomeric form, which implies that the protein does not require dimerisation to be functionally active. The *in vitro* conditions showed that *PfAdoMetDC* exists as two different dimers involving two sites on the protein surface. The C505S mutant results showed that disulphide linkage enhances the formation of the dimer at the predicted dimer interface [120] and butanol treatment showed that additional dimer formation is mediated by a site that could be involved in the native interaction with the *PfODC* domain [152].

3.3.6. Studies of the mechanism of processing in *PfAdoMetDC*

Processing of human and *T. cruzi* AdoMetDC is stimulated by putrescine binding in a charged-buried site distant from the active site. However, in the case of *P. falciparum* AdoMetDC, neither catalytic activity nor processing is stimulated by putrescine, which alludes to a different mechanism of processing for this protein. Heterologous expression of *PfAdoMetDC* within *E. coli* also showed that the processing reaction is not 100% efficient (Figure 3.2A). To elucidate

the mechanism of autocatalytic processing in *PfAdoMetDC* the residues involved in processing as well as the ones that assume the role of putrescine binding should be identified. Table 3.8 lists the residues that are predicted to be involved in the processing reactions of AdoMetDC from different organisms, which were identified with a multiple structure-based alignment of the sequences from human, plant and *Plasmodium* [120].

Table 3.8: Alignment of residues involved in the active site, processing reaction and the putrescine-binding site or charged-buried site for AdoMetDC from three organisms

Residues in the top row are numbered according to the human protein template while the residues in the bottom row are numbered according to the *P. falciparum* protein template. Residues in yellow are involved in the active site, green in the processing reaction and blue in the putrescine-binding site (*H. sapiens*) or charged-buried site (*P. falciparum* and *S. tuberosum*). Conserved residues are shown in grey.

	13	15	17	67	68	82	174	178	223	229	243	247	256
<i>H. sapiens</i>	L	E	W	E	S	C	D	E	F	S	H	E	E
<i>S. tuberosum</i>	R	E	S	E	S	C	R	E	F	S	H	E	E
<i>P. falciparum</i>	R	V	K	E	S	C	K	E	F	S	H	E	E
	11	13	15	72	73	87	215	219	415	421	434	438	447

Table 3.8 shows that the residues involved in the active site and processing reaction are highly conserved between the organisms, while the residues that have been shown to be involved in putrescine binding of the human protein are not well conserved and shows significant diversity. The *PfAdoMetDC* homology model showed that three basic amino acids (Arg11, Lys15 and Lys215) occupy the regions of the acidic residues that were shown to interact with putrescine in the human crystal structure (hGlu15, hAsp174, hGlu178 and hGlu256). In *P. falciparum* these residues correspond to Val13, Lys215, Glu219 and Glu447 (Figure 3.12). Therefore, in *P. falciparum*, hGlu15 is replaced by Val13 and positively-charged residues Arg11 and Lys15 are located approximate to the position where one terminal of putrescine would be positioned while Lys215 occupies the position of the other terminal, thereby mimicking putrescine binding (Figure 3.12) [120].

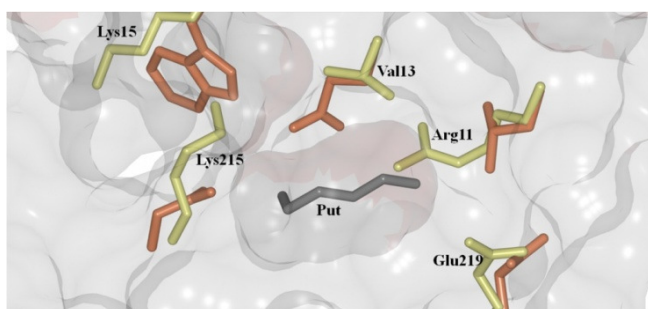


Figure 3.12: The charged-buried site of *PfAdoMetDC*.

Putrescine in grey from the human AdoMetDC crystal structure (1I7M) is shown with the residues that are predicted to stabilise putrescine binding in orange. The corresponding residues from the *PfAdoMetDC* homology model [120] that are predicted to mimic putrescine binding are shown in yellow. Taken from Birkholtz *et al.* (Biochemical Journal, in press).

In the current study, residues Ser421 and Arg11 were investigated for their roles in *PfAdoMetDC* processing. Mutagenesis of the Ser421 residue (corresponding to hSer229, previously shown to be essential for processing [125]) to Ala did not prevent processing of *PfAdoMetDC* since both the processed ~61 kDa mutant protein and the ~9 kDa dissociated β -subunit could be identified on the 12.5% acrylamide gel (Figure 3.13A and B, lane 2).

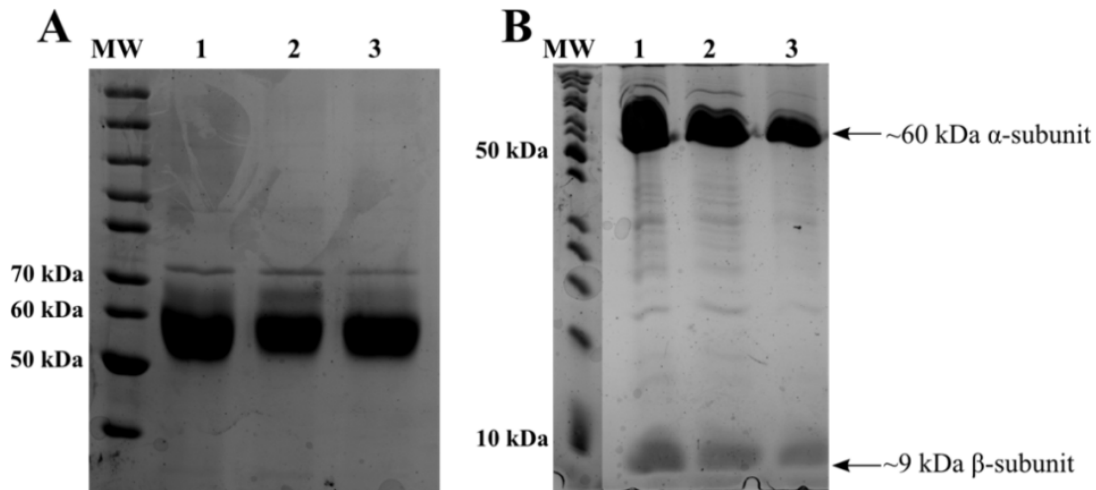


Figure 3.13: SDS-PAGE analysis of the S421A *PfAdoMetDC* mutant protein to determine the role of this residue in autocatalytic processing.

The Ser421 residue was mutated to Ala and the expressed mutant protein was analysed with (A) 7.5% and (B) 12.5% SDS-PAGE gels in order to identify the ~60 kDa α - and ~9 kDa β -subunits as an indication of processing taking place in the *PfAdoMetDC* protein. MW: PageRuler Unstained Protein Ladder. (A) and (B) lane 1: wild-type *PfAdoMetDC*; lane 2: *PfAdoMetDC*-C505S; lane 3: *PfAdoMetDC*-S421A. The positions of the ~60 kDa α - and ~9 kDa β -subunits of *PfAdoMetDC* are indicated with arrows.

In *T. cruzi*, it was previously shown that mutation of Arg34 in this parasite's AdoMetDC to the corresponding residue in human AdoMetDC (hLeu13) abolished processing while the crystal structure of plant AdoMetDC showed that the corresponding residue Arg18 is located at the approximate position that putrescine occupies in the human protein [184]. Similarly, in the current study Arg11 of *PfAdoMetDC* was mutated to Leu to observe its possible role in *PfAdoMetDC* processing. The results confirmed previous findings [120] and showed that the *PfAdoMetDC*-R11L mutant only expressed as the unprocessed protein at ~70 kDa (Figure 3.14A, lane 1) while the ~9 kDa β -subunit could not be identified on the 12.5% acrylamide gel (Figure 3.14B, lane 1).

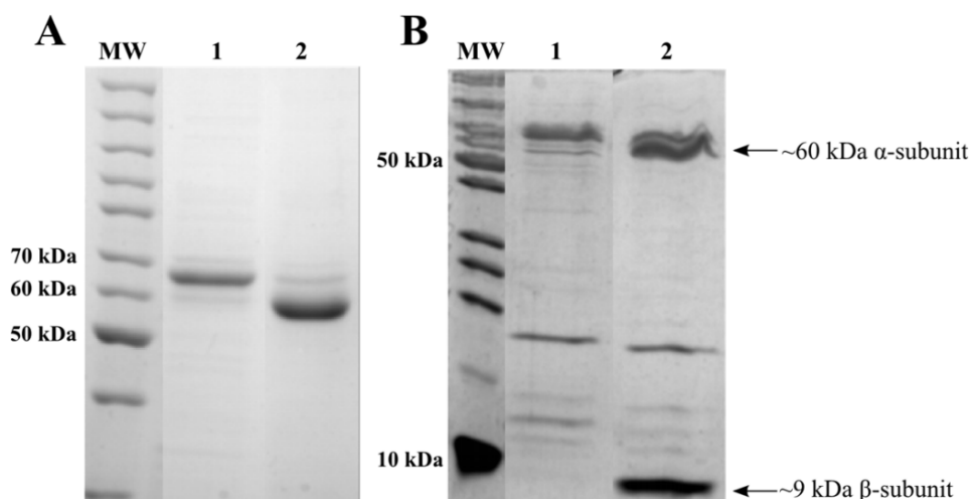


Figure 3.14: SDS-PAGE analysis of the R11L *PfAdoMetDC* mutant protein to determine the role of this residue in autocatalytic processing.

The Arg11 residue was mutated to Leu and the expressed mutant was analysed with (A) 7.5% and (B) 12.5% SDS-PAGE gels. MW: PageRuler Unstained Protein Ladder. (A) and (B) lane 1: *PfAdoMetDC*-R11L and lane 2: wild-type *PfAdoMetDC*.

Subsequent activity analyses showed that although mutagenesis of the Ser421 residue did not affect processing of *PfAdoMetDC*, enzyme activity decreased by 25% (Figure 3.15), which indicates that either the rate of the processing reaction was affected by the mutation or that the activity was disrupted due to the proximate position of Ser421 in the active site. Activity analysis of the *PfAdoMetDC*-R11L mutant confirmed the SDS-PAGE results in Figure 3.14 since the mutant enzyme showed no activity indicating complete disruption of processing (Figure 3.15).

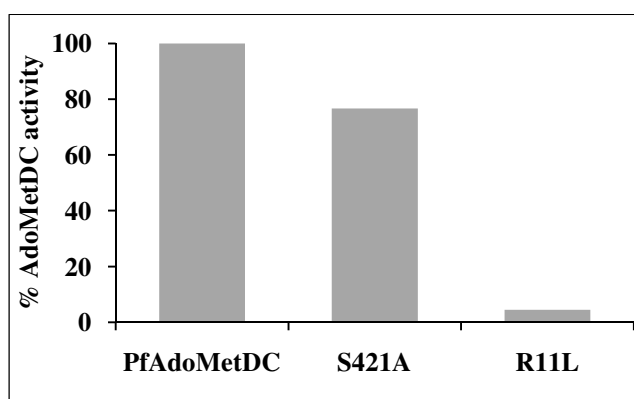


Figure 3.15: Activity analyses of the S421A and R11L *PfAdoMetDC* mutant enzymes.

The specific activities in nmol/min/mg were normalised to the wild-type protein activity and expressed as a percentage. The results were determined from a single experiment (n=1) carried out in duplicate.

3.3.7. Enzyme kinetics of monofunctional *PfAdoMetDC*

Since the oligomeric status of the active, mainly monomeric, monofunctional *PfAdoMetDC* protein that was expressed from a codon-harmonised construct has now been established and the secondary structure as well as mechanism of autocatalytic processing has been investigated, the

enzyme kinetics of this protein was repeated for comparison to that of other AdoMetDCs. Typical Michaelis-Menten kinetics was observed (Figure 3.16A) and linear transformation of the Michaelis-Menten equation with the Hanes-Woolf plot [198] resulted in a K_m of 250 μM and a V_{max} of 77 nmol/min/mg for *PfAdoMetDC* (Figure 3.18B). The K_m calculated here for *PfAdoMetDC* is approximately 4-fold higher than reported for the 660-residue wt*PfAdoMetDC*-hinge enzyme and approximately 6-fold higher when *PfAdoMetDC* is associated with *PfODC* in the bifunctional complex (Table 3.9) [71]. However, the K_m determined here is in a similar range to that of the homodimeric trypanosomal AdoMetDC orthologues (Table 3.9).

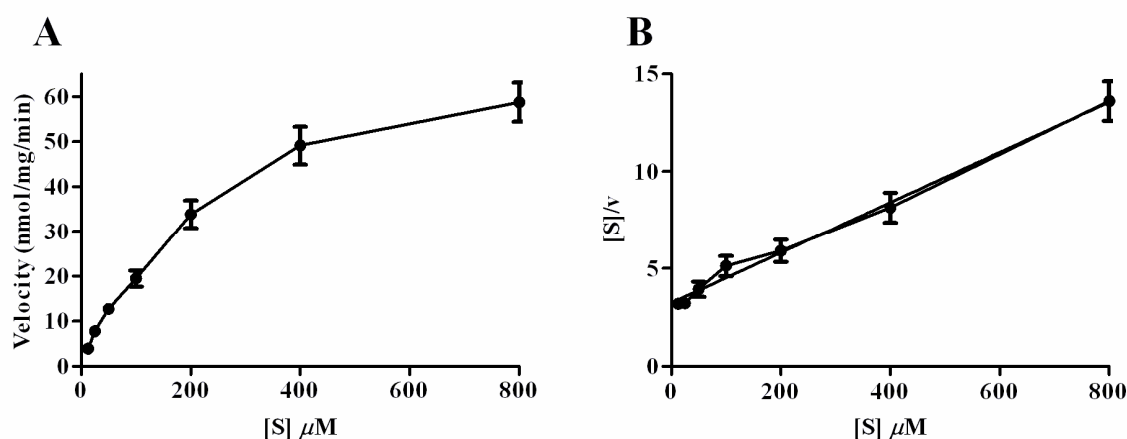


Figure 3.16: Michaelis-Menten curve (A) and linear Hanes-Woolf plot (B) of *PfAdoMetDC* reaction velocity measured at different substrate concentrations.

(A) The substrate affinity constant as well as V_{max} of *PfAdoMetDC* was determined using Michaelis-Menten kinetics. A substrate dilution series ([S]) ranging from 12.5 to 800 μM was used to determine the mean of the reaction velocities (v , nmol/mg/min) from three independent experiments carried out in duplicate. S.E.M is indicated. (B) The linear Hanes-Woolf plot was subsequently used to determine the K_m and V_{max} values.

The k_{cat} of *PfAdoMetDC* was calculated to be 5.3 min^{-1} , the enzyme therefore converts a molecule of substrate into product in approximately 11 s compared to the 0.4 s it takes for human AdoMetDC (Table 3.9). The k_{cat} values of the wt*PfAdoMetDC*-hinge and the bifunctional protein preparation of *PfAdoMetDC* are similar and in the range of 3.3 to 4 min^{-1} (Table 3.9). The specificity constant (k_{cat}/K_m) for *PfAdoMetDC* was calculated to be $332 \text{ M}^{-1}\text{s}^{-1}$. This value is 3- to 4-fold less than previously reported [71] and is the lowest of the proteins analysed (Table 3.9).

Thus, it appears that the presence of the hinge region (and/or *PfODC*) in some way improves the kinetics of *PfAdoMetDC* by increasing its substrate affinity. Importantly, compared to previous findings [71] a similar trend is observed in which monofunctional *PfAdoMetDC* shows less catalytic efficiency as indicated by the k_{cat} and K_m values compared to when the protein is in complex with *PfODC*.

Table 3.9: Comparison of enzyme kinetics for AdoMetDC from different organisms

The enzyme kinetics of *PfODC* are also included in order to show how the K_m and k_{cat} values of the monofunctional enzymes change when they become associated with the neighbouring domain of the bifunctional *PfAdoMetDC/ODC* complex.

Organism	Protein arrangement, oligomeric state	K_m^a	K_m^a +put	k_{cat} (min ⁻¹)	MDL73811	CGP48664 ^b	Putrescine effect	Reference
<i>H. sapiens</i>	Homodimer	74	59	114 (-put) 156 (+put)	0.56	5000 (-put) 0.005 (+put)	Stimulates activity and processing	[186,204,205]
	Monofunctional <i>PfAdoMetDC</i> , monomer	250		5.4	0.33	4.1		Current study
<i>P. falciparum</i>	Monofunctional <i>PfAdoMetDC</i> -hinge	58	-	4	-	3	No effect	[71,100]
	Bifunctional <i>PfAdoMetDC/ODC</i> , heterotetramer	43		3.3	1.6	-		[71,100]
	Homodimer	260	250	-	-	100 (-put) 6 (+put)		[186]
<i>T. cruzi</i>	Homodimer	540	130	0.3 (-put) 1.44 (+put)	-	-	Stimulates activity of homo- and heterodimer	[164]
	Monomer/prozyme, heterodimer	580	170	36 (-put) 50.4 (+put)	-	-		[164]
	Homodimer	380	240	0.096 (-put) 0.492 (+put)	-	0.49	Stimulates activity of homodimer	[164,206]
<i>T. brucei</i>	Monomer/prozyme, heterodimer	110	170	84 (-put) 102 (+put)	-	-		[164]

^a The K_m values (in μM) are given in the presence and absence of putrescine (put) in the organisms where putrescine stimulates the activity of the protein.

^b The K_i values (in μM) are given in the presence and absence of putrescine (put) in the organisms where putrescine stimulates the activity of AdoMetDC.

Analysis of enzyme kinetics in the presence of the irreversible inhibitor MDL73811 showed that *PfAdoMetDC* activity decreased in a concentration dependent manner (Figure 3.17A). A secondary plot yielded a linear graph from which a k_{inact} value of 0.46 min^{-1} and a K_i value of $0.33 \text{ }\mu\text{M}$ were determined for MDL73811 (Figure 3.17B). Comparison to the reported K_i of $1.6 \text{ }\mu\text{M}$ for MDL73811 on *PfAdoMetDC*/ODC [100] indicates stronger inhibition of the monofunctional enzyme (Table 3.9).

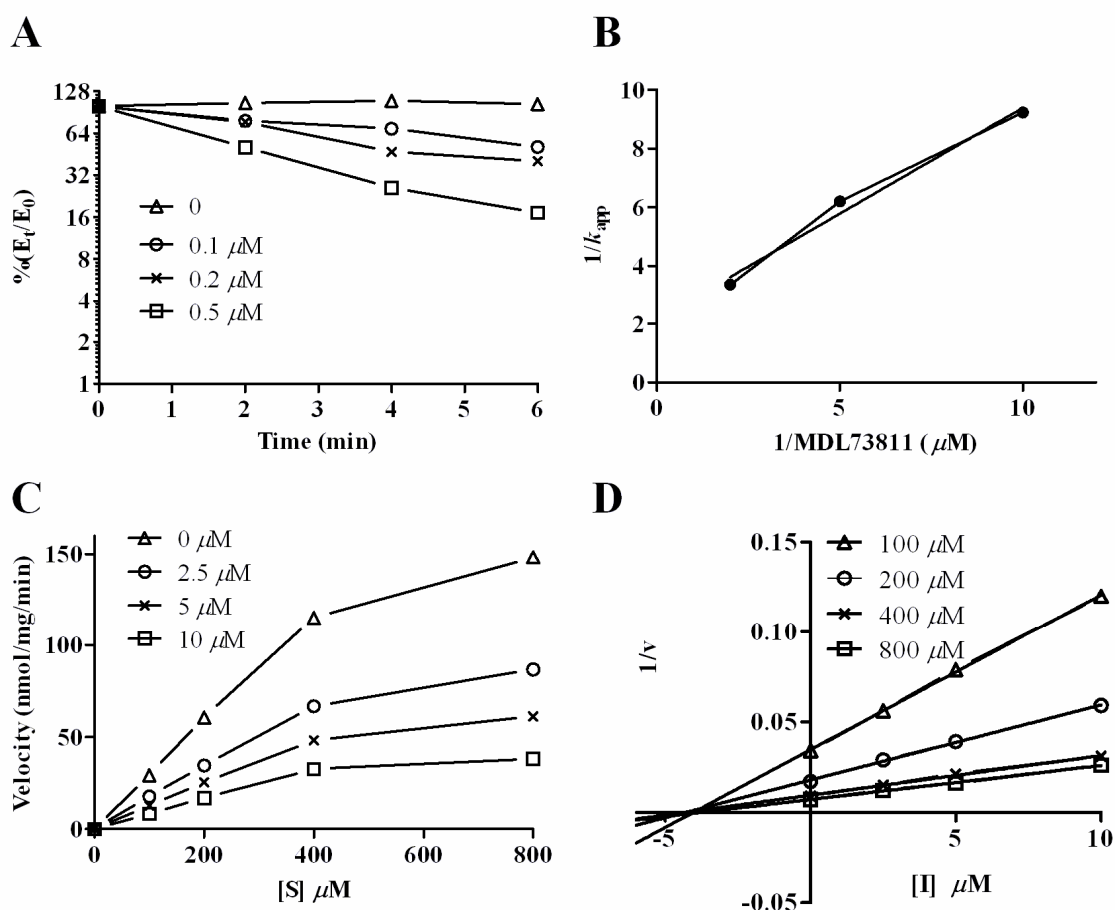


Figure 3.17: Inhibition kinetics of *PfAdoMetDC* treated with MDL73811 and CGP48664.

For the irreversible inhibitor MDL73811 the Kitz-Wilson method was used where the percentage enzyme activity (given by the maximal enzyme activity following pre-incubation with a specific $[I]$ for time interval t (E_t) over the enzyme activity following pre-incubation in the absence of inhibitor for each $[I]$ tested (E_0) against time is shown (A). Linearisation was performed by plotting the inverse of the slope from the primary plot versus the inverse of $[I]$. For inhibition with CGP48664 the Michaelis-Menten curves (C) showing the reaction velocities (v , nmol/mg/min) in the presence of a substrate ($[S]$) dilution series ranging from $100 \text{ }\mu\text{M}$ to $800 \text{ }\mu\text{M}$ and an inhibitor dilution series ranging from $2.5 \text{ }\mu\text{M}$ to $10 \text{ }\mu\text{M}$ are indicated. The linear Dixon plots (D) were obtained by plotting the inverse of the reaction velocities against $[I]$.

Inhibition kinetics of *PfAdoMetDC* with the CGP48664 showed that increasing concentrations of CGP48664 did not affect the K_m of *PfAdoMetDC* but instead decreased the V_{max} , which is typical of a non-competitive inhibitor whereby binding of the native substrate is not affected (constant K_m) but the efficiency of the reaction is decreased (Figure 3.17C). Linearisation of the



Michaelis-Menten curves resulted in a K_i of 4.1 μM (Figure 3.17D), which is similar to the reported value for wt*PfAdoMetDC*-hinge (Table 3.9) [100]. The finding that the inhibition of *PfAdoMetDC* by CGP48664 is non-competitive is similar to that observed for *T. cruzi* AdoMetDC [186]. In contrast, the inhibition of human AdoMetDC with CGP48664 is competitive [124].

3.4. Discussion

The polyamine biosynthetic activities of *P. falciparum* are uniquely arranged on a bifunctional *PfAdoMetDC*/ODC protein consisting of 1419 residues of which the hinge region is predicted to be encoded by residues 530-804 [71]. The evolutionary role of such a large complex has been extensively questioned. A possible reason could be the combined regulation of two enzymes in a pathway via the interference of a single domain, which then communicates the change to the adjacent domain. Another unique property of *PfAdoMetDC*/ODC is the presence of five parasite-specific inserts that range in size between 6 and 157 residues and are located within both the *PfAdoMetDC* [120] and *PfODC* [127] domains. Possible roles for these inserts, with unknown structure, in interdomain interactions mediating activity have been shown [69]. In this study, various biochemical and structural characteristics of the monofunctional *PfAdoMetDC* domain was investigated to provide an understanding of this protein's functionality as a monofunctional protein compared to its role within the bifunctional complex. This information would provide us with novel insights into the possible role of the bifunctional complex in the homeostatic maintenance of polyamine levels within *P. falciparum* parasites.

Homology modeling of the *PfAdoMetDC* monomer with the plant structure as template predicted the same four-layer $\alpha\beta\beta\alpha$ -sandwich fold [120] as was observed with the human and plant AdoMetDCs [123,184]. Furthermore, the active site and charged-buried site residues of *PfAdoMetDC* are conserved with similar conformation to that of the human counterpart. In contrast to *PfAdoMetDC*, which does not bind putrescine [71], the crystal structure of human AdoMetDC revealed the presence of an unusual collection of charged residues between the β -sheets of each monomer that binds putrescine in a positively cooperative manner [125,185,189,207]. The functional oligomeric unit of *PfAdoMetDC* has not been elucidated but since this protein does not bind putrescine, dimerisation of *PfAdoMetDC* is not expected to have a functional role. This is according to the postulation by Bale *et al.* in a study of human AdoMetDC where they showed that putrescine binding and dimerisation may be linked resulting



in positive cooperativity between the monomers of the human protein [185]. The lack of information on the biochemical characteristics of *PfAdoMetDC* could be ascribed to the ineffective heterologous expression of soluble forms of plasmodial proteins [208] such as *PfAdoMetDC/ODC*

In this study, codon harmonisation of the monofunctional *PfAdometdc* gene was carried out to test whether this technique could improve the heterologous protein expression within *E. coli*. Codon harmonisation looks at the frequency of codon usage for each amino acid in *P. falciparum* and their preference in *E. coli*, and then alters the code of the gene to the codon frequency of the non-natural host (*E. coli*) [209]. In contrast to codon optimisation, these changes thus ensure that the positional codon frequency of low/intermediate and high usage codons remain similar in the non-natural host, which then allows the speed of translation to match that of the natural host. Assuming that the translational machineries of the expression and natural host organisms are similar, translation and pausing at the particular sites where folding of the secondary and tertiary structures are required, is expected to occur as it would occur in the natural host. Additionally, any false Shine-Dalgarno sites are removed that may result in the truncation of the proteins within the expression host.

Comparison of the expression of the wt*PfAdoMetDC*-hinge and *PfAdoMetDC* proteins encoded from wild-type, unharmonised and harmonised sequences, respectively, showed that harmonisation improved the expression levels as well as protein stability of monofunctional *PfAdoMetDC*. The reduction of Hsp70 co-purification in the *PfAdoMetDC* sample also gives an indication that less pressure was placed on *E. coli* during protein translation and folding. However, the possible improvement of protein expression due to the removal of the Strep-tag at the N-terminus of *PfAdoMetDC* cannot be excluded. Addition of unharmonised nucleotides to the harmonised gene to produce a protein comparable in size to that of wt*PfAdoMetDC*-hinge (residues 1-660) [71] did not result in soluble protein. The hinge region may therefore affect soluble protein expression. Furthermore, soluble expression of *PfAdoMetDC* within *E. coli* showed the presence of both the unprocessed and processed proteins after affinity chromatography indicating that the heterologous expression prevented the 100% efficiency of the processing reaction. These results show that folding of the protein was not optimal to allow the correct positioning of the residues involved in the autocatalytic cleavage reaction. Subsequent analysis of the insoluble protein extracts showed that a considerable amount of these proteins were expressed as insoluble inclusion bodies. Refolding and purification of



monofunctional *PfAdoMetDC* from the insoluble inclusion bodies was therefore performed, firstly in an attempt to increase the yield and purity of the protein and secondly to determine if correct refolding under favourable *in vitro* conditions could lead to increased processing efficiency since it is generally accepted that simply the correct structural conformation of *PfAdoMetDC* is required for pyruvoyl co-factor formation. The results showed that even though significant amounts of pure protein (without Hsp70 contamination) could be obtained from the inclusion bodies, processing of both the *PfAdoMetDC* and *PfAdoMetDC*-hinge proteins were abolished and only resulted in the isolation of inactive, unprocessed proteins. Preliminary far-UV CD analyses of these samples showed similar overall secondary structural content compared to the proteins isolated from the soluble fraction but the conformation of the proteins are unknown.

Prior to the investigative experiments to determine the oligomeric structure and activity of the soluble *PfAdoMetDC* protein, different buffer screens were tested with DSF to ensure the stability of the protein. DSF identifies ideal buffer solutions, low molecular weight ligands or protein-inhibitor/substrate complexes that could contribute to protein stabilisation. In the presence of the SYPRO orange dye the protein's T_m corresponds to the temperature at which there exists an equivalent concentration of folded and unfolded proteins. If the stability of a protein is subsequently increased as a consequence of, for example, the co-incubation of substrate, the free energy contribution of substrate binding results in an increase in the temperature at which this equilibrium is obtained, which is consequently shown by an increase in the protein's T_m [193]. In this study, DSF analyses showed that, in comparison to a whole range of buffers that were tested, the stability of *PfAdoMetDC* in dialysis buffer consisting of 50 mM Tris/HCl, pH 8.0 and 150 mM NaCl was similar to the T_m obtained in the buffer that stabilised the protein the most. Co-incubation of the protein with substrate analogues also resulted in further increases of *PfAdoMetDC* stability.

Investigations into the oligomer formation of *PfAdoMetDC* were performed using SEC, non-reducing SDS-PAGE and DLS on a pure, stable form of the protein expressed from a harmonised gene. A concentration-dependent monomer-dimer equilibrium exists for the *PfAdoMetDC* protein that could be shifted towards the monomeric form when reducing conditions were applied. Subsequent inspection of the equivalent human AdoMetDC dimer interface in the *PfAdoMetDC* model [120] suggested the involvement of the Cys505 residue in disulphide bond formation between two monomeric proteins. This residue is not conserved amongst all AdoMetDCs but since it is located on the β_{15} strand at the proposed dimer interface,



it could form a disulphide bond with the same residue from a second monomer and thereby stabilise the dimeric form under oxidising conditions. This residue was subsequently mutated since it was predicted that if the *PfAdoMetDC* protein dimerises at the same dimer interface as the human protein, even if this occurs at a lower association constant, then both the *PfAdoMetDC* and Cys505 mutant proteins are expected to show dimeric forms with SEC. However, if the Cys505 residue does lie at the dimer interface and stabilises the dimeric form of the protein via disulphide bond formation, then the wild-type and mutant proteins would probably show different dimer propensities. Mutagenesis of Cys505 confirmed the modelling predictions and MALDI-MS results, which showed that Cys505 is indeed located at the native dimer interface since the mutant form reduced the propensity of *PfAdoMetDC* to dimerise (~7.5-fold increase in K_d).

The K_d of *PfAdoMetDC* in the low micromolar range indicated that this protein forms a much less stable dimer, which is 300-fold higher than that of the dimeric human protein [185] but similar to the monomeric plant protein [184]. DLS results also showed that mutation of Cys505 shifted the dimer-monomer equilibrium of *PfAdoMetDC* towards the monomer and treatment of *PfAdoMetDC* with a reducing agent immediately prior to DLS analysis was not as effective as this mutation in decreasing unwanted oligomer formation even at a concentration of the mutant protein double than the wild-type. The results show that while *PfAdoMetDC* forms a dimer that involves the same dimer interface as the human protein, dimerisation occurs at a much lower affinity and is stabilised *in vitro* by a disulphide bond across the dimer interface. It should also be noted that the formation of the disulphide bond mediated by Cys505 is not proposed to be essential for *PfAdoMetDC* quaternary structure formation or activity. *PfAdoMetDC* is a cytosolic protein and due to the presence of glutathione and thioredoxin redox systems in the cytoplasm it is unlikely that the protein will be in an oxidising environment to allow the formation of a disulphide bond *in vivo* [210]. Furthermore, even though the human AdoMetDC protein is predicted to be a dimer joined by an edge-on association of the β -sheets of each monomer at the dimer interface, inspection of the 1I7M structure shows that a distance of 4.27 Å exists between the C_β atoms of the hCys148 residues on strands β 7 of each monomeric protein, which could also result in the formation of a disulphide bond. The protein was, however, crystallised in the presence of 10 mM DTT [124].

Despite the prevention of disulphide bond formation at the dimer interface with the Cys505 mutation or addition of a reducing agent, SEC analyses showed that *PfAdoMetDC* still formed



dimers, especially at moderately high protein concentrations. Dimerisation *in vitro* could additionally occur on a surface of the *PfAdoMetDC* domain which is natively involved in an interaction with the *PfODC* domain within the bifunctional complex [69]. Protein-protein docking also identified the site on *PfAdoMetDC* where *PfODC* is most likely to bind [152] and involves the α -helices flanking the core β -strands of *PfAdoMetDC*. Such an interaction between two *PfAdoMetDC* monomers would therefore occur in a side-to-side fashion as opposed to the edge-on association of the β -strands at the dimer interface as seen for human *AdoMetDC* (Figure 3.9). In addition, since the relative positions of the parasite-specific inserts in the quaternary structure of *PfAdoMetDC* are unknown [120] their potential role in causing dimerisation and perhaps tetramerisation via hydrophobic/philic interactions cannot be excluded. Considering the site of the *PfAdoMetDC* interaction on the *PfODC* domain, the O1 insert is positioned such that it could form a possible interaction with *PfAdoMetDC*, which substantiates the results obtained in Chapter 2. However, since the C505S mutant has a significantly lower dimer affinity than the wild type, we could show here that *PfAdoMetDC* is able to dimerise at the same site which usually mediates dimerisation of the human protein [120] and thus more closely resembles the native conformation but is not essential for activity.

Figure 3.18 summarises the proposed *in vitro* model of monofunctional *PfAdoMetDC* oligomer formation as obtained from the results in this chapter. The inactive protomer which has not undergone autocatalytic processing was obtained with the heterologous expression of the protein as well as with protein refolding from insoluble inclusion bodies. Subsequent processing of this protomer to generate the pyruvoyl co-factor at Ser73 within the active site resulted in the formation of the α - and β -subunits which associates into the $\alpha\beta$ -monomer. These subunits could be resolved with SDS-PAGE and were catalytically active. The $\alpha\beta$ -monomer was shown with SEC to exist in equilibrium with an $(\alpha\beta)_2$ -dimer, which is similar to that of homodimeric human *AdoMetDC* since dimer formation takes place as an extension of the β -sheets mediated by edge-on interactions between the β -strands from each monomer. This dimer was additionally shown to be stabilised *in vitro* via disulphide formation between the Cys505 residues from each monomer. The calculated dimerisation constant of the C505S mutant protein confirmed the location of this residue on the β -sheet at the predicted dimer interface since mutation increased the dissociation constant 7.5-fold. Oligomerisation of monofunctional *PfAdoMetDC*, in the absence of *PfODC*, was also predicted to occur as a result of hydrophobic interactions at the native *PfODC* binding site, which involve the α -helices on the “sides” of the monomers. The inclusion of butanol during SEC of the *PfAdoMetDC*-C505S protein confirmed that hydrophobic sites were protected

by this organic solvent resulting in the presence of the monomeric form of the protein. Higher oligomers were also shown to occur with SEC, which could form as a result of hydrophobic association and/or dimer-interface mediated interactions.

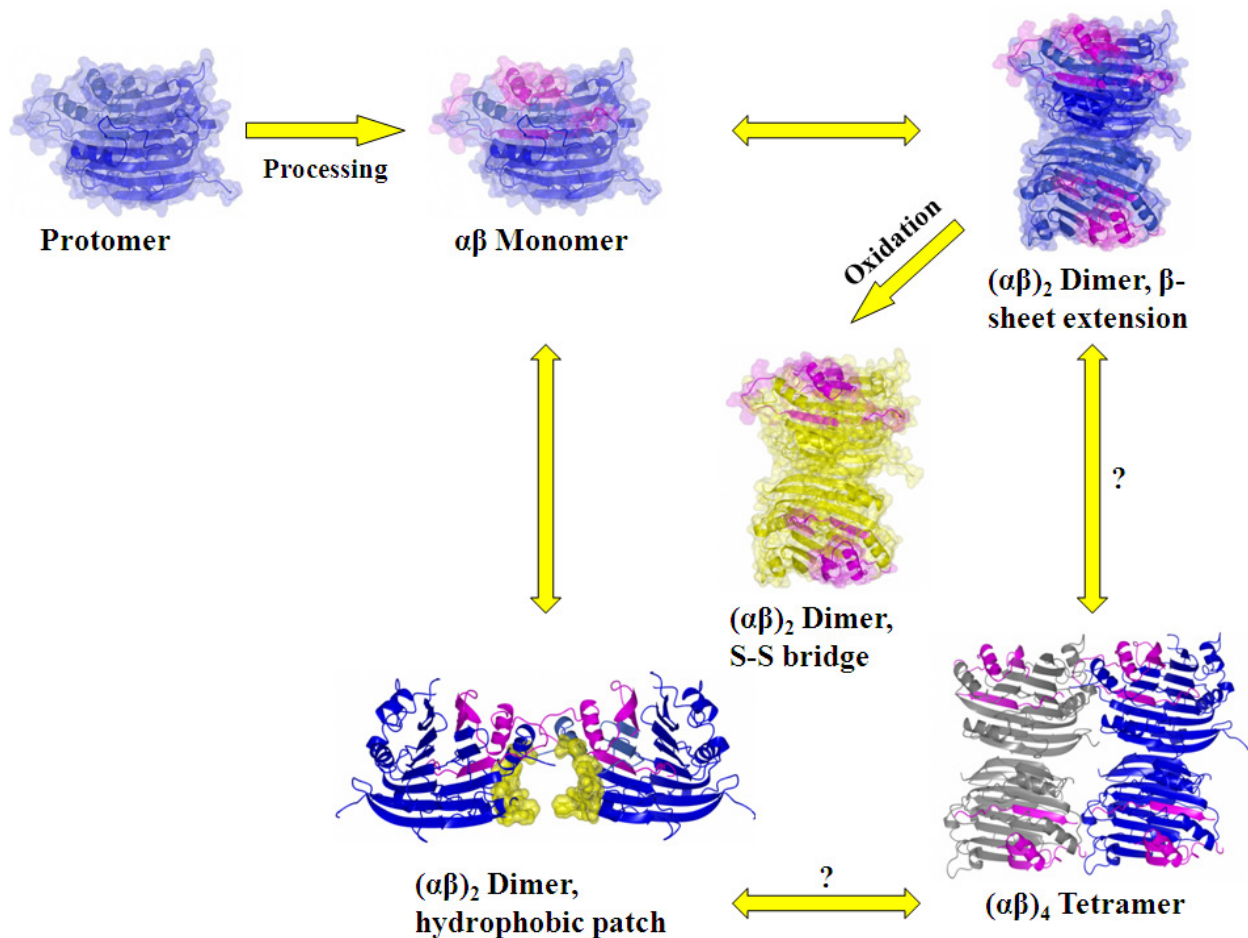


Figure 3.18: Model of monofunctional *Pf*AdoMetDC oligomerisation *in vitro*.

The protomer in blue undergoes autocatalytic processing to generate the pyruvoyl co-factor at Ser73 within the active site. Processing also forms the α - and β -subunits shown in blue and magenta, respectively, resulting in an $\alpha\beta$ -monomer. These monomers are in equilibrium with an $(\alpha\beta)_2$ -dimer, which is similar to that of homodimeric human AdoMetDC where dimer formation takes place as an extension of the β -sheets mediated by edge-on interactions between the β -strands from each monomer. Under oxidising conditions the *Pf*AdoMetDC dimer is further stabilised by disulphide bond formation between the CysC505 residues from each monomer (α - and β -subunits shown in yellow and pink, respectively) on the β -sheets at the predicted dimer interface. Oligomerisation of monofunctional *Pf*AdoMetDC, in the absence of *Pf*ODC, as a result of hydrophobic interactions at the native *Pf*ODC binding site (shown in yellow), can also occur and involve the α -helices on the “sides” of the monomers. Higher oligomers could also be formed due to hydrophobic association and/or dimer-interface mediated interactions.

Far-UV CD analyses was performed to obtain initial information on the fold of *Pf*AdoMetDC and to additionally determine whether the C505S mutation affected the structure of the protein. However, the prevention of disulphide bond formation at the dimer interface should not affect the folding properties of the protein and such a bond would only be detected in the near-UV range. The CD results showed that the AdoMetDC proteins from human and *P. falciparum* give similar spectra, with high contents of β -strands. Additionally, 30-40% of the *Pf*AdoMetDC



protein was calculated to be unordered structures and may be contributed by the parasite-specific inserts [120]. The far-UV CD analyses also confirmed identical spectra between *PfAdoMetDC* and the mainly monomeric C505S mutant, indicating that the prevention of covalently-linked dimer association did not cause a secondary structure change in the monomeric protein.

The recombinant monofunctional *PfAdoMetDC* protein produced here from a harmonised gene is therefore believed to be similar in conformation to the native protein. This is based on the secondary structure comparison as determined with far-UV CD that showed similarities between the *P. falciparum* and human AdoMetDCs as well as the confirmation that disulphide formation at the proposed dimer interface is mediated between closely situated Cys505 residues, which confirm the dimer interface predictions of Wells *et al.* [120]. The presence of the processed form of the recombinant protein, which is reliant on the exact positioning of the Arg11-Lys15-Lys215 triad, also indicates the correct conformation of the recombinant protein.

The mechanism of processing within AdoMetDC where a Ser residue undergoes serinolysis to produce the pyruvoyl co-factor has been extensively studied in the human and *T. cruzi* proteins where specific residues involved have been mutated and tested for their role in the processing reaction [125,185-189]. As mentioned previously, neither the catalytic activity nor processing of *P. falciparum* and plant AdoMetDC, is stimulated by putrescine. These two orthologues may therefore be constitutively processed to allow for continuously active protein, which is nonsensical in the case of plant AdoMetDC due to the various important functions that the polyamines mediate. Additionally plant AdoMetDC translation is also regulated by a well-characterised small upstream open reading frame [211,212]. For *PfAdoMetDC*, the activity may be regulated by a different mechanism. It is also important to note that dcAdoMet is exclusively used as a substrate in the polyamine pathway, thus once produced it is committed to this pathway. It is therefore unlikely that *PfAdoMetDC* would be constitutively active to continuously supply dcAdoMet. Moreover due to the important roles of AdoMet in various methylation reactions its abundance would be tightly regulated [178]. The expression of the constitutively active protein may therefore be regulated, which, once again, alludes to the bifunctional arrangement of *PfAdoMetDC* and its contribution to protein activities. Furthermore the roles of AdoMet or dcAdoMet as possible allosteric effectors need to be investigated.

In *PfAdoMetDC*, Ser73 is converted into a pyruvoyl group and previous studies have shown that mutation of this residue results in an inactive protein [71]. Residues involved in the active and



charged-buried site are conserved while those involved in putrescine-binding (human) and the charged-buried site (plant and *P. falciparum*) are diverse (Table 3.8). The *PfAdoMetDC* homology model showed that residues Arg11, Lys15 and Lys215 may mimic putrescine binding as their locations correspond to the positions of the amino terminals of putrescine [120]. Furthermore, for human AdoMetDC, residue hSer229 was shown to be situated close to the processing site and the hydroxyl group of this residue was shown to be essential for the processing reaction as confirmed with mutagenesis and subsequent 3D structure analysis [125]. In the current study, the corresponding Ser421 residue was mutated to Ala, however, the results showed that this residue has no effect on the processing reaction but its mutagenesis resulted in decreased enzyme activity. These results show that in the parasite an alternative mechanism is involved where another residue provides the hydroxyl group needed for processing but similarly to the human protein, Ser421 does influence enzyme activity, probably due to its proximate location to the active site. This result was unexpected and indicated that differences exist between the processing mechanisms of human and *P. falciparum* AdoMetDCs that needs to be investigated further.

Previously it was shown that residues Arg34 and Arg18 from *T. cruzi* and plant AdoMetDC, respectively, are essential for processing to occur [184,187]. Arg34 represents the key structural change to explain why *T. cruzi* AdoMetDC processing is not stimulated by putrescine. In this study, the corresponding residue Arg11 from *PfAdoMetDC* was also shown to be essential for the processing reaction [120]. These results did not only confirm the importance of Arg11 in the *PfAdoMetDC* processing reaction but also showed that expression of such a mutant protein results in the production of a single *PfAdoMetDC* species instead of the heterogeneous mixture of processed and unprocessed proteins obtained with wild-type protein expression. This protein, despite it being inactive, could be advantageous for future crystallisation studies in which a homogeneous protein solution is required.

This study has therefore shown that monofunctional *PfAdoMetDC* forms a dimer in solution and that dimerisation is stabilised by various factors. More information could also be obtained on the structure as well as the unique mechanism of processing of this protein. However, since the major aim of this study was to characterise *PfAdoMetDC* in order to obtain insights into the contribution of this domain to the bifunctional complex, enzyme kinetics of the monofunctional domain were compared to the kinetics of *PfAdoMetDC* within the bifunctional complex. Previous studies have shown increased substrate affinity of *PfAdoMetDC* within the bifunctional



complex [71], which is hypothesised to be introduced by subtle changes as a result of interdomain protein interactions with the *PfODC* domain. In Chapter 2 this was further investigated whereby the critical role of the O1 parasite-specific insert was implicated in these interactions. In this study, initial activity analyses of monofunctional *PfAdoMetDC* reinforced previous studies [69,71], which showed that both the hinge region and the *PfODC* domain play important roles in the kinetic properties of *PfAdoMetDC*. Previous studies have shown that the removal of a central part of the hinge region (residues 573-752) from the bifunctional protein decreases *PfAdoMetDC* activity by 24% relative to its activity within the bifunctional complex [69]. Further removal of both the *PfODC* domain as well as half of the hinge region to create the wt*PfAdoMetDC*-hinge protein (660 residues) increased activity by 20% [71] while, as shown in this study, the further deletion of 88 residues from the hinge region (572 residues) increased activity by 55% relative to the activity within the bifunctional complex (Figure 3.19). However, the kinetics analyses showed reduced substrate affinity of the latter enzyme (K_m of 250 μM) compared to that of the *PfAdoMetDC* domain in the bifunctional complex (K_m of 43 μM) (Figure 3.19) [71]. The K_m value obtained here is surprisingly similar to that of homodimeric trypanosomal AdoMetDC (Table 3.9) suggesting that, in the absence of the hinge or the *PfODC* domain, monofunctional *PfAdoMetDC* behaves like kinetoplastid AdoMetDCs. However, *PfAdoMetDC* is still a less catalytically efficient enzyme compared to AdoMetDCs that are activated by putrescine (human, *T. cruzi*) or prozyme (kinetoplastids). In the presence of prozyme the k_{cat} of *T. brucei* AdoMetDC is increased 1200-fold [163] while a similar situation was seen for *T. cruzi* where both prozyme and putrescine increased the enzyme efficiency to a level similar to that of the fully activated counterpart in *T. brucei* (Table 3.9) [164]. Therefore, it can be postulated that the bifunctionality of *PfAdoMetDC/ODC* allows the parasite to mediate regulatory mechanisms between the two decarboxylase domains but an allosteric effector remains to be identified that could increase the enzyme efficiency of *PfAdoMetDC* to the levels observed for human and heterodimeric trypanosomal AdoMetDCs.

The results show that binding of *PfODC* results in a 6-fold change in both the specific activity and K_m of *PfAdoMetDC* resulting in slightly lower enzyme efficiency (k_{cat} of 5.3 min^{-1} versus 3.3 min^{-1}) (Figure 3.19). The K_m of monofunctional *PfAdoMetDC* is therefore considerably increased so as to prevent the binding of metabolically important AdoMet when putrescine-producing *PfODC* is absent. Within the bifunctional complex, the affinities of both enzymes for their respective substrates improve (43 μM for *PfAdoMetDC* and 42 μM for *PfODC*) with synchronised enzyme catalytic rates of approximately 3 min^{-1} (Figure 3.19) [71] producing

dcAdoMet and putrescine every 18-20 s for the subsequent synthesis of spermidine by *Pf*SpdS. These property changes of the two enzymes in the bifunctional complex is hypothesised to be due to subtle changes in the active site centre induced by long-range effects [134] modulated by interdomain protein interactions with *Pf*ODC [69] to regulate the polyamine levels within the parasite.

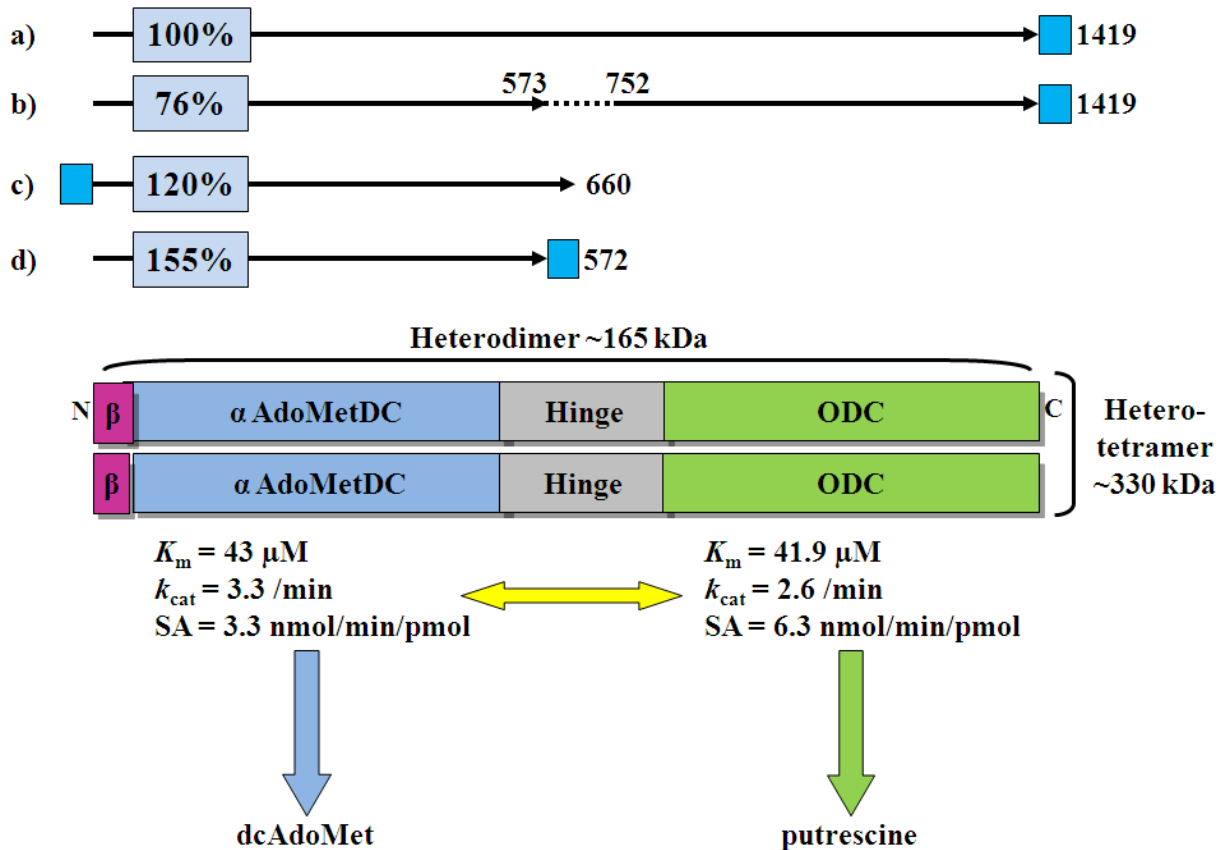


Figure 3.19: Schematic diagram describing the coordinated activities of the domains within the bifunctional AdoMetDC/ODC complex from *P. falciparum*.

In the central diagram, the *Pf*AdoMetDC/ODC bifunctional arrangement is shown with the processed α - and β -subunits of *Pf*AdoMetDC shown in blue and magenta, respectively. This domain is linked to the C-terminal *Pf*ODC domain (green) with the hinge region (grey). The approximate protein sizes of the heterodimeric complex (~165 kDa) as well as the heterotetrameric bifunctional complex (~330 kDa) are indicated [70]. Above the diagram the activities of the different constructs of *Pf*AdoMetDC are shown, which are expressed as a percentage of the *Pf*AdoMetDC activity in the bifunctional complex (a) [71] by taking into account the different sizes of the proteins in relation to the 1419-residue bifunctional protein. The lengths of the proteins are indicated as black lines in proportion to the schematic diagram of the bifunctional protein while the deleted hinge region in (b) is shown with a dashed line. The positions of the Strep-tags are shown as blue boxes. The AdoMetDC and ODC reactions produce dcAdoMet and putrescine, respectively, and enzyme kinetics have shown that within the bifunctional complex these domain activities are coordinated such that equimolar quantities of the products are synthesised. The activities of (a) and (c) as well as the enzyme kinetics data were obtained from [71], the activity of the hinge deletion mutant is from [69] while the result of the shortest protein was obtained in the current study.

Trypanosomal AdoMetDC behaviour was also observed when *Pf*AdoMetDC was treated with CGP48664. In contrast to what was shown for human AdoMetDC [124], this substrate analogue inhibited *Pf*AdoMetDC non-competitively. Similarly, non-competitive inhibition was also shown



for *T. cruzi* AdoMetDC [186] where enzyme activity was actually increased in the presence of <10 μM CGP48664 while inhibition was only observed at higher concentrations or in the presence of putrescine (K_i of 6 μM). The authors suggested that in the absence of putrescine, the compound binds to the putrescine-binding site and acts as an agonist of activity as putrescine would and when bound to the active site it acts as an inhibitor. The data also suggested that the inhibitor binds with higher affinity to the putrescine-binding site and only inhibits at higher concentrations when it saturates the active site. For *PfAdoMetDC*, the inhibitor concentrations used were below 10 μM and no increase in activity was observed, which was expected since the putrescine-binding site is absent and is replaced with analogous positively-charged residues. This result shows that both the substrate and inhibitor can either fit within the active site, which suggests that the active site is large enough to accommodate both or that another more complex kinetic model is required. Alternatively the inhibitor might be binding at a site different from that of the active site, thus resulting in a negative allosteric effect. For *T. cruzi* the observed effect could be explained by the presence of Leu242, which, if mutated to the human counterpart (Thr), abolished inhibitor activation of activity and resulted in pronounced inhibition at lower inhibitor concentrations [186]. In *PfAdoMetDC* this residue corresponds to Phe413, which is located adjacent to Phe415, an essential residue involved in substrate binding. Interestingly, human AdoMetDC inhibition with CGP48664 was shown to be extremely effective only in the presence of putrescine and subsequent co-crystallisation showed inhibitor binding within the active site [124].

Currently, AdoMetDC from various sources are classified into five distinct subclasses based on oligomeric structure (α - and β -subunits as well as prozyme binding), mechanism of autocatalytic processing and activation factors [196,197]. The subclasses can be divided into two main groups; those from bacterial or archeal origin are in Group 1 while the eukaryotic AdoMetDCs fall into the second group (Table 3.10). Group 1 is further subdivided based on oligomeric status and the requirement of a metal ion for activity (subclass 1a: gram-negative bacteria, tetramer) or an unknown activation factor (subclass 1b: gram-positive bacteria and archaea, dimer). Group 2 constitutes the eukaryotic enzymes that are not affected by putrescine (subclass 2a: plant, monomer) and those that do bind putrescine are further subdivided into the human (subclass 2b-I, dimer) and the trypanosomatids (subclass 2b-II, heterodimer with prozyme) AdoMetDC classes [196]. Based on these different groupings and with respect to monofunctional activity and oligomeric arrangement, *PfAdoMetDC* seems to belong to the parasitic AdoMetDC subclass 2b-II. However, properties such as the unique bifunctional arrangement, the presence of parasite-



specific inserts and lack of activation by putrescine or prozyme denote that AdoMetDC from *Plasmodium* spp does not fall within the subclasses that are currently described. We therefore propose a distinct subclass for plasmodial AdoMetDCs, namely subclass 2b-III for which a possible activation factor remains to be indentified (Table 3.10).

Table 3.10: Subclasses of AdoMetDCs from different organisms

Subclass	Fold	Oligomer	Stimulation/activation	Organism
1a	$(\alpha\beta)_4$	Tetramer	Metal ion	<i>E. coli</i>
1b	$(\alpha\beta)_2$	Dimer	Unknown	<i>T. maritima</i>
2a	$\alpha\beta$	Monomer	None	<i>S. tuberosum</i>
2b-I	$(\alpha\beta)_2$	Dimer	Putrescine	<i>H. sapiens</i>
2b-II	$\alpha\beta$ +prozyme	Heterodimer	Putrescine and prozyme	<i>T. cruzi, T. brucei</i>
2b-III	$(\alpha\beta)_2$ + <i>Pf</i> ODC	Heterotetramer	<i>Pf</i> ODC?	<i>P. falciparum</i>

3.5. Conclusion

In conclusion, this study has shown that *Pf*AdoMetDC expressed from a codon-harmonised gene appears as a monomer in moderate protein concentrations but we have strong indications that at high concentrations an oligomer appears that corresponds to that of the human protein, an $(\alpha\beta)_2$ dimer. This dimer was also shown to be stabilised under oxidising conditions by the formation of a disulphide bond between the Cys505 residues from each monomer. *Pf*AdoMetDC has therefore not lost its ability to dimerise and shares quaternary structure similarities to that of human AdoMetDC. Nevertheless the dimer affinity of *Pf*AdoMetDC is orders of magnitude lower than the human orthologue. The results also showed that, according to the estimated K_d values and at the concentration used for determining the specific activity of *Pf*AdoMetDC, more than 95% of the protein exists in the $(\alpha\beta)$ monomeric form. This correlates with a suggestion made previously that putrescine binding and dimerisation is linked [185]. Kinetics here and elsewhere [71] showed that monofunctional, monomeric *Pf*AdoMetDC behaves like other parasite AdoMetDCs while the bifunctional complex causes changes in the kinetic properties, which might be due to interdomain protein interactions imposed by the *Pf*ODC domain that result in coordinated domain activities. The results also show that an allosteric regulator remains to be identified that can activate the *in vitro* *Pf*AdoMetDC to the levels observed with the trypanosomal AdoMetDC and prozyme interaction [164,213]. Allosteric binding could induce conformational changes in one domain of the bifunctional complex that are then transmitted to the neighbouring domain. In our experiments *Pf*ODC seems the most likely target for such an effect as this domain is more refractory to change [69,103].



These studies contribute to the structural and functional characterisation of *PfAdoMetDC*, which points towards the classification of this protein into a distinct structural class, suggested as 2b-III. Furthermore, this study has provided important starting points for crystallography from which the structure can aid in the identification of drug-like lead compounds for the inhibition of *PfAdoMetDC* activity.

Chapter 4:

Validation of pharmacophore-identified inhibitors against *Plasmodium falciparum* SpdS with X-ray crystallography

4.1. Introduction

The ensemble of the polyamines; putrescine, spermidine and spermine has been shown to occur in millimolar concentrations within the parasite and correspondingly increase during the asexual, intra-erythrocytic developmental cycle of the parasite [10,67,100]. Upstream precursor metabolites required for the synthesis of polyamines including L-ornithine as substrate also increase during maturation of the parasites [214]. The stoichiometric by-product of spermidine formation, MTA, is catabolised and recycled to adenine and methionine within the parasites [215]. The level of spermidine exceeds that of other polyamines, emphasising the role of *PfSpdS* as a major polyamine flux determining protein [100]. Additionally, spermidine appears to have greater metabolic importance compared to the other polyamines as it is a prerequisite for the post-translational activation of eIF-5A (involved in translation initiation and elongation [216]) and in trypanosomes for the biosynthesis of the glutathione mimic, trypanothione [217]. Some effects of polyamine biosynthesis inhibitors have therefore been attributed to the accumulation of unmodified eIF-5A due to spermidine depletion while null mutants of SpdS have also demonstrated their essential role in the survival of *L. donovani* parasites [218]. Moreover, in the plasmodial parasite, biosynthesis of spermine has also been attributed to the action of *PfSpdS* [98], highlighting that attenuation of this protein holds promise to disrupt not only spermidine-dependent processes but also the formation of the downstream spermine metabolite [219].

The design of SpdS inhibitors has proven more challenging than expected with the most effective compound being 4MCHA (K_i of 1.4 μ M, Figure 4.1)[220]. Throughout the 1980s and early 1990s various putrescine and dcAdoMet analogues were synthesised but none were found to inhibit SpdS activity within the nanomolar range [221-226]. However, with the release of the first SpdS crystal structure from *T. maritima* (1JQ3) in 2002, which was co-crystallised with the multi-substrate, transition state analogue AdoDATO (Figure 4.1) [132], SpdS has again received attention. This is moreover evidenced by the release of 38 SpdS crystal structures of which ten are from *H. sapiens* and seven are from *P. falciparum*. Furthermore, *PfSpdS* and its importance as a possible drug target has also been revisited in the last couple of years with the use of transcriptomics and inhibitor co-crystallisation studies [119,182,227].

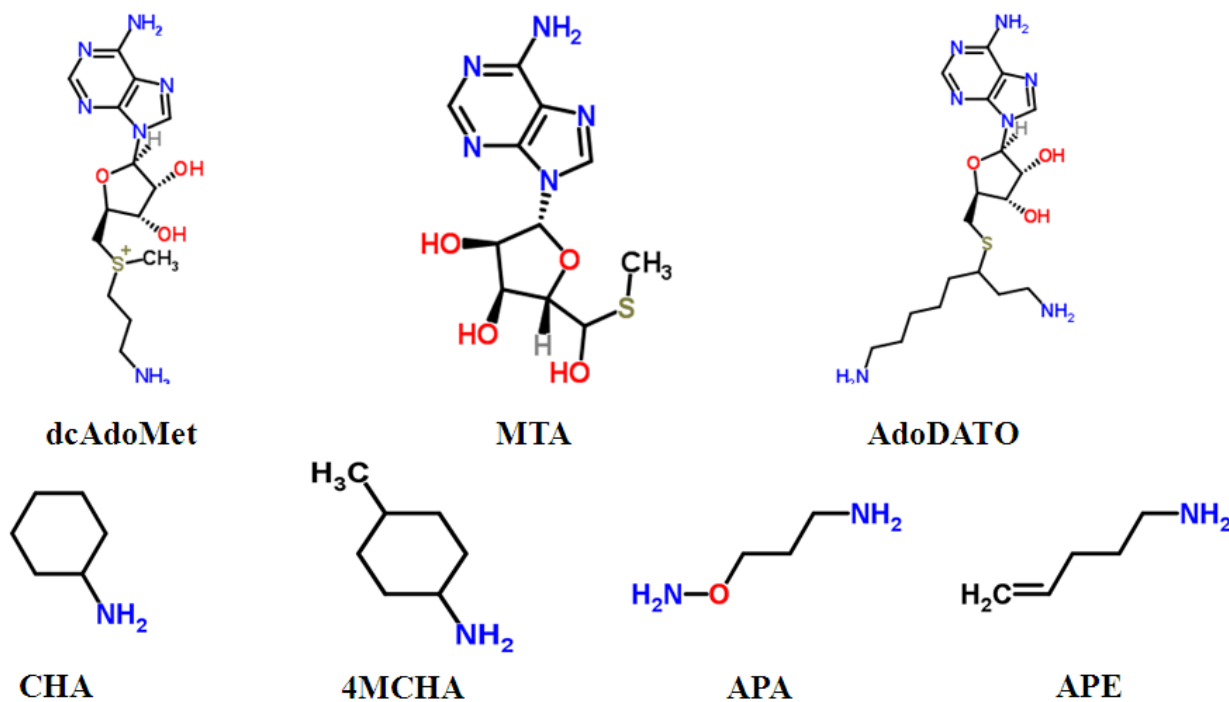


Figure 4.1: Chemical structures of various SpdS inhibitors.

Chemical structures were obtained from ChemSpider (<http://www.chemspider.com/>) where oxygen and hydroxyl groups are shown in red and nitrogen and amine groups are in blue. Abbreviations: AdoDATO, *S*-adenosyl-1,8-diamino-3-thio-octane; APA, 3-aminooxy-1-aminopropane; APE, 5-amino-1-pentene; CHA, cyclohexylamine; dcAdoMet, decarboxylated *S*-adenosyl-L-methionine; 4MCHA, *trans*-4-methylcyclohexyl amine; MTA, 5'-methylthioadenosine.

Despite the release of the *Pf*SpdS crystal structure, studies directed at polyamine biosynthesis as a drug target in *P. falciparum* have mainly been focused on *Pf*AdoMetDC and *Pf*ODC with attention only being paid to *Pf*SpdS in the last couple of years. Simultaneous targeting of these enzymes may also present a promising strategy in which to deplete polyamine biosynthesis within the parasite. In addition, since *Pf*SpdS is expressed during erythrocytic schizogony with both the mRNA and protein levels peaking at the late trophozoite stage [98], which coincides with the transcriptional abundance of the bifunctional *PfAdometdc/Odc* (Figure 1.7), simultaneous inhibition of all of the polyamine biosynthetic enzymes could take place during the same stage of the life cycle. Further studies are therefore needed to identify novel inhibitory compounds that can be used to explore *Pf*SpdS as a potential drug target for the chemotherapeutic treatment of malaria parasites.

The active site of SpdS contains two binding cavities, one for the adenosine substrate dcAdoMet and the other for the diamine putrescine. Early spatial deductions concerning the active site of SpdS suggested that the putrescine-binding cavity has favourable hydrophobic interactions with central primary alkyl components of putrescine and other alkylamines [226]. Other requirements for inhibitory activity of putrescine cavity binding compounds appeared to be related to the

atomic length of the alkyl chain and the flanking amine groups, illustrated by the fact that inhibitors 5-amino-1-pentene (APE), 4MCHA and APA have similar alkyl chains lengths (Figure 4.1) [98]. Of these, 4MCHA is considered as the most promising *Pf*SpdS inhibitor. This cyclohexylamine-based inhibitor was shown to occupy the putrescine-binding cavity where the cyclohexyl ring and methyl group align with the methylene groups of putrescine and the amine group occupies the region of the non-attacking nitrogen of putrescine [119]. Binding of the inhibitor was shown to be extremely effective with a K_i of 0.18 μM and an IC_{50} value of 35 μM on the parasites cultured *in vitro*. However, spermidine supplementation did not reverse the effects of inhibition and the possibility of 4MCHA having non-selective inhibition could unfortunately not be excluded [98]. Continuous *in vivo* administration of 4MCHA only reduced body-weight gain in rats and resulted in non-lethal altered spermine content in various tissues [228]. The inhibitor also had no effect on parasite proliferation *in vivo* and failed to cure *P. berghei*-infected mice [93], possibly due to assimilation of 4MCHA in the host organism. Extensive structure-activity relationship studies of this compound did not result in improved inhibitory compounds [226]. AdoDATO, resembling the dcAdoMet and putrescine transition state, has been shown to have remarkably good binding characteristics to *Pf*SpdS with an *in vitro* enzyme inhibitory activity of 8.5 μM . Subsequent X-ray co-crystallisation studies confirmed that the compound occupies both the dcAdoMet and putrescine-binding cavities [119].

Crystallographic evidence has sparked interest for the development and application of computational structure-based drug design approaches against *Pf*SpdS [119]. A study by Jacobsson *et al.* in 2008 identified several active site binders using a structure-based pharmacophore model, virtual screening and experimental validation with NMR. Two of the compounds were predicted to bind in the putrescine-binding cavity. Interestingly, these two compounds were shown to have stronger binding affinity in the presence of MTA, which could be due to the known feedback regulatory effects of MTA on *Pf*SpdS activity thereby providing additive inhibitory effects [98] or that the occupied dcAdoMet-binding site stabilises the binding of the compounds within the putrescine-binding pocket [97,119]. Several other compounds were predicted to bind in the dcAdoMet-binding cavity and were shown to compete with MTA. However, two weaknesses of this study include the treatment of the protein as a rigid body, which means that induced fit effects of compounds were not considered and several promising compounds could therefore have been missed as well as the similarity of the compounds to AdoMet. Since the binding interactions of AdoDATO were used as the search model in the pharmacophore model, many of the compounds resemble the AdoMet structure and may

therefore display off-target effects and reduced specificity due to the many important functions that AdoMet perform [178].

The lack of the discovery of effective compounds against *Pf*SpdS activity by following both ligand and receptor-based approaches warranted the need of a different approach to identify novel lead compounds. The development of a receptor-based, “dynamic” pharmacophore model (DPM) was consequently selected as the method of choice. This methodology was developed by Carlson *et al.* and attempts to account for the inherent flexibility of the active site, thereby aiming to reduce the entropic penalties associated with ligand binding [229]. The need to incorporate protein flexibility during virtual screening has been a long standing challenge and it is estimated that top docking algorithms incorrectly predict binding poses 50 to 70% of the time when a single rigid receptor structure is used [230].

In the doctoral study by P. B. Burger (University of Pretoria, [231]), a receptor-based DPM was developed to identify potential inhibitory compounds against *Pf*SpdS that could be optimised as good inhibitors of *Pf*SpdS [231]. The results from this study form the basis of this chapter in which the compounds that were identified were validated with the use of protein X-ray crystallography.

4.1.1. Identification of novel compounds against *Pf*SpdS with the use of a dynamic pharmacophore model

At the start of this study, several *Pf*SpdS structures had been deposited in the PDB database and therefore provided valuable starting points to develop a novel, receptor-based DPM for *Pf*SpdS. An area of 7 Å² containing 62 residues of the *Pf*SpdS active site co-crystallised with AdoDATO (2I7C, chain C) was used to create a subensemble, which was subsequently used in a MD simulation. This approach ensured a better sampling of the active site conformational changes than using a rigid protein backbone [229]. The clustering was performed separately for each monomer of the simulated dimer and the centre structures of the top five representative clusters of both monomers were selected and compared based on their root mean square deviation (RMSD) values. From these structures five structures were selected to best represent the RMSD range between the structures and were subsequently used in further studies (Figure 4.2). These selected structures were representative of 96.2% of the sampled phase space and should therefore be statistically more meaningful than randomly selected structures from the MD simulation.

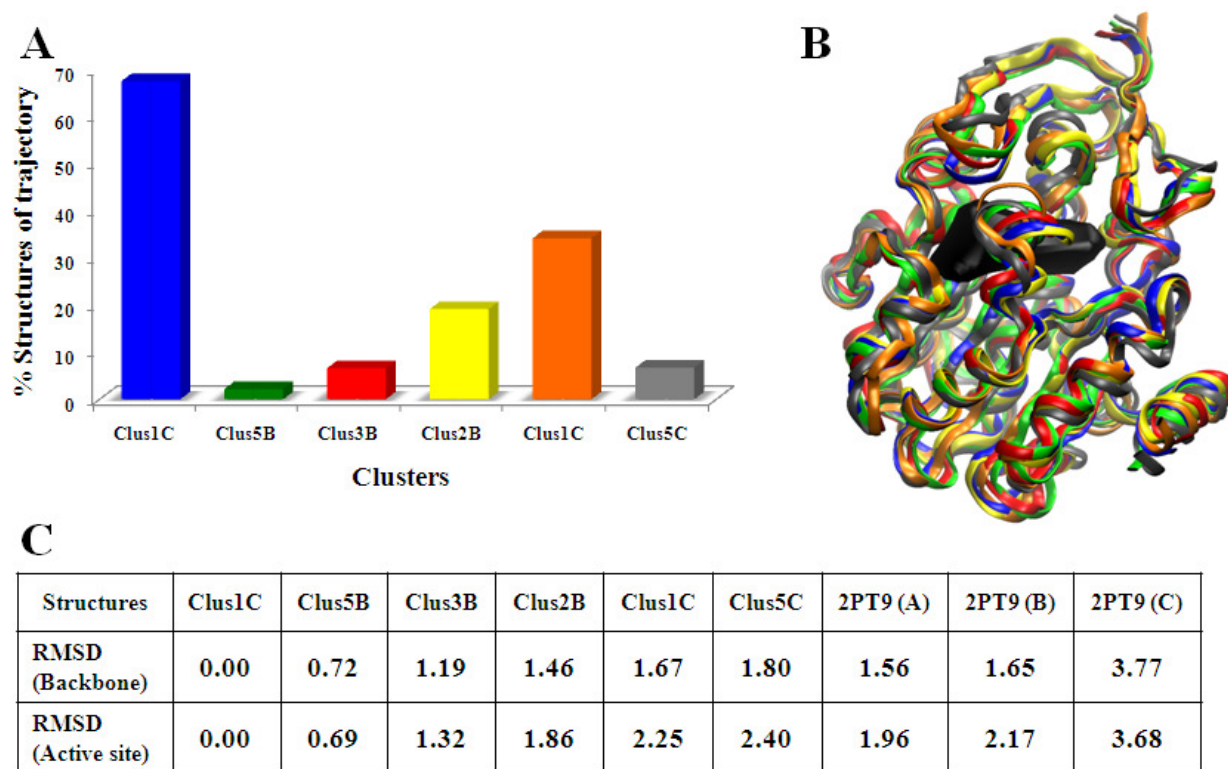


Figure 4.2: Clustering of the MD trajectory of *PfSpdS* in the absence of ligands.

(A) The representative cluster sizes in percentage of total structures sampled for both monomers B and C of the structures selected to represent the *PfSpdS* subensemble (i.e. Cluster 1 of monomer B (Clus1B) represents 68% of the total structures sampled for monomer B). (B) The representative structure ensemble obtained during phase space sampling of *PfSpdS* using MD. The active site surface is displayed in black. (C) The RMSD values of both the backbone and active site residues of the substructure ensemble. The RMSD values of the crystal structure of *PfSpdS* (2PT9 monomers A to C) are also included.

A comparison between the MD starting structure and the subensemble of structures revealed important conformational changes within the putrescine-binding cavity. Most significant is the conformational change that residue Gln229 undergoes in the absence of AdoDATO. The amide group of this residue orientates itself perpendicular in the apo-state compared to the orientation within the holo-state, which was later confirmed by the release of the apo-*PfSpdS* crystal structure (2PSS). The adopted orientation of Gln229 would not allow for the identification of pharmacophore features (PhFs) that represent binding of the attacking nitrogen of putrescine. Therefore, although the conformation of Gln229 adopted during the MD simulation was confirmed by the apo-*PfSpdS* structure, it was clear that using only the subensemble of structures for the development of a DPM would not adequately represent the binding characteristics of the active site and in particular the putrescine-binding cavity. Subsequently, the three monomers of *PfSpdS* co-crystallised with 4MCHA and dcAdoMet (2PT9) were included in the negative image construction of the *PfSpdS* active site. It was concluded that these structures provided adequate phase space sampling for both the bound- and apo-states.

The chemical space within the active site was subsequently explored using molecular interaction field (MIF) analysis to find energetically favourable binding hotspots by using probes representing hydrogen bond donor (HBD), hydrogen bond acceptor (HBA) and hydrophobic (HYD) pharmacophore features (PhFs). Visual inspection of the active site of the *Pf*SpdS crystal structures 2I7C and 2PT9 containing AdoDATO and 4MCHA, respectively, revealed two solvent molecules that make important interactions with their respective PhFs (residues Glu231 and Glu46) [119]. A water probe was therefore used to identify these binding hotspots for the water molecules within the subensemble of structures. These water molecules therefore facilitate PhF identification by providing important HBD and HBA characteristics within the binding areas of interest. The most common chemical moieties were found to be the NH, OH, CH₂ and NH₃⁺ entities and were subsequently considered in the selection of probes to explore the *Pf*SpdS active site.

As mentioned before, the active site of *Pf*SpdS is divided into two binding cavities, one for putrescine and one for dcAdoMet. The r-shaped cavity of the active site and its dimensions led to the subdivision of the entire active site into four binding regions, namely DPM1 through to DPM4, to facilitate the pharmacophore searches as well as to explore specific regions of interest within the protein (Figure 4.3). For each of these regions various DPMs represented by different combinations of PhFs were constructed. Figure 4.3A shows a 2D representation of the *Pf*SpdS active site with the natural occurring substrates within their respective binding cavities.

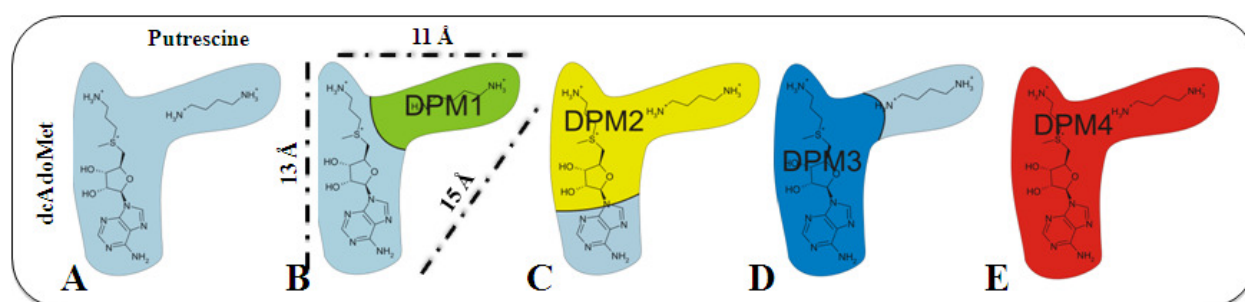


Figure 4.3: 2D representation of the active site of *Pf*SpdS illustrating different regions used to explore and construct DPMs.

(A) The *Pf*SpdS active site containing the natural occurring substrates dcAdoMet and putrescine within their respective binding cavities. (B) to (E) DPMs 1 to 4. The distances in Å between the furthest apart HBD PhFs within the entire binding cavity are shown in (B).

The DPM1 binding region was selected to explore the putrescine-binding cavity (Figure 4.3B, green). DPM2 was selected to explore the chemical space extending from the putrescine-binding cavity into the dcAdoMet-binding cavity by bridging of the catalytic centre (Figure 4.3C, yellow). DPM3 included the catalytic centre and was used to explore the dcAdoMet-binding

cavity (Figure 4.3D, dark blue) while DPM4 was used to explore the entire active site of *Pf*SpdS (Figure 4.3E, red).

The drug-like subset of the ZINC database containing 2 011 000 unique entries was screened for compounds using the DPMs. The compounds identified during these searches were fitted to their corresponding DPM to obtain the best fitting compounds and these were ranked accordingly. Visual inspection of these compounds was then performed to select the top compounds based on their fit values and orientation within the active site. Selected compounds were finally docked using AutoDock 4 [232] to evaluate their energy scores and poses within the active site. Representative compounds were selected for the four DPMs to test *in vitro* against the recombinant enzyme but only one of the nine compounds, which targets the DPM2 binding cavity, showed significant inhibitory activity and will therefore be discussed here.

4.1.1.1. Identification of compounds targeting the DPM2 binding cavity

Besides for AdoDATO that occupies the entire active site, there are currently no inhibitors that bind within the DPM2 cavity, which involves the catalytic centre. PhFs within this cavity were specifically selected (Figure 4.4A) and fourteen DPMs were constructed. The ZINC database screen resulted in 1800 hits for which the best-fit values were calculated and subsequently used in combination with visual inspection as selection criteria. Twenty-four compounds were selected and docked to evaluate the docking poses and related docking energies before they were considered for *in vitro* testing.

The compound *N*-(3-aminopropyl)-*trans*-cyclohexane-1,4-diamine (NACD) was rationally derived by taking into consideration the information obtained from MIF analysis as well as confirmed PhFs (protein-ligand interactions) and represents a basic structure or scaffold for an inhibitor of *Pf*SpdS, which is similar in structure to spermidine (Figure 4.4B). NACD is not commercially available but has been tested for inhibition against deoxyhypusine synthase and found not to inhibit the latter [233]. NACD was docked to *Pf*SpdS resulting in the expected binding poses with good binding energies. The cyclohexylamine ring of NACD would bind in a similar manner as 4MCHA does while the aminopropyl chain would bind to the same cavity as the aminopropyl group of dcAdoMet (Figure 4.4B). It is also expected that the hydrogen bonds between the nitrogen connecting the aminopropyl chain of NACD to the cyclohexylamine ring would reduce the binding penalty an aliphatic carbon would have by bridging the catalytic centre and thus increase the binding affinity and inhibition.

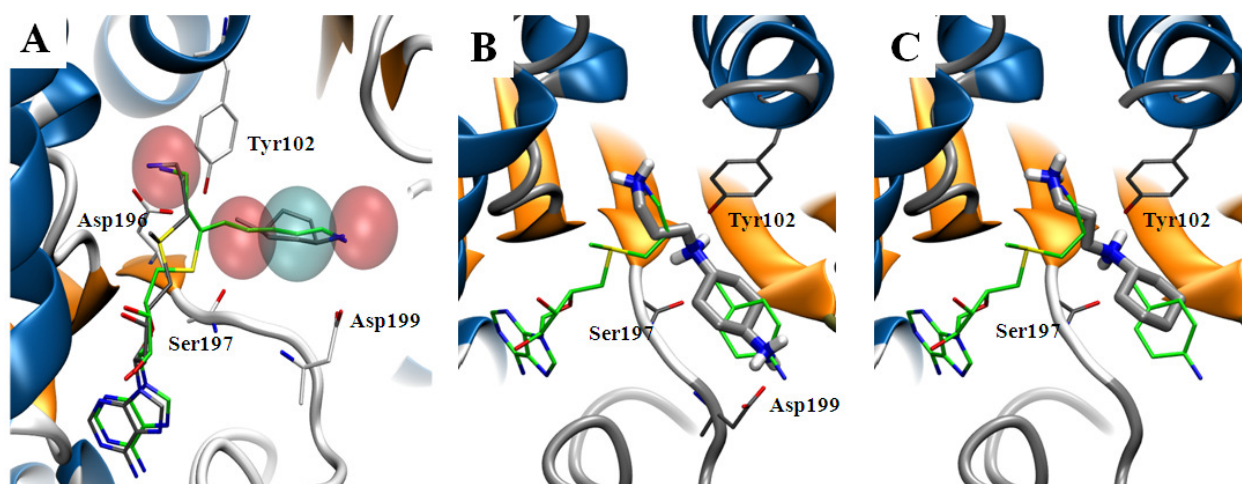


Figure 4.4: PhFs selected to describe the most important binding characteristics of the DPM2 binding cavity as well as the proposed docking poses of NAC and NACD within *Pf*SpdS.

(A) The PhFs best describing the binding characteristics of the DPM2 binding cavity within *Pf*SpdS. The red spheres represent the positive ionisable features and the blue sphere represents the hydrophobic feature. AdoDATO is shown in green and 4MCHA and dcAdoMet are shown in grey. The residues in white represent some of the residues that define the PhFs shown. (B) The docking pose of NACD (grey). Hydrogen bonds are predicted to form with Ser197 and Tyr102 upon binding. The aminopropyl chain of NACD bridges the catalytic centre and binds within a similar chemical space as the aminopropyl chain of dcAdoMet. 4MCHA and dcAdoMet are shown in green. (C) The docking pose of NAC (grey). NACD only differs in the additional amino group on the cyclohexyl ring, which is predicted to form a hydrogen bond with Asp199 that forms part of the gate-keeping loop (grey ribbon). 4MCHA and dcAdoMet are shown in green.

However, since NACD was not commercially available at the time, substructure searches using SciFinder were performed to identify similar compounds. *N*-(3-aminopropyl)-cyclohexylamine (NAC) was subsequently identified and was docked to *Pf*SpdS to evaluate its binding pose and docking energies. Good binding poses and low binding energies were obtained. NAC differs from NACD in that its ring moiety is a cyclohexylamine and not a 1,4-diaminocyclohexyl ring and therefore assumes the same binding pose and hydrogen bond pattern as NACD except for the missing amino group (Figures 4.4B and C). This made NAC a good alternative to test.

In this study we report the evaluation of two lead inhibitory compounds against *Pf*SpdS that were identified *in silico* with the use of a dynamic DPM with the aim of further chemical optimisation to promote these to potential antimalarial therapeutics. These hits were tested against the recombinant *Pf*SpdS protein followed by the kinetics of inhibition. These compounds were furthermore tested for their effect on the survival of *in vitro* cultured malaria parasites. Finally, protein crystallography was performed to validate the *in silico* predicted interactions of these compounds within the active site of the protein. Besides for the large AdoDATO complex, this is the first study that has identified an inhibitory compound that crosses the catalytic centre of the *Pf*SpdS active site and thereby competes with putrescine and dcAdoMet binding.

4.2. Methods

4.2.1. Enzyme kinetics of *PfSpdS* treated with lead inhibitor compounds

These studies were performed by S.B. Reeksting [101]. A 87 bp N-terminus deletion of *PfSpdS* cloned into pTRCHisB (Invitrogen) was expressed and purified from *E. coli* BLR (DE3) according to Haider *et al.* [98]. Purified *PfSpdS* was subsequently assayed and the spermidine reaction product was visualised and quantified using thin layer chromatography and liquid scintillation counting as described previously [98]. Statistical analysis was performed using paired Students t-test with GraphPad Prism v5.0 (GraphPad Software, Inc.) in which *P*-values below 0.01 were considered statistically significant.

Additional kinetic experiments were performed to determine the K_i of NAC (TCI Europe, 251 g/mol) by varying the putrescine concentrations and keeping the concentration of dcAdoMet fixed at 100 μ M. Reaction incubation and enzyme inactivation was performed as before.

4.2.2. *In vitro* growth inhibition of *P. falciparum*

These studies were performed by D. Le Roux [234]. *P. falciparum* strain 3D7 was maintained as described in the method of Trager and Jensen [235]. Parasites were synchronised with D-sorbitol (Sigma-Aldrich) according to established methods [236]. *In vitro* growth inhibition was monitored with the Malaria SYBR Green I Fluorescence assay [237,238]. The binding of SYBR[®] Green I (Invitrogen) to parasitic nucleic acids during the ring stage of parasite growth (1% parasitaemia, 2% haematocrit) was monitored at the end of a 96 h incubation period at 37°C. NAC and NACD (PharmaAdvance Inc, China, 280.61 g/mol) were selected for IC₅₀ determination. NAC was dissolved in dddH₂O and NACD in 1xPBS and the compounds were diluted two-fold from starting concentrations of 1 mM and 600 μ M in culture medium. Treated and untreated parasites were run in parallel and all assays were performed in triplicate in 96-well micro titre plates. A volume of 0.2 μ l of SYBR Green I/ml of lysis buffer (20 mM Tris/HCl pH 7.5, 5 mM EDTA, 0.008% (w/v) Saponin, 0.08% (v/v) Triton X-100) was added to each well followed by gentle mixing. After 1 h of incubation in the dark at RT, fluorescence was measured with a Flourosan Ascent FL Fluorimeter 2.4 with excitation and emission wavelengths of 490 nm and 520 nm, respectively and an integration time of 1000 ms.

Analysis of the fluorescence obtained was performed with SigmaPlot v11.0. Fluorescence readings were plotted against the logarithm of the compound concentration to produce a sigmoidal dose response curve. Curve fitting by non-linear regression was performed to yield the

IC₅₀ values, which represent the concentrations that produced 50% of the observed decline from the maximum counts in the untreated control wells.

4.2.3. Near-UV CD of *PfSpdS* in the presence of active site ligands

Near-UV CD was performed to test whether any structural changes take place when the active site is occupied by substrates or the NAC and NACD inhibitors. The results could also be used to validate possible structural changes observed with the protein co-crystallised with the inhibitors. Previous results have shown that binding of dcAdoMet or MTA stabilise the active site gate-keeping loop, which contains residues DSSDDPIGPAETLFNQN. The JASCO J815 CD instrument was used to determine the near-UV spectra of the purified *PfSpdS* protein at a concentration of 1 mg/ml (28.9 μM) in crystal buffer (10 mM HEPES pH7.5, 500 mM NaCl). The protein samples were incubated at RT for 30 min with [2.5 mM NAC] or [2.5 mM NACD], [2.5 mM putrescine], [20 μM dcAdoMet+2.5 mM spermidine] and [20 μM dcAdoMet]. The low amount of dcAdoMet relative to the protein concentration (20 μM versus 29.8 μM) that was used due to limited quantities of this compound could mean that possible structural changes as a result of dcAdoMet binding would not be detected. As control, the spectrum of the apo-protein was also measured. Measurements were conducted in 10 mm cuvettes at a wavelength range of 320 to 250 nm at 20°C, using a wavelength interval of 0.5 nm, a bandwidth of 1 nm and a scanning speed of 20 nm/min. Five readings were accumulated per sample, the spectrum of crystal buffer was subtracted and the data points were averaged.

Since near-UV CD gives a much weaker signal than far-UV CD double the amount of protein was used (1 mg/ml) than before (section 3.2.6) as well as a cuvette with a longer path length (10 mm versus 1 mm). The molar ellipticity ($[\theta]_M$) of each data point in units deg cm² dmol⁻¹ was calculated as follows according to Bale *et al.* [185]:

$$[\theta]_M = \frac{\Delta\theta \times MW}{10 \times l \times C}$$

Where $\Delta\theta$ is the reading in degree, MW is the molecular weight of the protein in g/mol, l is the path length in cm and C is the concentration of the protein in mg/ml.

Signals that arise in the region from 250-270 nm are attributable to Phe, signals from 270-290 nm are from Tyr and those from 280-300 nm are from Trp. Disulphide bonds give rise to broad weak signals throughout the spectrum.

4.2.4. Protein crystallisation of *PfSpdS* in complex with lead inhibitor compounds

4.2.4.1. Protein purification

For protein crystallisation of *PfSpdS*, the gene sequence corresponding to a protein lacking 39 residues at the N-terminus and cloned into the p15-TEV-LIC vector was obtained from the Structural Genomics Consortium in Toronto (<http://www.sgc.utoronto.ca/>). Protein expression and isolation was followed according to Dufe *et al.* and included purification via both anion exchange (aIEX) and SEC [119]. Briefly, clear cell lysate after cell disruption and ultracentrifugation was loaded onto a DEAE Sepharose column (GE Healthcare) previously activated with 2.5 M NaCl and equilibrated with binding buffer (50 mM HEPES pH 7.5, 500 mM NaCl, 5 mM imidazole, 5% (v/v) glycerol). The column was washed with 20 ml binding buffer and the flow-through was collected in 0.5 ml fractions at a flow rate of 0.5 ml/min. The sizes of the proteins within the fractions that gave rise to large protein peaks at an absorbency of 280 nm were analysed with SDS-PAGE to identify the monomeric *PfSpdS* with a size of ~30 kDa. These fractions were then combined and loaded onto a 2 ml Ni-NTA column (Sigma-Aldrich), pre-equilibrated with binding buffer. The beads were subsequently washed with 200 ml wash buffer (50 mM HEPES pH 7.5, 500 mM NaCl, 30 mM imidazole, 5% glycerol) followed by protein elution with 15 ml elution buffer (50 mM HEPES pH 7.5, 500 mM NaCl, 250 mM imidazole, 5% glycerol). A final concentration of 1 mM EDTA was added to the eluate followed by 5 mM DTT approximately 15 min later. The eluate was concentrated using a 15 ml Amicon Ultra centrifugal filter device (MWCO 3000, Millipore) to a volume of 1 ml. The concentrated protein was subsequently loaded onto a Superdex[®]-S200 10/300 GL SE column (Tricorn, GE Healthcare) connected to an Äkta Prime System (Amersham Pharmacia Biotech) pre-equilibrated with crystal buffer at a flow rate of 0.5 ml/min and 0.5 ml fractions corresponding to the homodimeric ~60 kDa protein were collected.

His-tag cleavage with 500 U ProTEV protease (Promega) was performed overnight at 4°C in the presence of 1 mM DTT. ProTEV protease contains an N-terminal HQ-tag (HQQHQ, Promega) such that, together with the cleaved His-tag from the recombinant *PfSpdS* protein, it can be removed from the reaction by incubating it with a metal-affinity resin. The *PfSpdS* protein without the His-tag was therefore purified via a second Ni-NTA purification by collection of the flow-through. The column was washed with an additional 10 ml of binding buffer and the eluates were combined. The ProTEV and cleaved His-tag was subsequently eluted with elution buffer. Cleavage of the His-tag was confirmed with Western immunodetection using 1:2500 HisProbe[™]-HRP (Pierce Biotechnology) and 1:2500 of polyclonal *PfSpdS* antiserum, which

was raised in rabbits. For the latter Western blot goat anti-rabbit IgG-HRP was used as secondary antibody. Western blotting was then performed as stipulated in section 2.2.6. Finally, buffer exchange was performed in crystal buffer with a centrifugal filter to a protein concentration of 22.8 mg/ml and stored at 4°C.

4.2.4.2. Protein crystallisation

Purified *PfSpdS* was crystallised in the presence of NACD, MTA and NAC using the hanging drop vapour diffusion method at 293 K. Protein solution was mixed with reservoir solution containing 25% (w/v) PEG3350 (Sigma-Aldrich), 0.1 M MES pH 5.6 and 0.1 M $(\text{NH}_4)_2\text{SO}_4$. The *PfSpdS*-NACD complex was obtained by using 10 mg/ml protein pre-incubated with 2.5 mM NACD for 30 min at RT before mixing 1 μl with 2 μl reservoir solution. The *PfSpdS*-NACD-MTA complex was obtained with pre-incubation of 5 mg/ml protein with 2.5 mM of both NACD and MTA followed by mixing 1 μl with 1 μl of reservoir solution while 10 mg/ml protein was used at the same ratio for the *PfSpdS*-NAC-MTA complex.

Prior to data collection, crystals were transferred to cryo protectant solution containing the reservoir solution and 15% glycerol before being flash frozen in a liquid nitrogen stream at 100 K. Data was collected at beam line I911-2 (MAX-lab, Lund, Sweden) and processed using the XDS package [239].

Molecular replacement was performed with CNS v1.2 [240,241] using apo-*PfSpdS* (2PSS) as template for *PfSpdS*-NACD and *PfSpdS*-MTA (2HTE) for both *PfSpdS*-NACD-MTA and NAC-MTA. The programmes Coot, CNS v1.2 [240,241] and CCP4 [242] were used for model building and refinement. The library files for NAC and NACD were generated using the PRODRG server [243]. The electron density maps were visualised to localise the traces of the polypeptide chains in the molecular graphics programme COOT. Model refinement was then performed with reftmac v5.5 (CCP4 v6.1.13) [242,244] and CNS v1.2 followed by the manual adjustment of residues according to several geometrical constraints and also for improved fitting of atoms within their respective densities. The updated coordinate files were then used to calculate improved electron density maps, which was followed by another cycle of model building. With each iterative cycle of model building, map generation and model refinement, the side chains became correctly assigned with acceptable peptide geometries (bond lengths and angles) and side chain rotamers.

The main chain polypeptide conformations of the crystal structures were verified by Ramachandran plots [245] with the programme RAMPAGE [246]. In these plots the dihedral peptide angles phi (ϕ) and psi (ψ) are plotted for each residue (i.e. for each residue in all of the monomeric chains that are solved), and the positions of these data points should then lie in the allowed regions of ϕ and ψ angles that correspond to energetically acceptable protein secondary structures [247]. The goal is to obtain a structure in which all the solved residues lie within the favoured or at least allowed regions except for Gly residues, which are not restricted by ϕ and ψ angles and may therefore be located at any position.

Model quality was evaluated with PROCHECK (Appendices I, II, III) [153] and the Joint Structural Genomics Consortium (JCSG) Quality Control v2.7 (<http://smb.slac.stanford.edu/jcsg/QC/>), which contains MolProbity (<http://molprobity.biochem.duke.edu/>) [248] and ADIT (<http://deposit.pdb.org/validate/>) checks.

4.3. Results

4.3.1. Enzyme kinetics and *in vitro* parasite treatment of novel inhibitory compounds against *PfSpdS*

In vitro testing of NAC at a 100 μM concentration showed a remarkable 86% reduction in *PfSpdS* activity, which warranted further investigation of this compound. Enzyme kinetics was subsequently performed for the compound and the K_i value was determined (Figure 4.5A). Data from a Lineweaver-Burk extrapolation indicated a similar K_m value for putrescine at 25.1 ± 3.2 μM and a slightly lowered V_{max} value at 96.4 ± 2.7 $\mu\text{mol}/\text{min}/\text{mg}$ than previously reported [98]. Additionally, in the presence of NAC the K_m and V_{max} parameters of *PfSpdS* were affected. For NAC to be a true competitive inhibitor of the putrescine-binding site, only the K_m value is expected to change. However, the kinetic data showed that the V_{max} was not re-established at putrescine concentrations far greater than its K_m , suggesting that NAC also affected the binding of the second substrate, dcAdoMet and that the additional putrescine was not able to disrupt the tight binding interaction of NAC. A secondary plot from the Lineweaver-Burk plot was used to calculate the K_i value of NAC, which was found to be 2.8 μM (Figure 4.5B). Inhibition kinetics with NACD was unfortunately not performed due to the compound not being commercially available at the time of recombinant protein testing.

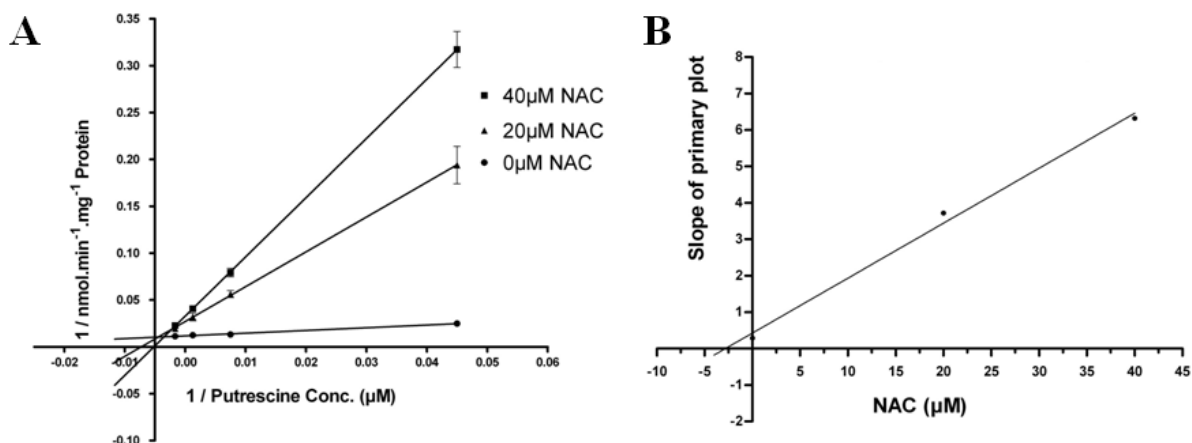


Figure 4.5: Inhibition kinetics of *PfSpdS* treated with NAC.

(A) Lineweaver-Burk plot and (B) secondary Lineweaver-Burk plot of the slopes obtained from the plot in (A) versus inhibitor concentration to determine K_i . Results are the mean of five independent experiments \pm S.E.M.

Furthermore, the ability of compounds NAC and NACD to inhibit the growth of *P. falciparum* parasites cultured *in vitro* was determined using standard growth inhibition assays. Subsequent IC_{50} determinations showed that NAC has an inhibitory activity of $105 \pm 13 \mu\text{M}$ ($n=5$) while that of NACD is slightly more effective at $81.2 \pm 13 \mu\text{M}$ ($n=7$) (Figures 4.6A and B). The physiological effects of the inhibitors on parasite growth were also investigated via the treatment of the parasite cultures with $2 \times IC_{50}$ concentrations of each inhibitor immediately following the infection stage. Parasite morphology showed changes at 72 h post-treatment with NAC whereas changes were observed as soon as 48 h post-treatment with NACD [234]. Treatment also resulted in delayed cell cycle progression compared to the untreated culture. Furthermore, co-treatment of either NAC or NACD with the AdoMetDC inhibitor MDL73811 or ODC inhibitor DFMO showed additive inhibition [234]. These results indicate that the simultaneous inhibition of *PfODC* and *PfSpdS* could result in a polyamine depleted state within the parasites.

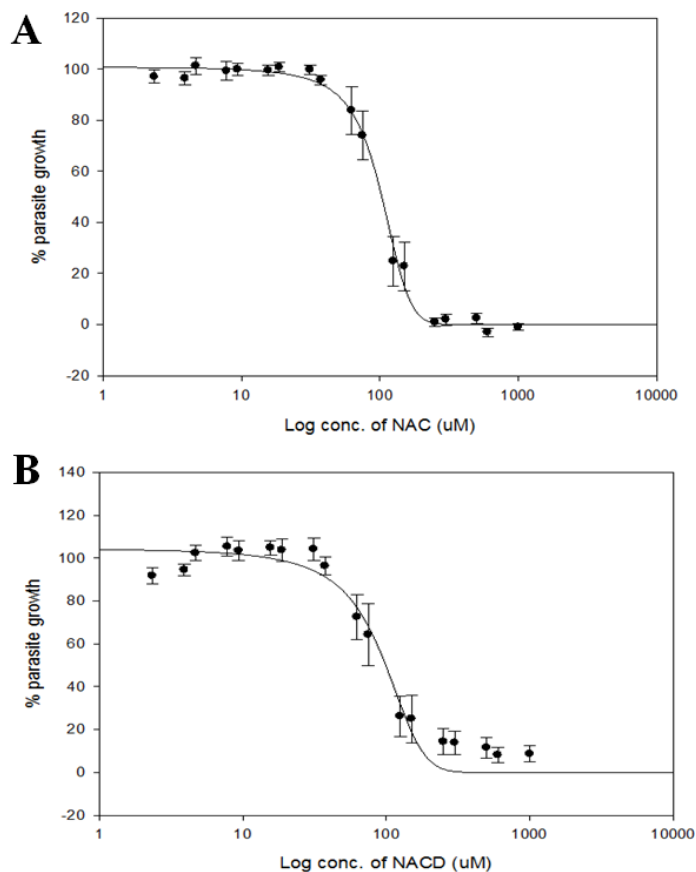


Figure 4.6: Dose response curves of *P. falciparum* cultures treated with NAC (A) and NACD (B) for determination of IC_{50} values.

Results are shown as S.E.M and were obtained from five individual experiments for NACD (n=5) and seven experiments for NACD (n=7), performed in triplicate.

Based on the *in vitro* results it is anticipated that, compared to NAC, the inhibition efficiency of NACD on the recombinant protein would be more effective, since the extra amine group on the cyclohexyl moiety is predicted to stabilise inhibitor binding within the active site via interaction with Asp199. Subsequently, the *in silico* predicted binding interactions of the lead inhibitor compounds were validated with the use of X-ray crystallography of the protein in complex with these compounds.

4.3.2. Preparation of high yields of pure *Pf*SpdS for protein crystallography

Large-scale expression of *Pf*SpdS for crystallisation studies was obtained from 2.5 liters of bacterial culture followed by protein purification involving aIEX, batch purification with Ni-NTA resin and SEC. aIEX analyses of the total soluble lysate collected after cell disruption and ultracentrifugation showed the elution of four major peaks corresponding to fractions #7 (V_e 5 ml), #17 (10 ml), #21 (11.8 ml), #26 (14.2 ml) (Figure 4.7A). *Pf*SpdS consists of 283 residues and has a pI of 6.18. The presence of *Pf*SpdS within these fractions was confirmed with SDS-PAGE with an expected monomeric protein size of ~31 kDa under denaturing conditions.

The SDS-PAGE results showed the presence of a protein ~31 kDa in size in fractions #17 and #21, with a small amount in #26 (Figure 4.7B), which could correspond to the monomeric *PfSpdS* protein under the denaturing SDS-PAGE conditions. Several contaminating proteins were also present within the collected samples to be removed during the secondary and tertiary purification steps. Fractions 12-24 were pooled and concentrated for subsequent affinity chromatography using Ni-NTA resin. The 5 mM imidazole within the binding buffer should not interfere with His-tag binding and was therefore not removed prior to column loading.

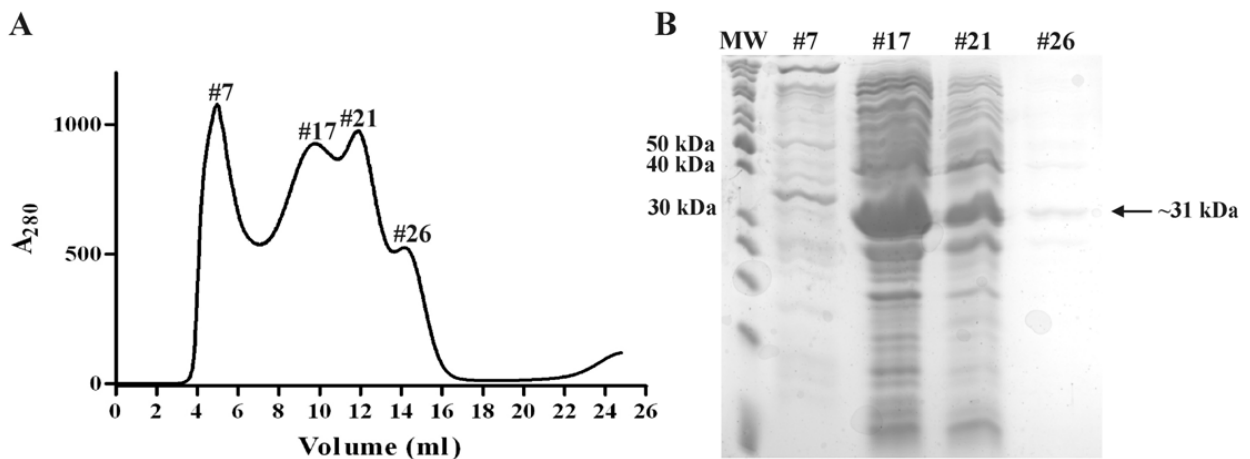


Figure 4.7: The aEX chromatogram (A) and subsequent SDS-PAGE analysis (B) of the *PfSpdS* fractions. MW: PageRuler Unstained Protein Ladder; #7, #17, #21, #26: fractions collected with aEX. The expected size of the monomeric *PfSpdS* protein is shown.

The His-tagged *PfSpdS* sample eluted from the Ni-NTA resin in 15 ml elution buffer was further purified by separation with SEC. The results showed the presence of a major protein peak at a V_e of 16.3 ml (Figure 4.8A), indicating the successful removal of the untagged, contaminating proteins as seen in Figure 4.7B during the washing step of affinity chromatography. The protein peak corresponds to a calculated size of the ~60 kDa homodimer and fractions 13-18 were collected and pooled (Figure 4.8). Denaturing SDS-PAGE analyses of the affinity and SE chromatography-purified proteins showed the presence of the pure monomeric *PfSpdS* protein at ~31 kDa. A small amount of protein ~70 kDa in size could represent *E. coli* Hsp70, a protein that often co-purifies during plasmidial proteins expression in *E. coli*, but still needs to be verified with MS.

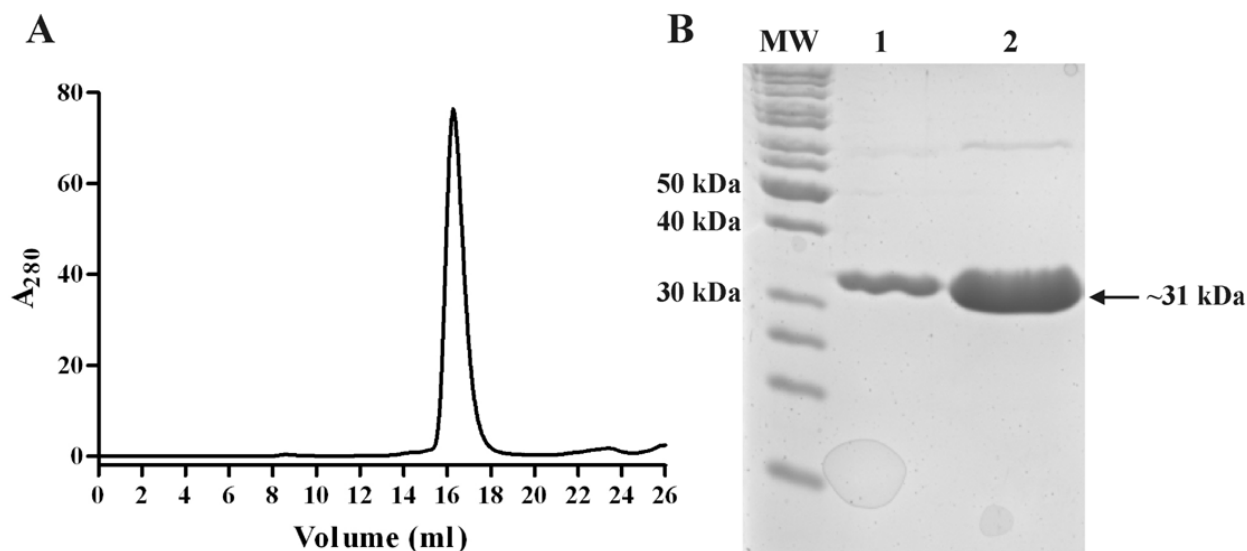


Figure 4.8: SEC of affinity-purified *Pf*SpdS (A) followed by SDS-PAGE analysis (B).

(A) The protein sample eluted with affinity chromatography and the concentrated pooled fractions obtained from SEC are shown in lanes 1 and 2, respectively (B). MW: PageRuler Unstained Protein Ladder. The expected size of the monomeric *Pf*SpdS protein is shown.

Affinity tags such as 6xHis and Strep are short, flexible peptides and can often hamper the crystallisation process by interfering with the establishment of crystal contacts. In general it is therefore beneficial to remove these prior to crystallisation screens with the use of proteases that cleave the tags at engineered protease recognition sites. In the case of *Pf*SpdS, a seven residue ProTEV cleavage site (EXXYXQG/S) is present prior to the C-terminal His-tag, which could therefore be removed with the use of the highly site-specific ProTEV enzyme. The cleavage reaction in the presence of DTT was optimised for *Pf*SpdS-His in terms of reaction temperature and duration. Subsequent Western immunodetection with both the HisProbe[®]-HRP (Figure 4.9A) and a polyclonal *Pf*SpdS antibody (Figure 4.9B) confirmed the absence of the His-tag in the *Pf*SpdS protein after Ni-NTA elution (lane 2).

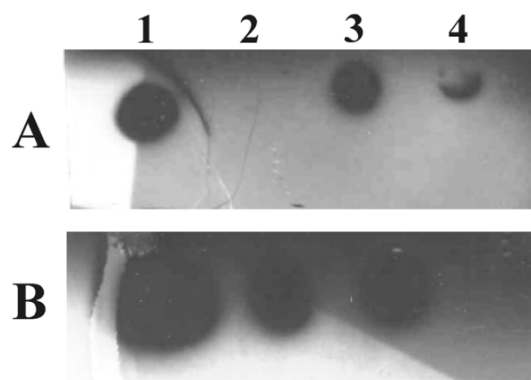


Figure 4.9: Western immunodetection of the ProTEV cleavage products collected after affinity chromatography using HisProbe[®]-HRP (A) and a polyclonal *Pf*SpdS antibody (B).

Lane 1: *Pf*SpdS-His collected from SEC as control of recombinantly expressed protein containing a His-tag; lane 2: flow-through of *Pf*SpdS (cleaved His-tag) collected from Ni-NTA; lane 3: eluted His-tag and Pro-TEV (containing HQ-tag) with elution buffer; lane 4: sample collected during washing of the Ni-NTA resin.

Western immunodetection confirmed the absence of the His-tag on *PfSpdS* collected from the flow-through during Ni-NTA purification since removal of the tag prevents the protein from binding to the resin (Figures 4.9A and B, lane 2). The cleavage reaction was, however not 100% efficient, since His-tagged *PfSpdS* protein was detected in the sample collected during the elution step (Figures 4.9B, lane 3) while the eluate probably contained cleaved His-tags, ProTEV protease (with HQ-tag) and *PfSpdS*-His (Figures 4.9A, lane 3). Cleaved His-tags were also eluted during the washing step (Figures 4.9A, lane 4). The flow through collected (sample in lane 2) was finally concentrated to 22.8 mg/ml (total yield of 11.4 mg) and the protein was stored at 4°C until the crystallisation trials were performed.

4.3.3. Near-UV CD analyses of *PfSpdS* in the presence of NAC or NACD

Prior to solving the crystal structures, the tertiary structures of *PfSpdS* in the presence of various active site ligands were determined with near-UV CD (Figure 4.10). In this way, changes in specifically the aromatic amino acids (as an indicator of tertiary structure) and possible effects that the compounds may have on the conformation of the active site and gate-keeping loop can be observed, which can then be validated with the crystal structures. Previously it was suggested that the sulphide atom on dcAdoMet or MTA is involved in stabilisation of the loop [119] and from a drug discovery perspective it would therefore be of interest to determine the effect of NAC or NACD in the presence of MTA or dcAdoMet on this loop.

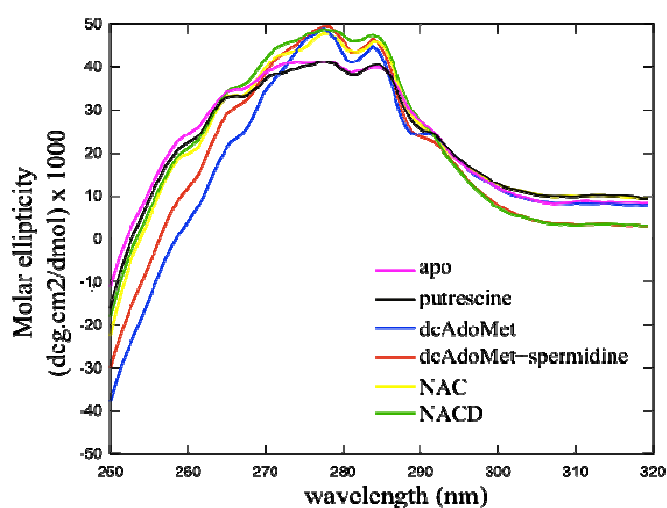


Figure 4.10: Near-UV CD analyses of *PfSpdS* in the presence of various ligands.

The purified *PfSpdS* protein was treated with putrescine, spermidine, dcAdoMet, NAC and NACD in different combinations and at specific concentrations and the spectra in the near-UV CD wavelength range of 250 nm to 320 nm were measured. Results are given as molar ellipticity ($[\theta]_M$) in units $\text{deg cm}^2 \text{dmol}^{-1}$.

The spectra of the *PfSpdS* incubated with NAC (yellow line), NACD (green) and dcAdoMet (blue) showed remarkable similarity with no major differences therefore indicating that the

tertiary structures of these proteins are similar (Figure 4.10). Additionally, this result may indicate that binding of these ligands results in similar conformations of the active site and gate-keeping loop. On the other hand, in comparison to the spectra of the apo (Figure 4.10, pink line) and putrescine (black) samples, the ligand-bound samples show differences in terms of the signal strength and peak overlaps. The spectra of the apo and putrescine samples show high similarity and could indicate that the structures of the *PfSpdS* protein with empty or partially filled active sites are similar. As previously suggested, the flexibility of the gate-keeping loops of these protein samples may also contribute to the observed spectra [119]. Finally, the difference in the Tyr absorption area (270-290 nm) between the apo and NAC/NACD spectra may be due to the movement of Ty264, which could be involved in the stabilisation of the cyclohexyl rings, as previously observed for 4MCHA binding [119].

4.3.4. Growth of diffraction quality *PfSpdS* protein crystals in complex with NAC or NACD

To validate the predicted binding of NACD and NAC within the active site of *PfSpdS*, the compounds were co-crystallised with the protein to provide atomic resolution information on the inhibitor interactions. Several manual crystal screens of the His-cleaved, pure *PfSpdS* protein in complex with NAC, NACD and MTA were performed using the hanging drop vapour diffusion method at temperatures of 288 and 295 K. The buffer system, pH, amount of PEG3350, protein concentration and drop sizes were varied until diffraction quality crystals were obtained. All crystals grew within a couple of days at 295 K in either 2 or 3 μ l drops of 5 or 10 mg/ml protein treated with 2.5 mM inhibitor in 0.1 M MES pH 5.6 precipitant solution containing 25% PEG3350 and 0.1 M $(\text{NH}_4)_2\text{SO}_4$. The crystals were shaped as three-dimensional hexagons with average dimensions of 0.1x0.3x0.06 mm (Figure 4.11). The crystal structures previously published for *PfSpdS* were crystallised in 0.1 M BisTris pH 5.5 containing 23% PEG3350 and 0.1 M $(\text{NH}_4)_2\text{SO}_4$.

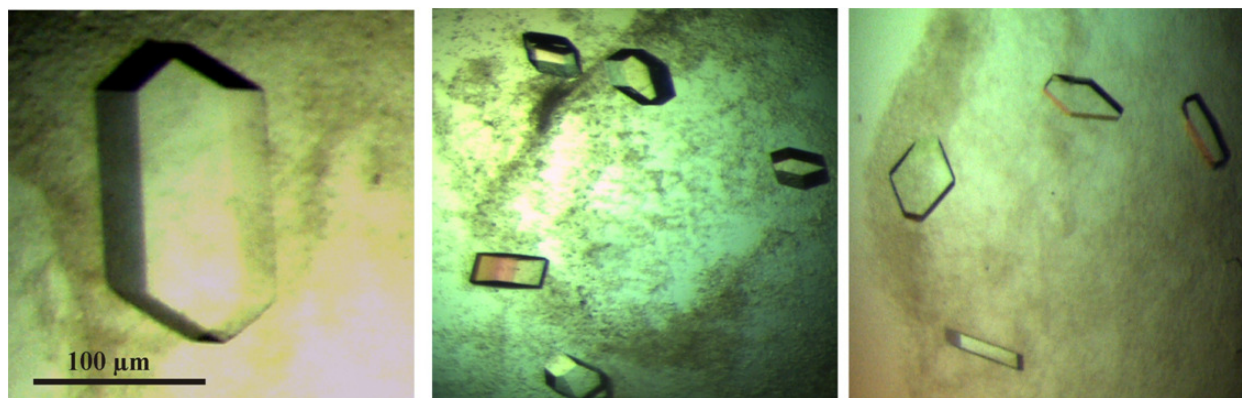


Figure 4.11: Images of *PfSpdS* crystals in complex with NAC or NACD.

Crystals were grown at 295 K in 0.1 M MES pH 5.6 precipitant solution containing 25% PEG3350 and 0.1 M $(\text{NH}_4)_2\text{SO}_4$ with the hanging drop vapour diffusion method.

4.3.5. X-ray crystallography verifies binding of NAC and NACD in the active site of *PfSpdS*

4.3.5.1. Crystal structure refinement results

Following crystal rotation data collection, several key steps were followed to arrive at the stage where the models could be built, these included 1) analysis of the observed reflections and positions thereof in the detector plane and optimisation of the detector distance; 2) integration of the diffraction intensities; 3) spacegroup definition and 4) correction of data followed by data scaling. Prior to the collection of the full data sets, several parameters were studied to examine the quality of data and to assign the spacegroup. The correct parameters could then be specified as required by the spacegroup in order to collect the maximum number of possible reflections. The observed diffraction patterns showed the positions of the recorded reflections for a particular plane of the crystal. The crystals were then rotated at specified angles such that exposure with X-ray could detect the remaining reflections. The XDS package was used in this study to perform these initial tasks [239].

In the case of the *PfSpdS*-NACD crystal, two data sets were collected; firstly for the intensities in the low resolution range (1-8 Å), 200 frames were collected at an oscillation of 1° and an exposure time of 50 s after which the exposure time was decreased to 15 s for collection of 100 frames with an oscillation of 2° to collect the intensities in the high resolution range (1-2.5 Å). This strategy ensured that the intensities at low resolution were detected with the longer exposure time while overloading of the intensities at high resolution was prevented by collection of the high-resolution data with the shorter exposure time. These two data sets were then integrated separately and merged prior to reflection scaling. A single dataset was collected for *PfSpdS*-NACD-MTA consisting of 200 frames of 20 s per frame. Although crystals for the

PfSpdS-NAC complex were obtained, diffraction data could not be collected possibly due to a high degree of crystal disorder. In addition, only 132 frames were collected for the *PfSpdS*-NAC-MTA crystal due to a problem that occurred with the cryo stream during diffraction, however with the collected data ~93% completeness in the high-resolution shell was still obtained.

The reflection files were then used to solve the phase problem, which in this study was performed by molecular replacement with published crystal structures of *PfSpdS* as templates. These structures provided information on the phase angles and by incorporating translation and rotation functions the test and template molecules could be aligned within the asymmetric unit (ASU), such that, together with the structure factors, the models could be built with the corresponding electron density maps. The data collection and refinement statistics of the solved crystal structures are listed in Table 4.1.

The cell dimensions of the *PfSpdS*-NACD-MTA and NACD structures are identical and data was collected in the same resolution ranges for both. The data collection for NACD-MTA was complete in the high resolution shell and provided good estimates for the quality of data scaling and averaging as given R_{meas} (Table 4.1). The latter is the multiplicity-independent factor, which means that it does not increase with an increase in redundancy (multiplicity) as R_{merge} does [249]. The multiplicity for the NACD data sets was between 4 and 5, which means that each reflection was measured 4 to 5 times during data collection, these were then averaged during data scaling to give rise to approximately 98 000 unique reflections (multiple observations of the same and symmetry-related reflections). Finally, $I/\sigma(I)$ gives an indication of the signal strength of the observed intensities and, as observed for the data here, should not be less than two (Table 4.1).

Table 4.1: Crystallography data collection and refinements statistics

Data collection			
	NACD-MTA	NACD	NAC-MTA
Space group	C121	C121	C121
Unit cell dimensions	a=196.8 Å, b=134.6 Å, c=48.5 Å, β=94.6°	a=196.80 Å, b=134.59 Å, c=48.46 Å, β=94.55	a=196.71 Å, b=134.33, c=48.33 Å, β=94.7
Molecules per asymmetric unit	3	3	3
Resolution range (Å)	20.1-1.89	20.0-1.89	19.8-2.39
No. of reflections	413846	492876	137713
No. of unique reflections	98147	98435	45723
Completeness (%) ^a	99.8 (100)	99.6 (99.8)	92.4 (94.3)
Multiplicity	4.2	5	3
R_{meas} (%) ^{a, b}	5.9 (41.1)	5.1 (39.8)	8 (43.6)
$I/\sigma(I)$ ^a	18.5 (3.9)	19.3 (4.1)	13.9 (4.3)
Refinement statistics			
Number of reflections	93239	93506	43435
$R_{\text{work}}/R_{\text{free}}$ ^c	0.18/0.21	0.21/0.24	0.19/0.24
No. of atoms	7493	6780	6999
protein	6745	6481	6656
water	617	211	243
NACD	36	36	-
MTA	60	-	60
glycerol	18	18	18
1PG	17	34	17
SO ₄	-	-	5
 (Å ²)	25.4	36.5	29.6
RMS deviations			
Bond length (Å)	0.029	0.026	0.022
Bond angles (°)	2.08	1.995	1.938
Ramachandran statistics (%) ^d			
Favoured	97.2	96.2	96.1
Allowed	99.9	100	99.9
Outliers	0.1	0	0.1

^a The numbers in parentheses are of the highest resolution shell.

^b $R_{\text{meas}} = (\sum_i \sqrt{\frac{n_i}{n_i-1}} \sum_j |I_{ij} - \langle I_i \rangle|) / (\sum_i \sum_j \langle I_i \rangle)$, the redundancy-independent factor, where n is the number of observations for reflection i .

^c R_{free} is the same as R_{work} , but calculated on 5% of the data excluded from refinement. $R_{\text{work}} = (\sum |F_o - F_c|) / (\sum F_o)$, where F_o and F_c are the observed and calculated structure factor amplitudes, respectively.

^d Ramachandran statistics were calculated using Molprobity [248].

Model refinement resulted in well defined structures such that crystallographic solvent molecules could be identified. A good indicator of model progression was given by the R -factor (R_{work}), which was calculated throughout the refinement steps and gave an indication of the agreement between the observed and the calculated data (Table 4.1). However, the over interpretation or over fitting of data, for example when too many solvent molecules are fitted resulting in a compensation for model errors, can result in a value that is too low regardless of the correctness of the model. The so-called R_{free} factor was therefore assessed, which used reflection data from a test set (representing 5% of the total data) that was not subjected to model refinement and therefore represented an unbiased indicator of model quality [247]. The R_{free} is therefore slightly higher than the R_{work} . For the *PfSpdS* structures the R_{work} values were in a range that resulted in

well defined structures from which residues and solvent molecules could be clearly localised (Table 4.1).

The main chain polypeptide conformations of the crystal structures were verified by RAMPAGE-generated Ramachandran plots [245] (Figures 4.12 and 4.13) [246]. RAMPAGE uses a plot in which the borders of areas were computed by analyses of 81234 non-Gly, non-Pro, and non-pre-Pro residues with B-factors of less than 30 from 500 high resolution protein crystal structures. This resulted in a plot with sharp boundaries at the critical edges between regions as well as clear delineations between the empty areas and regions that are allowed but not favoured. The Ramachandran plot of the structure of *Pf*SpdS co-crystallised with NACD showed that no residues were located in the outlier regions (white areas) while 96.5% of the residues were positioned in the favoured regions (Figure 4.12 and Table 4.1). In addition, all Gly and Pro residues were in the favoured areas while a few pre-Pro residues were located in the allowed regions.

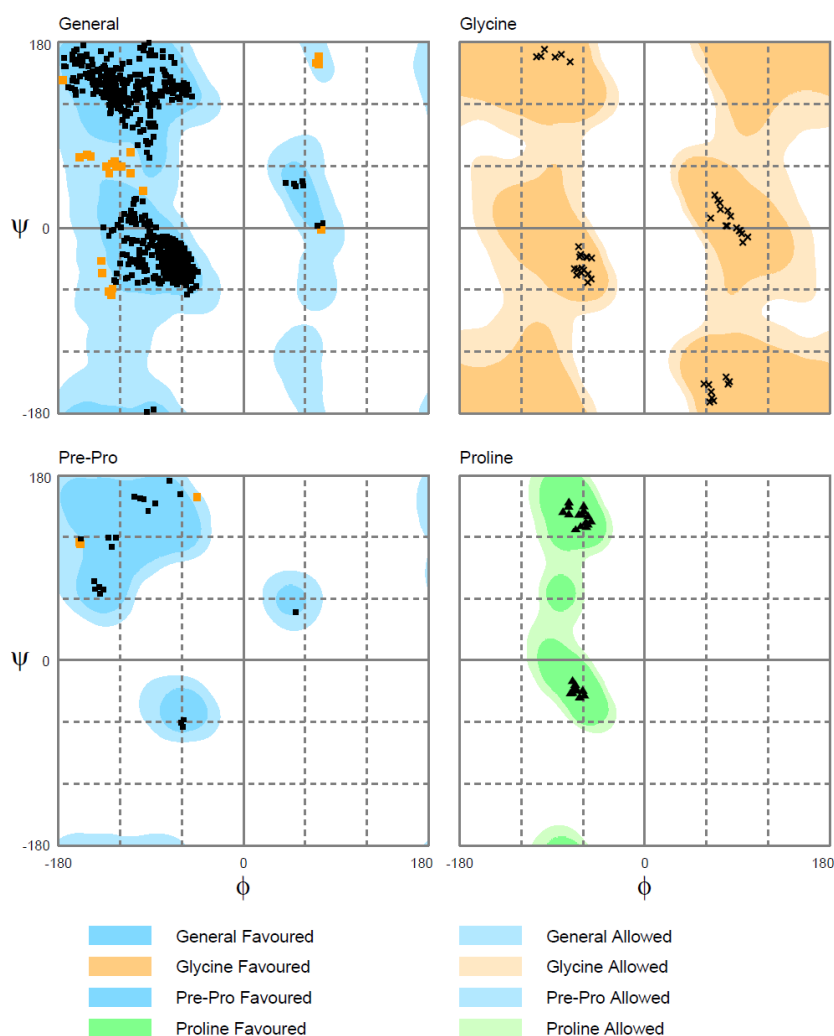


Figure 4.12: Ramachandran plot of the *Pf*SpdS-NACD structure.

For both the *Pf*SpdS-NACD-MTA and NAC-MTA structures residue Glu231 was detected as the single outlier on chain C and A, respectively. Interestingly, this residue is located within the active site and has been shown to interact with 4MCHA [119]. The observed geometric differences for this residue between the NACD and NACD-MTA/NAC-MTA structures alludes to a difference in ligand binding in the absence or presence of MTA, respectively, which will be clarified by the structures themselves. Nonetheless, the overall geometries were of high quality with >95% of the residues being in the allowed regions (Figures 4.13 and 4.14, Table 4.1).

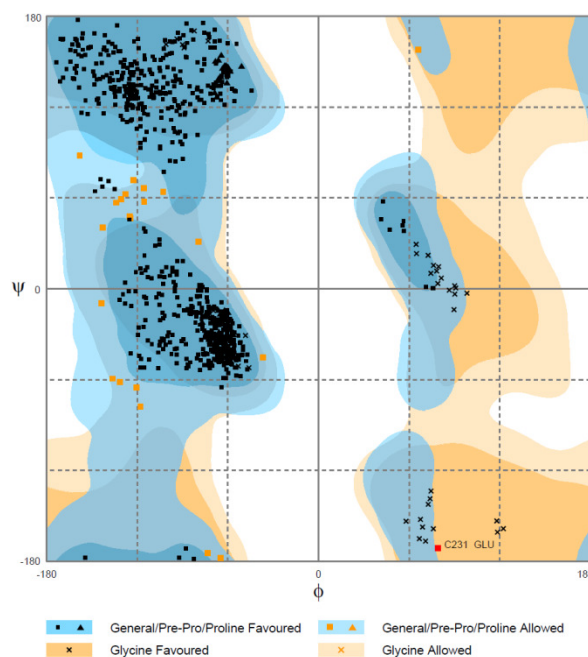


Figure 4.13: Ramachandran plot of the *Pf*SpdS-NACD-MTA crystal structure.

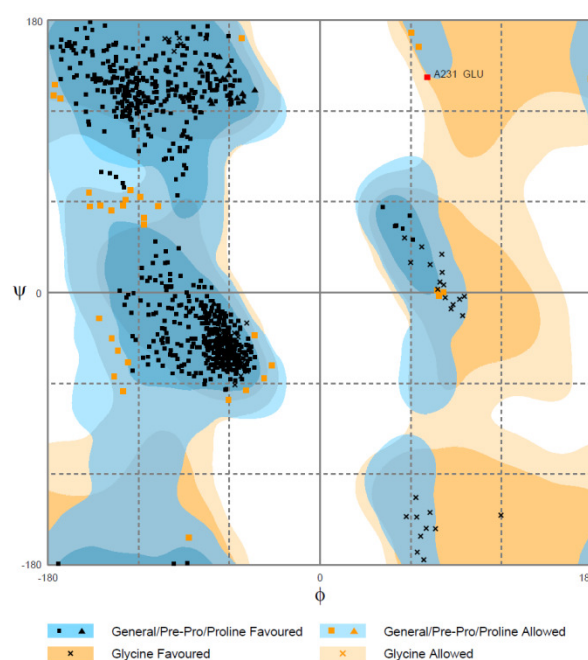


Figure 4.14: Ramachandran plot of the *Pf*SpdS-NAC-MTA crystal structure.

4.3.5.2. Overall structure of *Pf*SpdS

Crystallisation was performed with the addition of the inhibitors as well as in combination with the byproduct of the SpdS reaction, MTA. This was done as a result of previous studies that showed that inclusion of only one substrate leads to disordered gate-keeping loops [97,119]. Additionally, MTA was included since the kinetics results showed that NAC binding competes with dcAdoMet and could therefore result in a structure that does not have both the inhibitor bound within the active site and an inflexible loop (section 4.3.1).

The results of PROCHECK analyses of the three models are included in Appendices I to III. *Pf*SpdS was crystallised in space group C121 with three monomers (Matthews coefficient of 3.04) in the ASU and the solvent area occupying 50-60% of the unit cell. A representation of the crystal packing within the unit cell is shown in Figure 4.15 while the unit cell dimensions for the three structures are listed in Table 4.1. Subsequent analysis with PISA [250] showed that two of these subunits (chains B and C) form a homodimer with a buried interface of 1424 Å².

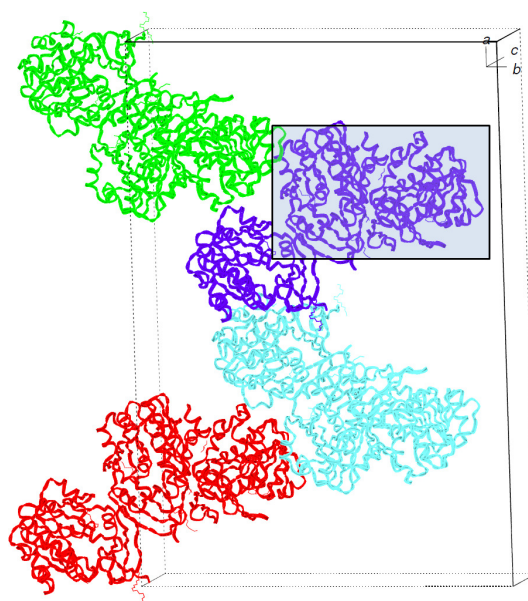


Figure 4.15: Diagram to illustrate the crystal packing of *Pf*SpdS-NACD crystallised in spacegroup C121. The diagram was obtained with the RCSB Atlas programme. Each colour represents the three monomers within the ASU of which two interact to form the homodimer (an example of such a homodimer is shown within the blue box).

*Pf*SpdS consists of two domains including an N-terminal β -sheet consisting of six anti-parallel strands and a catalytic domain consisting of a 7-stranded β -sheet flanked by 9 α -helices forming a Rossmann-like fold, which is typical of methyltransferases and nucleotide-binding proteins (Figure 4.16A) [97]. Each monomer contains its own independent active site, which is located between the two domains and is enclosed by a flexible gate-keeping loop (Figure 4.16A).

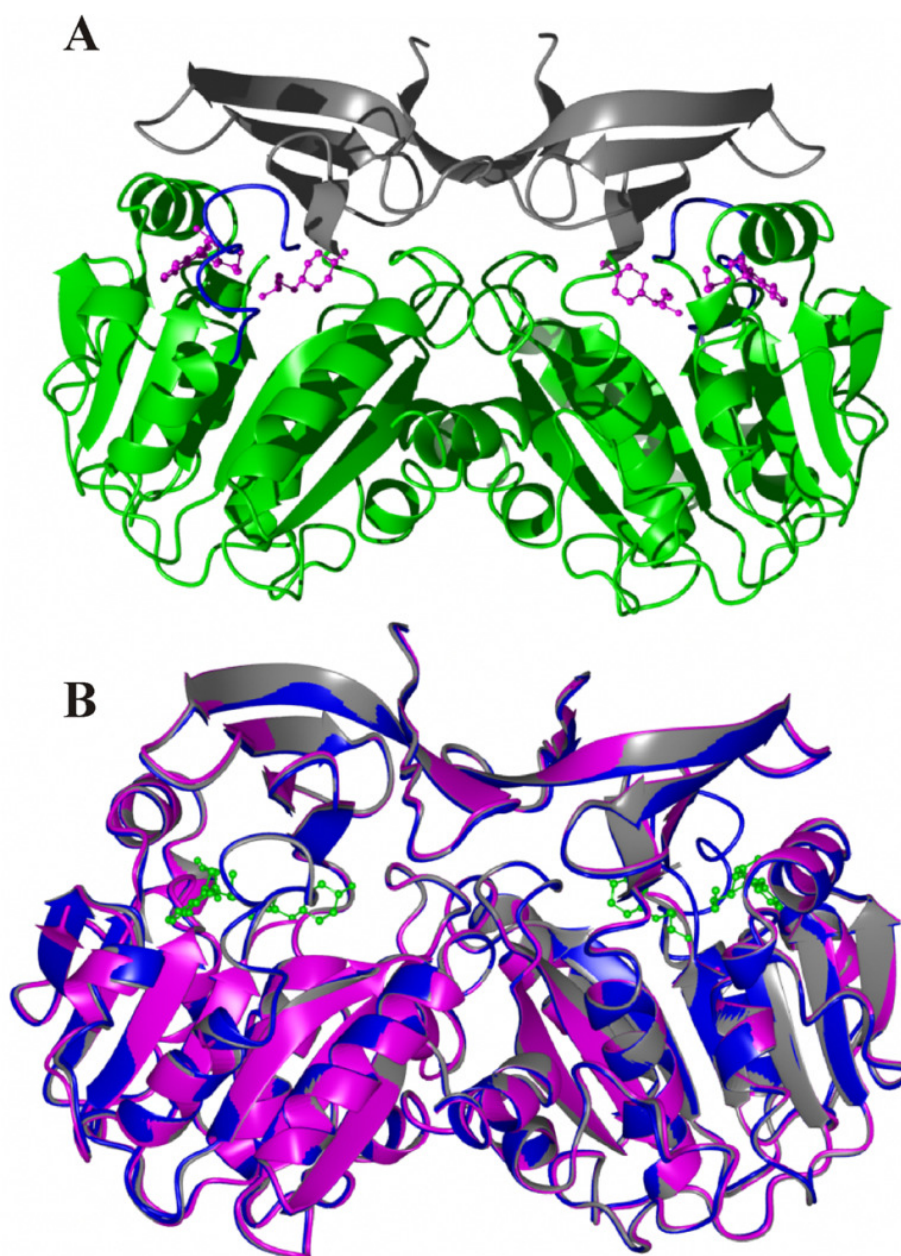


Figure 4.16: Overall fold of *Pf*SpdS (A) and superimposition of the solved crystal structures (B).

(A) The N-terminal and catalytic domains of each monomer are shown in grey and green, respectively. The active sites containing MTA and NACD are shown in magenta while the gate-keeping loops are in blue. (B) Alignment of the *Pf*SpdS-NACD (magenta), NACD-MTA (blue) and NAC-MTA (grey) crystal structures are shown. The active site ligands are shown in green.

The overall structures of all complexes obtained were nearly identical except for the gate-keeping loop, which was disordered in the *Pf*SpdS-NACD structure (residues 199-210 located between strand β -10 and helix α 5) (Figure 4.16B). The RMSD value between *Pf*SpdS-NACD and the apo structure (2PSS), which was used for its molecular replacement during structure solving, is 0.21 Å. The RMSD values between the *Pf*SpdS-MTA structure (2HTE) and *Pf*SpdS-NAC-MTA and NACD-MTA structures are 0.18 Å and 0.29 Å, respectively. The active site consists of the two substrate-binding pockets for putrescine (identified here with NACD/NAC binding) and dcAdoMet (identified here with MTA binding) (Figure 4.16B). As will be

described in the next sections, the residues involved in substrate binding are conserved and were also shown to play a role in inhibitor binding.

4.3.5.3. Binding of NACD and MTA

In vitro studies on malaria parasites showed that the NACD inhibitor is effective in the micromolar range, with slightly improved activity compared to NAC, possibly due to the inclusion of an extra amine group on the cyclohexyl ring, which is predicted to align with the amine of 4MCHA (2PT9) and in turn aligns with the non-attacking nitrogen of putrescine. Subsequent crystallisation of *Pf*SpdS co-incubated with NACD and MTA confirmed the binding orientation of NACD within the putrescine-binding pocket (Figure 4.17). The N^3 amine on the cyclohexylamine ring is hydrogen bonded to Glu46 via a solvent molecule (2.8 Å) and directly to the side chain of Asp199 (3 Å). Even though density was observed for the solvent molecule that was identified in the dcAdoMet-4MCHA structure (2PT9) as being involved in hydrogen bonding with the amine of 4MCHA [119], a bond was not observed between Glu231 and one of the solvent molecules due to a distance of >6 Å between them. Tyr102 (3.4 Å) and the carbonyl group of Ser197 (3.2 Å) interact with the bridging amino group (N^2 , the nitrogen connecting the aminopropyl chain of NACD to the cyclohexylamine ring) while Asp127 and Asp196 bind to the terminal amine N^1 , which crosses the catalytic centre. These interactions confirm the *in silico* predictions of NACD binding (Figure 4.4). The gate-keeping loop was also clearly defined (Figure 4.17), which corroborates previous studies in which binding of a ligand to only the putrescine-binding pocket resulted in a flexible loop [119].

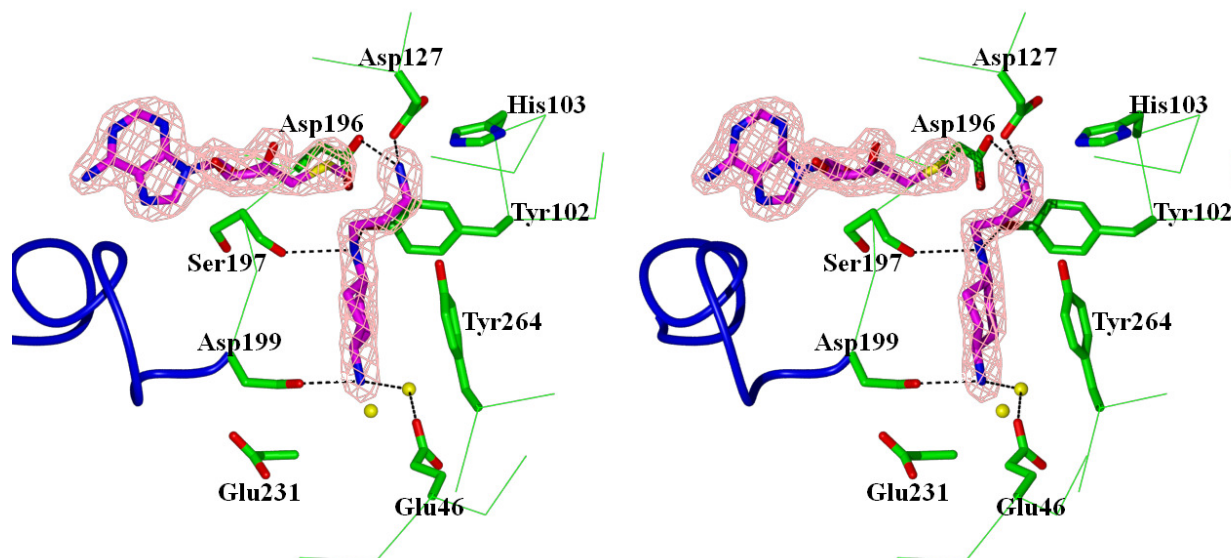


Figure 4.17: Stereo view of the *Pf*SpdS-NACD-MTA active site.

The MTA and NACD ligands together with their electron densities are shown in magenta. The residues involved in NACD binding are annotated while the gate-keeping loop is shown in blue. Solvent molecules involved in inhibitor binding are shown as yellow spheres.

The *Pf*SpdS-NACD-MTA structure superimposes well with the apo structure (2PSS) with an RMSD value of 0.31 Å, however, several conformational changes take place in order to accommodate the cyclohexylamine ring of NACD (Figure 4.18A). Most notably is the 90° rotation of Tyr264 to allow stacking of the aromatic side chain to the cyclohexylamine ring. The C_δ atom of Gln93 is shifted 1.7 Å to accommodate interactions with the C2 and C9 atoms of NACD. Ser197 also undergoes an almost 180° flip such that its carbonyl group can interact with the bridging amino group (Figures 4.17 and 4.18A). As previously predicted, Gln229 undergoes a significant conformational change in the presence of the inhibitor, which corroborates the DPM in which PhFs that represent binding of the attacking nitrogen of putrescine were identified by inclusion of the 2PT9 structure during negative image construction. Without the inclusion of this structure, NACD would probably not have been identified as a possible inhibitor due to the short distance of <1.86 Å between the position of Gln229 in the apo-state and the ring. The structures of *Pf*SpdS-NACD-MTA and dcAdoMet-4MCHA (2PT9) are very similar with an RMSD value of 0.33 Å. Residues involved in ligand binding are also conserved (Figure 4.18B).

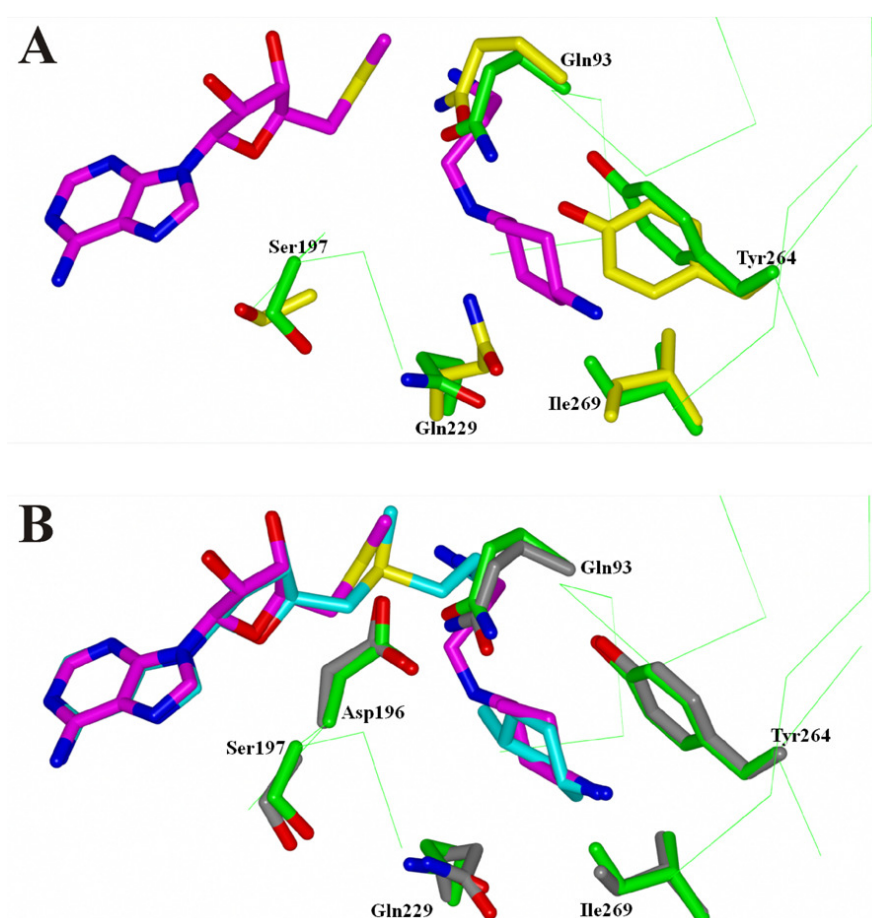


Figure 4.18: The active site of *Pf*SpdS-NACD-MTA superimposed with the 2PSS (A) and 2PT9 (B) crystal structures.

The MTA and NACD ligands of *Pf*SpdS-NACD-MTA are shown in magenta while the residues involved in NACD binding are shown in green. The corresponding residues of the apo structure are shown in yellow while those of the dcAdoMet-4MCHA (cyan) structure are shown in grey.

Protein crystallography provided important insights into the inhibitor efficiency of NACD in the presence of MTA, which binds within the DPM2 site and competes with both putrescine and dcAdoMet binding (section 4.3.1 and Figure 4.18). In addition and compared to 4MCHA, NACD forms additional binding interactions within the active site since the aminopropyl chain of NACD aligns with the terminal amine of dcAdoMet and further stabilises ligand binding (Figure 4.19). The structure also shows the binding of NACD to Asp199, which forms part of the gate-keeping loop.

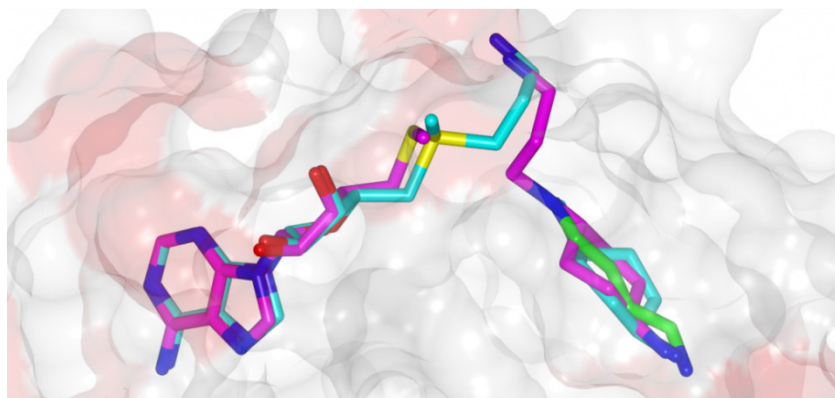


Figure 4.19: Electrostatic surface potential of the *Pf*SpdS active site.

Alignment of NACD and MTA (magenta), 4MCHA and dcAdoMet (2PT9, cyan) and putrescine (human structure 2O06, green). Blue represents nitrogen atoms, red represents oxygen and yellow represents sulphur atoms.

4.3.5.4. Binding of NACD

Crystallisation of *Pf*SpdS in the presence of only NACD did not show electron density of the inhibitor at the expected putrescine-binding site where NACD was located in the *Pf*SpdS-NACD-MTA structure. Instead the density map showed that NACD was bound within the dcAdoMet-binding pocket (Figure 4.20). The density was, however, much less defined than that observed for the NACD-MTA structure, which could be due to the flexibility of the aminopropyl chain and/or cyclohexylamine ring at this position. Furthermore, and as predicted from previous studies [119], the gate-keeping loop of the structure was disordered (residues 199 to 210) and loop flexibility could further have contributed to the flexibility of NACD. The suggestion that the sulphide atom of dcAdoMet or MTA is required for loop stabilisation is therefore supported by this result [97,119]. Binding of the inhibitor at the dcAdoMet-binding site could be substantiated by the ionic interactions that are detected between the carbonyl group of Cys146 and the terminal N^1 amino group (2.96 Å), Gln93 and the N^3 amine as well as between Ser197 and the bridging N^2 nitrogen (3.1 Å) of NACD. Residues that normally bind the natural substrate such as Glu147, Gln72 and Asp178 can also stabilise the interaction and favour the binding of NACD at this position (Figure 4.20).

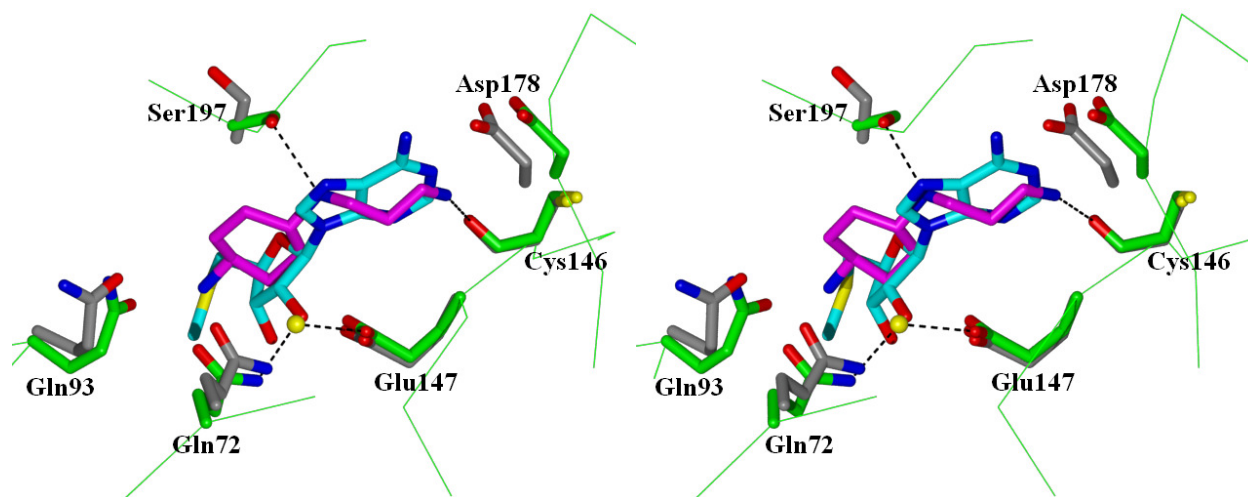


Figure 4.20: Stereo view of the *Pf*SpdS-NACD active site.

The MTA (2HTE) and NACD ligands are shown in cyan and magenta, respectively. Residues involved in NACD binding are annotated and shown in green while the corresponding residues of 2HTE are shown in grey. The solvent molecule is shown as a yellow sphere.

The cyclohexylamine ring is positioned perpendicular to the ribosyl group of MTA and the N^1 and N^2 amino groups of the inhibitor overlap with N^1 and N^9 from MTA, which allows NACD to form interactions with Cys146 and Ser197, respectively (Figure 4.20). Interestingly, a water molecule was identified in the *Pf*SpdS-NACD structure that occupies the site of one of the hydroxyls on the ribosyl moiety of MTA. Previously, it was shown that solvent molecules do not mediate interactions between ligands within the dcAdoMet-binding site and the active site residues [119]. However, in the absence of the ribosyl moiety, a solvent molecule was detected that forms hydrogen bonds with Gln72 (2.6 Å) and Glu147 (2.7 Å) and may thereby stabilise the ring moiety of NACD (3.1–3.3 Å) (Figure 4.20).

Superimposition of the *Pf*SpdS-NACD structure with the MTA complex (2HTE) showed several changes in active site residues to accommodate inhibitor binding. Ser197 rotated 90° towards NACD to form an interaction with the bridging amino group. Gln93 shifted 2.2 Å towards the amine group on the cyclohexylamine ring (Figure 4.20). The cause of the movement of Asp178 away from the ligand to a distance of >7 Å is unclear.

These results showed that the efficiency of the NACD compound may be more pronounced in the presence of MTA, which shifts binding to the putrescine-binding pocket. In the presence of MTA the gate-keeping loop also becomes inflexible and may be locked in a fixed or closed position, resulting in an increase in the inhibitor binding efficiency. Nonetheless, the crystal

structures of *Pf*SpdS in complex with NACD validated the *in vitro* inhibition results as well as the use of a DPM to identify novel lead compounds.

4.3.5.5. Binding of NAC

The last structure that was solved was of *Pf*SpdS co-crystallised with NAC and MTA. Similar results to that of the NACD-MTA complex were expected, except for the absence of the terminal amine on the cyclohexyl ring. Docking results of NAC predicted a very similar binding pose to that of NACD (Figure 4.4). However, upon solving of the crystal structure at a lower resolution than that of the NACD structures (2.39 Å versus 1.9 Å), some unexpected results were observed. Firstly, density of NAC within the putrescine-binding pocket that could fit the ligand could not be identified but instead showed the presence of two well defined solvent molecules occupying the sites where the N^1 and N^3 nitrogen atoms of the ligand were expected to be located (Figure 4.21). Furthermore, even though NAC was absent, the residues previously identified as being involved in NACD binding were orientated in such a way that indicated the presence of the ligand. As expected, binding of MTA resulted in the gate-keeping loop being inflexible and could therefore be solved in the structure (Figure 4.21).

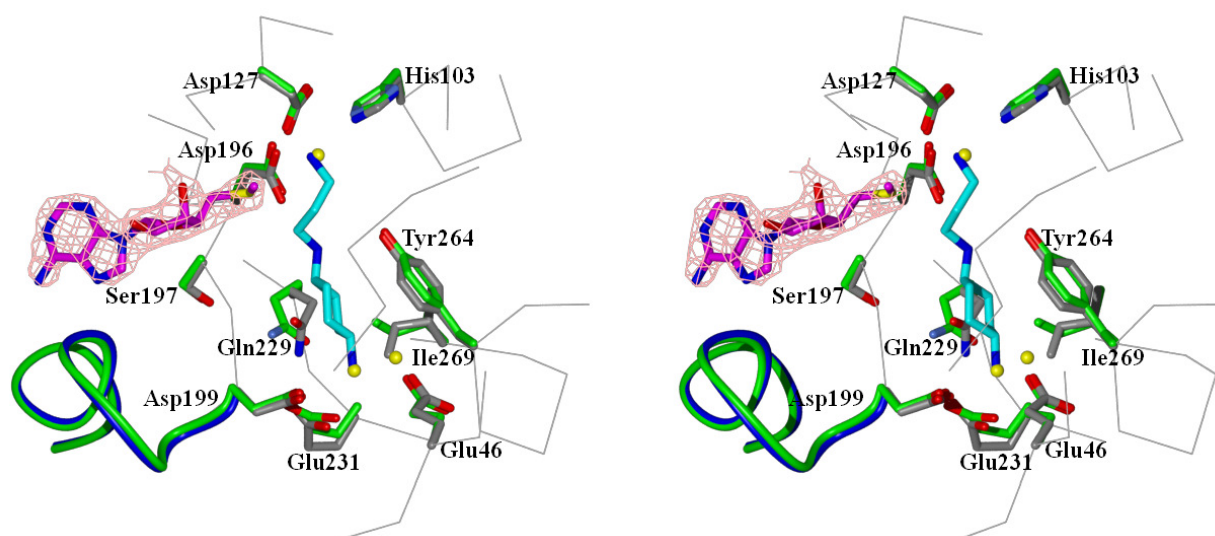


Figure 4.21: Stereo view of the *Pf*SpdS-NAC-MTA active site.

NACD from the *Pf*SpdS-NACD-MTA structure is shown in cyan while MTA from the NAC-MTA structure is shown in magenta together with its electron density. Residues previously shown to be involved in NACD binding are annotated and shown in green while the corresponding residues of the NAC-MTA structure are in grey. The gate-keeping loops are also shown. The solvent molecules are shown as yellow spheres.

The orientations of the residues, which suggested a ligand-bound state of the protein becomes even more obvious when the *Pf*SpdS-NAC-MTA structure is superimposed with the apo structure (2PSS) (Figure 4.22). Tyr264 is positioned in such a way to allow stacking against a ligand with its aromatic side chain, Ser197 is orientated perpendicular to that of the residue in the

apo structure while Gln229 and Glu231 are also shifted as if to participate in interactions with the ligand. Furthermore, even though the majority of the solvent molecules in the active site of the NAC-MTA structure align with that of the apo one, the molecule occupying the site where the non-attacking nitrogen (N^1) of NAC is predicted to be positioned is not conserved (Figures 4.21 and 4.22) and could indicate that this molecule fulfills the binding interactions with the repositioned residues in the absence of NAC.

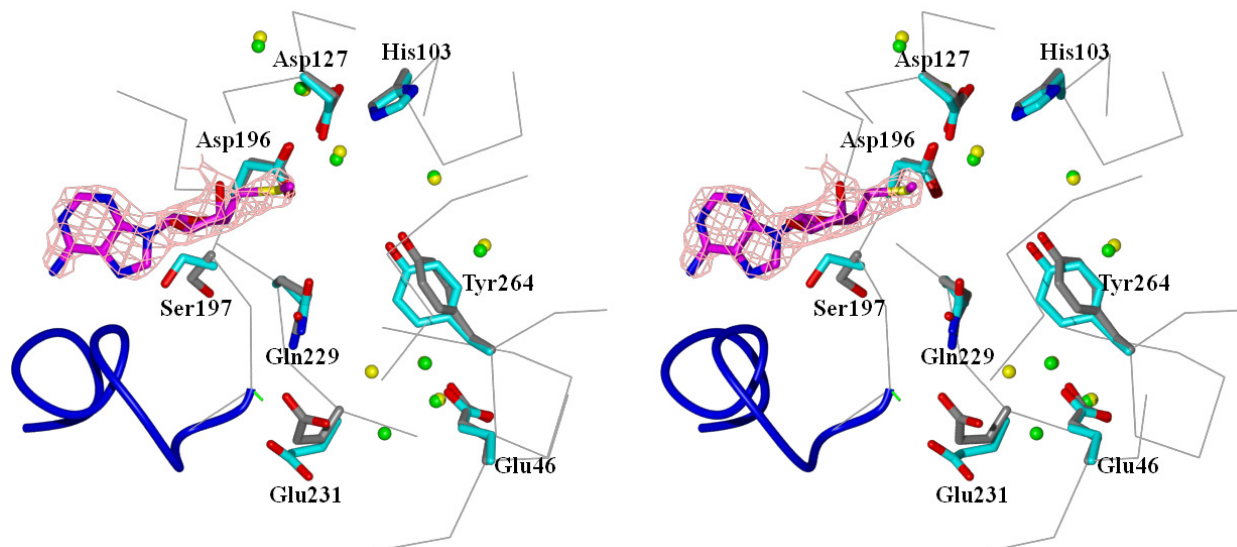


Figure 4.22: Stereo view of the *Pf*SpdS-NAC-MTA active site superimposed with the apo structure.

MTA from the NAC-MTA structure is shown in magenta together with its electron density. Residues previously shown to be involved in NACD binding are annotated and shown in grey for the NAC-MTA structure while the corresponding residues of the apo structure are in cyan. The gate-keeping loop of *Pf*SpdS-NAC-MTA is also shown as a blue ribbon. The solvent molecules belonging to the NAC-MTA structure are shown as yellow spheres while that of the apo structure are in green.

These results show that either the flexibility of the ligand was too high such that density could not be detected where NAC was predicted to bind, or the protein was not co-crystallised with the inhibitor. Another possibility could be that the observed residue orientations that were previously shown with the NACD-MTA structure to accommodate ligand binding could indicate that the ligand was in fact present within the active site but was replaced with solvent molecules during crystal soaking in the cryo protectant due to the weaker binding interaction of the ligand within the active site compared to NACD. No direct conclusions could therefore be obtained from the crystal structure of *Pf*SpdS bound with NAC. However, based on the inhibitory efficiency of NAC as well as the detailed results obtained from the NACD-MTA crystal structure it is likely that the binding pose predicted in Figure 4.4 pertains to that of NAC binding within *Pf*SpdS.

4.4. Discussion

The identification of effective inhibitors against SpdS with the application of ligand- or receptor-based approaches has proven difficult and largely ineffective [226,251]. 4MCHA was identified with a ligand-based approach by synthesising putrescine analogues and, despite its poor target specificity [98], still represents the best inhibitor of *Pf*SpdS to date [220]. In 2008 the first structure-based study for *Pf*SpdS was released and although no promising leads were identified it provided a proof of principle for the application of *in silico* methods to screen thousands of compounds for subsequent *in vitro* testing [251]. Due to the lack of highly effective and specific inhibitors of *Pf*SpdS activity, we decided to follow a different approach for inhibitor design, which could add to the list of current *Pf*SpdS inhibitors (Table 4.2).

Table 4.2: Inhibitors tested *in vitro* on *Pf*SpdS or in whole-cell assays against *P. falciparum*.

Only inhibitors for which *in vitro* *Pf*SpdS inhibitory values are available are included, which are listed from the most to the least effective. When available, the IC₅₀ values of the inhibitors against *in vitro* *P. falciparum* are also included.

Inhibitors	K _i (μM)	IC ₅₀ (μM)	Binding cavity	Size (Da)
4MCHA	1.4	34.2	putrescine and unknown	113
NAC	2.8	105	-	159
NACD	-	81	putrescine (in presence of MTA)	281
APE	6.5	83.3	putrescine	85
AdoDATO	8.5	-	dcAdoMet and putrescine	425
Cyclohexylamine	19.7	198	putrescine	99
2-Mercaptoethylamine	76	254	unknown	77
APA	84	1.0	putrescine	90
MTA	159	-	dcAdoMet	313
Dicyclohexylamine	>1000	342	unknown	181

Interaction of the inhibitors within the putrescine, dcAdoMet, the entire active site or unknown binding sites is indicated. All the results were obtained from [98] except for the AdoDATO data [119].

The DPM computational approach used in this study allowed individual pharmacophore sites to be probed using distinct chemical moieties that displayed favourable binding properties. Pharmacophore modelling therefore provided a powerful tool for extracting representative biologically active components from both inhibitor ligands and their intended protein target receptors. It also allowed for the incorporation of information from previous studies as well as information derived during the discovery process. The methodology furthermore addressed the problem of protein flexibility during structure-based drug design, which is one of the major challenges that computational chemists currently face [229,230]. This approach resulted in the identification of novel inhibitors against SpdS of *P. falciparum*, which were tested on the recombinant *Pf*SpdS protein (Table 4.2).

Binding cavities were selected to identify specific binding hotspots that could be used in the identification of ligands. For this purpose the *PfSpdS* active site was divided into four binding cavities. Most relevant to this study was the DPM2 binding cavity, which was selected to identify compounds that favourably bind within the putrescine- and a part of the dcAdoMet-binding sites and therefore represented an area that has not been studied. The premise for selecting this binding cavity is based on the knowledge that SpdS catalyses the aminopropyl transfer from dcAdoMet to putrescine, wherein product release is mediated by a gate-keeping loop that opens and closes over the active site. It was therefore hypothesised that compounds binding favourably to the DPM2 cavity will also form interactions with residues from the loop (Ser197 and Asp199) and thereby maintain the loop in a closed conformation for longer periods of time resulting in increased inhibitor potency. Alternatively, the loop may be locked in a closed position, which inactivates the protein indefinitely.

Currently, AdoDATO is the only known inhibitor that crosses the negatively-charged catalytic centre of *PfSpdS*. The crossing of the catalytic centre by the aliphatic aminopentyl chain of AdoDATO can be attributed to the substrate-like characteristics of this compound, which are strong enough to overcome this unfavourable interaction. The 4MCHA and APE inhibitors are more effective against *PfSpdS* than AdoDATO [98], and they are also much smaller molecules with sizes of 85 and 113 Da compared to the 425 Da of AdoDATO (Table 4.2). Furthermore, it is known that the strong inhibition characteristics of 4MCHA and APE are due to cooperative binding with either dcAdoMet or MTA. It can therefore be postulated that the higher K_i value of AdoDATO is partly due to the unfavourable interactions of the aliphatic part of the aminopropyl moiety, which crosses the negatively-charged catalytic centre. This highlights the importance of finding chemical entities that are able to link ligands bound within the dcAdoMet-binding cavity to ones within the putrescine-binding site by bridging the catalytic centre. It is also known that the catalytic centre binds positive ionisable groups to catalyse the transfer of an aminopropyl group and the residues involved in binding the attacking nitrogen of putrescine are Tyr102, Asp196 and the backbone carbonyl group of Ser197 [97]. Therefore in this study, the PhFs and binding poses of AdoDATO, dcAdoMet and 4MCHA were used to derive compounds, which could bridge the catalytic centre and favourably bind within this region.

The compound NACD was identified by taking into account these considerations and represents a basic scaffold for an inhibitor of *PfSpdS*. NACD docking to *PfSpdS* was used to predict its binding poses and it was shown that the cyclohexylamine moiety binds in a similar manner to

4MCHA. It was anticipated that hydrogen bond formations would reduce the penalty that an aliphatic carbon would have by binding within the catalytic centre and thereby increase the binding affinity as well as inhibitory activity. The aminopropyl chain of NACD was also predicted to bind in the same cavity as the aminopropyl chain of dcAdoMet. Due to the unavailability of NACD at the time, NAC was identified as a similar, commercially available compound. The compound is an analogue of cyclohexylamine containing an additional aminopropyl chain. Similar binding poses and hydrogen bond patterns as NACD were therefore predicted, except for the missing amino group. This made NAC a good alternative to test and subsequent enzyme kinetics of this compound showed a high inhibitor activity against *Pf*SpdS with a K_i of 2.8 μM , which is comparable to that of 4MCHA (Table 4.2). Kinetics also showed competitive binding, which suggested that the interaction involves competitive interaction with both putrescine and dcAdoMet. The low K_i could be due to specific hydrogen bond formation of NAC with *Pf*SpdS, which can only be true if NAC binds in the predicted docking pose by bridging the catalytic centre and if the aminopropyl chain binds in the aminopropyl binding pocket of the dcAdoMet cavity. This binding mode of NAC would also accommodate the simultaneous binding of MTA, which would allow the gate-keeping loop to close over the active site. Furthermore, the ability of the compound to form hydrogen bonds with residues Tyr102 and Ser197 may significantly contribute to the strong binding of the compound in the active site, which could play a role in the stabilisation of the gate-keeping loop and to keep it closed for a longer period over the active site. A similar phenomenon was observed in the co-crystallisation of *Pf*SpdS and 4MCHA where the binding of 4MCHA could only be resolved in the presence of dcAdoMet. It was therefore suggested by the authors that dcAdoMet binding occurs prior to 4MCHA or putrescine binding hence resulting in inhibition or catalysis, respectively [119]. A similar phenomenon was observed for putrescine and MTA binding to human SpdS [97]. With this information in mind, it can be speculated that, if the kinetic data holds true and NAC also requires cooperative binding of a second compound within the dcAdoMet cavity, then the true K_i of NAC is observed when MTA is bound within the dcAdoMet-binding pocket.

Even though NAC was shown to be extremely effective on the recombinant enzyme level, *in vitro* determination of the effect of NAC and NACD on the parasite cultures resulted in 50% growth inhibition in the micromolar range, which is approximately double the IC_{50} of 4MCHA and in the range of inhibition provided by APE (Table 4.2). These results suggest poor uptake or instability problems of the compounds *in vitro*. Analyses of the druggability of NAC showed that it conforms to the Lipinski's rule of five, which makes the drug orally active [252]. NAC

contains only two hydrogen bond donors, no hydrogen bond acceptors, it has a LogP value of 1.57 and the size of the compound is 159 Da, which is below the required limit of 500 Da. Alternative drug-delivery strategies may improve the *in vitro* whole-cell activity of these compounds to acceptable ranges (<1 μ M) as specified by e.g. the MMV (<http://www.mmv.org/>). However, preliminary results provided by the co-inhibition of *Pf*SpdS with either NAC or NACD and the rate-limiting enzymes of the polyamine pathway showed additive inhibition. These results indicate that the specific and simultaneous inactivation of the parasite-specific bifunctional *Pf*AdoMetDC/ODC enzyme together with the flux-determining *Pf*SpdS enzyme could result in improved inhibitory effects and lead to possible cessation of *in vivo* synthesised polyamines. Currently, inhibitors such as MDL73811, DFMO and 4MCHA can be used to simultaneously target these enzymes but these only result in cytostatic growth effects and we therefore need to find strategies beyond those that are currently available. Future studies, in combination with the crystal structure results, could improve the inhibition efficiency, target specificity and drug delivery of these compounds that may have an increased inhibitory effect on the parasite cultures by targeting the polyamine biosynthetic pathway.

Protein crystallisation is an extremely valuable tool in the field of drug discovery for the validation of predicted binding sites of inhibitors as well as to obtain insights into the improvement of target specificity. In this study, the *in silico* predicted binding poses and active site interactions of NAC and NACD with *Pf*SpdS were therefore confirmed via the co-crystallisation of these compounds with the protein. Analyses of near-UV CD results as well as geometric analyses of the residues with Ramachandran plots provided an early indication of different binding interactions of NAC and NACD in the presence or absence of MTA. The CD results showed a difference in the tertiary structures depending on the presence of a substrate in the dcAdoMet-binding cavity. Furthermore, the presence of Glu231 in the outlier regions of the Ramachandran plots when both the binding cavities were filled indicated that this residue in the NACD crystal structure may not be involved in inhibitor binding. This could be hypothesised since it was previously shown that this residue orientates itself differently in the presence of both 4MCHA and dcAdoMet [119]. The residue is therefore strained in the presence of the ligand in such a way as to accommodate the ring moiety of the inhibitor.

The crystal structure of *Pf*SpdS-NACD-MTA confirmed the *in silico* predicted binding poses and highlighted the interactions of this inhibitor within the active site that allowed it to display its inhibitory properties. The observed interactions also showed how the flanking acidic regions

of the putrescine-binding pocket accommodates the ligand with its terminal positive ionisable groups, which forms hydrogen bonds with Glu231 and Glu46 at the non-attacking nitrogen, and Asp127 and Asp196 at the attacking nitrogen. Hydrogen bonds involving Ser197 and Tyr102 with the bridging nitrogen group also showed how the ligand is accommodated despite its presence within the hydrophobic cavity of the putrescine-binding site. Furthermore, the gate-keeping loop became inflexible and therefore enabled diffraction data collection of the residues. This indicates that MTA followed by inhibitor binding resulted in the closure of the loop, which could be mediated by the sulphide atom (as previously suggested [97,119]) and/or binding of the ligand, respectively. This hypothesis was confirmed with the crystal structure of *PfSpdS*-NACD where the loop was not resolved either due to the absence of MTA or the binding of NACD within the dcAdoMet cavity and therefore the absence of stabilising interactions with the loop. However, a different hypothesis is proposed here where the sulphide atom of MTA is not primarily responsible for loop stabilisation but as a result of the contribution of various interactions of both the ligands with the loop in such a way that it becomes inflexible. From the 10 residues that constitute the loop spanning residues Asp196 to Glu205, six interactions are formed between the two ligands and residues Asp196, Ser197, Ser198, Asp199, Pro203 and Ala204. It therefore seems that the contribution of several stabilising interactions could close the loop over the active site. In fact, only a single interaction mediated by the sulphide atom could be deduced from the 2PT9 crystal structure and involves Asp127, which would hardly constitute loop stabilisation to a residue that is not even present on the loop.

Furthermore, even though electron density of NAC in the *PfSpdS*-NAC-MTA was not detected, it could be deduced that the NAC was present within putrescine-binding site since MTA was bound in the dcAdoMet cavity and the conformational changes of the residues that were identified in the NACD-MTA structure were similar. The loop was also stabilised in this structure, which indicates that both binding sites were filled. Therefore the improved inhibitory activity of NACD is predicted to be due to the additional amino group on the ring moiety, which forms ionic interactions within the acidic region of the non-attacking nitrogen of the active site. This additional nitrogen also improved stability of ligand binding such that the ligand did not diffuse out during cryo protectant soaking as is suggested to be the case for NAC.

The *PfSpdS*-NACD-MTA structure showed that the sulphide atom of MTA may additionally interact with the aminopropyl chain of NACD and thereby contribute to its binding within the active site. It can therefore be deduced that a compound that includes the chemical properties of

NACD as well as the essential elements of MTA may represent an important candidate to test, which would still follow the strategy of bridging the catalytic centre of *Pf*SpdS. Previous suggestions by P. B. Burger include *N*³-cyclohexylpentane-1,3,5-triaminium (NACDS), *N*²-cyclohexylbutane-1,2,4-triaminium (NACDS-alternative) and *N*³-[(1*R*,4*R*)-4-ammonio-cyclohexyl]pentane-1,3,5-triaminium (NACDSW) as derivatives of NAC and NACD, whereby the extra groups (boxed in Figure 4.23) can bind within the sulphide-binding cavity of MTA and thereby display the combined inhibitory effects of NACD and MTA.

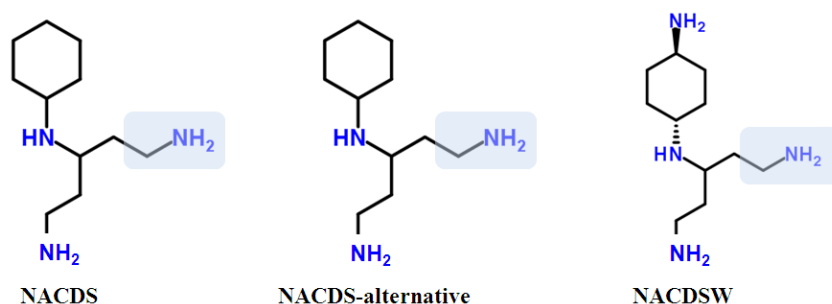


Figure 4.23: Derivatives of NAC and NACD as alternative chemical compounds to test for inhibition of *Pf*SpdS activity.

Chemical structures were obtained from ChemSpider (<http://www.chemspider.com/>) where nitrogen and amine groups are shown in blue. The boxed areas represent the chemical entities that are predicted to bind in the sulphide-binding cavity of MTA. Abbreviations: NACDS, *N*³-cyclohexylpentane-1,3,5-triaminium; NACDS-alternative, *N*²-cyclohexylbutane-1,2,4-triaminium; NACDSW, *N*³-[(1*R*,4*R*)-4-ammonio-cyclohexyl]pentane-1,3,5-triaminium.

The opening of the gate-keeping loop once the aminopropyl chain of dcAdoMet has been transferred to putrescine resulting in the formation of MTA and spermidine also indicates that the loop opening following catalysis may be mediated by the interactions of the aminopropyl chain. One would expect that the presence of MTA would relieve the loop closure such that the reaction products can be released while dcAdoMet would stabilise loop closure. A crystal structure containing putrescine would provide more information on the possible role of the aminopropyl chain in loop movement. An important aspect to take into account in terms of identifying a drug that locks the *Pf*SpdS gate-keeping loop in closed formation is the half-life of *Pf*SpdS. The stability of *Pf*SpdS enzyme has not been determined but it is generally known that SpdS is more stable than AdoMetDC and ODC [253] and studies on mouse mammary epithelium showed a half-life of >12 h [254]. In *P. falciparum* it has been shown that transcription occurs with a just-in-time manufacturing process whereby induction of a gene occurs once per intra-erythrocytic cycle and only at a time when it is required [4]. The drug candidate therefore needs to be specific enough such that its inhibitory properties will have an effect during this period. In addition, target specificity therefore becomes a critical issue such that inhibitor binding does not result in prolonged inhibition of the host protein if the drug is not

target specific. Future studies include testing of the compounds identified with the DPM against mammalian cell lines since the active site of SpdS is highly conserved. As can be seen in Figure 4.24 superimposition of the *Pf*SpdS-NACD-MTA structure with the human protein (2O06, [97]) shows that only His103 (corresponding to hGln80) is not conserved between the two proteins. Whether this change is significant enough to produce a target specific response should be determined *in vitro*.

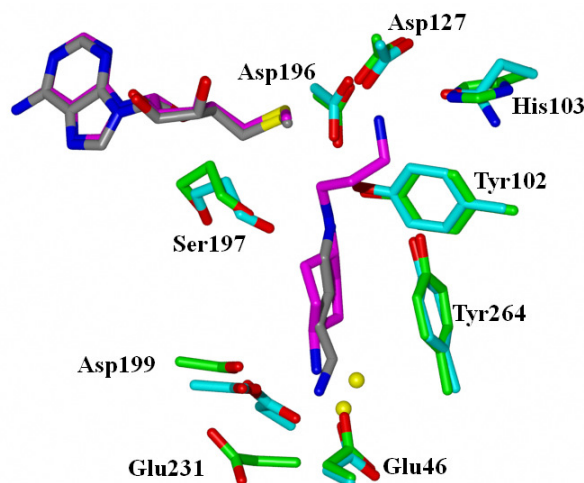


Figure 4.24: The *Pf*SpdS-NACD-MTA active site superimposed with the human structure.

MTA and NACD from the *Pf*SpdS-NACD-MTA structure are shown in magenta while MTA and putrescine from the human structure (2O06) is shown in grey [97]. Residues previously shown to be involved in NACD binding are annotated and shown in green while the corresponding residues of the human structure are in cyan. The solvent molecules belonging to the NACD-MTA structure are shown as yellow spheres. His103 is the only unique *P. falciparum* residue within the active site that is involved in NACD binding.

4.5. Conclusion

The compounds identified in this study have been shown to cross the catalytic centre of *Pf*SpdS in an energetically favourable manner by hydrogen bonding to Tyr102 and Ser197, and cooperatively bind MTA within the dcAdoMet cavity. Inhibition was also in the range of 4MCHA activity, while improved potency was expected since the inhibitor competes with both putrescine and dcAdoMet. Protein X-ray crystallography subsequently confirmed the binding of the novel inhibitory compound within the *Pf*SpdS active site and showed how NACD is stabilised within the active site by additional hydrogen bonds. Novel insights into the stabilisation of the gate-keeping loop of the holo-protein were also obtained from the structures.

Therefore the promising results of these two inhibitors which target both the putrescine and dcAdoMet binding activities emphasise the value of incorporating a “dynamic”, receptor-based pharmacophore model and represent a valuable tool for the future design of possible therapeutics.

Chapter 5:

Concluding discussion

Currently, the first ever Phase III clinical trials are being conducted on a vaccine against malaria. Unfortunately, it has already been established that its efficacy will not be 100% [255] but the important fact is that it would contribute to a decrease in the number of new malaria cases. Malaria prevention and eradication requires the concerted efforts of various disease-control factors and a constant vigilance of each of these would hopefully, one day, lead to a malaria-free world. A reduction in malaria prevalence requires the control of its transmission with methods such as IRS and ITNs, while prevention of malaria infection requires prophylaxis and once infected we need to be able to effectively treat the disease to prevent further transmission.

Disease-controlling factors require the joint cooperation of not only the individuals who are at risk of contracting the disease but also the government, health authorities, aid organisations, funding agencies, public awareness campaigns and the scientists in the field of malaria research. Extensive malaria research has been made possible by funding from large organisations and has become a highly competitive field in the race towards finding a novel, effective and cheap antimalarial agent. As a result, scientists are making groundbreaking findings in both the understanding of parasite pathogenesis as well as strategies to curb the infection of humans. Malaria research has also become highly attractive from a scientific point of view due to the many unique characteristics of the malarial parasite, its complicated life cycle, successful immune evasion, advanced gene transcription and translation mechanisms as well as general metabolism, which contains characteristics of both plants and prokaryotes alike. Understanding this complexity has become a major challenge for scientists, which has resulted in the development of sophisticated methods and technologies. Ultimately, we can only hope that our research findings would contribute to the understanding of the malarial disease, which forms the foundation in an attempt to relieve the burden of not only malaria but other debilitating diseases including HIV-AIDS and tuberculosis.

To date, progress towards novel drug targets and antimalarials has been hampered by the incomplete knowledge of the parasite's biochemistry, particularly the enzymes of parasite origin that could represent useful drug targets. However, this knowledge has increased substantially through the application of biochemical and molecular biology studies that compare the biochemical aspects of the malaria parasite to that of the host cell. A rational approach to achieve



selective chemotherapy requires a thorough understanding of the metabolic and biochemical differences between the parasite and its host cell. In this way, several parasite-specific and novel targets have been identified by their cloning and expression, biochemical characterisation and subsequent inhibitor screening followed by structure-function relationship studies. The success of such an approach relies on the highly specific and selective inhibition of a specific parasite biochemical process that is vital to parasite growth and survival without affecting the process of the host cell. In this regard the polyamine biosynthetic pathway of the plasmodial parasite is particularly attractive and represents a novel strategy to interfere with parasite viability. This is particularly relevant since polyamines themselves are essential for growth and differentiation of all cells, but has drawn little interest from investigators worldwide mainly due to the difficulty of working with this pathway's constituent enzymes.

Research of the polyamine biosynthetic pathway in *P. falciparum* as well as other parasites such as *T. brucei* has identified sufficiently unique properties that would allow for its selective targeting. Despite the availability of a considerable number of inhibitors and some structural data of the polyamine biosynthetic enzymes already published, little information is available for the *P. falciparum* polyamine biosynthetic rate-limiting enzymes. This may be due to the technical difficulties involved in obtaining sufficiently large amounts of these proteins that are required for structural studies. Although previous studies have reported the successful recombinant expression of active bifunctional *PfAdoMetDC/ODC* as well as the monofunctional *PfAdoMetDC* and *PfODC* proteins in *E. coli*, further optimisation is still needed to increase the level of expression and to overcome the poor solubility as well as instability of these expressed proteins before the structures can be solved through X-ray crystallography. In the absence of crystal structures, the modelling of the proteins has been useful to permit exploration of the predicted catalytic mechanism and effects of potential drug interactions [120,127,130]. However, a homology model is highly dependent on the degree of sequence homology, which is generally low for *P. falciparum* and can thus only provide guidance to the correct structure. Homology models nonetheless represent a powerful tool for the rational design of substrate analogues and screening for potential inhibitors.

Various similarities can be drawn between the bifunctional *P. falciparum* DHFR/TS enzyme and that of bifunctional *PfAdoMetDC/ODC*. Like *PfAdoMetDC/ODC*, *PfDHFR/TS*, is also a validated target for the inhibition of *de novo* folate biosynthesis in the parasite and antimalarials such as pyrimethamine and sulphadoxine have been used as successful antimalarial strategies for a considerable period of time. The emergence of resistance has rendered these antimalarials



largely ineffective but they are still being used today in combination therapies and in certain malaria treatment cases (WHO 2010). The biochemical and structural characterisation of these two enzymes as well as the other folate biosynthetic enzymes has allowed researchers to pinpoint the mechanism of resistance development, methods to delay this and the identification of novel inhibitors that could in future be used to replace the current antifolates, either as single drugs or in combinations [256]. *PfDHFR/TS* is a dimeric enzyme with extensive interdomain interactions significantly mediated by the junction region (known as the hinge region in *PfAdoMetDC/ODC*) as well as additional parasite-specific inserts in the *PfDHFR* domain. The activity of the *PfTS* domain depends on the integrity of the N-terminal *PfDHFR* as well as the junction region [122,257] and therefore represents a unique feature that may be exploited in the development of *PfTS*-specific inhibitors. Interestingly, it was shown that deletion of only five residues at the N-terminus of *PfDHFR/TS* resulted in significant impairment of DHFR function, and further deletion of 15 residues resulted in an inactive bifunctional enzyme [257]. These results indicated that the N-terminal residues play an important role in both activities of the bifunctional complex, even if the start of the *PfTS* domain is 320 residues away from the N-terminus. The crystal structure of *C. hominis* DHFR/TS showed that, while parasite-specific insert 1 extends away from the domain surface and does not interact with the core *ChDHFR* structure, it forms an interaction with the *ChTS* domain and thereby contributes to the stabilisation of the interdomain attachment [258]. The junction region, notably the “donated helix”, also forms extensive interactions with the other *ChDHFR* domain and includes part of insert 2.

In *P. falciparum*, *AdoMetDC/ODC* also exists as a dimer of the two *PfAdoMetDC/ODC* polypeptides, which are connected by a hinge region. Autocatalytic cleavage within the *PfAdoMetDC* domain for its activation as well as α - and β -subunit formation, results in the formation of the heterotetrameric protein [70]. Biochemical studies have previously shown that the hinge region as well as the *PfAdoMetDC* domain is important for the C-terminal *PfODC* activity and that this domain is more refractory to change [69,103]. Like *PfDHFR*, *PfAdoMetDC* is not dependent on the C-terminal domain and removal of this domain actually improves the enzyme efficiency of *PfAdoMetDC* [71]. However, various interdomain interactions are formed [69] and their interaction sites have been predicted with the help of homology models [120] and *in silico* protein-protein docking experiments [152]. Delineation of these exact sites awaits the crystal structure of the bifunctional complex, which could be identified for *PfDHFR/TS* and *ChDHFR/TS* once their structures were solved. Further studies have also identified various parasite-specific inserts within *PfAdoMetDC/ODC* that are important for protein activities and are predicted to mediate interactions within the two domains [69] as has been observed for



DHFR/TS from both *P. falciparum* and *C. hominis* [122,258]. However, and in contrast to *PfDHFR/TS*, the activities of *PfAdoMetDC/ODC* are not involved in substrate channelling and the basis for the bifunctional arrangement is largely unknown. It has been shown that *PfODC* is feedback regulated by its product putrescine, which has no effect on *PfAdoMetDC* activity [71]. Furthermore, while *PfAdoMetDC* can function independently, monofunctional *PfODC* is inactive [71,103].

The evolutionary role of such a large bifunctional arrangement has extensively been questioned. Possible reasons include the regulated biosynthesis of polyamines in *Plasmodium* spp [70] via the interference of a single domain, which then communicates the change to the adjacent domain. In addition to the enormous 5'-UTR of *PfAdometdc/Odc* consisting of nearly 3000 nucleotides, the hinge region has been suggested to represent the remnants of the 5'-UTR of *PfOdc* as it is not predicted to have any conformational role but is within the reading frame of translation from *PfAdometdc*. Further studies are needed to identify specific areas within the UTRs that may mediate transcriptional and translational control as well as possible sites that could bind polyamines as a feedback control mechanism as seen for the plant and human transcripts [211,212,259]. In addition, while antizyme [102] is absent in *P. falciparum* and the presence of a prozyme [213] seems improbable, *PfODC* may behave in an analogous fashion to the *PfDHFR/TS* association, and have adopted a role as regulator of the activity of *PfAdoMetDC* (and *vice versa*) in the bifunctional complex. This is evidenced by the improved enzyme kinetics of the recombinantly expressed, monofunctional *PfAdoMetDC* protein compared to its activity in complex with *PfODC* [71]. This has led to the postulation that the bifunctional arrangement could mediate the co-regulation of both activities of the polyamine rate-limiting enzymes and that these are made possible by the various interdomain activities, which can regulate the domain activities. Comparison between *PfDHFR/TS* and *PfAdoMetDC/ODC* has thus revealed that the parasite may employ the bifunctional arrangement of enzymes for 1) the coordinated regulation of enzyme activities in essential metabolic pathways; 2) to allow for the dependence of the activity of the C-terminal domain on the N-terminal domain within the complex; 3) in the case of *PfDHFR/TS* to allow for substrate channelling; and 4) to allow for additional interdomain protein-protein interactions for the metabolic regulation of important metabolites such as folates and polyamines.

In this study, the possibility of interdomain regulation between *PfAdoMetDC* and *PfODC* in the bifunctional complex was studied via the delineation of specifically the O1 parasite-specific insert of the *PfODC* domain and its role in interdomain interactions as well as with the



biochemical and structural characterisation of monofunctional *PfAdoMetDC*. Peptides as probes to determine the possible roles of the O1 insert in interdomain interactions showed that these peptides that are identical to the insert itself could displace the binding sites of this insert and resulted in an increase in *PfAdoMetDC* activity that was comparable to the activity of this enzyme when it exists in its monofunctional form [71]. These peptides therefore mimic the monofunctional arrangement of the *PfAdoMetDC* domain and a peptide that specifically targeted the O1 insert reduced *PfODC* activity, thereby mimicking the effect of expressing *PfODC* in its monofunctional form [103]. These results alluded to the possibility that this insert represents the delineating site that could mediate the activities within the bifunctional *PfAdoMetDC/ODC* complex. In addition, future studies involving the crystallisation of the *PfAdoMetDC* domain could utilise the stabilising effects of the peptides on *PfAdoMetDC* activity to increase its crystallisation in the absence of its protein partner. It was subsequently necessary to characterise the enzyme kinetics of the monofunctional *PfAdoMetDC* domain in order to determine whether the kinetics of this domain are improved in the presence of *PfODC* and would therefore corroborate the O1 insert peptide results. In addition, the biochemical characterisation of *PfAdoMetDC* represents novel results as only limited information is available on this protein in its monofunctional form.

Expression of monofunctional *PfAdoMetDC* (without the majority of the hinge region) showed that while the specific activity of this enzyme is higher in this form, the substrate affinity decreased compared to the K_m in the bifunctional complex. In addition, comparison of the *PfODC* kinetics showed that this monofunctional enzyme is inactive while the presence of *PfAdoMetDC* increases its specific activity as well as substrate binding affinity [71,103]. Furthermore, analyses of the turnover numbers of monofunctional and bifunctional *PfAdoMetDC* or *PfODC* showed that the bifunctional arrangement resulted in matched rates, which would allow for balanced synthesis of the products of the decarboxylase reactions. The results therefore show that the rate-limiting enzymes of the polyamine pathway in *P. falciparum* are co-regulated within the bifunctional complex such that their rates can concurrently be controlled for the subsequent synthesis of the metabolically relevant polyamines via the reaction of *PfSpdS* [98]. We have thus shown for the first time that polyamine biosynthesis in *P. falciparum* is regulated via the arrangement of activities in a bifunctional protein. Future studies should focus on the crystallisation of the monofunctional proteins as well as bifunctional complex such that rational drug design can be facilitated. The studies on monofunctional *PfAdoMetDC* provide important starting points for crystallisation in which a stable protein should be used. These results also prove the relevance of targeting the already validated drug

target, *Pf*AdoMetDC/ODC, with a compound that could simultaneously affect both enzyme activities and thereby inhibit the synthesis of downstream polyamines. The latter studies will have to be performed in combination with the characterisation of polyamine transport in *P. falciparum* since the uptake of polyamines as a means for the parasite to overcome polyamine biosynthesis inhibition will have to be taken into account.

AdoMetDC represents an important drug target due to various factors, including 1) its key responsibility in the synthesis of polyamines by downstream aminopropyl transferases; 2) the unique utilisation of a covalently bound pyruvate as co-factor synthesised by an autocatalytic cleavage event; 3) the maintenance of low steady-state levels of its product, dcAdoMet, as a result of the importance of AdoMet in methyl transfer reactions; and 4) the strict control of its activity in response to the requirement of polyamines by means of its transcription, translation, post-translational modification (pyruvoyl formation), enzyme activity as well as its degradation [258]. It therefore seems that AdoMetDC represents the most important enzyme in the polyamine pathway while SpdS is involved in flux control due to its dependence on the products of both the AdoMetDC and ODC reactions for the synthesis of spermidine. However, in *P. falciparum*, the association of AdoMetDC with ODC within a bifunctional complex allows for a unique opportunity to not only target AdoMetDC activity but also ODC. In addition, the identification of protein-protein interactions between these two domains, especially those mediated by the O1 parasite-specific insert, has allowed for additional strategies to target enzyme activities with the use of non-active site inhibitors. The use of such inhibitors are beneficial due to the limitations involved in targeting inhibitors to the enzyme active site when high structural conservation exists between the active sites of the host and the disease-causing parasite. The greater structural variability of protein-protein interfaces suggests that these interface contact sites may provide important target sites that are sufficiently different between the host and the parasite. The large *Pf*AdoMetDC/ODC complex possesses several protein-protein interaction regions that are absent in the host monofunctional counterparts and can thus be selectively targeted. Another advantage of targeting areas other than the active site is the reduced resistance pressure that is placed on the organism when a non-active site-based drug is used. Resistance to the drug via the introduction of mutations in the active site, as is seen for *Pf*DHFR/TS [146], will develop at a slower rate, which is extremely valuable in drug development against the multidrug resistant malaria-causing *P. falciparum* parasites [169]. Several other advantages of using peptides as therapeutic molecules include: 1) high activity and specificity; 2) unique 3D characteristics; 3) no accumulation in organs due to small size; 4) low toxicity; and 5) low immunogenicity [259].



Alternatively, the use of structure-based drug design was also evaluated by using the well-characterised *PfSpdS* protein as drug target in a study that applied a dynamic, receptor-based pharmacophore model together with *in silico* chemical library screening. This approach identified important factors that should be taken into account to identify a promising lead compound and it specifically identified the importance of identifying a ligand that could bridge the catalytic centre of this two-substrate enzyme and thereby efficiently compete with both substrates. Two lead compounds were subsequently tested *in vitro* for their effects on enzyme inhibition and whole cell-based parasite cultures. The compounds also showed promising interactions and stabilisation within the active site as determined by the atomic resolution (1.9 Å) crystal structures. While the inhibitory results showed potential, these drugs still need to be effectively delivered into the parasites to obtain increased inhibition in the nanomolar range. However, in contrast to prior studies that focussed on ligand-based approaches, the dynamic, receptor-based pharmacophore model employed here identified a compound that could bind to a restricted site within the active site and cause inhibition. The co-crystallisation of these lead compounds with the purified *PfSpdS* protein validated the *in silico* predictions and thus shows the relevance of applying such a study for prioritisation of potential inhibitors to be tested experimentally.

The results of this dissertation have thus completed a full circle in terms of identification of a novel drug target (polyamine biosynthesis), biochemical and structural characterisation thereof in order to identify potential unique properties that are exploitable for selective drug targeting (*PfAdoMetDC* and *PfODC*, Chapters 2 and 3), followed by the identification of potential inhibitors via rational structure-based drug design and validation of the mechanism of inhibition with these novel compounds (*PfSpdS*, Chapter 4). This study thus shows the importance of combining *in vitro* with *in silico* experiments to streamline the required studies that are needed to be performed in the laboratory and shows a successful interplay of three different, yet dependent scientific approaches, namely biochemistry, bioinformatics and medicinal chemistry. Future studies should focus on further structural characterisation of the bifunctional *PfAdoMetDC/ODC* complex as well as validation of interdomain interactions, followed by the identification of novel inhibitory compounds. The efficiency of the inhibitory compounds identified for *PfSpdS* should also be improved in terms of delivery into the parasites and selectivity against host cells. Ultimately, the aim would be to apply a combination-based approach to target bifunctional *PfAdoMetDC/ODC* with a non-active site based inhibitor as well as the flux-controlling activity of *PfSpdS* with a highly selective, active site inhibitor that would result in a drastic reduction of polyamine levels within the parasite.

References

- 1 Gardner, M. J., Hall, N., Fung, E., White, O., Berriman, M., Hyman, R. W., Carlton, J. M., Pain, A., Nelson, K. E., Bowman, S., Paulsen, I. T., James, K., Eisen, J. A., Rutherford, K., Salzberg, S. L., Craig, A., Kyes, S., Chan, M., Nene, V., Shallom, S. J., Suh, B., Peterson, J., Angiuoli, S., Pertea, M., Allen, J., Selengut, J., Haft, D., Mather, M. W., Vaidya, A. B., Martin, D. M. A., Fairlamb, A. H., Fraunholz, M. J., Roos, D. S., Ralph, S. A., McFadden, G. I., Cummings, L. M., Subramanian, G. M., Mungall, C., Venter, J. C., Carucci, D. J., Hoffman, S. L., Newbold, C., Davis, R. W., Fraser, C. M. and Barrell, B. (2002) Genome sequence of the human malaria parasite *Plasmodium falciparum*. *Nature*. **419**, 498-511
- 2 Holt, R. A., Subramanian, G. M., Halpern, A., Sutton, G. G., Charlab, R., Nusskern, D. R., Wincker, P., Clark, A. G., Ribeiro, J. M., Wides, R., Salzberg, S. L., Loftus, B., Yandell, M., Majoros, W. H., Rusch, D. B., Lai, Z., Kraft, C. L., Abril, J. F., Anthouard, V., Arensburger, P., Atkinson, P. W., Baden, H., de Berardinis, V., Baldwin, D., Benes, V., Biedler, J., Blass, C., Bolanos, R., Boscus, D., Barnstead, M., Cai, S., Center, A., Chatuverdi, K., Christophides, G. K., Chrystal, M. A., Clamp, M., Cravchik, A., Curwen, V., Dana, A., Delcher, A., Dew, I., Evans, C. A., Flanagan, M., Grundschober-Freimoser, A., Friedli, L., Gu, Z., Guan, P., Guigo, R., Hillenmeyer, M. E., Hladun, S. L., Hogan, J. R., Hong, Y. S., Hoover, J., Jaillon, O., Ke, Z., Kodira, C., Kokoza, E., Koutsos, A., Letunic, I., Levitsky, A., Liang, Y., Lin, J.-J., Lobo, N. F., Lopez, J. R., Malek, J. A., McIntosh, T. C., Meister, S., Miller, J., Mobarry, C., Mongin, E., Murphy, S. D., O'Brochta, D. A., Pfannkoch, C., Qi, R., Regier, M. A., Remington, K., Shao, H., Sharakhova, M. V., Sitter, C. D., Shetty, J., Smith, T. J., Strong, R., Sun, J., Thomasova, D., Ton, L. Q., Topalis, P., Tu, Z., Unger, M. F., Walenz, B., Wang, A., Wang, J., Wang, M., Wang, X., Woodford, K. J., Wortman, J. R., Wu, M., Yao, A., Zdobnov, E. M., Zhang, H., Zhao, Q., Zhao, S., Zhu, S. C., Zhimulev, I., Coluzzi, M., della Torre, A., Roth, C. W., Louis, C., Kalush, F., Mural, R. J., Myers, E. W., Adams, M. D., Smith, H. O., Broder, S., Gardner, M. J., Fraser, C. M., Birney, E., Bork, P., Brey, P. T., Venter, J. C., Weissenbach, J., Kafatos, F. C., Collins, F. H. and Hoffman, S. L. (2002) The genome sequence of the malaria mosquito *Anopheles gambiae*. *Science*. **298**, 129-149
- 3 Aurrecochea, C., Brestelli, J., Brunk, B. P., Dommer, J., Fischer, S., Gajria, B., Gao, X., Gingle, A., Grant, G., Harb, O. S., Heiges, M., Innamorato, F., Iodice, J., Kissinger, J. C., Kraemer, E., Li, W., Miller, J. A., Nayak, V., Pennington, C., Pinney, D. F., Roos, D. S., Ross, C., Stoeckert, C. J., Treatman, C. and Wang, H. (2009) PlasmoDB: A functional genomic database for malaria parasites. *Nucleic Acids Res.* **37**, 539-543
- 4 Bozdech, Z., Llinás, M., Pulliam, B. L., Wong, E. D., Zhu, J. and DeRisi, J. L. (2003) The transcriptome of the intra-erythrocytic developmental cycle of *Plasmodium falciparum*. *PLoS Biol.* **1**, e5
- 5 Le Roch, K. G., Johnson, J. R., Florens, L., Zhou, Y., Santrosyan, A., Grainger, M., Yan, S. F., Williamson, K. C., Holder, A. A., Carucci, D. J., Yates, J. R. and Winzeler, E. A. (2004) Global analysis of transcript and protein levels across the *Plasmodium falciparum* life cycle. *Genome Res.* **14**, 2308-2318
- 6 Le Roch, K. G., Zhou, Y., Blair, P. L., Grainger, M., Moch, J. K., Haynes, J. D., De la Vega, P., Holder, A. A., Batalov, S., Carucci, D. J. and Winzeler, E. A. (2003) Discovery of gene function by expression profiling of the malaria parasite life cycle. *Science*. **301**, 1503-1508
- 7 Llinás, M., Bozdech, Z., Wong, E. D., Adai, A. T. and DeRisi, J. L. (2006) Comparative whole genome transcriptome analysis of three *Plasmodium falciparum* strains. *Nucleic Acids Res.* **34**, 1166-1173
- 8 Nirmalan, N., Sims, P. F. G. and Hyde, J. E. (2004) Quantitative proteomics of the human malaria parasite *Plasmodium falciparum* and its application to studies of development and inhibition. *Mol. Microbiol.* **52**, 1187-1199
- 9 Sims, P. F. G. and Hyde, J. E. (2006) Proteomics of the human malaria parasite

- Plasmodium falciparum*. Expert Review of Proteomics. **3**, 87-95
- 10 Teng, R., Junankar, P. R., Bubb, W. A., Rae, C., Mercier, P. and Kirk, K. (2008) Metabolite profiling of the intra-erythrocytic malaria parasite *Plasmodium falciparum* by ¹H NMR spectroscopy. NMR Biomed. **22**, 292-302
 - 11 Cohen, J., Bennis, S., Vekemans, J. and Leach, A. (2010) The malaria vaccine candidate RTS,S/AS is in phase III clinical trials. Ann. Pharm. Fr. **68**, 370-379
 - 12 Greenwood, B. M., Fidock, D. A., Kyle, D. E., Kappe, S. H. I., Alonso, P. L., Collins, F. H. and Duffy, P. E. (2008) Malaria: Progress, perils, and prospects for eradication. J. Clin. Invest. **118**, 1266-1276
 - 13 Christophides, G. K. (2005) Transgenic mosquitoes and malaria transmission. Cell. Microbiol. **7**, 325-333
 - 14 Dondorp, A. M., Nosten, F., Yi, P., Das, D., Phyto, A. P., Tarning, J., Lwin, K. M., Ariey, F., Hanpithakpong, W., Lee, S. J., Ringwald, P., Silamut, K., Imwong, M., Chotivanich, K., Lim, P., Herdman, T., An, S. S., Yeung, S., Singhasivanon, P., Day, N. P. J., Lindergardh, N., Socheat, D. and White, N. J. (2009) Artemisinin resistance in *Plasmodium falciparum* malaria. N. Engl. J. Med. **361**, 455-467
 - 15 Cox-Singh, J., Davis, T. M. E., Lee, K.-S., Shamsul, S. S. G., Matusop, A., Ratnam, S., Rahman, H. A., Conway, D. J. and Singh, B. (2008) *Plasmodium knowlesi* malaria in humans is widely distributed and potentially life threatening. Clin. Infect. Dis. **46**, 165-171
 - 16 Hoffman, S. L., Subramanian, G. M., Collins, F. H. and Venter, J. C. (2002) *Plasmodium*, human and *Anopheles* genomics and malaria. Nature. **415**, 702-709
 - 17 Cowman, A. F. and Crabb, B. S. (2006) Invasion of red blood cells by malaria parasites. Cell. **124**, 755-766
 - 18 Wirth, D. F. (2002) The parasite genome: Biological revelations. Nature. **419**, 495-496
 - 19 Nwaka, S. and Hudson, A. (2006) Innovative lead discovery strategies for tropical diseases. Nat. Rev. Drug Discov. **5**, 941-955
 - 20 Maharaj, R., Mthembu, D. J. and Sharp, B. L. (2005) Impact of DDT re-introduction on malaria transmission in KwaZulu-Natal. S. Afr. Med. J. **95**, 871-874
 - 21 Rogan, W. J. and Chen, A. (2005) Health risks and benefits of bis (4-chlorophenyl)-1,1,1-trichloroethane (DDT). Lancet. **366**, 763-773
 - 22 Weissmann, G. (2006) DDT is back: Let us spray! FASEB J. **20**, 2427-2429
 - 23 Coleman, C. S., Stanley, B. A., Viswanath, R. and Pegg, A. E. (1994) Rapid exchange of subunits of mammalian ornithine decarboxylase. Eur. J. Biochem. **269**, 3155-3158
 - 24 Bray, R. S., Burgess, R. W., Fox, R. M. and Miller, M. J. (1959) Effect of pyrimethamine upon sporogony and pre-erythrocytic schizogony of *Laverinia falciparum*. Bull. W.H.O. **21**, 233-238
 - 25 Gillet, J. M., Charlier, J., Boné, G. and Mulamba, P. L. (1983) *Plasmodium berghei*: Inhibition of the sporogonous cycle by α -difluoromethylornithine. Exp. Parasitol. **56**, 190-193
 - 26 Knols, B. G. J., Bukhari, T. and Farenhorst, M. (2010) Entomopathogenic fungi as the next-generation control agents against malaria mosquitoes. Future Microbiol. **5**, 339-341
 - 27 Blanford, S., Chan, B. H. K., Jenkins, N., Sim, D., Turner, R. J., Read, A. F. and Thomas, M. B. (2005) Fungal pathogen reduces potential for malaria transmission. Science. **308**, 1638-1641
 - 28 Farenhorst, M., Mouatcho, J. C., Kikankie, C. K., Brooke, B. D., Hunt, R. H., Thomas, M. B., Koekemoer, L. L., Knols, B. G. J. and Coetzee, M. (2009) Fungal infection counters insecticide resistance in African malaria mosquitoes. Proc. Natl. Acad. Sci. USA. **106**, 17443-17447
 - 29 Miller, L. H. and Hoffman, S. L. (1998) Research toward vaccines against malaria. Nat. Med. **4**, 520-524
 - 30 Bull, P. C. and Marsh, K. (2002) The role of antibodies to *Plasmodium falciparum*-infected-erythrocyte surface antigens in naturally acquired immunity to malaria. Trends Microbiol. **10**, 55-58

- 31 Todryk, S. M. and Hill, A. V. S. (2007) Malaria vaccines: The stage we are at. *Nat. Rev. Microbiol.* **5**, 487-489
- 32 Doolan, D. L. and Hoffman, S. L. (1997) Multi-gene vaccination against malaria: A multistage, multi-immune response approach. *Parasitol. Today.* **13**, 171-178
- 33 Ghumra, A., Khunrae, P., Ataide, R., Raza, A., Rogerson, S. J., Higgins, M. K. and Rowe, J. A. (2011) Immunisation with recombinant PfEMP1 domains elicits functional rosette-inhibiting and phagocytosis-inducing antibodies to *Plasmodium falciparum*. *PLoS ONE.* **6**, e16414
- 34 Anders, R. F. and Saul, A. (2000) Malaria vaccines. *Parasitol. Today.* **16**, 444-447
- 35 Chauhan, P. M. S. and Srivastava, R. (2001) Present trends and future strategy in chemotherapy of malaria. *Curr. Med. Chem.* **8**, 1535-1542
- 36 Müller, I. B. and Hyde, J. E. (2010) Antimalarial drugs: Modes of action and mechanisms of parasite resistance. *Future Microbiol.* **5**, 1857-1873
- 37 Olliaro, P. (2001) Mode of action and mechanisms of resistance for antimalarial drugs. *Pharmacol. Ther.* **89**, 207-219
- 38 Aviado, D. M., Rosen, R., Dacanay, H. and Plotkin, S. H. (1969) Antimalarial and antiarrhythmic activity of plant extracts. 1. Cinchona and quinine in *Plasmodium berghei* in immature rats. *Med. Exp. Int. J. Exp. Med.* **19**, 79-94
- 39 Bjorkman, A. and Phillips-Howard, P. A. (1990) The epidemiology of drug-resistant malaria. *Trans. R. Soc. Trop. Med. Hyg.* **84**, 177-180
- 40 Yeh, I. and Altman, R. B. (2006) Drug targets for *Plasmodium falciparum*: A post-genomic review/survey. *Mini Rev. Med. Chem.* **6**, 177-202
- 41 White, N. J. (1992) Antimalarial drug resistance: the pace quickens. *J. Antimicrob. Chemother.* **30**, 571-585
- 42 Bathurst, I. and Hentschel, C. (2006) Medicines for Malaria Venture: Sustaining antimalarial drug development. *Trends Parasitol.* **22**, 301-307
- 43 Reed, M. B., Saliba, K. J., Caruana, S. R., Kirk, K. and Cowman, A. F. (2000) *Pgh1* modulates sensitivity and resistance to multiple antimalarials in *Plasmodium falciparum*. *Nature.* **403**, 906-909
- 44 Ivanetich, K. M. and Santi, D. V. (1990) Thymidylate synthase-dihydrofolate reductase in protozoa. *Exp. Parasitol.* **70**, 367-371
- 45 Wang, P., Wang, Q., Sims, P. F. G. and Hyde, J. E. (2007) Characterisation of exogenous folate transport in *Plasmodium falciparum*. *Mol. Biochem. Parasitol.* **154**, 40-51
- 46 Cowman, A. F. and Lew, A. M. (1990) Chromosomal rearrangements and point mutations in the DHFR/TS gene of *Plasmodium chabaudi* under antifolate selection. *Mol. Biochem. Parasitol.* **42**, 21-29
- 47 Plowe, C. V., Cortese, J. F., Djimde, A., Okey, C., Winstanley, P. A. and Doumbo, C. K. (1997) Mutations in *Plasmodium falciparum* dihydrofolate reductase and dihydropteroate synthase and epidemiological patterns of pyrimethamine-sulphadoxine use and resistance. *J. Infect. Dis.* **176**, 1590-1596
- 48 Hyde, J. E. (1989) Point mutations and pyrimethamine resistance in *Plasmodium falciparum*. *Parasitol. Today.* **5**, 252-255
- 49 Zolg, J. W., Plitt, J. R., Chen, G. X. and Palmer, S. (1989) Point mutations in the dihydrofolate reductase-thymidylate synthase gene as the molecular basis for pyrimethamine resistance in *Plasmodium falciparum*. *Mol. Biochem. Parasitol.* **36**, 253-262
- 50 Peterson, D. S., Walliker, D. and Wellem, T. E. (1988) Evidence that a point mutation in dihydrofolate reductase-thymidylate synthase confers resistance to pyrimethamine in falciparum malaria. *Proc. Natl. Acad. Sci. USA.* **85**, 9114-9118
- 51 Nirmalan, N., Sims, P. F. G. and Hyde, J. E. (2004) Translational up-regulation of antifolate drug targets in the human malaria parasite *Plasmodium falciparum* upon challenge with inhibitors. *Mol. Biochem. Parasitol.* **136**, 63-70
- 52 Hayton, K., Ranford-Cartwright, L. C. and Walliker, D. (2002) Sulphadoxine-

- pyrimethamine resistance in the rodent malaria parasite *Plasmodium chabaudi*. Antimicrob. Agents Chemother. **46**, 2482-2489
- 53 Nzila-Mounda, A., Mberu, E. K., Sibley, C. H., Plowe, C. V., Winstanley, P. A. and Watkins, W. M. (1998) Kenyan *Plasmodium falciparum* field isolates: correlation between pyrimethamine and chlorocycloguanil activity *in vitro* and point mutations in the dihydrofolate reductase domain. Antimicrob. Agents Chemother. **42**, 164-169
- 54 Luzzatto, L. (2010) The rise and fall of the antimalarial Lapdap: a lesson in pharmacogenetics. Lancet. **376**, 739-741
- 55 Price, R. N., Nosten, F., Luxemburger, C., ter Kuile, F. O., Paiphun, L., Chongsuphajaisiddhi, T. and White, N. J. (1996) Effects of artemisinin derivatives on malaria transmissibility. Lancet. **347**, 1654-1658
- 56 O'Neill, P. M., Barton, V. E. and Ward, S. A. (2010) The molecular mechanism of action of artemisinin: The debate continues. Molecules. **15**, 1705-1721
- 57 Krishna, S., Uhlemann, A. and Haynes, R. K. (2004) Artemisinins: Mechanisms of action and potential for resistance. Drug Resist. Updates. **7**, 233-244
- 58 de Vries, P. J. and Dien, T. K. (1996) Clinical pharmacology and therapeutic potential of artemisinin and its derivatives in the treatment of malaria. Drugs. **52**, 818-836
- 59 Kremsner, P. G. and Krishna, S. (2004) Antimalarial combinations. Lancet. **364**, 285-294
- 60 Meshnick, S. R. (2002) Artemisinin: Mechanisms of action, resistance and toxicity. Int. J. Parasitol. **32**, 1655-1660
- 61 Jambou, R., Legrand, E., Niang, M., Khim, N., Lim, P., Volney, B., Ekala, M. T., Bouchier, C., Esterre, P., Fandeur, T. and Mercereau-Puijalon, O. (2005) Resistance of *Plasmodium falciparum* field isolates to *in vitro* artemether and point mutations of the SERCA-type PfATPase6. Lancet **366**, 1960-1963
- 62 Edwards, G. and Biagini, G. (2006) Resisting resistance: Dealing with the irrepressible problem of malaria. Br. J. Clin. Pharmacol. **61**, 690-693
- 63 Fanello, C. I., Karema, C., Avellino, P., Bancone, G., Uwimana, A., Lee, S. J., d'Alessandro, U. and Modiano, D. (2008) High risk of severe anaemia after chlorproguanil-dapsone+artesunate antimalarial treatment in patients with G6PD (A-) deficiency. PLoS ONE. **3**, e4031
- 64 Gelb, M. H. (2007) Drug discovery for malaria: A very challenging and timely endeavor. Curr. Opin. Chem. Biol. **11**, 440-445
- 65 Dahl, E. L., Shock, J. L., Shenai, B. R., Gut, J., DeRisi, J. L. and Rosenthal, P. J. (2006) Tetracyclines specifically target the apicoplast of the malaria parasite *Plasmodium falciparum*. Antimicrob. Agents Chemother. **50**, 3124-3131
- 66 Wilson, R. J., Denny, P. W., Preiser, P. R., Rangachari, K., Roberts, K., Roy, A., Whyte, A., Strath, M., Moore, D. J. and Williamson, D. H. (1996) Complete map of the plastid-like DNA of the malaria parasite *Plasmodium falciparum*. J. Mol. Biol. **261**, 155-172
- 67 Assaraf, Y. G., Golenser, J., Spira, D. T. and Bachrach, U. (1984) Polyamine levels and the activity of their biosynthetic enzymes in human erythrocytes infected with the malarial parasite, *Plasmodium falciparum*. Biochem. J. **222**, 815-819
- 68 Wang, C. C. (1995) Molecular mechanisms and therapeutic approaches to treatment of African trypanosomiasis. Annu. Rev. Pharmacol. Toxicol. **35**, 93-127
- 69 Birkholtz, L., Wrenger, C., Joubert, F., Wells, G. A., Walter, R. D. and Louw, A. I. (2004) Parasite-specific inserts in the bifunctional *S*-adenosylmethionine decarboxylase/ornithine decarboxylase of *Plasmodium falciparum* modulate catalytic activities and domain interactions. Biochem. J. **377**, 439-448
- 70 Müller, S., Da'dara, A., Lüersen, K., Wrenger, C., Das Gupta, R., Madhubala, R. and Walter, R. D. (2000) In the human malaria parasite *Plasmodium falciparum*, polyamines are synthesised by a bifunctional ornithine decarboxylase, *S*-adenosylmethionine decarboxylase. J. Biol. Chem. **275**, 8097-8102
- 71 Wrenger, C., Lüersen, K., Krause, T., Müller, S. and Walter, R. D. (2001) The

- Plasmodium falciparum* bifunctional ornithine decarboxylase, *S*-adenosylmethionine decarboxylase enables a well-balanced polyamine synthesis without domain-domain interaction J. Biol. Chem. **276**, 29651-29656
- 72 Hamana, K. and Matsuzaki, S. (1992) Polyamines as a chemotaxonomic marker in bacterial systematics. Crit. Rev. Microbiol. **18**, 261-283
- 73 Bachrach, U. (1973) Function of naturally occurring polyamines. Academic Press, New York
- 74 Cohen, S. S. (1971) Introduction to the polyamines. Prentice hall, New York
- 75 Heby, O. (1981) Role of polyamines in the control of cell proliferation and differentiation. Differentiation. **19**, 1-20
- 76 Tabor, C. W. and Tabor, H. (1976) 1,4-Diaminobutane (putrescine), spermidine, and spermine. Annu. Rev. Biochem. **45**, 285-306
- 77 Russell, D. H. (1985) Ornithine decarboxylase: A key regulatory enzyme in normal and neoplastic growth. Drug Metab. Rev. **16**, 1-88
- 78 Poulin, R., Pelletier, G. and Pegg, A. E. (1995) Induction of apoptosis by excessive polyamine accumulation in ornithine decarboxylase-overproducing L1210 cells. Biochem. J. **311**, 723-727
- 79 Tobias, K. E. and Kahana, C. (1995) Exposure to ornithine results in excessive accumulation of putrescine and apoptic cell death in ornithine decarboxylase-overproducing mouse myeloma cells. Cell Growth Differ. **6**, 1279-1285
- 80 Xie, X., Tome, M. E. and Gerner, E. W. (1997) Loss of intracellular putrescine pool-size regulation induces apoptosis. Exp. Cell Res. **230**, 386-392
- 81 Feuerstein, B. G., Pattabiraman, N. and Marton, L. J. (1986) Spermine-DNA interactions: A theoretical study. Proc. Natl. Acad. Sci. USA. **83**, 5948-5952
- 82 Feuerstein, B. G., Pattabiraman, N. and Marton, L. J. (1989) Molecular dynamics of spermine-DNA interactions: Sequence specificity and DNA bending for a simple ligand. Nucleic Acids Res. **17**, 6883-6892
- 83 Kerppola, T. K. (1998) Transcriptional cooperativity: Bending over backwards and doing the flip. Structure. **6**, 549-554
- 84 Tabor, H. (1962) The protective effect of spermidine and other polyamines against heat denaturation of deoxyribonucleic acid. Biochemistry. **1**, 496-501
- 85 Hobbs, C. A., Paul, B. A. and Gilmour, S. K. (2002) Deregulation of polyamine biosynthesis alters intrinsic histone acetyltransferase and deacetylase activities in murine skin and tumors. Cancer Res. **62**, 67-74
- 86 Kang, H. A. and Hershey, J. W. (1994) Effect of initiation factor eIF-5A depletion on protein synthesis and proliferation of *Saccharomyces cerevisiae*. Mol. Cell. Biol. **269**, 3934-3940
- 87 Molitor, I. M., Knöbel, S., Dang, C., Spielmann, T., Alléra, A. and König, G. M. (2004) Translation initiation factor eIF-5A from *Plasmodium falciparum*. Mol. Biochem. Parasitol. **137**, 65-74
- 88 Thomas, T. and Thomas, T. J. (2001) Polyamines in cell growth and cell death: Molecular mechanisms and therapeutic applications. Cell. Mol. Life Sci. **58**, 244-258
- 89 Tome, M. E., Fiser, S. M., Payne, C. M. and Gerner, E. W. (1997) Excess putrescine accumulation inhibits the formation of modified eukaryotic initiation factor 5A (eIF-5A) and induces apoptosis. Biochem. J. **328**, 847-854
- 90 Seiler, N. (2003) Thirty years of polyamine-related approaches to cancer therapy. Retrospect and prospect Curr. Drug Targets. **4**, 537-585
- 91 Heby, O., Persson, L. and Rentala, M. (2007) Targeting the polyamine biosynthetic enzymes: A promising approach to therapy of African sleeping sickness, Chagas' disease, and leishmaniasis. Amino Acids. **33**, 359-366
- 92 Müller, S., Coombs, G. H. and Walter, R. D. (2001) Targeting polyamines of parasitic protozoa in chemotherapy. Trends Parasitol. **17**, 242-249
- 93 Müller, I. B., das Gupta, R., Lüersen, K. L., Wrenger, C. and Walter, R. D. (2008)

- Assessing the polyamine metabolism of *Plasmodium falciparum* as chemotherapeutic target. *Mol. Biochem. Parasitol.* **160**, 1-7
- 94 Casero, R. A. and Pegg, A. E. (2009) Polyamine catabolism and disease. *Biochem. J.* **421**, 323-338
- 95 Fairlamb, A. H. and Cerami, A. (1992) Metabolism and functions of trypanothione in the Kinetoplastida. *Annu. Rev. Microbiol.* **46**, 695-729
- 96 Hunter, K. J., Le Quesne, S. A. and Fairlamb, A. H. (1994) Identification and biosynthesis of N^1, N^9 -bis(glutathionyl)aminopropylcadaverine (homotrypanothione) in *Trypanosoma cruzi*. *Eur. J. Biochem.* **226**, 1019-1027
- 97 Wu, H., Min, J., Ikeguchi, Y., Zeng, H., Dong, A., Loppnau, P., Pegg, A. E. and Plotnikov, A. N. (2007) Structure and mechanism of spermidine synthases. *Biochemistry.* **46**, 8331-8339
- 98 Haider, N., Eschbach, M., de Souza Dias, S., Gilberger, T., Walter, R. D. and Lüersen, K. (2005) The spermidine synthase of the malaria parasite *Plasmodium falciparum*: Molecular and biochemical characterisation of the polyamine synthesis enzyme. *Mol. Biochem. Parasitol.* **142**, 224-236
- 99 Wu, H., Min, J., Zeng, H., McCloskey, D. E., Ikeguchi, Y., Loppnau, P., Michael, A. J., Pegg, A. E. and Plotnikov, A. N. (2008) Crystal structure of human spermine synthase: implications of substrate binding and catalytic mechanism. *J. Biol. Chem.* **283**, 16135-16146
- 100 Das Gupta, R., Krause-Ihle, T., Bergmann, B., Müller, I. B., Khomutov, A., Müller, S., Walter, R. D. and Lüersen, K. (2005) 3-Aminoxy-1-aminopropane and derivatives have an antiproliferative effect on cultured *Plasmodium falciparum* by decreasing intracellular polyamine concentrations. *Antimicrob. Agents Chemother.* **49**, 2857-2864
- 101 Reeksting, S. B. (2009) Metabolomic analyses of the malaria parasite after inhibition of polyamine biosynthesis. Thesis, University of Pretoria
- 102 Hayashi, S. and Murakami, Y. (1995) Rapid and regulated degradation of ornithine decarboxylase. *Biochem. J.* **306**, 1-10
- 103 Krause, T., Lüersen, K., Wrenger, C. and Gilberger, T. W. (2000) The ornithine decarboxylase domain of the bifunctional ornithine decarboxylase/S-adenosylmethionine decarboxylase of *Plasmodium falciparum*: recombinant expression and catalytic properties of two different constructs. *Biochem. J.* **352**, 287-292
- 104 Palmer, A. J. and Wallace, H. M. (2010) The polyamine transport system as a target for anticancer drug development. *Amino Acids* **38**, 415-422
- 105 Deitsch, K. W. and Wellems, T. E. (1996) Membrane modifications in erythrocytes parasitised by *Plasmodium falciparum*. *Mol. Biochem. Parasitol.* **76**, 1-10
- 106 Ginsberg, H. (1990) Alterations by the intra-erythrocytic malaria parasite in the permeability of its host cell membrane. *Comp. Biochem. Physiol.* **95**, 31-39
- 107 Seiler, N., Delcros, J. G. and Moulinoux, J. P. (1996) Polyamine transport in mammalian cells. An update. *Int. J. Biochem. Cell Biol.* **28**, 843-861
- 108 Singh, S., Puri, S. K., Singh, S. K., Srivastava, R., Gupta, R. C. and Pandey, V. C. (1997) Characterisation of simian malaria parasite (*Plasmodium knowlesi*)-induced putrescine transport in Rhesus monkey erythrocytes. *J. Biol. Chem.* **272**, 13506-13511
- 109 Assaraf, Y. G., Abu-Elheiga, L., Spira, D. T., Desser, H. and Bachrach, U. (1987) Effect of polyamine depletion on macromolecular synthesis of the malaria parasite, *Plasmodium falciparum*, cultured in human erythrocytes. *Biochem. J.* **242**, 221-226
- 110 Niemand, J. (2011) Biochemical characterisation of putrescine and spermidine uptake as a potential therapeutic target against the human malaria parasite, *Plasmodium falciparum*. Thesis, University of Pretoria
- 111 Palmer, A. J., Ghani, R. A., Kaur, N., Phanstiel, O. and Wallace, H. M. (2009) A putrescine-anthracene conjugate: A paradigm for selective drug delivery. *Biochem. J.* **424**, 431-438
- 112 Chadwick, J., Jones, M., Mercer, A. E., Stocks, P. A., Ward, S. A., Park, B. K. and

- O'Neill, P. M. (2010) Design, synthesis and antimalarial/anticancer evaluation of spermidine linked artemisinin conjugates designed to exploit polyamine transporters in *Plasmodium falciparum* and HL-60 cancer cell lines. *Bioorg. Med. Chem.* **18**, 2586-2597
- 113 Fairlamb, A. H., Henderson, G. B., Bacchi, C. J. and Cerami, A. (1987) *In vivo* effects of difluoromethylornithine on trypanothione and polyamine levels in bloodstream forms of *Trypanosoma brucei* *Mol. Biochem. Parasitol.* **24**, 185-191
- 114 Phillips, M. A., Coffino, P. and Wang, C. C. (1987) Cloning and sequencing of the ornithine decarboxylase gene from *Trypanosoma brucei*. Implications for enzyme turnover and selective difluoromethylornithine inhibition. *J. Biol. Chem.* **262**, 8721-8727
- 115 Wright, P. S., Byers, T. L., Cross-Doersen, D. E., McCann, P. P. and Bitonti, A. J. (1991) Irreversible inhibition of *S*-adenosylmethionine decarboxylase in *Plasmodium falciparum*-infected erythrocytes: Growth inhibition *in vitro*. *Biochem. Pharmacol.* **41**, 1713-1718
- 116 Bitonti, A. J., Dumont, J. A., Bush, T. L., Edwards, M. L., Stemerick, D. M., McCann, P. P. and Sjoerdsma, A. (1989) Bis(benzyl)polyamine analogues inhibit the growth of chloroquine-resistant human malaria parasites (*Plasmodium falciparum*) *in vitro* and in combination with α -difluoromethylornithine cure murine malaria. *Proc. Natl. Acad. Sci. USA.* **86**, 651-655
- 117 Kaiser, A. E., Gottwald, A. M., Wiersch, C. S., Lindenthal, B., Maier, W. A. and Seitz, H. M. (2001) Effect of drugs inhibiting spermidine biosynthesis and metabolism on the *in vitro* development of *Plasmodium falciparum*. *Parasitol. Res.* **87**, 963-972
- 118 Assaraf, Y. G., Golenser, J., Spira, D. T., Messer, G. and Bachrach, U. (1987) Cytostatic effect of DL- α -difluoromethylornithine against *Plasmodium falciparum* and its reversal by diamines and spermidine. *Parasitol. Res.* **73**, 313-318
- 119 Dufe, V. T., Qui, W., Müller, I. B., Hui, R., Walter, R. D. and Al-Karadaghi, S. (2007) Crystal structure of *Plasmodium falciparum* spermidine synthase in complex with the substrate decarboxylated *S*-adenosylmethionine and the potent inhibitors 4MCHA and AdoDATO. *J. Mol. Biol.* **373**, 167-177
- 120 Wells, G. A., Birkholtz, L., Joubert, F., Walter, R. D. and Louw, A. I. (2006) Novel properties of malarial *S*-adenosylmethionine decarboxylase as revealed by structural modelling. *J. Mol. Graph. Model.* **24**, 307-318
- 121 Roux, S. (2006) Modulation of functional properties of bifunctional *S*-adenosylmethionine decarboxylase/ornithine decarboxylase of *Plasmodium falciparum* by structural motifs in parasite-specific inserts. Thesis, University of Pretoria
- 122 Shallom, S., Zhang, K., Jiang, L. and Rathod, P. K. (1999) Essential protein-protein interactions between *Plasmodium falciparum* thymidylate synthase and dihydrofolate reductase domains. *J. Biol. Chem.* **274**, 37781-37786
- 123 Ekstrom, J. L., Mathews, I. I., Stanley, B. A., Pegg, A. E. and Ealick, S. E. (1999) The crystal structure of human *S*-adenosylmethionine decarboxylase at 2.25 Å resolution reveals a novel fold. *Structure.* **5**, 583-595
- 124 Tolbert, W. D., Ekstrom, J. L., Mathews, II, Secrist, J. A., Kapoor, P., Pegg, A. E. and Ealick, S. E. (2001) The structural basis for substrate specificity and inhibition of human *S*-adenosylmethionine decarboxylase. *Biochemistry.* **40**, 13124-13124
- 125 Xiong, H. and Pegg, A. E. (1999) Mechanistic studies of the processing of human *S*-adenosylmethionine decarboxylase proenzyme. *J. Biol. Chem.* **274**, 35059-35066
- 126 Müller, I. B., Walter, R. D. and Wrenger, C. (2005) Structural metal dependency of the arginase from the human malaria parasite *Plasmodium falciparum*. *Biochem. J.* **386**, 117-126
- 127 Birkholtz, L., Joubert, F., Neitz, A. W. H. and Louw, A. I. (2003) Comparative properties of a three-dimensional model of *Plasmodium falciparum* ornithine decarboxylase. *Proteins.* **50**, 464-473
- 128 Almrud, J. J., Oliveira, M. A., Kern, A. D., Grishin, N. V., Phillips, M. A. and Hackert, M. L. (2000) Crystal structure of human ornithine decarboxylase at 2.1 Å resolution: structural insights to antizyme binding. *J. Mol. Biol.* **295**, 7-16
- 129 Poulin, R., Ackermann, B., Bey, P. and Pegg, A. E. (1992) Mechanism of the irreversible

- inactivation of mouse ornithine decarboxylase by alpha-difluoromethylornithine. Characterisation of sequences at the inhibitor and coenzyme binding sites. *J. Biol. Chem.* **267**, 150-158
- 130 Burger, P. B., Birkholtz, L., Joubert, F., Haider, N., Walter, R. D. and Louw, A. I. (2007) Structural and mechanistic insights into the action of *Plasmodium falciparum* spermidine synthase. *Bioorg. Med. Chem.* **15**, 1628-1637
- 131 Ikeguchi, Y., Bewley, M. C. and Pegg, A. E. (2006) Aminopropyltransferases: Function, structure and genetics. *J. Biochem.* **139**, 1-9
- 132 Korolev, S., Ikeguchi, Y., Skarina, T., Beasley, S., Arrowsmith, C., Edwards, A., Joachimiak, A., Pegg, A. E. and Savchenko, A. (2002) The crystal structure of spermidine synthase with a multisubstrate adduct inhibitor. *Nat. Struct. Biol.* **9**, 27-31
- 133 Rattanachuen, W., Jönsson, M., Swedberg, G. and Sirawaraporn, W. (2009) Probing the roles of non-homologous insertions in the N-terminal domain of *Plasmodium falciparum* hydroxymethylpterin pyrophosphokinase-dihydropteroate synthase. *Mol. Biochem. Parasitol.* **168**, 135-142
- 134 Jackson, L. K., Baldwin, J., Akella, R., Goldsmith, E. J. and Phillips, M. A. (2004) Multiple active site conformations revealed by distant site mutation in ornithine decarboxylase. *Biochemistry.* **43**, 12990-12999
- 135 Pizzi, E. and Frontali, C. (2000) Divergence of noncoding sequences and of insertions encoding nonglobular domains at a genomic region well conserved in Plasmodia. *J. Mol. Evol.* **50**, 474-480
- 136 Bzik, D. J. (1991) The structure and role of RNA polymerase in *Plasmodium*. *Parasitol. Today.* **7**, 211-214
- 137 Lüersen, K., Walter, R. D. and Müller, S. (1998) The putative γ -glutamylcysteine synthetase from *Plasmodium falciparum* contains large insertions and a variable tandem repeat. *Mol. Biochem. Parasitol.* **98**, 131-142
- 138 Bzik, D. J., Li, W. B., Horri, T. and Inselburg, J. (1987) Molecular cloning and sequence analysis of the *Plasmodium falciparum* dihydrofolate reductase/thymidylate synthase gene. *Proc. Natl. Acad. Sci. USA.* **84**, 8360-8364
- 139 Cheesman, S., McAleese, S., Goman, M., Johnson, D., Horrocks, P., Ridley, R. G. and Kilbey, B. J. (1994) The gene encoding topoisomerase II from *Plasmodium falciparum*. *Nucleic Acids Res.* **22**, 2547-2551
- 140 Dyson, H. J. and Wright, P. E. (2005) Intrinsically unstructured proteins and their functions. *Nat. Rev. Mol. Cell Biol.* **6**, 197-208
- 141 Pizzi, E. and Frontali, C. (2001) Low-complexity regions in *Plasmodium falciparum* proteins. *Genome Res.* **11**, 218-229
- 142 Zilversmit, M. M., Volkman, S. K., DePristo, M. A., Wirth, D. F., Awadalla, P. and Hartl, D. L. (2010) Low-complexity regions in *Plasmodium falciparum*: missing links in the evolution of an extreme genome. *Mol. Biol. Evol.* **27**, 2198-2209
- 143 Feng, Z.-P., Zhang, X., Han, P., Arora, N., Anders, R. F. and Norton, R. S. (2006) Abundance of intrinsically unstructured proteins in *P. falciparum* and other apicomplexan parasite proteomes. *Mol. Biochem. Parasitol.* **150**, 256-267
- 144 Coletta, A., Pinney, J., Solis, D., Marsh, J., Pettifer, S. and Attwood, T. (2010) Low-complexity regions within protein sequences have position-dependent roles. *BMC Syst. Biol.* **4**, 43
- 145 Wright, P. E. and Dyson, H. J. (1999) Intrinsically unstructured proteins: re-assessing the protein structure-function paradigm. *J. Mol. Biol.* **293**, 321-331
- 146 Srinivasan, R. and Rose, G. D. (1999) A physical basis for protein secondary structure. *Proc. Natl. Acad. Sci. USA.* **96**, 14258-14263
- 147 Larkin, M. A., Blackshields, G., Brown, N. P., Chenna, R., McGettigan, P. A., McWilliam, H., Valentin, F., Wallace, I. M., Wilm, A., Lopez, R., Thompson, J. D., Gibson, T. J. and Higgins, D. G. (2007) Clustal W and Clustal X version 2.0. *Bioinformatics.* **23**, 2947-2948

- 148 Cole, C., Barber, J. D. and Barton, G. J. (2008) The Jpred 3 secondary structure prediction server. *Nucleic Acids Res.* **36**, W197-W201
- 149 Rychlik, W., Spencer, W. J. and Rhoads, R. E. (1990) Optimisation of the annealing temperature for DNA amplification *in vitro*. *Nucleic Acids Res.* **18**, 6409-6412
- 150 Bradford, M. M. (1976) A rapid and sensitive method for the quantitation of microgram quantities of protein utilising the principle of protein-dye binding. *Anal. Biochem.* **72**, 248-254
- 151 Merrill, C. R., Goldman, D., Sedman, S. A. and Ebert, M. H. (1981) Ultrasensitive stain for proteins in polyacrylamide gels shows regional variation in cerebrospinal fluid proteins. *Anal. Biochem.* **72**, 248-254
- 152 Wells, G. A. (2010) Molecular modeling elucidates parasite-specific features of polyamine pathway enzymes of *Plasmodium falciparum*. Thesis, University of Pretoria
- 153 Laskowski, R. A., MacArthur, M. W., Moss, D. S. and Thornton, J. M. (1993) PROCHECK: A program to check the stereochemical quality of protein structures. *J. Appl. Cryst.* **26**, 283-291
- 154 Vriend, G. (1990) WHAT IF: A molecular modeling and drug design program. *J. Mol. Graph.* **8**, 52-56
- 155 Humphrey, W., Dalke, A. and Schulten, K. (1996) VMD: Visual molecular dynamics. *J. Mol. Graph.* **14**, 33-38, 27-38
- 156 Phillips, J. C., Braun, R., Wang, W., Gumbart, J., Tajkhorshid, E., Villa, E., Chipot, C., Skeel, R. D., Kalé, L. and Schulten, K. (2005) Scalable molecular dynamics with NAMD. *J. Comput. Chem.* **26**, 1781-1802
- 157 Jackson, R. M., Gabb, H. A. and Sternberg, M. J. (1998) Rapid refinement of protein interfaces incorporating solvation: Application to the docking problem. *J. Mol. Biol.* **276**, 265-285
- 158 Yan, B. X. and Sun, Y. Q. (1997) Glycine residues provide flexibility for enzyme active sites. *J. Biol. Chem.* **272**, 3190-3194
- 159 Maupetit, J., Derreumaux, P. and Tuffery, P. (2009) PEP-FOLD: an online resource for *de novo* peptide structure prediction. *Nucleic Acids Res.* **37**, 498-503
- 160 Dasgupta, T. and Anderson, K. S. (2008) Probing the role of parasite-specific, distant structural regions on communication and catalysis in the bifunctional thymidylate synthase/dihydrofolate reductase from *Plasmodium falciparum*. *Biochemistry.* **47**, 1336-1345
- 161 Vargo, M. A., Martucci, W. E. and Anderson, K. S. (2009) Disruption of the crossover helix impairs dihydrofolate reductase activity in the bifunctional enzyme TS-DHFR from *Cryptosporidium hominis*. *Biochem. J.* **417**, 757-764
- 162 Murakami, Y., Matsufuji, S., Hayashi, S., Tanahashi, N. and Tanaka, K. (2000) Degradation of ornithine decarboxylase by the 26S proteasome. *Biochem. Biophys. Res. Commun.* **267**, 1-6
- 163 Willert, E. K., Fitzpatrick, R. and Phillips, M. A. (2007) Allosteric regulation of an essential trypanosome polyamine biosynthetic enzyme by a catalytically dead homologue. *Proc. Natl. Acad. Sci. USA.* **104**, 8275-8280
- 164 Willert, E. K. and Phillips, M. A. (2009) Cross-species activation of trypanosome S-adenosylmethionine decarboxylase by the regulatory subunit prozyme. *Mol. Biochem. Parasitol.* **168**, 1-6
- 165 Dufe, V. T., Ingner, D., Heby, O., Khomutov, A. R., Persson, L. and Al-Karadaghi, S. (2007) A structural insight into the inhibition of human and *Leishmania donovani* ornithine decarboxylase by 1-amino-oxy-3-aminopropane. *Biochem. J.* **405**, 261-268
- 166 Birkholtz, L. (2001) Functional and structural characterisation of the unique bifunctional enzyme complex involved in regulation of polyamine metabolism in *Plasmodium falciparum* Thesis, University of Pretoria
- 167 Marceau, M., Lewis, S. D. and Shafer, J. A. (1988) The glycine-rich region of *Escherichia coli* D-serine dehydratase. *J. Biol. Chem.* **263**, 16934-16941
- 168 Osterman, A., Brooks, H. B., Rizo, J. and Phillips, M. A. (1997) Role of Arg-277 in the

- binding of pyridoxal 5'-phosphate to *Trypanosoma brucei* ornithine decarboxylase. *Biochemistry*. **36**, 4558-4567
- 169 Singh, S. K., Maithal, K., Balaram, H. and Balaram, P. (2001) Synthetic peptides as inactivators of multimeric enzymes: Inhibition of *Plasmodium falciparum* triosephosphate isomerase by interface peptides. *FEBS Lett.* **501**, 19-23
- 170 Babe, L. M., Rose, J. and Craik, C. S. (1992) Synthetic "interface" peptides alter the assembly of the HIV 1 and 2 proteases. *Protein Sci.* **1**, 1244-1253
- 171 Schramm, H. J., Boetzel, J., Büttner, J., Fritsche, E., Göhring, W., Jaeger, E., König, S., Thumfart, O., Wenger, T., Nagel, N. E. and Schramm, W. (1996) The inhibition of human immunodeficiency virus proteases by "interface peptides". *Antiviral. Res.* **30**, 155-170
- 172 Prasanna, V., Bhattacharjya, S. and Balaram, P. (1998) Synthetic interface peptides as inactivators of multimeric enzymes: Inhibitory and conformational properties of three fragments from *Lactobacillus casei* thymidylate synthase. *Biochemistry*. **37**, 6883-6893
- 173 Okhanda, J., Buckner, F. S., Lockman, J. W., Yokoyama, K., Carrico, D., Eastman, R., de Luca-Fradley, K., Davies, W., Croft, S. L., Van Voorhis, W. C., Gelb, M. H., Sebt, S. M. and Hamilton, A. D. (2004) Design and synthesis of peptidomimetic protein farnesyltransferase inhibitors as anti-*Trypanosoma brucei* agents. *J. Med. Chem.* **47**, 432-445
- 174 Kuriyan, J. and Eisenberg, D. (2007) The origin of protein interactions and allostery in colocalisation. *Nature*. **450**, 983-990
- 175 Bitonti, A. J., Byers, T. L., Bush, T. L., Casara, P. J., Bacchi, C. J., Clarkson, A. B. J., McCann, P. P. and Sjoerdsma, A. (1990) Cure of *Trypanosoma brucei brucei* and *Trypanosoma brucei rhodesiense* infections in mice with an irreversible inhibitor of S-adenosylmethionine decarboxylase. *Antimicrob. Agents Chemother.* **34**, 1485-1490
- 176 Byers, T. L., Bush, T. L., McCann, P. P. and Bitonti, A. J. (1991) Antitrypanosomal effects of polyamine biosynthesis inhibitors correlate with increases in *Trypanosoma brucei brucei* S-adenosyl-L-methionine. *Biochem. J.* **274**, 527-533
- 177 Bacchi, C. J., Nathan, H. C., N., Y., Goldberg, B., McCann, P. P., Bitonti, A. J. and Sjoerdsma, A. (1992) Cure of murine *Trypanosoma brucei rhodesiense* infections with an S-adenosylmethionine decarboxylase inhibitor. *Antimicrob. Agents Chemother.* **36**, 2736-2740
- 178 Reguera, R. M., Redondo, C. M., Perez-Pertejo, Y. and Balana-Fouce, R. (2007) S-adenosylmethionine in protozoan parasites: functions, synthesis and regulation. *Mol. Biochem. Parasitol.* **152**, 1-10
- 179 Miao, J., Fan, Q., Cui, L., Li, J., Li, J. and Cui, L. (2006) The malaria parasite *Plasmodium falciparum* histones: organization, expression, and acetylation. *Gene*. **369**, 53-65
- 180 Frostesjö, L., Holm, I., Grahn, B., Page, A., Bestor, T. and Heby, O. (1997) Interference with DNA methyltransferase activity and genome methylation during F9 teratocarcinoma stem cell differentiation induced by polyamine deletion. *J. Biol. Chem.* **272**, 4359-4366
- 181 Blavid, R., Kusch, P., Hauber, J., Eschweiler, U., Sarite, S., Specht, S., Deininger, S., Hoerauf, A. and Kaiser, A. (2010) Down-regulation of hypusine biosynthesis in *Plasmodium* by inhibition of S-adenosyl-methionine-decarboxylase. *Amino Acids*. **38**, 461-469
- 182 van Brummelen, A. C., Olszewski, K. L., Wilinski, D., Llinás, M., Louw, A. I. and Birkholtz, L. (2009) Co-inhibition of *Plasmodium falciparum* S-adenosylmethionine decarboxylase/Ornithine decarboxylase reveals perturbation-specific compensatory mechanisms by transcriptome, proteome, and metabolome analyses. *J. Biol. Chem* **284**, 4635-4646
- 183 Bale, S., Baba, K., McCloskey, D. E., Pegg, A. E. and Ealick, S. E. (2010) Complexes of *Thermotoga maritima* S-adenosylmethionine decarboxylase provide insights into substrate specificity. *Acta Crystallogr. Sect. D Biol. Crystallogr.* **D66**, 181-189
- 184 Bennett, E. M., Ekstrom, J. L., Pegg, A. E. and Ealick, S. E. (2002) Monomeric S-adenosylmethionine decarboxylase from plants provides an alternative to putrescine stimulation. *Biochemistry*. **41**, 14509-14517
- 185 Bale, S., Lopez, M. M., Makhatadze, G. I., Fang, Q., Pegg, A. E. and Ealick, S. E. (2008) Structural basis for putrescine activation of human S-adenosylmethionine decarboxylase.

- Biochemistry. **47**, 13404-13417
- 186 Clyne Beswick, T., Willert, E. K. and Phillips, M. A. (2006) Mechanisms of allosteric regulation of *Trypanosoma cruzi* S-adenosylmethionine decarboxylase. *Biochemistry*. **45**, 7797-7807
- 187 Clyne, T., Kinch, L. N. and Phillips, M. A. (2002) Putrescine activation of *Trypanosoma cruzi* S-adenosylmethionine decarboxylase. *Biochemistry*. **41**, 13207-13216
- 188 Ekstrom, J. L., Tolbert, W. D., Xiong, H., Pegg, A. E. and Ealick, S. E. (2001) Structure of a human S-adenosylmethionine decarboxylase self-processing ester intermediate and mechanism of putrescine stimulation of processing as revealed by the H243A mutant. *Biochemistry*. **40**, 9495-9504
- 189 Xiong, H., Stanley, B. A., Tekwani, B. L. and Pegg, A. E. (2009) Processing of mammalian and plant S-adenosylmethionine decarboxylase proenzymes. *J. Biol. Chem.* **272**, 28342-28348
- 190 Birkholtz, L., Blatch, G., Coetzer, T., Hoppe, H. C., Human, E., Morris, J., Ngcete, Z., Oldfield, L., Roth, R., Shonhai, A., Stephens, L. and Louw, A. I. (2008) Heterologous expression of plasmodial proteins for structural studies and functional annotation. *Malaria J.* **7**, 197
- 191 Sprenger, J. (2010) Structural studies on S-adenosylmethionine decarboxylase from *Plasmodium falciparum*. Thesis, University of Potsdam
- 192 Sirawaraporn, W., Prapunwattana, P., Sirawaraporn, R., Yuthavong, Y. and Santi, D. V. (2003) The dihydrofolate reductase domain of *Plasmodium falciparum* thymidylate synthase-dihydrofolate reductase: gene synthesis, expression, and anti-folate-resistant mutants. *J. Biol. Chem.* **268**, 21637-21644
- 193 Niesen, F. H., Berglund, H. and Vedadi, M. (2007) The use of differential scanning fluorimetry to detect ligand interactions that promote protein stability. *Nature Protocols*. **2**, 2212-2221
- 194 Everberg, H., Peterson, R., Rak, S., Tjerneld, F. and Emanuelsson, C. (2006) Aqueous two-phase partitioning for proteomic monitoring of cell surface biomarkers in human peripheral blood mononuclear cells. *J. Proteome Res.* **5**, 1168-1175
- 195 Williams, M., Louw, A. I. and Birkholtz, L. (2007) Deletion mutagenesis of large areas in *Plasmodium falciparum* genes: A comparative study. *Malaria J.* **6**, 64
- 196 Greenfield, N. J. (2006) Using circular dichroism spectra to estimate protein secondary structure. *Nature Protocols*. **1**, 2876-2890
- 197 Lees, J. G., Smith, B. R., Wien, F., Miles, A. J. and Wallace, B. A. (2004) CDtool - An integrated software package for circular dichroism spectroscopic data processing, analysis and archiving. *Anal. Biochem.* **332**, 285-289
- 198 Wilson, K. and Walker, J. (2000) *Practical Biochemistry: Principles and Techniques*. Cambridge
- 199 Kitz, R. and Wilson, I. B. (1962) Esters of methanesulfonic acid as irreversible inhibitors of acetylcholinesterase. *J. Biol. Chem.* **237**, 3245-3249
- 200 Segel, I. H. (1976) *Biochemical calculations: how to solve mathematical calculations in General Biochemistry*. John Wiley & Sons
- 201 Li, X., Han, Y. and Pan, X. M. (2001) Cysteine-25 of adenylate kinase reacts with dithiothreitol to form an adduct upon aging of the enzyme. *FEBS Lett.* **507**, 169-173
- 202 Alliegro, M. C. (2000) Effects of dithiothreitol on protein activity unrelated to thiol-disulfide exchange: for consideration in the analysis of protein function with Cleland's reagent. *Anal. Biochem.* **282**, 102-106
- 203 van Beers, M. M. C., Sauerborn, M., Gilli, F., Brinks, V., Schellekens, H. and Jiskoot, W. (2010) Aggregated recombinant human interferon beta induces antibodies but no memory in immune-tolerant transgenic mice. *Pharmacol. Res.* **27**, 1812-1824
- 204 Danzin, C., Marchal, P. and Casara, P. (1990) Irreversible inhibition of rat S-adenosylmethionine decarboxylase by 5'-[(Z)-4-amino-2-butenyl]methylamino)-5'-deoxyadenosine. *Biochem. Pharmacol.* **40**, 1499-1503

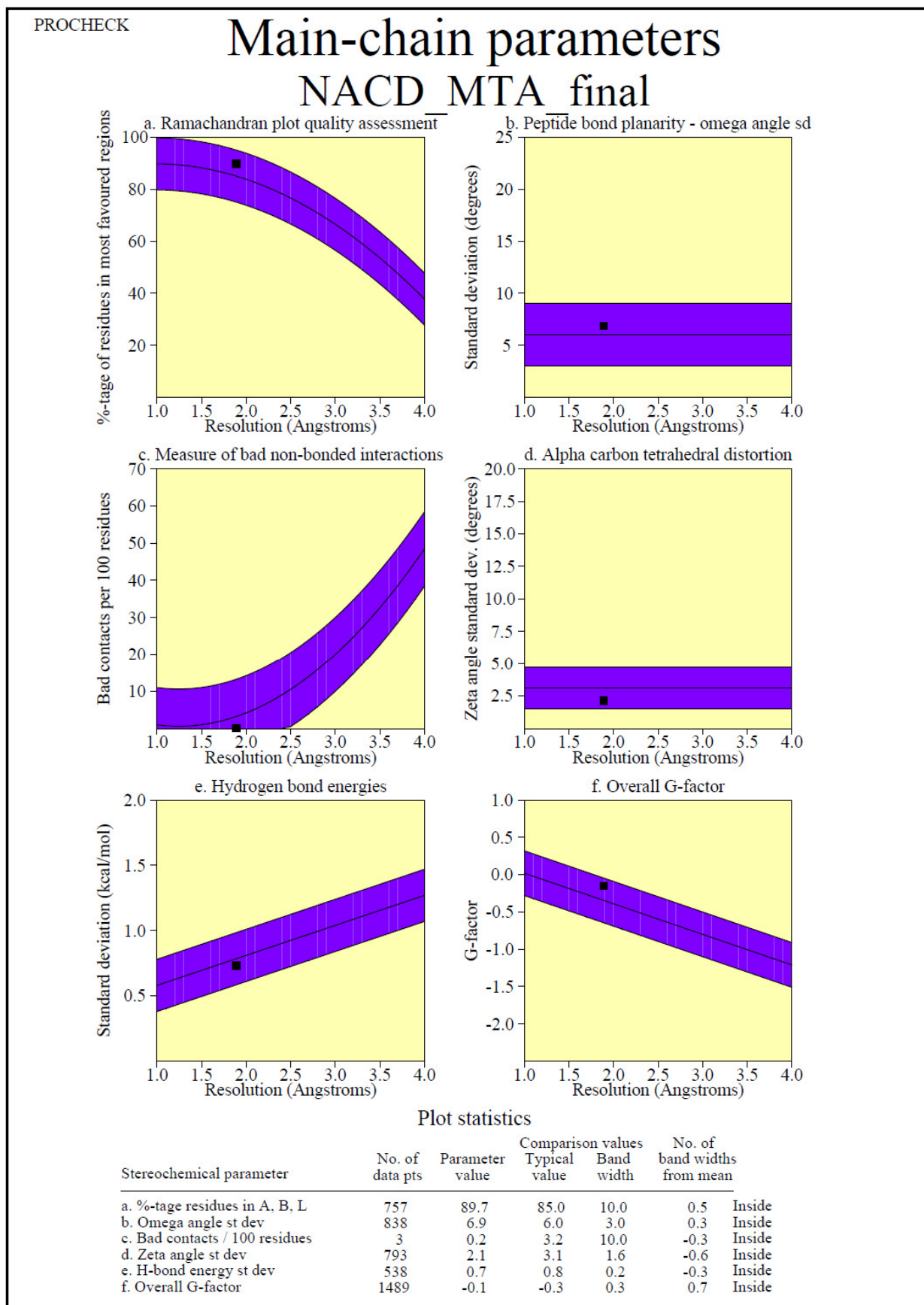
- 205 Regenass, U., Mett, H., Stanek, J., Mueller, M., Kramer, D. and Porter, C. W. (1994) CGP48664, a new *S*-adenosylmethionine decarboxylase inhibitor with broad spectrum antiproliferative and antitumor activity. *Cancer Res.* **54**, 3210-3217
- 206 Brun, R., Bühhler, Y., Sandmeier, U., Kaminsky, R., Bacchi, C. J., Rattendi, D., Lane, S., Croft, S. L., Snowdon, D., Yardley, V., Caravatti, G., Frei, J., Stanek, J. and Mett, H. (1996) *In vitro* trypanocidal activities of new *S*-adenosylmethionine decarboxylase inhibitors. *Antimicrob. Agents Chemother.* **40**, 1442-1447
- 207 Tolbert, W. D., Cottet, S. E., Bennet, E. M., Ekstrom, J. L., Pegg, A. E. and Ealick, S. E. (2003) Mechanism of human *S*-adenosylmethionine decarboxylase proenzyme processing as revealed by the structure of the S68A mutant. *Biochemistry.* **42**, 2386-2395
- 208 Vedadi, M., Lew, J., Artz, J., Amani, M., Zhao, Y., Dong, A., Wasney, G. A., Gao, M., Hills, T., Brokx, S., Qiu, W., Sharma, S., Diassiti, A., Alam, Z., Melone, M., Mulichak, A., Wernimont, A., Bray, J., Loppnau, P., Plotnikova, O., Newberry, K., Sundararajan, E., Houston, S., Walker, J., Tempel, W., Bochkarev, A., Koziaradski, I., Edwards, A., Arrowsmith, C., Roos, D. S., Kain, K. and Hui, R. (2006) Genome-scale protein expression and structural biology of *Plasmodium falciparum* and related Apicomplexan organisms. *Mol. Biochem. Parasitol.* **151**, 100-110
- 209 Angov, E., Hillier, C. J., Kincaid, R. L. and Lyon, J. A. (2008) Heterologous protein expression is enhanced by harmonising the codon usage frequencies of the target gene with those of the expression host. *PLoS ONE.* **3**, e2189
- 210 Müller, S. (2004) Redox and antioxidant systems of the malaria parasite *Plasmodium falciparum*. *Mol. Microbiol.* **53**, 1291-1305
- 211 Hanfrey, C., Elliott, K. A., Franceschetti, M., Mayer, M. J., Illingworth, C. and Michael, A. J. (2005) A dual upstream open reading frame-based autoregulatory circuit controlling polyamine responsive translation. *J. Biol. Chem.* **280**, 39229-39237
- 212 Hanfrey, C., Franceschetti, M., Mayer, M. J., Illingworth, C. and Michael, A. J. (2002) Abrogation of upstream open reading framed mediated translational control of a plant *S*-adenosylmethionine decarboxylase results in polyamine disruption and growth perturbations. *J. Biol. Chem.* **277**, 44131-44139
- 213 Willert, E. K., Fitzpatrick, R. and Phillips, M. A. (2007) Allosteric regulation of an essential trypanosome polyamine biosynthetic enzyme by a catalytically dead homologue. *Proc. Natl. Acad. Sci. USA* **104**, 8275-8280
- 214 Olszewski, K. L., Morrissey, J. M., Wilinski, D., Burns, J. M., Vaidya, A. B., Rabinowitz, J. D. and Llinás, M. (2009) Host-parasite interactions revealed by *Plasmodium falciparum* metabolomics. *Cell.* **5**, 191-199
- 215 Walker, J. and Barrett, J. (1997) Parasite sulphur amino acid metabolism. *Int. J. Parasitol.* **27**, 883-897
- 216 Landau, G., Bercovich, Z., Park, M. H. and Kahana, C. (2010) The role of polyamines in supporting growth of mammalian cells is mediated through their requirement for translation initiation and elongation. *J. Biol. Chem.* **285**, 12474-12481
- 217 Kaiser, A. E., Gottwald, A. M., Wiersch, C. S., Maier, W. A. and Seitz, H. M. (2003) Spermidine metabolism in parasitic protozoa - a comparison to the situation in prokaryotes, viruses, plants and fungi. *Folia Parasitol.* **50**, 3-18
- 218 Roberts, S. C., Jiang, Y., Jardim, A., Carter, N. S., Heby, O. and Ullman, B. (2001) Genetic analysis of spermidine synthase from *Leishmania donovani*. *Mol. Biochem. Parasitol.* **115**, 217-226
- 219 Clark, K., Dhoogra, M., Louw, A. I. and Birkholtz, L. (2009) Transcriptional responses of *Plasmodium falciparum* to α -difluoromethylornithine-induced polyamine depletion. *Biol. Chem.* **389**, 111-125
- 220 Shirahata, A., Morohoshi, T. and Samejima, K. (1988) *Trans*-4-methylcyclohexylamine, a potent new inhibitor of spermidine synthase. *Chem. Pharm. Bull. (Tokyo)* **36**, 3220-3222
- 221 Coward, J. K. and Pegg, A. E. (1987) Specific multisubstrate adduct inhibitors of

- aminopropyltransferases and their effect on polyamine biosynthesis in cultured cells. *Adv. Enzyme Regul.* **26**, 107-113
- 222 Eloranta, T. O., Khomutov, A. R., Khomutov, R. M. and Hyvönen, T. (1990) Aminoxy analogues of spermidine as inhibitors of spermine synthase and substrates of hepatic polyamine acetylating activity. *J. Biochem.* **108**, 593-598
- 223 Hibasami, H., Borchardt, R. T., Chen, S. Y., Coward, J. K. and Pegg, A. E. (1980) Studies of inhibition of rat spermidine synthase and spermine synthase. *Biochem. J.* **187**, 419-428
- 224 Khomutov, R. M., Hyvönen, T., Karvonen, E., Kauppinen, L., Paalanen, T., Paulin, L., Eloranta, T., Pajula, R. L., Andersson, L. C. and Pösö, H. (1985) 1-Aminoxy-3-aminopropane, a new and potent inhibitor of polyamine biosynthesis that inhibits ornithine decarboxylase, adenosylmethionine decarboxylase and spermidine synthase. *Biochem. Biophys. Res. Commun.* **130**, 596-602
- 225 Nakashima, K., Tsukada, T., Hibasami, H. and Maekawa, S. (1986) Synthesis of N-chlorosulfonyl dicyclohexylamine as a potent inhibitor for spermidine synthase and its effects on human leukemia molt4B cells. *Biochem. Biophys. Res. Commun.* **141**, 718-722
- 226 Shirahata, A., Morohohi, T., Fukai, M., Akatsu, S. and Samejima, K. (1991) Putrescine or spermidine binding site of aminopropyltransferases and competitive inhibitors. *Biochem. Pharmacol.* **41**, 205-212
- 227 Becker, J., Mtwisha, L., Crampton, B., Stoychev, S., van Brummelen, A., Reeksting, S. B., Louw, A. I., Birkholtz, L. and Mancama, D. (2010) *Plasmodium falciparum* spermidine synthase inhibition results in unique perturbation-specific effects observed on transcript, protein and metabolite levels. *BMC Genomics.* **11**, 235
- 228 Kobayashi, M., Watanabe, T., Xu, Y. J., Tatemori, M., Goda, H., Niitsu, M., Shirahata, A. and Samejima, S. (2005) Control of spermidine and spermine levels in rat tissues by *trans*-4-Methylcyclohexylamine, a spermidine-synthase inhibitor. *Biol. Pharm. Bull.* **28**, 569-573
- 229 Carlson, H. A. and McCammon, J. A. (2000) Accommodating protein flexibility in computational drug design. *Mol. Pharmacol.* **57**, 213-218
- 230 Totrov, M. and Abagyan, R. (2008) Flexible ligand docking to multiple receptor conformations: A practical alternative. *Curr. Opin. Struct. Biol.* **18**, 178-184
- 231 Burger, P. B. (2008) Development of a dynamic receptor-based pharmacophore model of *Plasmodium falciparum* spermidine synthase for selective inhibitor identification. Thesis, University of Pretoria
- 232 Morris, G. M., Goodsell, D. S., Halliday, R. S., Huey, R., Hart, W. E., Belew, R. K. and Olson, A. J. (1998) Automated docking using a Lamarckian genetic algorithm and an empirical binding free energy function. *J. Comput. Chem.* **19**, 1639-1662
- 233 Jakus, J., Wolff, E. C., Park, M. H. and Folk, J. E. (1993) Features of the spermidine-binding site of deoxyhypusine synthase as derived from inhibition studies. Effective inhibition by bis- and mono-guanylated diamines and polyamines. *J. Biol. Chem.* **268**, 13151-13159
- 234 le Roux, D. (2010) *In vitro* antiplasmodial activity of inhibitors on polyamine metabolism targeting *Plasmodium falciparum* spermidine synthase. Thesis, University of Pretoria
- 235 Trager, W. and Jensen, J. (1976) Human malaria parasites in continuous culture. *Science* **193**, 673-675
- 236 Lambros, C. and Vanderberg, J. P. (1979) Synchronisation of *Plasmodium falciparum* erythrocytic stages in culture. *J. Parasitol.* **65**, 418-420
- 237 Bennett, T. N., Paguio, M., Gligorijevic, B., Seudieu, C., Kosar, A. D., Davidson, E. and Roepe, P. D. (2004) Novel, rapid, and inexpensive cell-based quantification of antimalarial drug efficacy. *Antimicrob. Agents Chemother.* **48**, 1807-1810
- 238 Smilkstein, M., Sriwilajaroen, N., Kelly, J. X., Wilairat, P. and Riscoe, M. (2004) Simple and inexpensive fluorescence-based technique for high-throughput antimalarial drug screening. *Antimicrob. Agents Chemother.* **48**, 1803-1806
- 239 Kabsch, W. (2010) XDS. *Acta Crystallogr. Sect. D Biol. Crystallogr.* **66**, 125-132

- 240 Brunger, A. T. (2007) Version 1.2 of the Crystallography and NMR system. *Nat. Protocols*. **2**, 2728-2733
- 241 Brunger, A. T., Adams, P. D., Clore, G. M., DeLano, W. L., Gros, P., Grosse-Kunstleve, R. W., Jiang, J.-S., Kuszewski, J., Nilges, M., Pannu, N. S., Read, R. J., Rice, L. M., Simonson, T. and Warren, G. L. (1998) Crystallography & NMR System: A new software suite for macromolecular structure determination. *Acta Crystallogr. Sect. D Biol. Crystallogr.* **54**, 905-921
- 242 Collaborative Computational Project, n. (1994) The CCP4 suite: Programs for protein crystallography. *Acta Crystallogr. Sect. D Biol. Crystallogr.* **50**, 760-763
- 243 Schuettelkopf, A. W. and van Aalten, D. M. F. (2004) PRODRG-A tool for high-throughput crystallography of protein-ligand complexes. *Acta Crystallogr. Sect. D Biol. Crystallogr.* **60**, 1355-1363
- 244 Vagin, A. A., Steiner, R. S., Lebedev, A. A., Potterton, L., McNicholas, S., Long, F. and Murshudov, G. N. (2004) REFMAC5 dictionary: Organisation of prior chemical knowledge and guidelines for its use. *Acta Crystallogr. Sect. D Biol. Crystallogr.* **60**, 2284-2295
- 245 Ramachandran, G. N., Ramakrishnan, C. and Sasisekharan, V. (1963) Stereochemistry of polypeptide chain configurations. *J. Mol. Biol.* **7**, 95-99
- 246 Lovell, S. C., Davis, I. W., Arendall, W. B., de Bakker, P. I. W., Word, J. M., Prisant, M. G., Richardson, J. S. and Richardson, D. C. (2003) Structure validation by C α geometry: ϕ , ψ and C β deviation. *Proteins*. **50**, 437-450
- 247 Messerschmidt, A. (2007) X-ray crystallography of biomacromolecules: A practical guide. Wiley-VCH, Weinheim
- 248 Davis, I. W., Leaver-Fay, A., Chen, V. B., Block, J. N., Kapral, G. J., Wang, X., Murray, L. W., Arendall, W. B., Snoeyink, J., Richardson, J. S. and Richardson, D. C. (2007) MolProbity: all-atom contacts and structure validation for proteins and nucleic acids. *Nucleic Acids Res.* **35**, W375-W383
- 249 Diederichs, K. and Karplus, P. A. (1997) Improved R-factors for diffraction data analysis in macromolecular crystallography. *Nat. Struct. Mol. Biol.* **4**, 269-275
- 250 Krissinel, E. and Henrick, K. (2007) Inference of macromolecular assemblies from crystalline state. *J. Mol. Biol.* **372**, 774-797
- 251 Jacobsson, M., Gäredal, M., Schultz, J. and Karlén, A. (2008) Identification of *Plasmodium falciparum* spermidine synthase active site binders through structure-based virtual screening. *J. Med. Chem.* **51**, 2777-2786
- 252 Lipinski, C. A., Lombardo, F., Dominy, B. W. and Feeney, P. J. (2001) Experimental and computational approaches to estimate solubility and permeability in drug discovery and development settings. *Adv. Drug Deliv. Rev.* **46**, 3-26
- 253 Klein, G. and Weinhouse, S. (1981) Advances in cancer research. Academic Press, New York
- 254 Oka, T., Perry, J. W. and Kano, K. (1977) Hormonal regulation of spermidine synthase during the development of mouse mammary epithelium. *Biochem. Biophys. Res. Commun.* **79**, 979-986
- 255 Aponte, J. J., Aide, P., Renom, M., Mandomando, I., Bassat, Q., Sacarlal, J., Manaca, M. N., Lafuente, S., Barbosa, A., Leach, A., Lievens, M., Vekemans, J., Sigauque, B., Dubois, M., Demoitié, M., Sillman, M., Savarese, B., McNeil, J. G., Macete, E., Ballou, W. R., Cohen, J. and Alonso, P. L. (2007) Safety of the RTS,S/AS02D candidate malaria vaccine in infants living in a highly endemic area of Mozambique: A double blind randomised controlled phase I/IIb trial. *Lancet*. **370**, 1543-1551
- 256 Yuthavong, Y., Yuvaniyama, J., Chitnumsub, P., Vanichtanankul, J., Chusacultanachai, S., Tarnchompoo, B., Vilavivan, T. and Kamchonwongpaisan, S. (2005) Malarial (*Plasmodium falciparum*) dihydrofolate reductase-thymidylate synthase: structural basis for antifolate resistance and development of effective inhibitors. *Parasitology*. **130**, 249-259
- 257 Wattanarangsana, J., Chusacultanachai, S., Yuvaniyama, J., Kamchonwongpaisan, S. and Yuthavong, Y. (2003) Effect of N-terminal truncation of *Plasmodium falciparum* dihydrofolate

- reductase on dihydrofolate reductase and thymidylate synthase activity. *Mol. Biochem. Parasitol.* **126**, 97-102
- 258 O'Neil, R. H., Lilien, R. H., Donald, B. R., Stroud, R. M. and Anderson, A. C. (2003) The crystal structure of dihydrofolate reductase-thymidylate synthase from *Cryptosporidium hominis* reveals a novel architecture for the bifunctional enzyme. *J. Eukaryot. Microbiol.* **50**
- 259 Persson, K., Aslund, L., Grahn, B., Hanke, J. and Heby, O. (1998) *Trypanosoma cruzi* has not lost its *S*-adenosylmethionine decarboxylase: Characterisation of the gene and the encoded enzyme. *Biochem. J.* **333**, 527-537

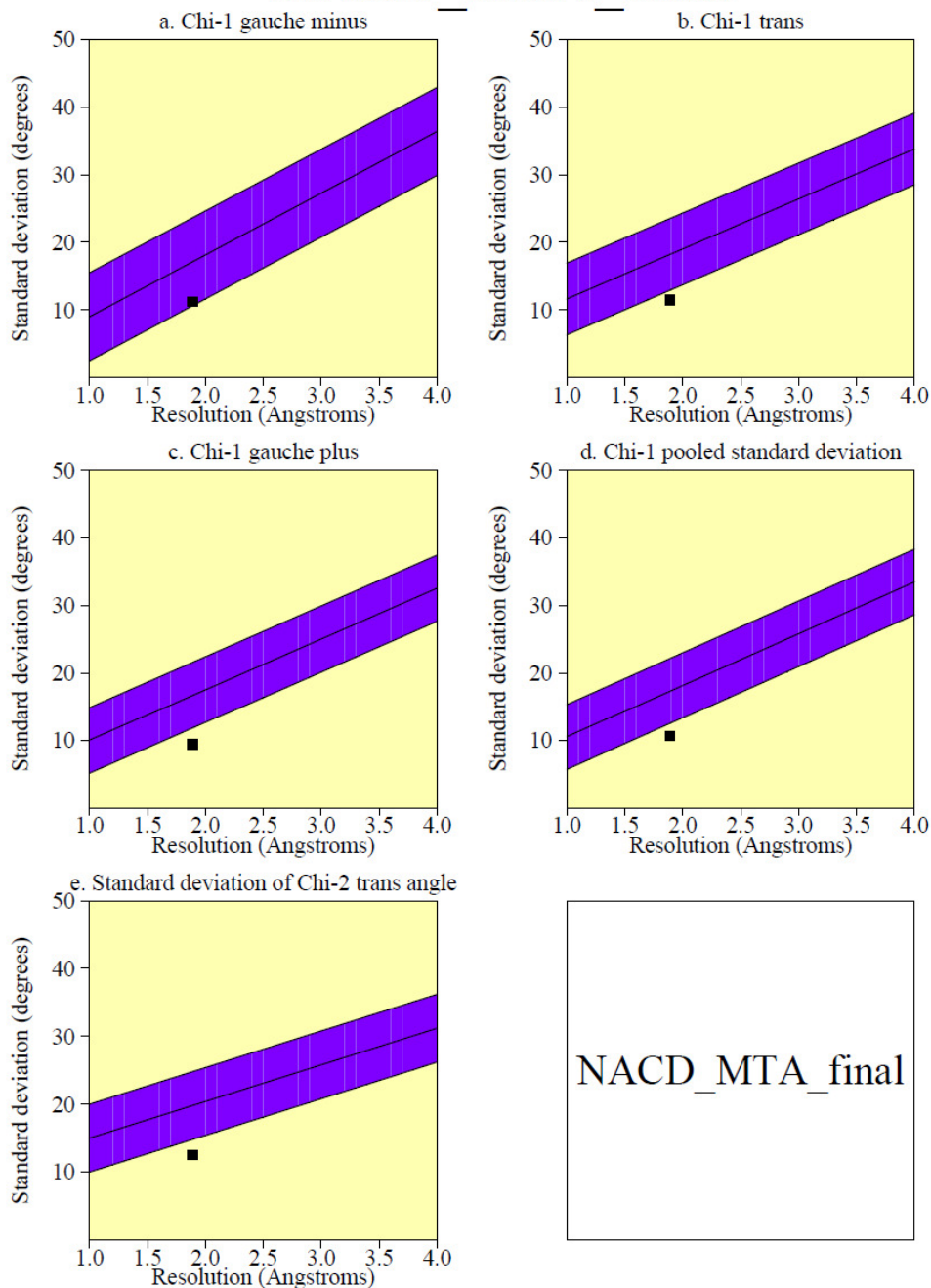
Appendix I: PROCHECK results for the *Pf*SpdS-NACD-MTA crystal structure



PROCHECK

Side-chain parameters

NACD_MTA_final



NACD_MTA_final

Plot statistics

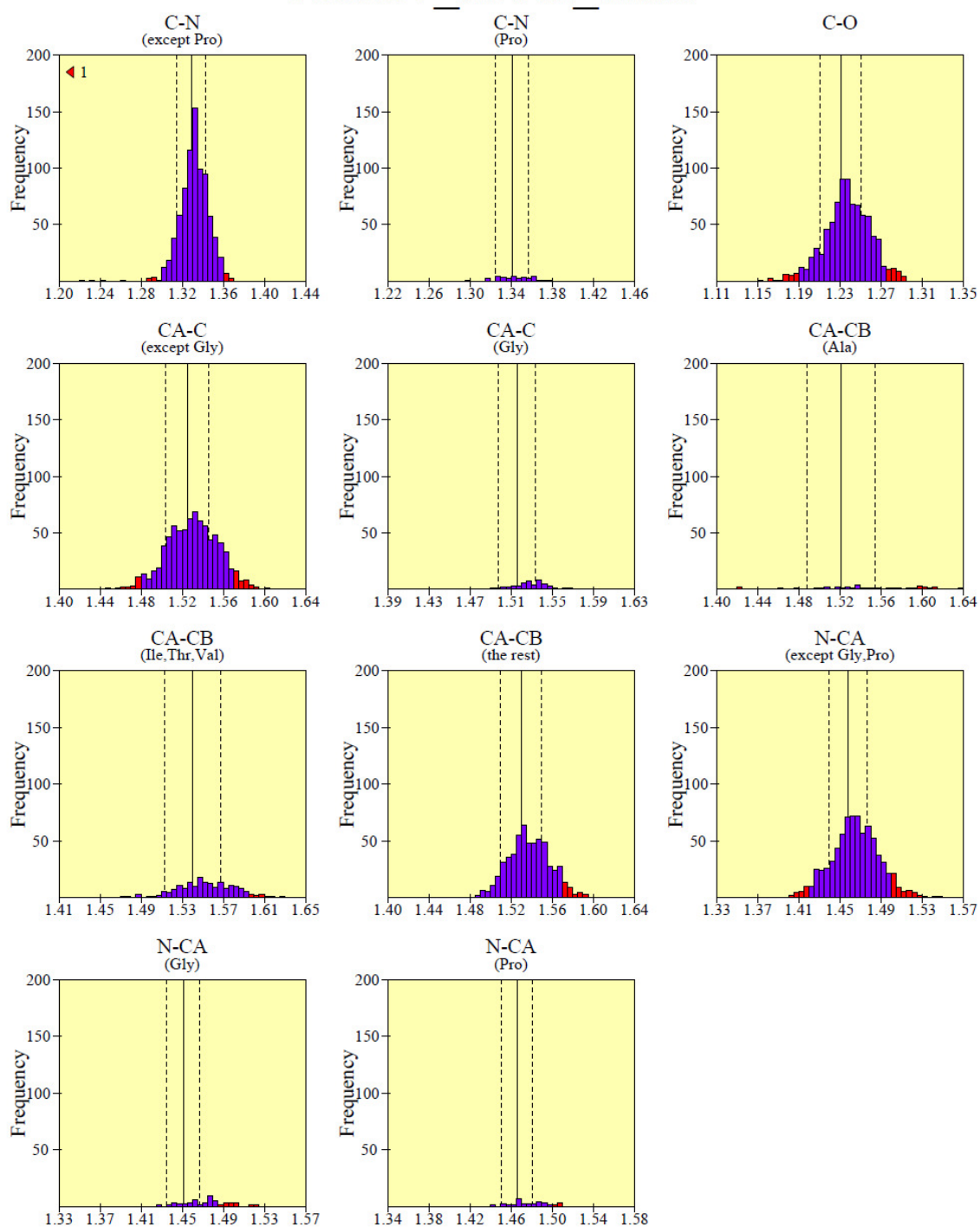
Stereochemical parameter	No. of data pts	Parameter value	Comparison values		No. of band widths from mean	
			Typical value	Band width		
a. Chi-1 gauche minus st dev	125	11.2	17.1	6.5	-0.9	Inside
b. Chi-1 trans st dev	230	11.5	18.2	5.3	-1.3	BETTER
c. Chi-1 gauche plus st dev	371	9.3	16.7	4.9	-1.5	BETTER
d. Chi-1 pooled st dev	726	10.6	17.3	4.8	-1.4	BETTER
e. Chi-2 trans st dev	243	12.5	19.8	5.0	-1.5	BETTER

PROCHECK

Page 1

Main-chain bond lengths

NACD_MTA_final



Black bars > 2.0 st. devs. from mean.

◀ or ▶ signifies data points off the graph in the direction shown.

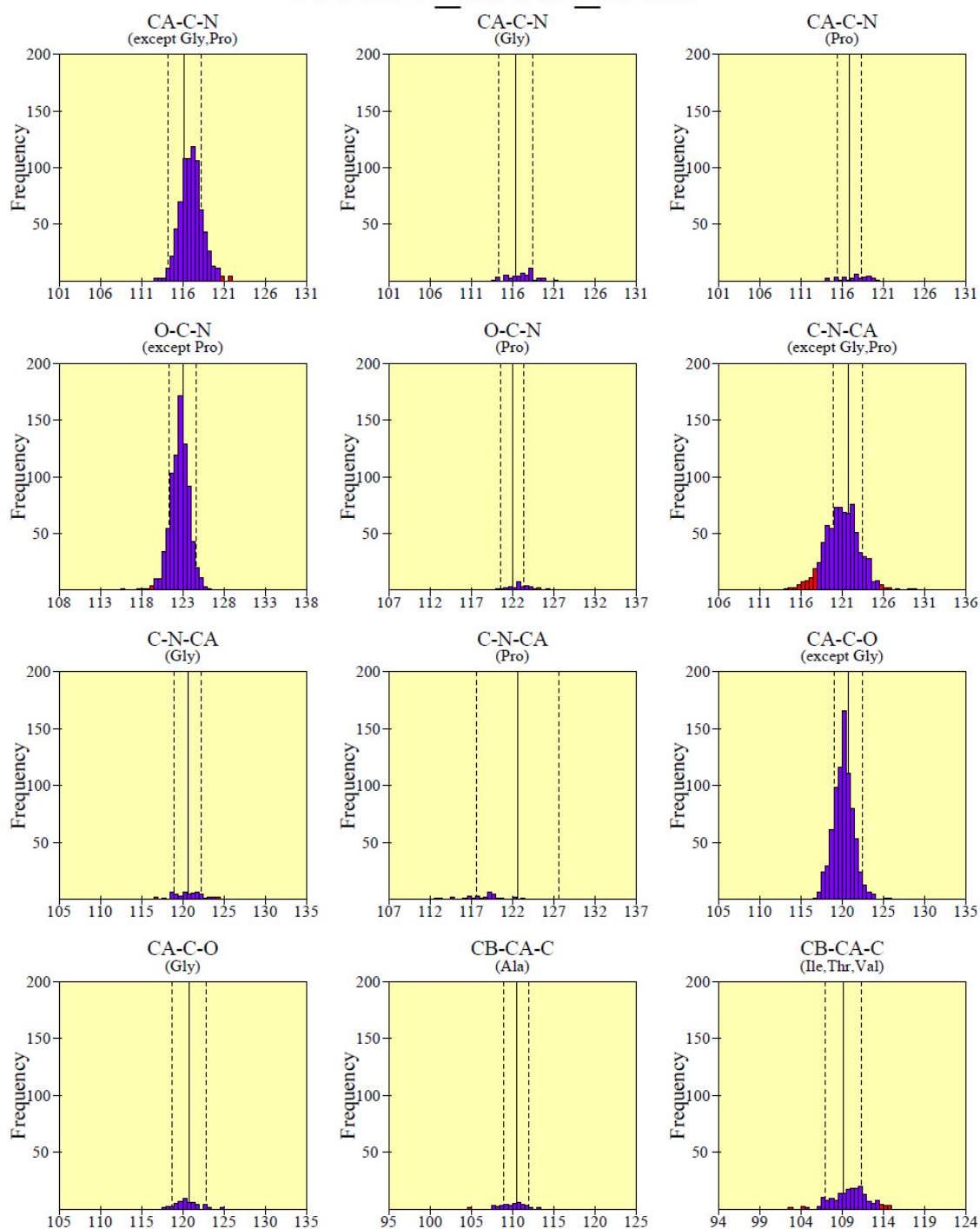
Solid and dashed lines represent the mean and standard deviation values as per Engh & Huber small-molecule data.

PROCHECK

Page 1

Main-chain bond angles

NACD_MTA_final



Black bars > 2.0 st. devs. from mean.

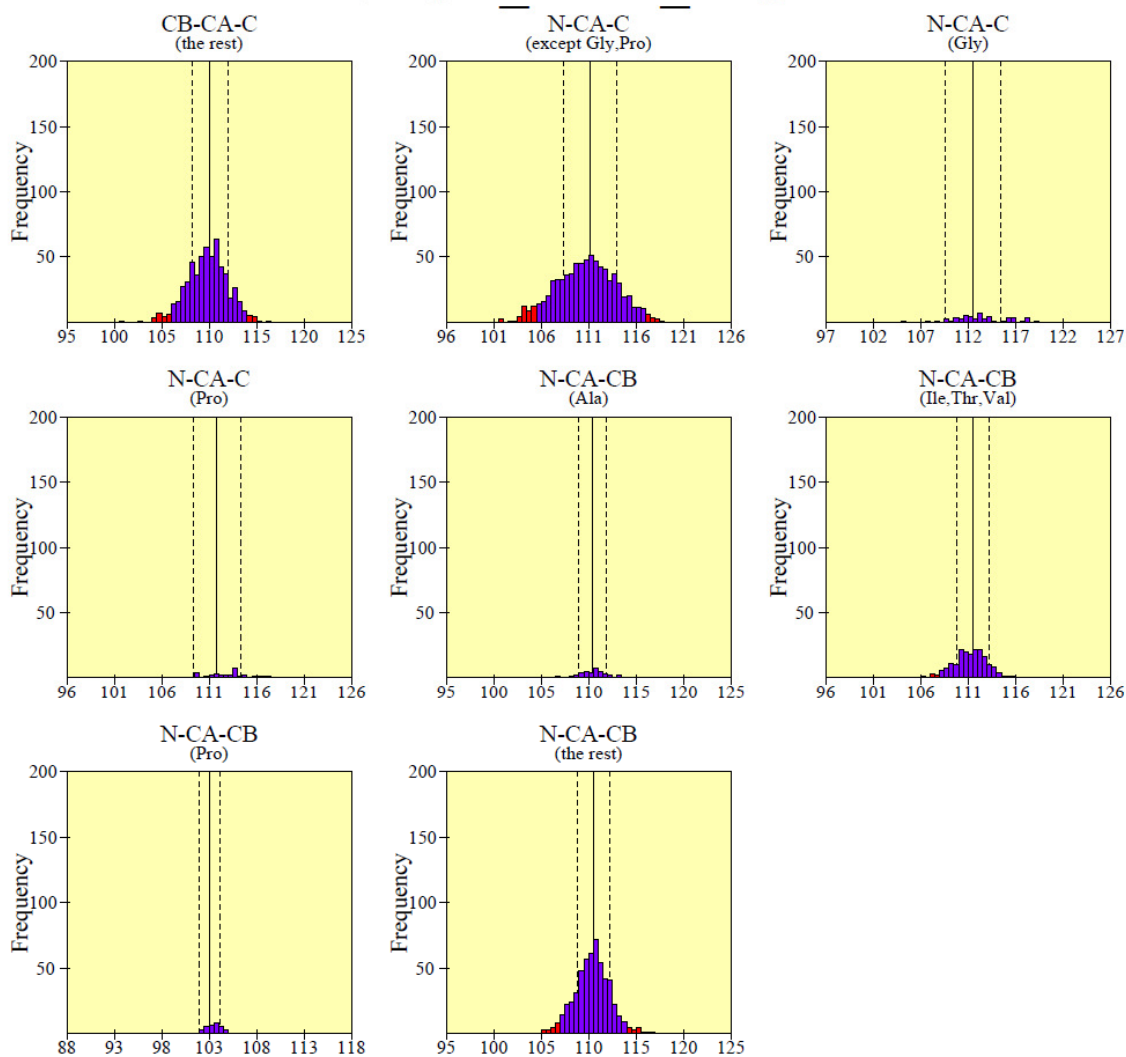
Solid and dashed lines represent the mean and standard deviation values as per Engh & Huber small-molecule data.



PROCHECK

Page 2

Main-chain bond angles NACD_MTA_final



Black bars > 2.0 st. devs. from mean.

Solid and dashed lines represent the mean and standard deviation values as per Engh & Huber small-molecule data.

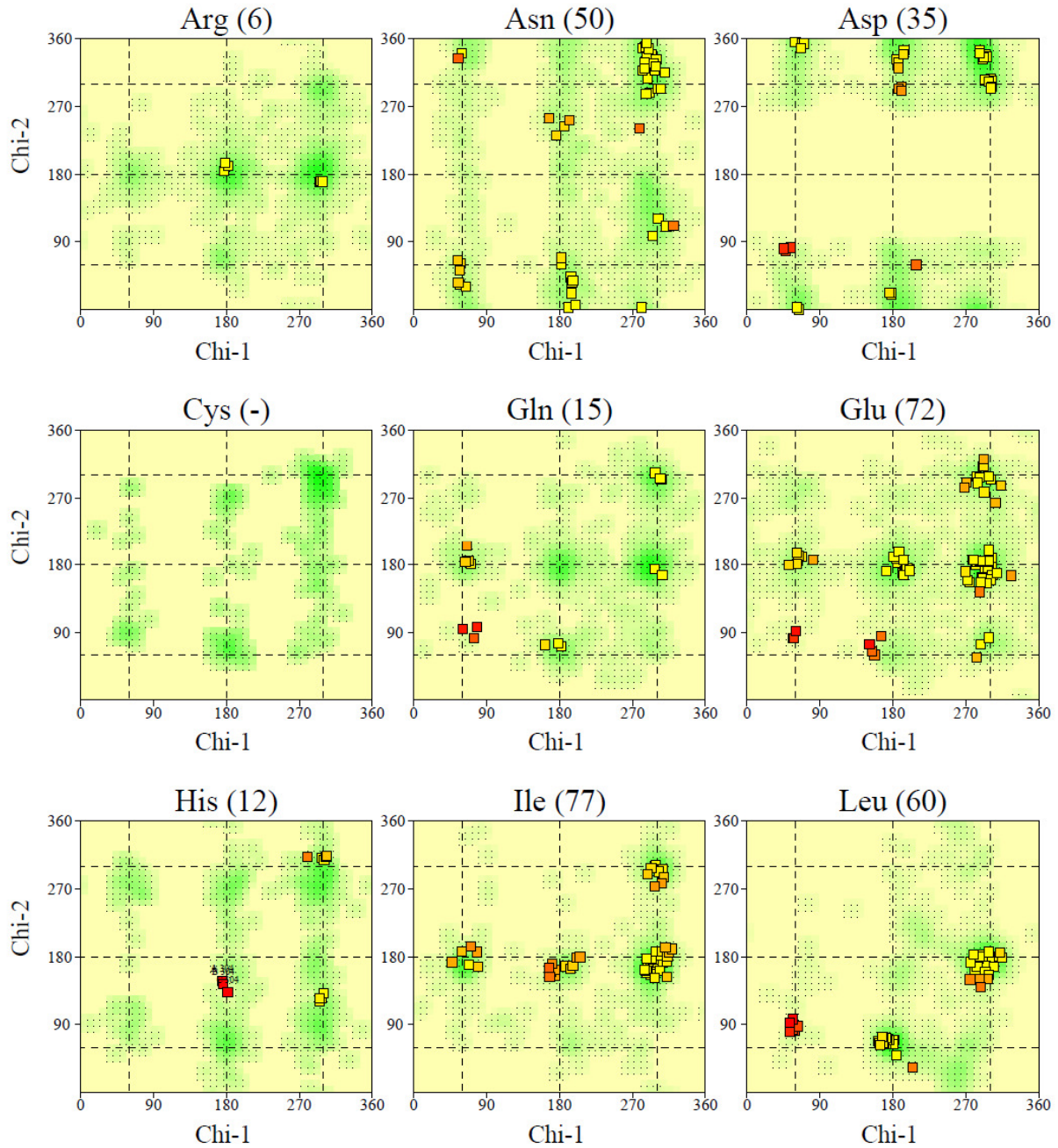


PROCHECK

Page 1

Chi1-Chi2 plots

NACD_MTA_final



Numbers of residues are shown in brackets. Those in unfavourable conformations (score < -3.00) are labelled. Shading shows favourable conformations as obtained from an analysis of 163 structures at resolution 2.0Å or better.

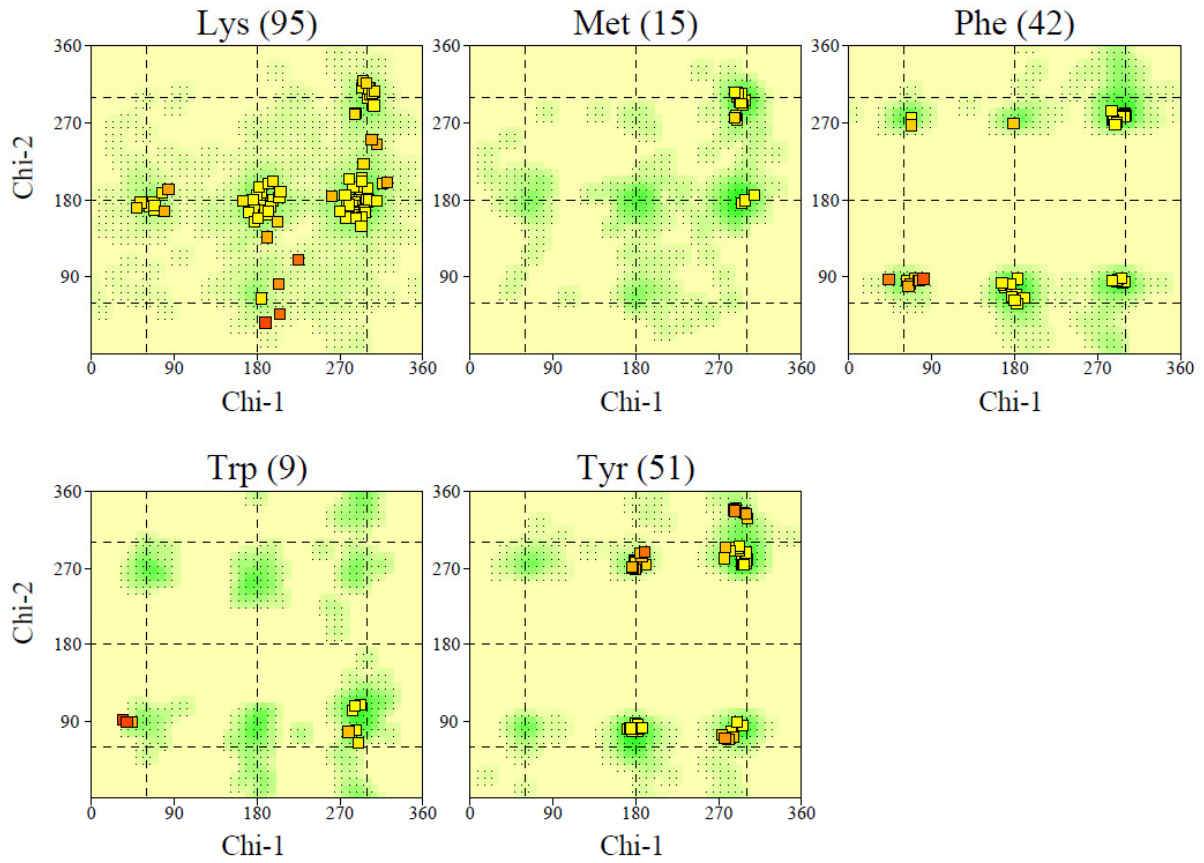


PROCHECK

Page 2

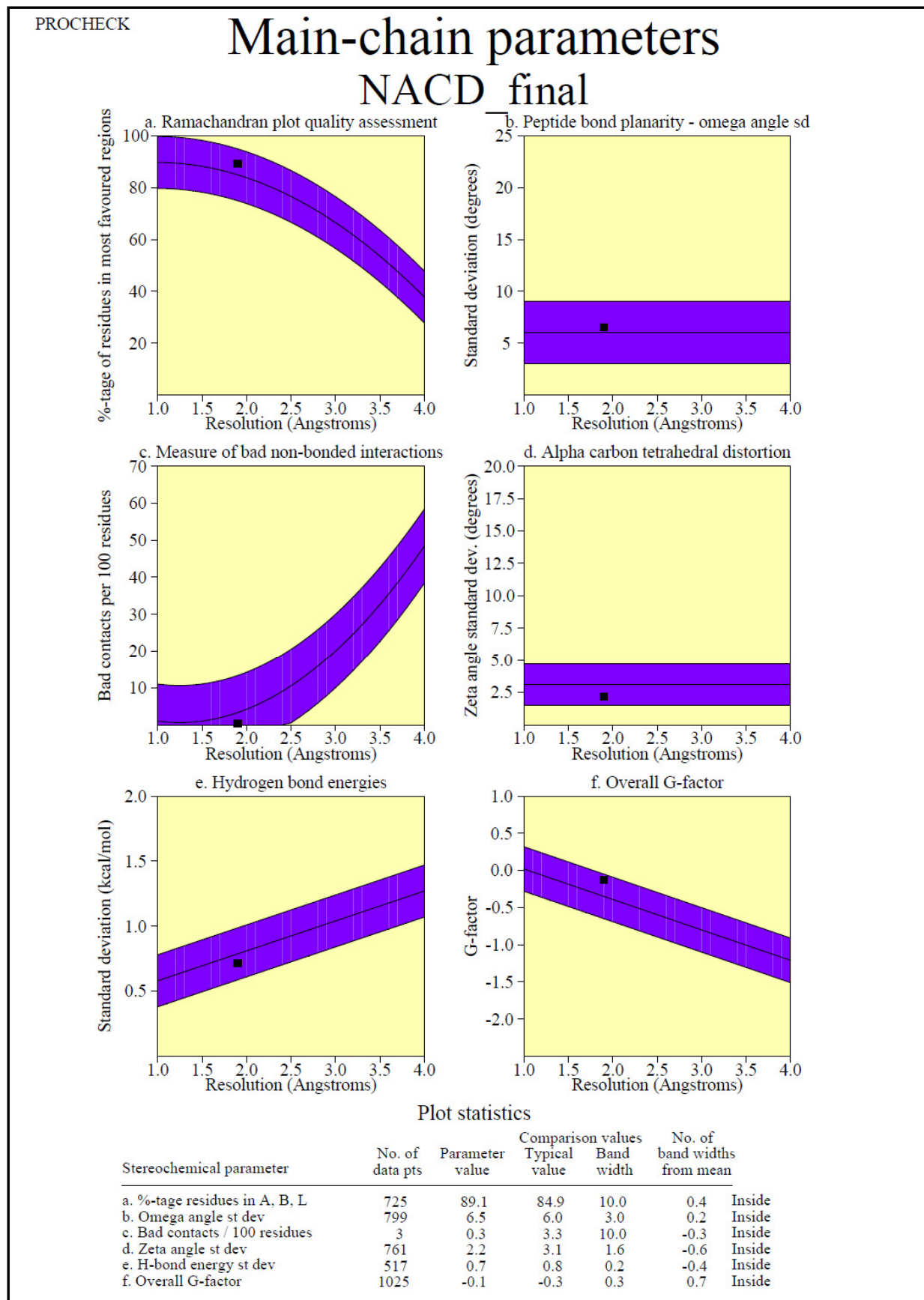
Chi1-Chi2 plots

NACD_MTA_final



Numbers of residues are shown in brackets. Those in unfavourable conformations (score < -3.00) are labelled. Shading shows favourable conformations as obtained from an analysis of 163 structures at resolution 2.0Å or better.

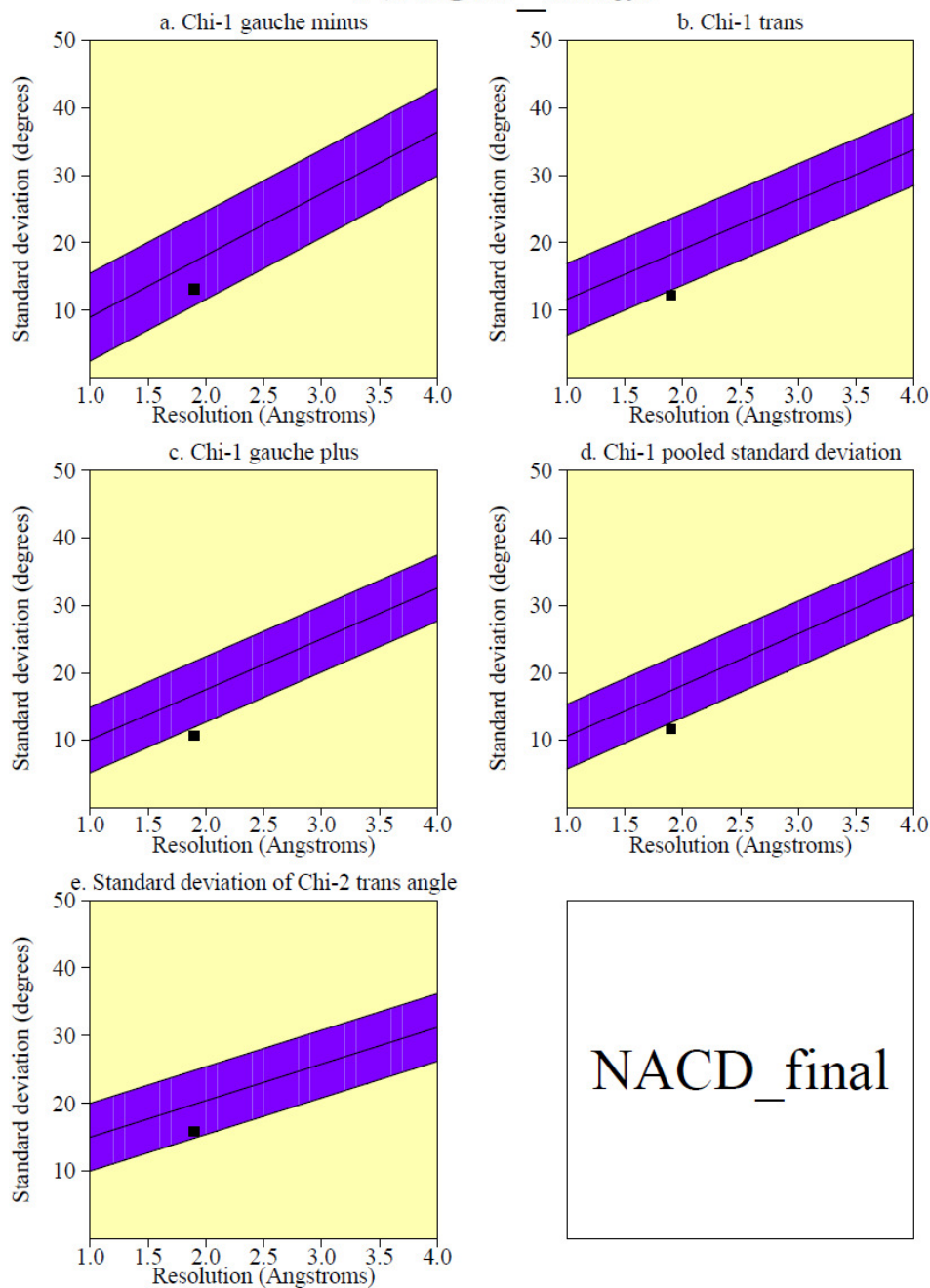
Appendix II: PROCHECK results for the *PfSpdS*-NACD crystal structure



PROCHECK

Side-chain parameters

NACD_final



NACD_final

Plot statistics

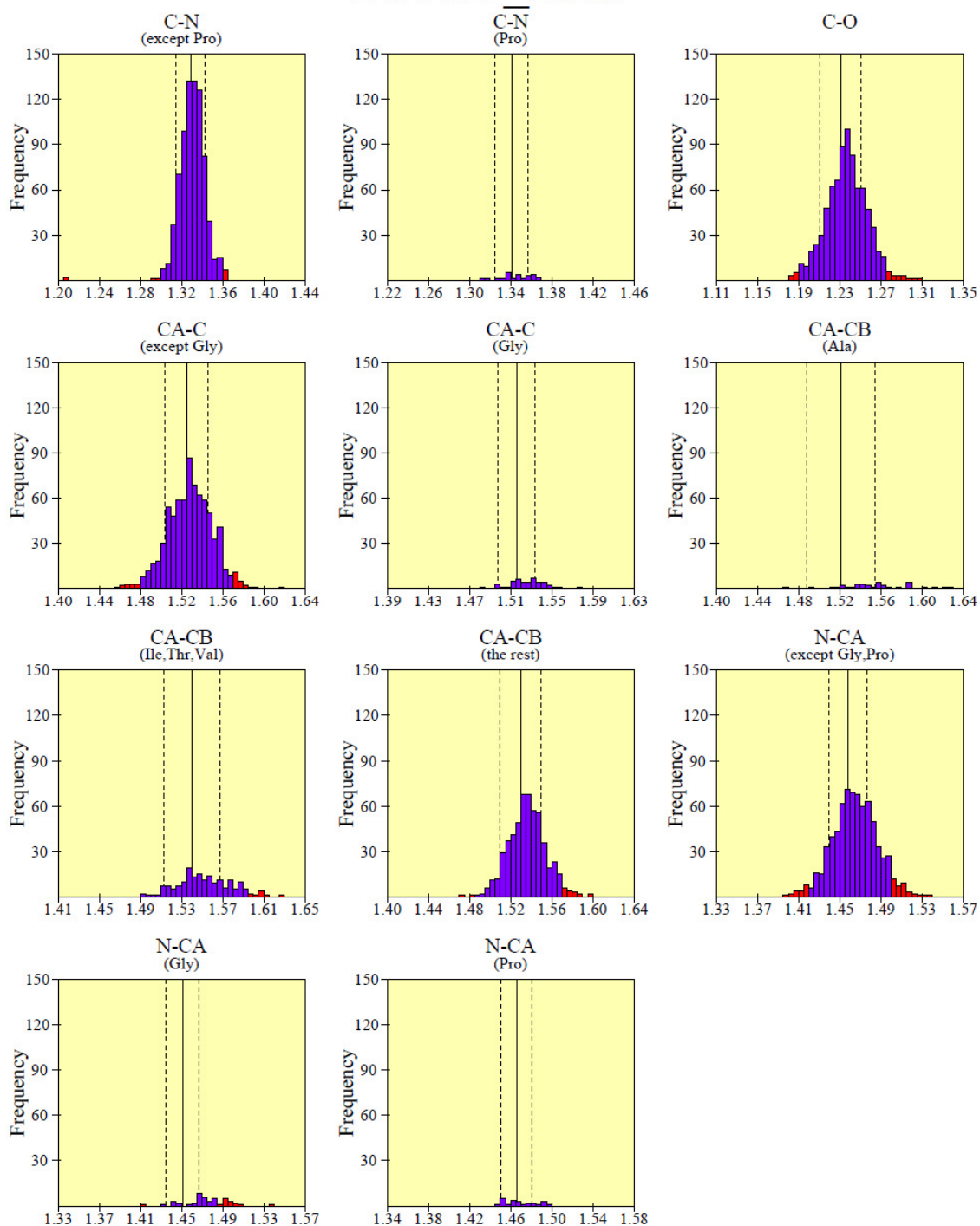
Stereochemical parameter	No. of data pts	Parameter value	Comparison values		No. of band widths from mean	
			Typical value	Band width		
a. Chi-1 gauche minus st dev	108	13.1	17.2	6.5	-0.6	Inside
b. Chi-1 trans st dev	233	12.3	18.3	5.3	-1.1	BETTER
c. Chi-1 gauche plus st dev	363	10.7	16.8	4.9	-1.2	BETTER
d. Chi-1 pooled st dev	704	11.7	17.4	4.8	-1.2	BETTER
e. Chi-2 trans st dev	236	15.9	19.9	5.0	-0.8	Inside

PROCHECK

Page 1

Main-chain bond lengths

NACD_final



Black bars > 2.0 st. devs. from mean.

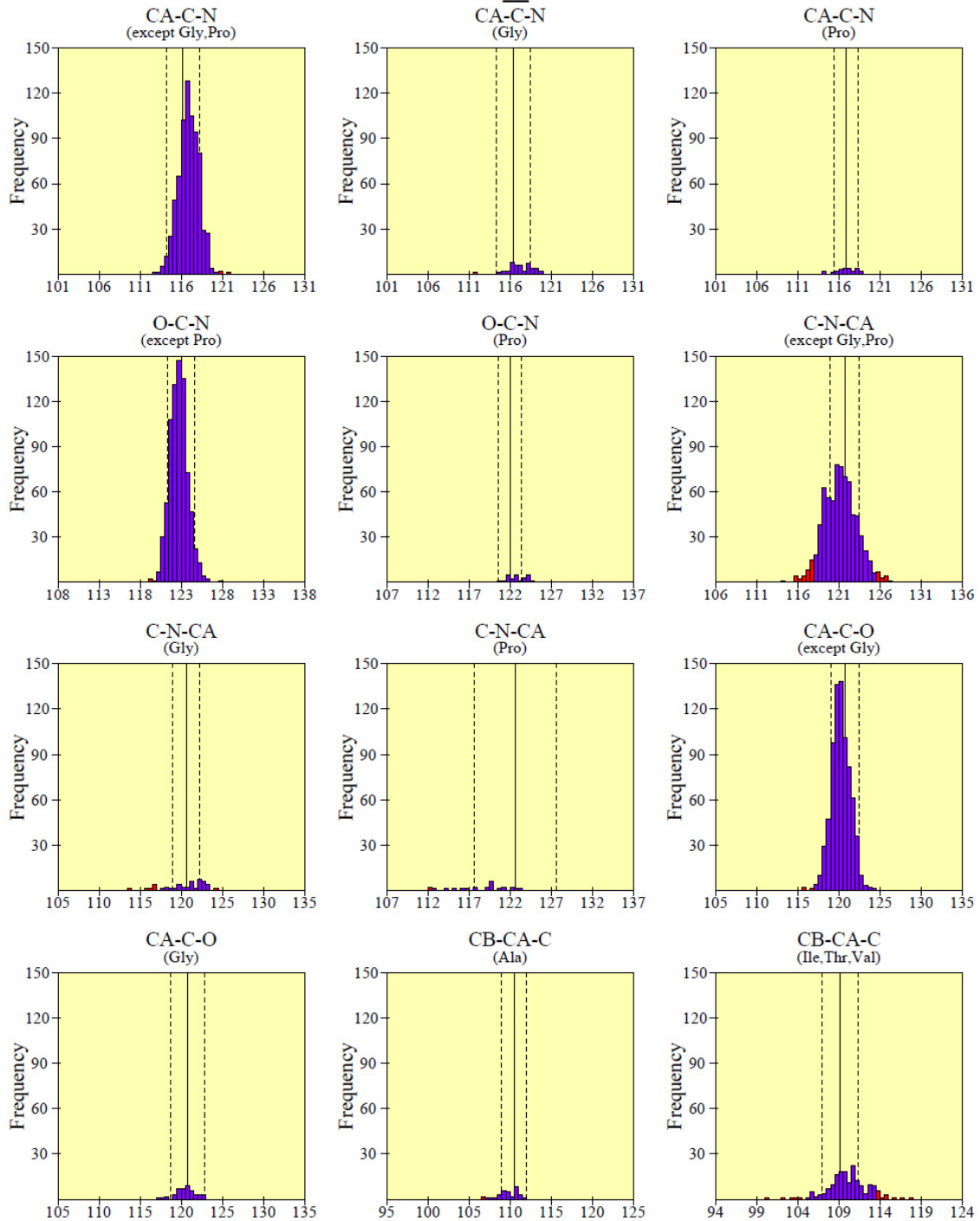
Solid and dashed lines represent the mean and standard deviation values as per Engh & Huber small-molecule data.



PROCHECK

Page 1

Main-chain bond angles NACD_final



Black bars > 2.0 st. devs. from mean.

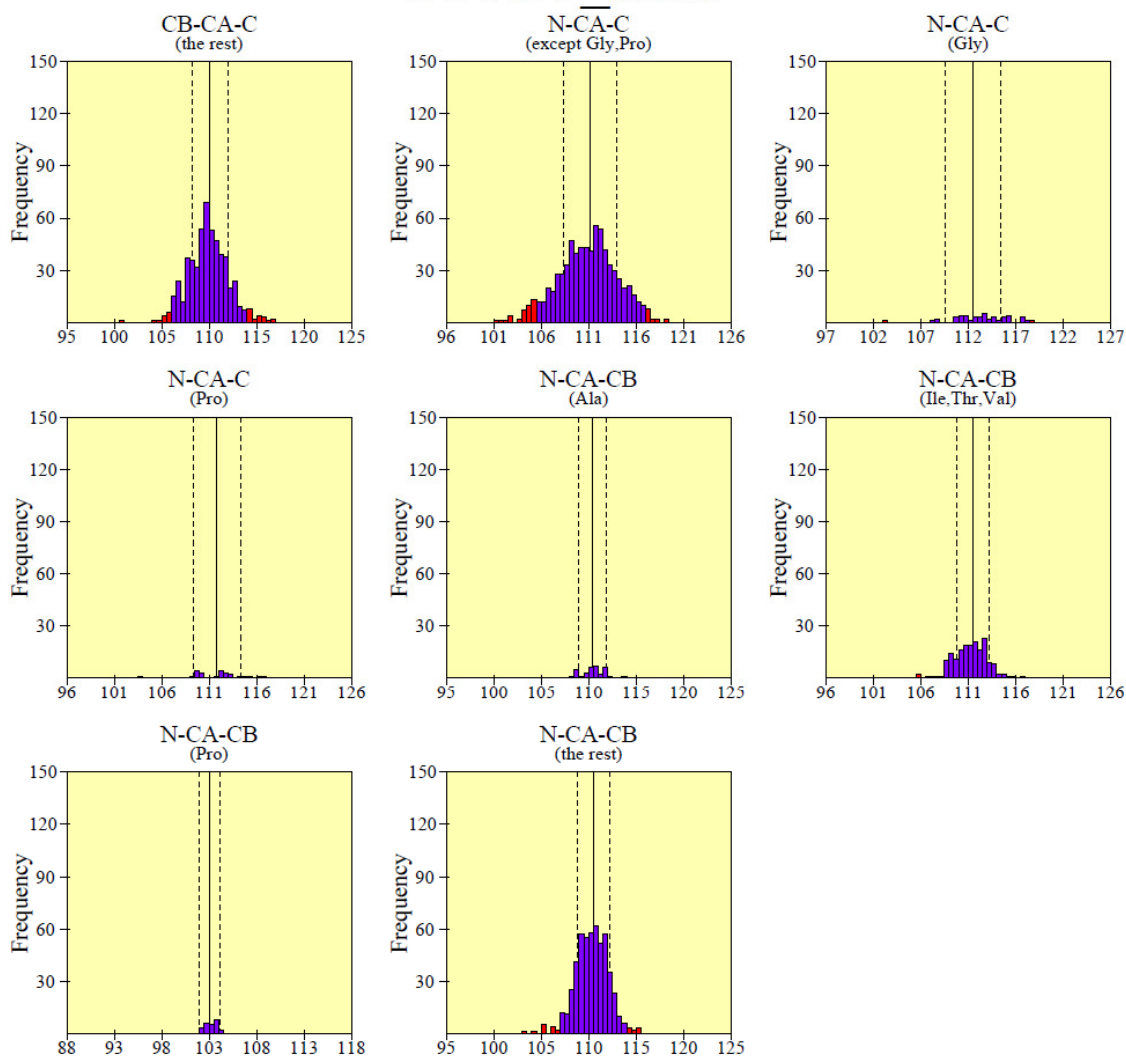
Solid and dashed lines represent the mean and standard deviation values as per Engh & Huber small-molecule data.



PROCHECK

Page 2

Main-chain bond angles NACD_final



Black bars > 2.0 st. devs. from mean.

Solid and dashed lines represent the mean and standard deviation values as per Engh & Huber small-molecule data.

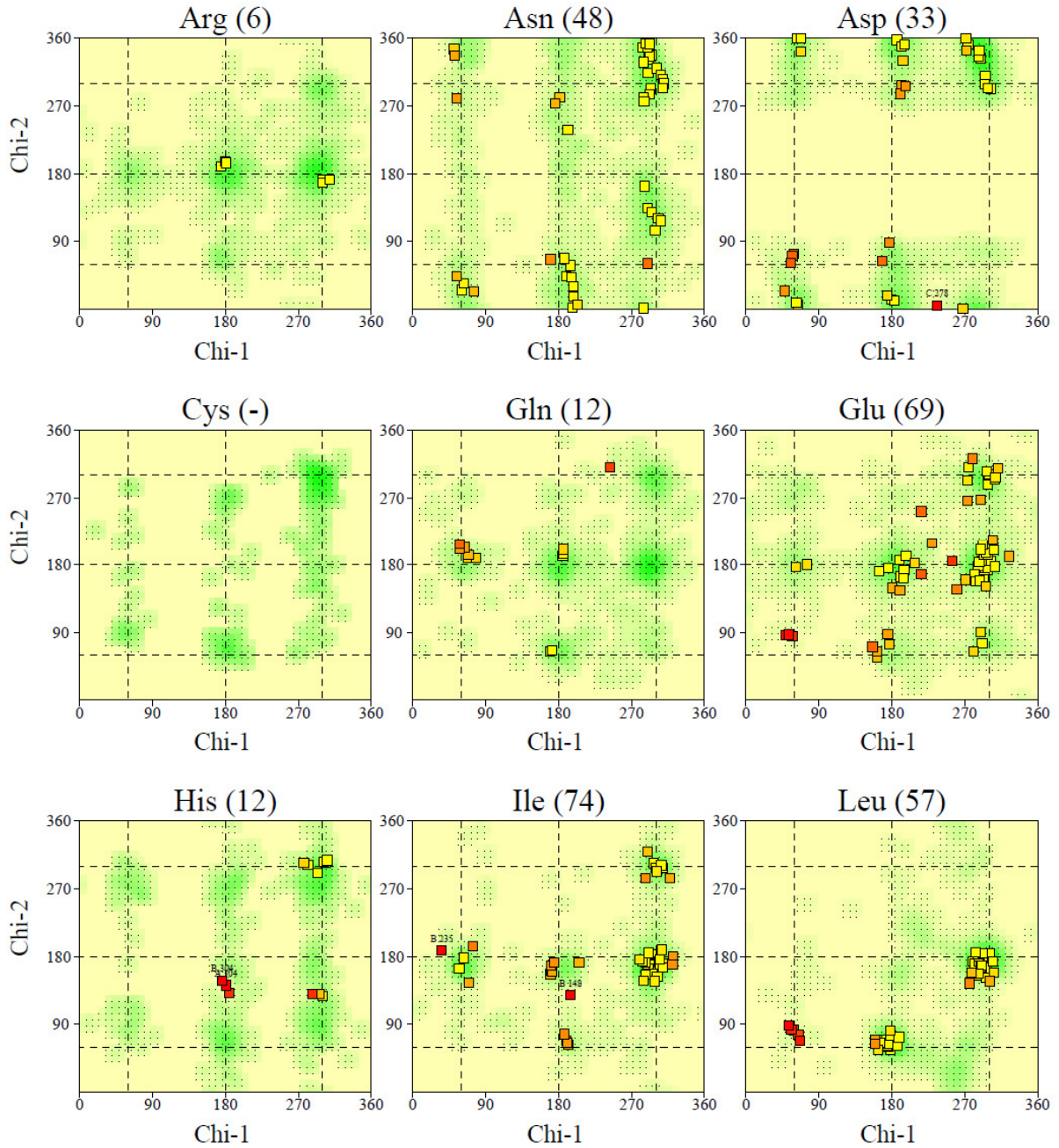


PROCHECK

Page 1

Chi1-Chi2 plots

NACD_final



Numbers of residues are shown in brackets. Those in unfavourable conformations (score < -3.00) are labelled. Shading shows favourable conformations as obtained from an analysis of 163 structures at resolution 2.0Å or better.

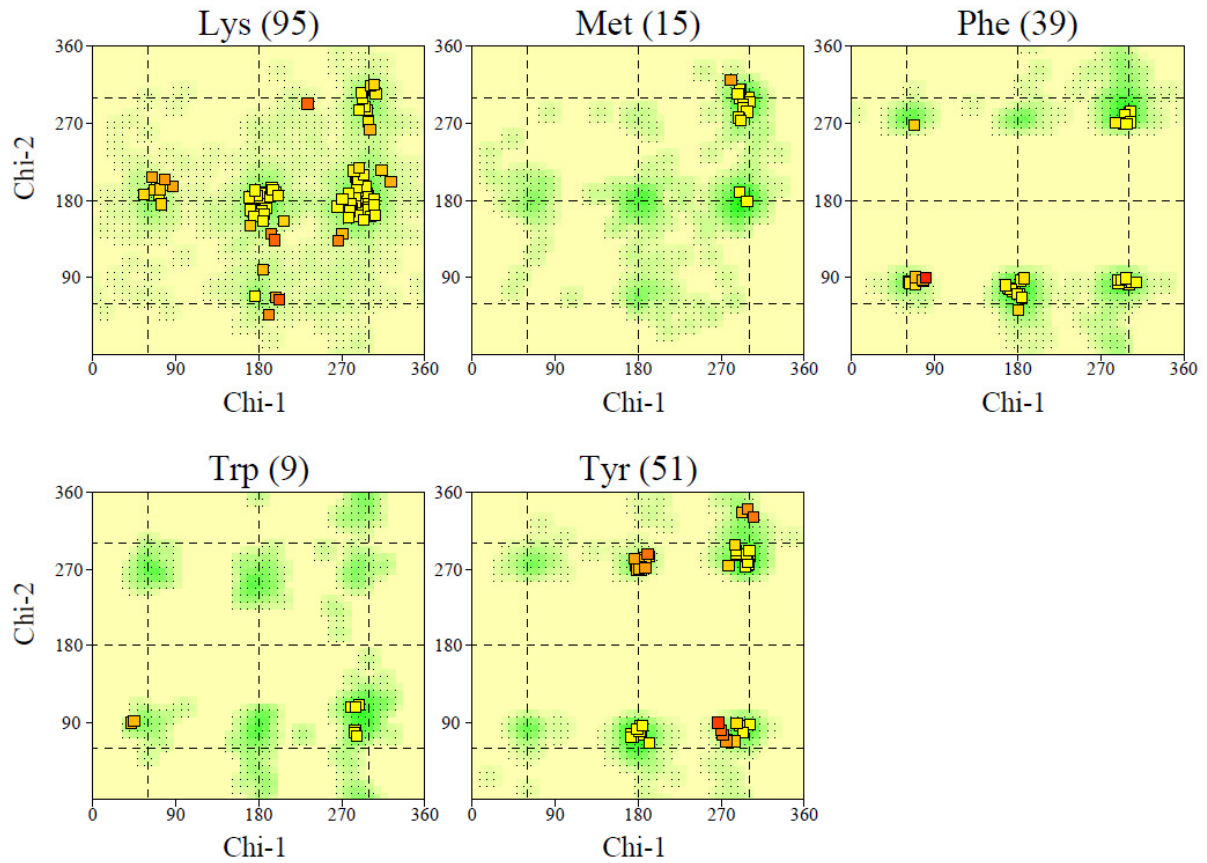


PROCHECK

Page 2

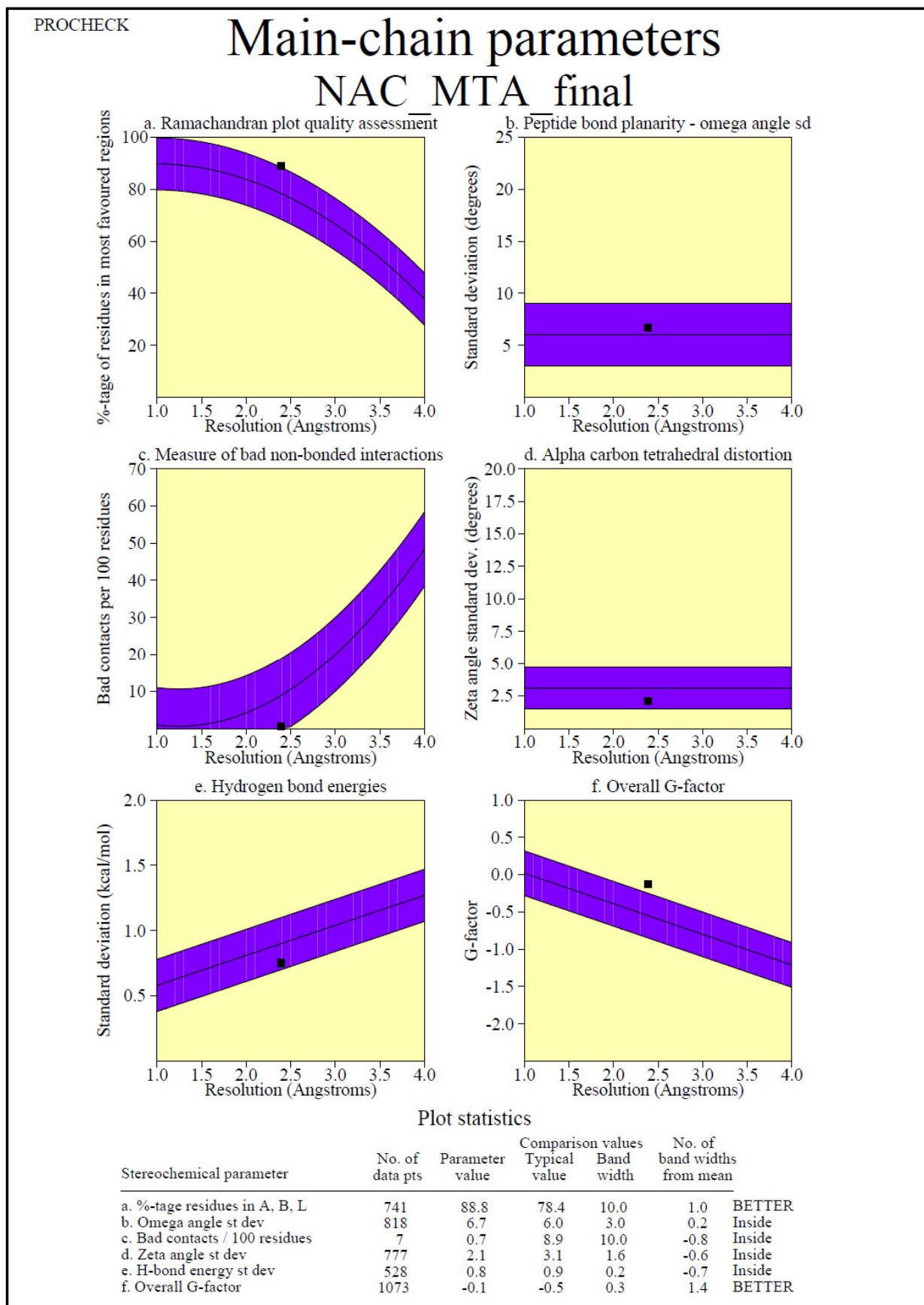
Chi1-Chi2 plots

NACD_final



Numbers of residues are shown in brackets. Those in unfavourable conformations (score < -3.00) are labelled. Shading shows favourable conformations as obtained from an analysis of 163 structures at resolution 2.0Å or better.

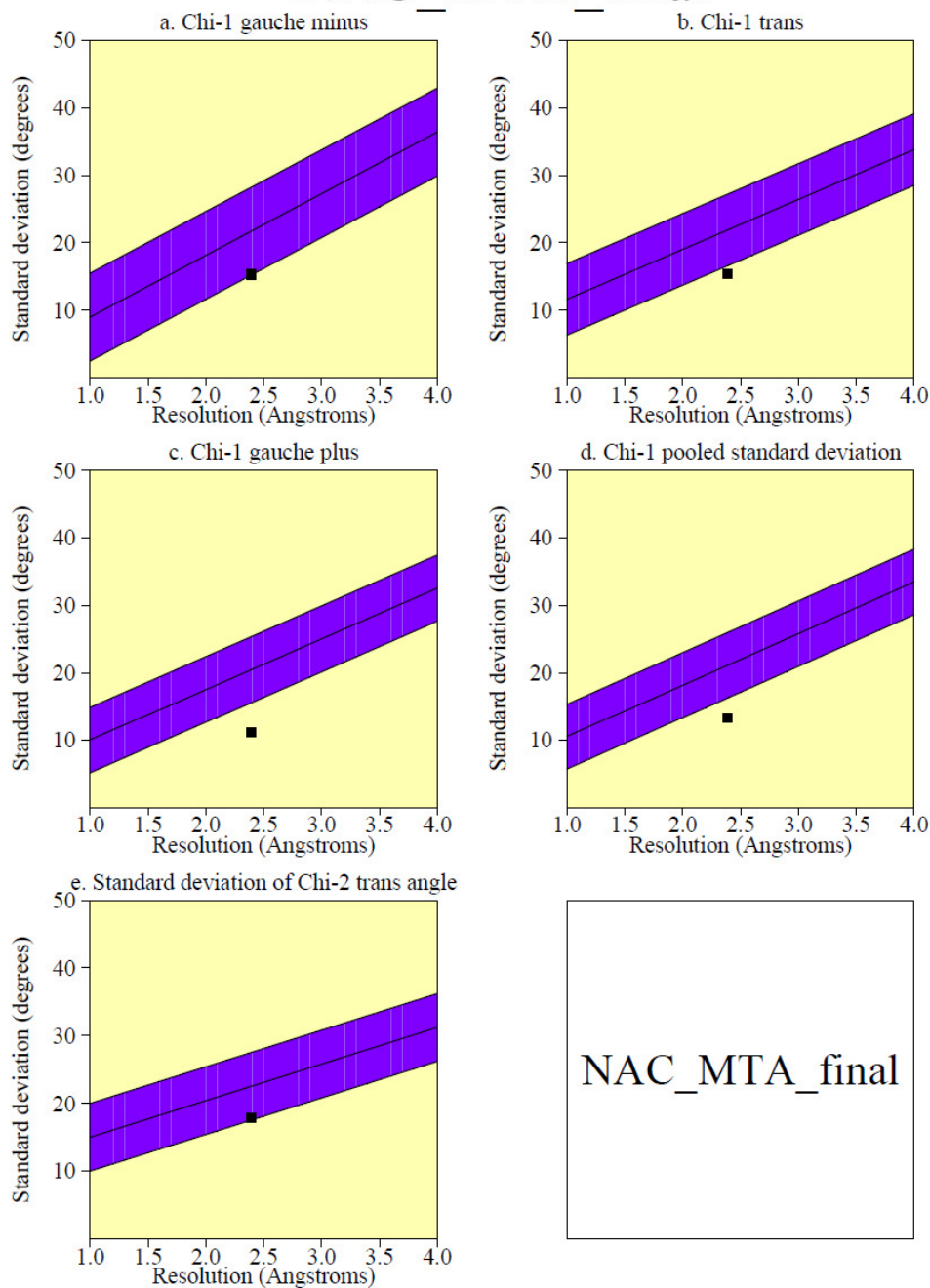
Appendix III: PROCHECK results for the *Pf*SpdS-NAC-MTA crystal structure



PROCHECK

Side-chain parameters

NAC_MTA_final



NAC_MTA_final

Plot statistics

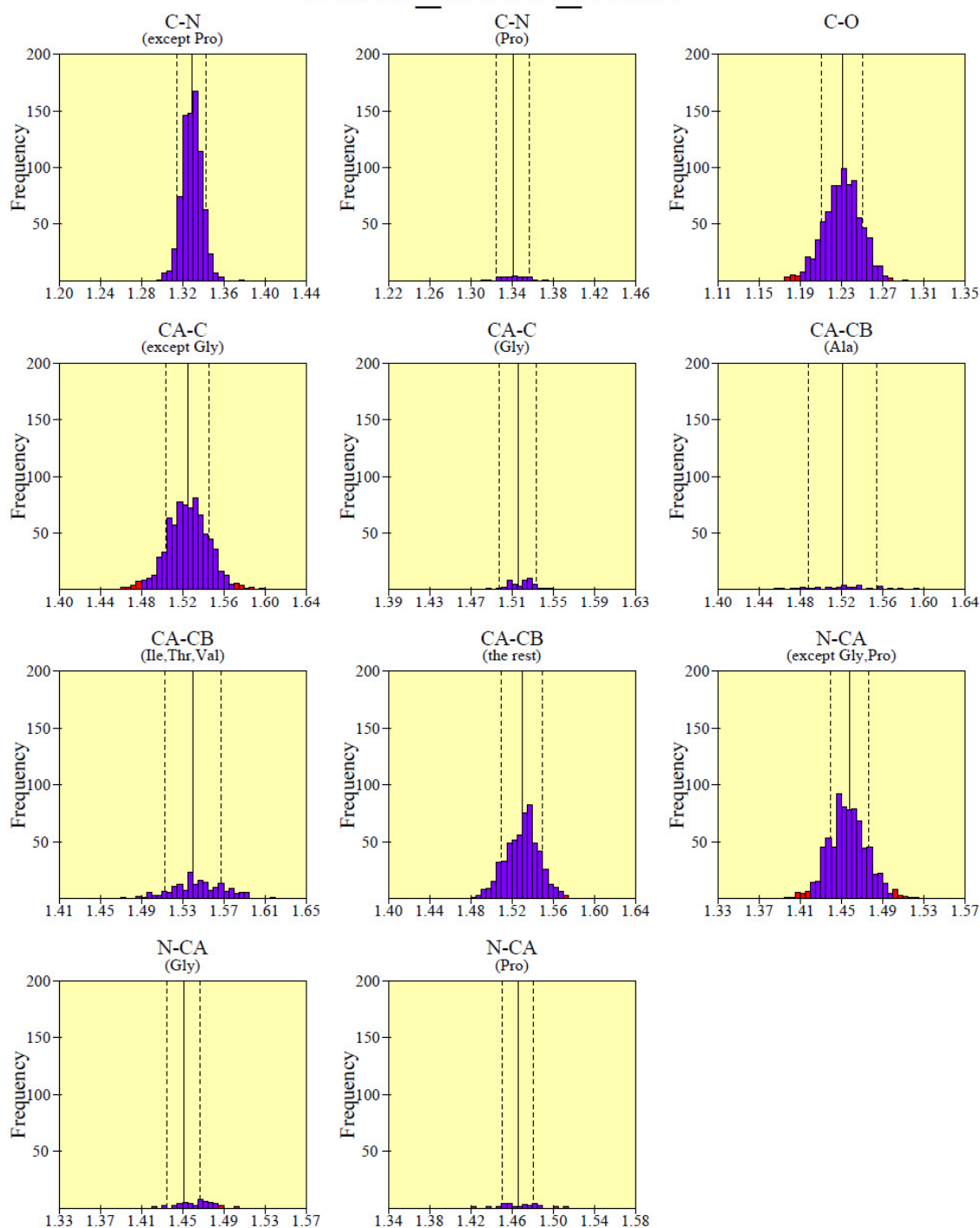
Stereochemical parameter	No. of data pts	Parameter value	Comparison values		No. of band widths from mean	
			Typical value	Band width		
a. Chi-1 gauche minus st dev	123	15.3	21.7	6.5	-1.0	Inside
b. Chi-1 trans st dev	234	15.3	21.9	5.3	-1.2	BETTER
c. Chi-1 gauche plus st dev	360	11.2	20.5	4.9	-1.9	BETTER
d. Chi-1 pooled st dev	717	13.3	21.2	4.8	-1.6	BETTER
e. Chi-2 trans st dev	238	17.9	22.5	5.0	-0.9	Inside

PROCHECK

Page 1

Main-chain bond lengths

NAC_MTA_final



Black bars > 2.0 st. devs. from mean.

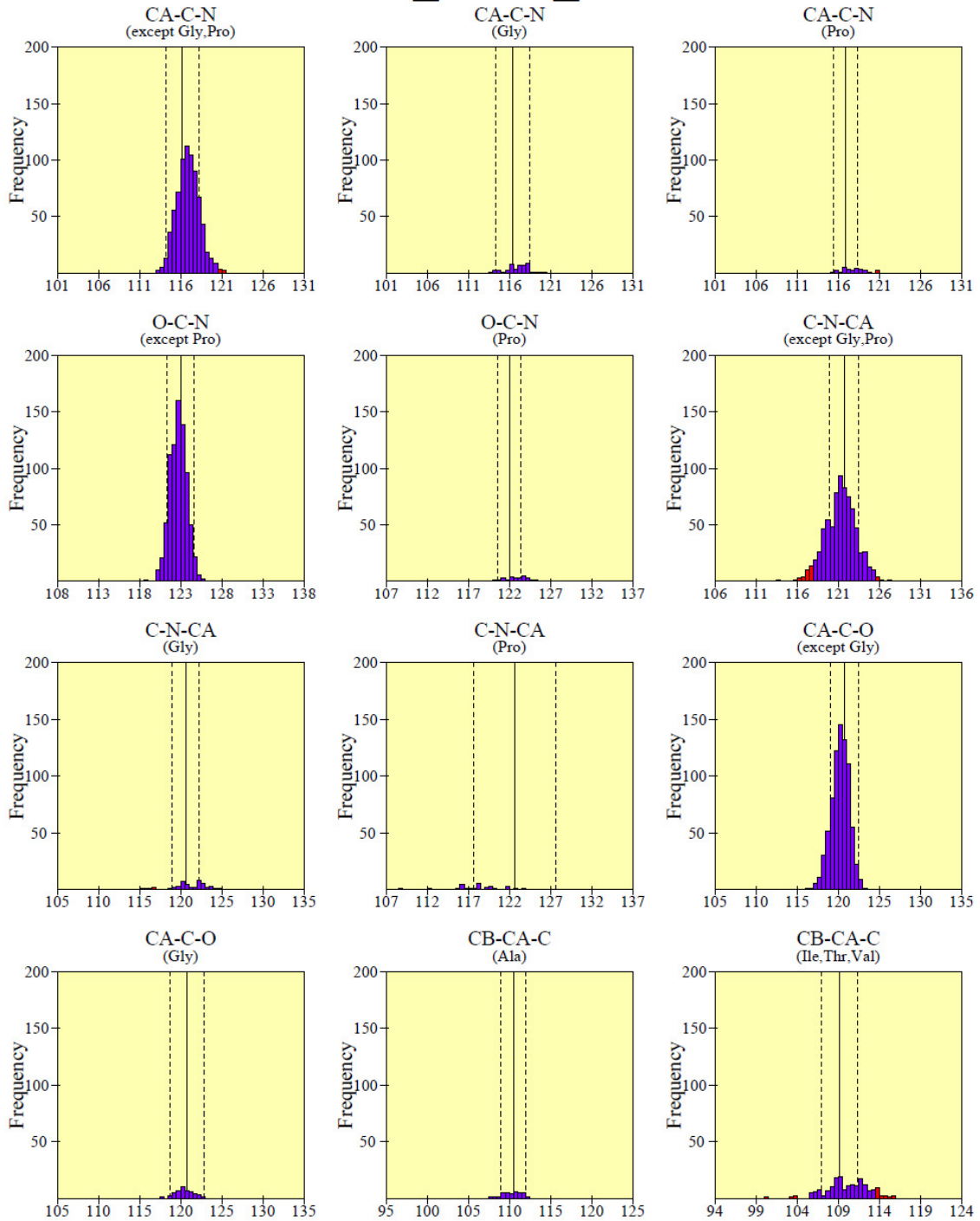
Solid and dashed lines represent the mean and standard deviation values as per Engh & Huber small-molecule data.



PROCHECK

Page 1

Main-chain bond angles NAC_MTA_final



Black bars > 2.0 st. devs. from mean.

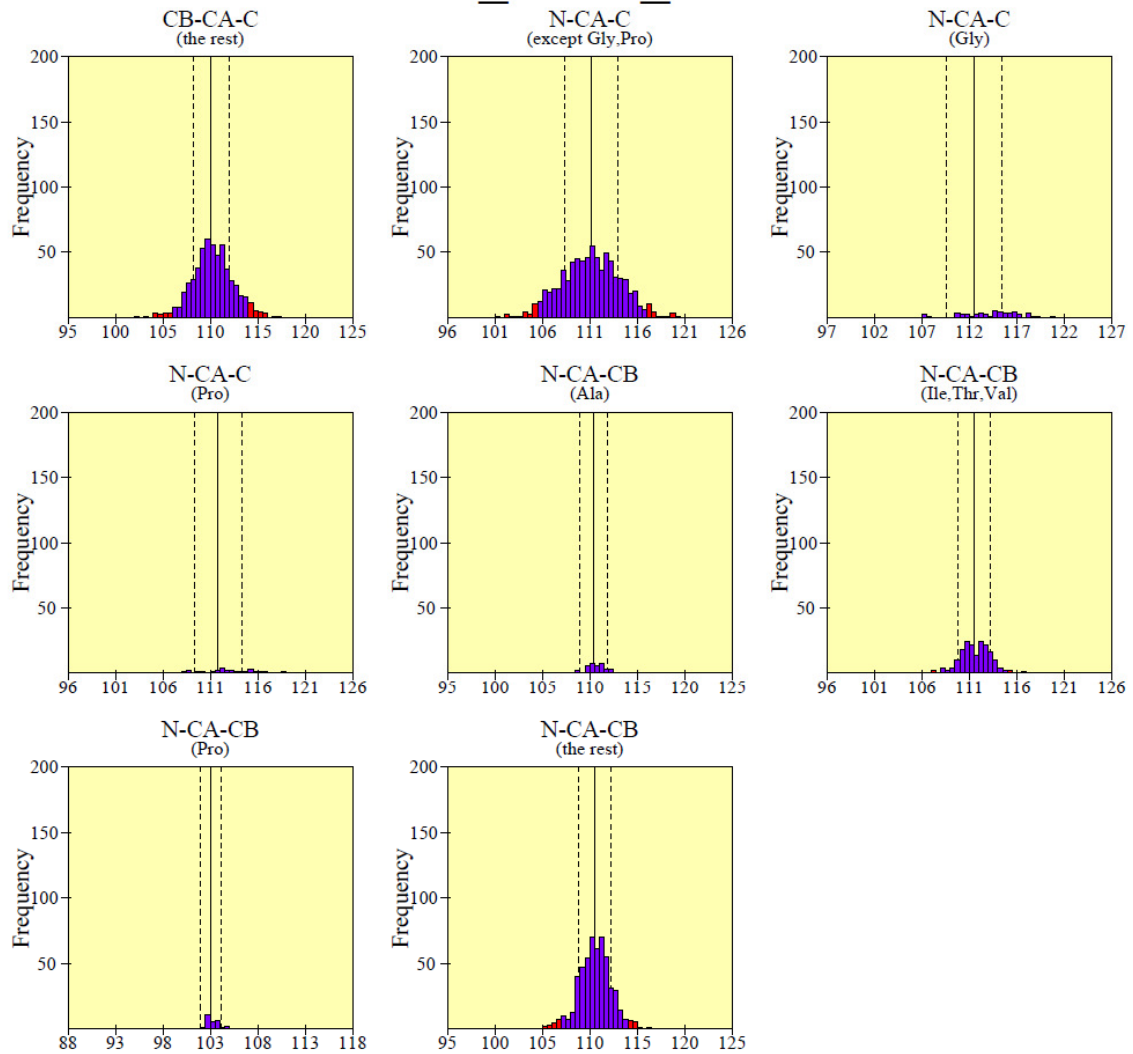
Solid and dashed lines represent the mean and standard deviation values as per Engh & Huber small-molecule data.



PROCHECK

Page 2

Main-chain bond angles NAC_MTA_final



Black bars > 2.0 st. devs. from mean.

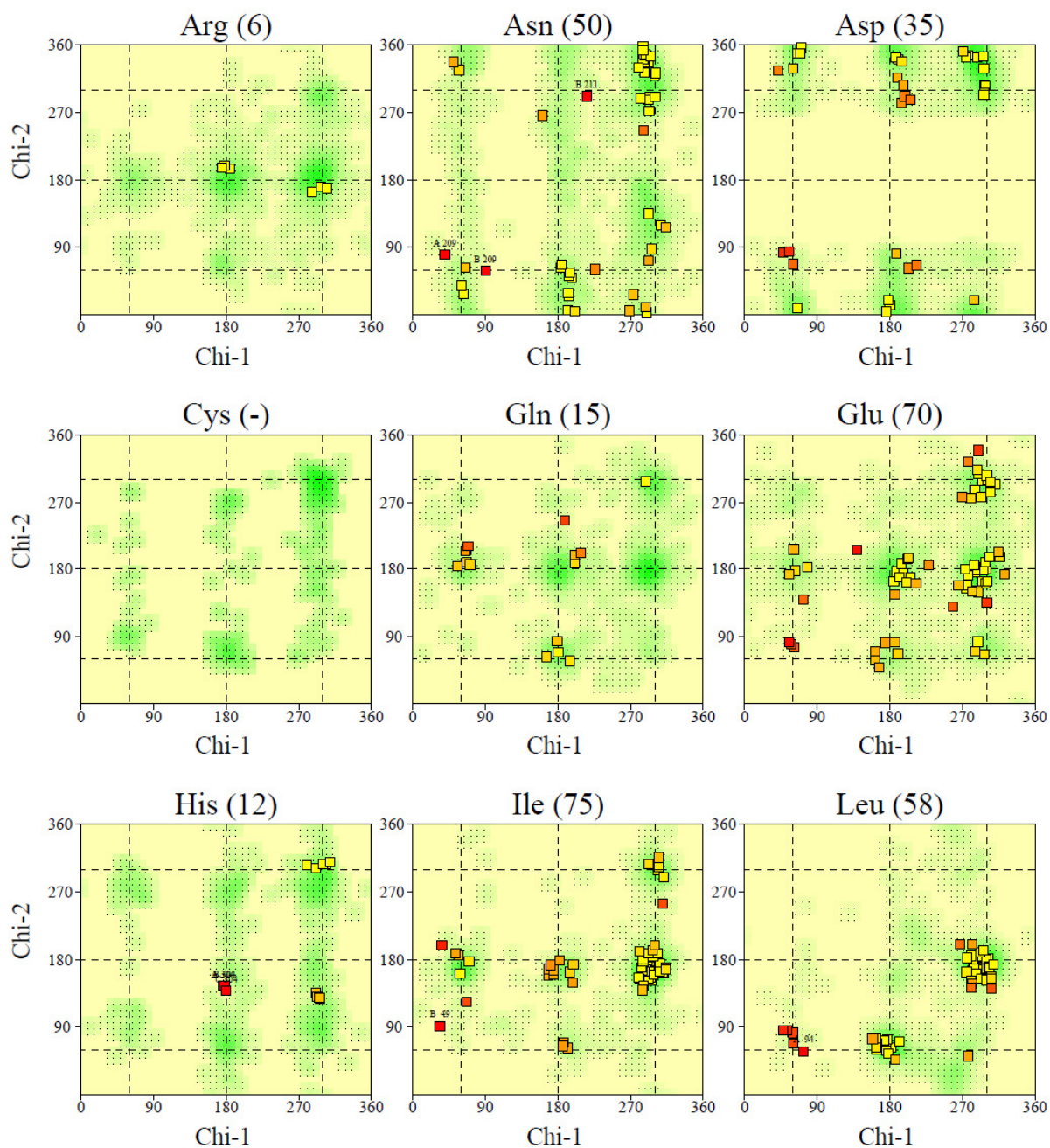
Solid and dashed lines represent the mean and standard deviation values as per Engh & Huber small-molecule data.

PROCHECK

Page 1

Chi1-Chi2 plots

NAC_MTA_final



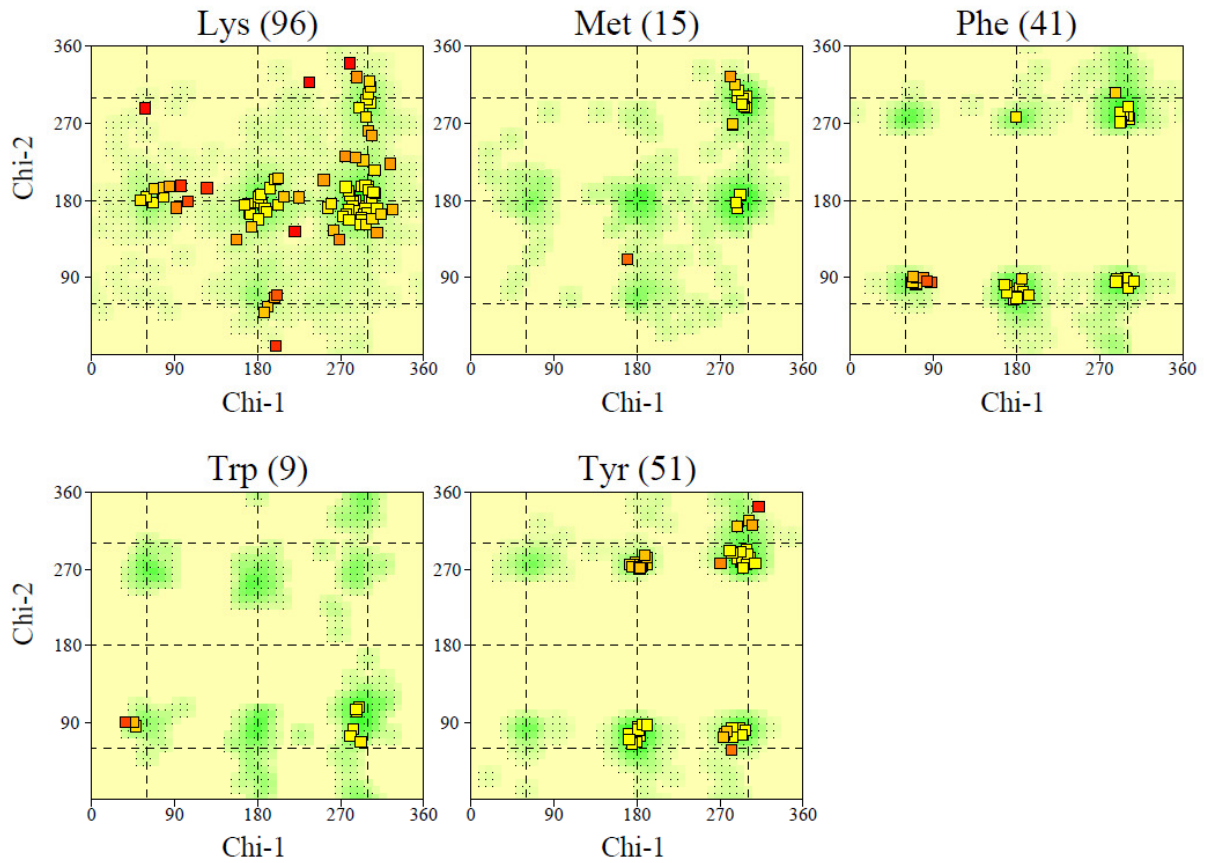
Numbers of residues are shown in brackets. Those in unfavourable conformations (score < -3.00) are labelled. Shading shows favourable conformations as obtained from an analysis of 163 structures at resolution 2.0Å or better.

PROCHECK

Page 2

Chi1-Chi2 plots

NAC_MTA_final



Numbers of residues are shown in brackets. Those in unfavourable conformations (score < -3.00) are labelled. Shading shows favourable conformations as obtained from an analysis of 163 structures at resolution 2.0Å or better.